Progress in Silicones and Silicone-Modified Materials

ACS SYMPOSIUM SERIES **1154**

Progress in Silicones and Silicone-Modified Materials

Stephen J. Clarson, Editor
University of Cincinnati, Cincinnati, Ohio, United States

Michael J. Owen, Editor
Michigan Molecular Institute, Midland, Michigan, United States

Steven D. Smith, Editor
Procter and Gamble, Cincinnati, Ohio, United States

Mark Van Dyke, Editor
Virginia Tech, Blacksburg, Virginia, United States

Michael Brook, Editor
McMaster University, Hamilton, Ontario, Canada

Joseph Mabry, Editor
AFRL, Andrews Air Force Base, California, United States

Foreword

The ACS Symposium Series was first published in 1974 to provide a mechanism for publishing symposia quickly in book form. The purpose of the series is to publish timely, comprehensive books developed from the ACS sponsored symposia based on current scientific research. Occasionally, books are developed from symposia sponsored by other organizations when the topic is of keen interest to the chemistry audience.

Before agreeing to publish a book, the proposed table of contents is reviewed for appropriate and comprehensive coverage and for interest to the audience. Some papers may be excluded to better focus the book; others may be added to provide comprehensiveness. When appropriate, overview or introductory chapters are added. Drafts of chapters are peer-reviewed prior to final acceptance or rejection, and manuscripts are prepared in camera-ready format.

As a rule, only original research papers and original review papers are included in the volumes. Verbatim reproductions of previous published papers are not accepted.

ACS Books Department

Preface

The ***Silicones and Silicone-Modified Materials*** symposium has been held six times at the ***American Chemical Society (ACS)*** National Meetings. The locations were: Dallas (1998); San Diego (2001); Anaheim (2004); San Francisco (2006); Washington, DC (2009); and San Diego (2012).

At ***ACS*** in San Diego in 2012 we had 34 talks and 16 posters in the ***Silicones and Silicone-Modified Materials*** symposium. Some of these contributions are represented herein, some will be in a forthcoming ***"SILICON"*** book and others were given in the ***ACS Polymer Preprints*** Volume 53(01), 2012.

Our previous book ***Advances in Silicone and Silicone-Modified Materials*** title came from Dr. Michael Owen, however the tile this time comes from me. It is to our good fortune that the ***American Chemical Society*** and ***Oxford University Press*** have kept our ***"SILICONE"*** books in press for us all to enjoy and utilize in our studies.

We would like to thank Mr. Bob Hauserman and Mr. Tim Marney of ***ACS*** books for commissioning this book and for moving it forward to production and publication.

We would also like to thank Professor Mark Dadmun ***POLY*** treasurer. We couldn't do these ***POLY*** symposia without the ever delightful Kathy, Neta and Leisa and we therefore thank them for every kind of help and encouragement.

I would like to thank Dr. H. N. Cheng for help, encouragement and poetry in the wee hours, when I was busy on ***"The Late Shift"***.

We hope that you find ***Progress in Silicone and Silicone-Modified Materials*** to be useful. We shall look forward to seeing you all again at ***Silicones and Silicon-Modified Materials VII*** which we are organizing for the ***251st ACS National Meeting & Exposition*** in San Diego (March 13-17, 2016).

SJC (Cincinnati on Saturday 24th August, 2013)

Stephen J. Clarson
Department of Biomedical, Chemical and Environmental Engineering (BCEE) and the Polymer Research Centre
The University of Cincinnati
Cincinnati, OH 45221-0012
USA
stephen.clarson@uc.edu (e-mail)

Dedication

To our Mothers and to our Fathers …
… with our deepest respect and gratitude.

Chapter 1

Amorphous Silica Preservation in an Anthropogenic Soil: An Explorative Study of "*Plaggen*" Soils

Wim Clymans,*,1,† Toon Verbeeck,1 Sander Tielens,1 Eric Struyf,2 Floor Vandevenne,2 and Gerard Govers1

1Department of Earth and Environmental Sciences, KU Leuven, Heverlee, B-3001, Belgium
2Department of Biology - Ecosystem Management Research Group, University Antwerp, Wilrijk, B-2610, Belgium
***E-mail: wim.clymans@geol.lu.se**
†Present affiliation: Department of Geology, Lund University, Lund, SE-22362, Sweden

Amorphous Silica (ASi) is present in considerable amounts in most soils and serves as a (micro-)nutrient for many plants. However, our understanding of the response of this important nutrient pool to human or natural disturbances is still very limited. One of the reasons for this is the long time scales involved. This explorative study focuses on the effect of a historical agricultural system, called *plaggen* management, that was applied on sandy areas in Belgium, the Netherlands and Germany over a period of ca. 1000 yrs on ASi dynamics. The system was designed to maintain high nutrient levels (including C and Si) on arable fields through the addition of mixtures rich in animal manure and vegetation residues. The continuous addition of ASi over such a long time period allows to study if and to what extent ASi is preserved in such a soil system and how Si addition affects the build-up and availability of ASi pools. We quantified ASi pools (Na_2CO_3 extraction) in a soil profile with *plaggen* application, and a reference soil without *plaggen* application. Other measured soil properties were soil organic carbon (SOC) and grain size distribution. There was an important SOC (+20%) and ASi accumulation (+70%) and

preservation at the plaggen site. Si losses from the soil column through leaching and crop harvest might thus be restricted by application of organic residue and Si fertilisation to maintain sustainable nutrient concentrations in the topsoil. Net C and Si accumulation rates were 45 kg C ha^{-1} y^{-1} and 77 kg SiO$_2$ ha^{-1} y^{-1} respectively, not accounting for the removal of ASi through plant uptake nor for the mineralisation of part of the SOC. The vertical distribution of ASi within the profile, suggests that, contrary to SOC, most of the added ASi has remained stably stored in the soils and that only a smaller, labile pool was removed, most likely through dissolution rather than through plant uptake. Our results indicate that ASi addition leads to a build-up of Si pools in these sandy soils. While this results in increased Si availability, this effect is limited because most ASi remains stored for long time spans. To consolidate our preliminary research results, to answer unresolved questions and to validate proposed hypotheses, future research should: (1) collect additional profiles with higher vertical resolution; (2) include other Si fractions; (3) analyse the relationship between ASi and SOC to better understand the coupling of the ASi and C cycles; (4) develop a modelling approach that would allow one to investigate how ASi pools in soils may respond to future changes.

Introduction

Large amounts of Si are stored in terrestrial soils in a more soluble amorphous form than mineral Si. The amorphous Si (ASi) consists mainly of biogenic silica (BSi), primarily in the form of plant siliceous bodies called phytoliths (*1*), but also as different pedogenic Si forms (*2*). The uptake of dissolved silica (DSi) in the vegetation and dissolution of ASi in soils has been shown to be an important controlling factor for the DSi export to rivers from catchments dominated by boreal wetlands (*3*), forests (*4*) and grasslands (*5*). This implies that riverine Si fluxes will be affected by biological and pedological processes (*6*). Quantitative mass-balance studies are necessary to improve our estimates of ASi storage and cycling within terrestrial ecosystems to accurately estimate its effect on Si delivery (*7*). The few studies performed (1) lack sufficient spatial distribution to integrate in global Si models (*8*), (2) focus on natural ecosystems, dominantly forests (e.g. (*4*, *9*, *10*)) and some grassland (e.g. (*5*)) or wetland studies (e.g. (*11*)) and (3) rarely account for the total ASi pool, including both biogenic and pedogenic Si forms (e.g. (*12*, *13*)).

Natural ecosystem studies contributed significantly to the contemporary knowledge of terrestrial Si cycling (*14*). One can however not neglect the effect of human perturbations on Si-mobilisation and Si-storage. Historically land management has altered Si- mobilisation (*10*, *15*, *16*), and Si-storage (*13*, *17*). Research interests have therefore shifted to disturbed landscapes (e.g. arable lands

and pastures), and processes specific to human land use types (*18*, *19*), like ASi depletion or conversion towards more stable Si forms (*20*), direct mobilisation of accumulated ASi through soil erosion (*21*) and the net loss due to harvest into the *so-called agricultural loop* (*22–24*). A robust estimate for temperate regions showed that agricultural expansion led to a 10% decrease in the soil ASi pool, and potentially a 20% increase in annual Si delivery towards aquatic systems (*13*). Acknowledging the uncertainty on this estimate, this finding corroborated the hypothesis that biotic processes rather than abiotic processes control Si dynamics on biological timescales (*7*).

In cultivated areas the harvest of Si accumulating crops (and grasses) leads to a depletion of the plant-available Si stock as large parts of plant Si are not returned (*13*, *23*). Only a part of the harvested crops will re-enter the cropland through direct re-application of biomass or organic fertilisation, i.e. manure (*24*). As a consequence of reduced Si availability, Si-concentrations in plants may be reduced making them more vulnerable for biotic and abiotic stresses (*25*), potentially reducing yields (*26*). In theory, anthropogenic Si addition could lead to a build-up of a bio-available Si pool, as shown for re- established natural vegetation (*23*). It is however unclear whether original levels can be re-established on relevant timescales, and whether the added Si is available to plants. Although positive effects on crop yields after Si fertilisation have previously been observed (*27*), studies looking at the effect of Si addition to agricultural systems on ASi pools received limited attention.

This study focuses on the effect on soil ASi stocks of a historically applied agricultural system, called *plaggen* management. In the sandy areas of Western Europe *plaggen* management was introduced (since 10th century) to improve soil fertility by adding a mixture of manure and organic top layer of neighbouring heathland that was used for grazing. It thus implicitly included Si fertilisation. Nowadays *plaggen* management has completely been replaced by mineral fertilisation, and arable lands as well as the former heathlands are partly converted to pasture or forest and vice versa. Here, we present a first exploration of the Si dynamics within anthropogenic soils that were formed during periods of *plaggen* management as they might offer an opportunity to investigate (1) how Si addition built up amorphous silica pools, (2) how present land-use practices could influence these increased amorphous silica pools, and more generally (3) add to our understanding of the controls ASi soil storage, specifically under human disturbed land. Therefore, we quantified the ASi distribution and pools in one anthropogenic soil, i.e. with *plaggen* application, and one reference soil, without *plaggen* application. The current land use on both study sites was arable land.

Background

The cultural landscape on sandy soils in Western Europe at 1000CE typically consisted of arable fields in the vicinity of the settlements (i.e. infields), and the extensively grazed heathlands at a distance (i.e. outfields) (Fig. 1). These heathlands developed from about 4000 years ago, as a result of forest clearances followed by use of the land for grazing cattle, cutting turf, burning and cutting

vegetation for fuel and fodder, activities which all prevented the regeneration of the forest (*28*). Low intrinsic soil fertility characterised the sandy soils. Persistent agricultural production on arable infields further degraded the nutrient balance of the sandy soils, and therefore their fertility. To sustain sufficient food supply for the growing population, a new agricultural management practice was introduced around 1000 BP: *plaggen* management.
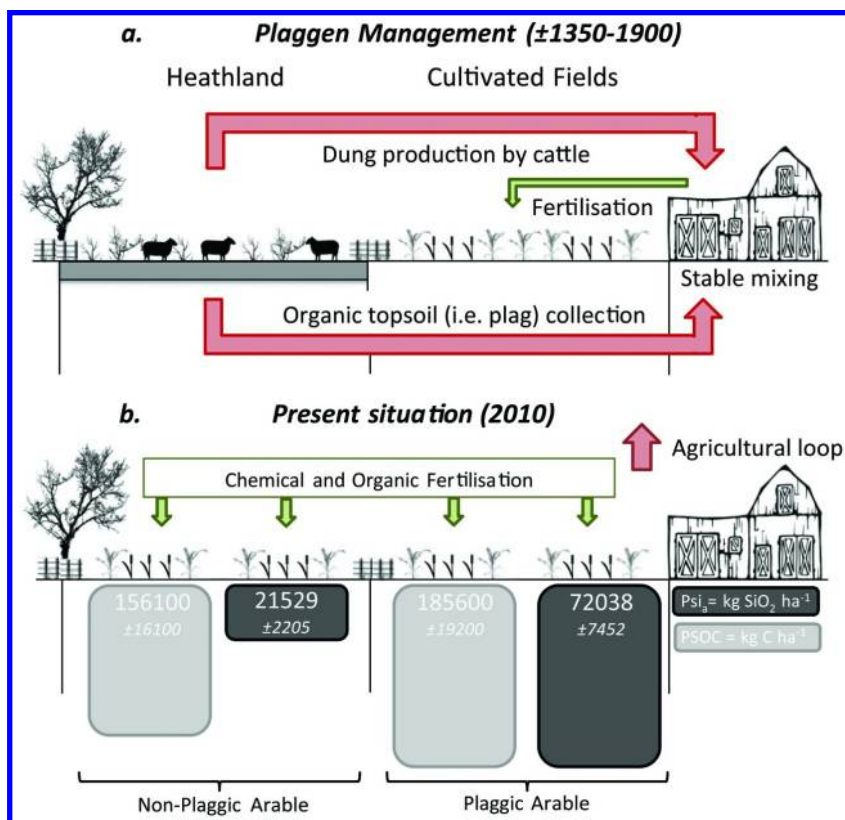
Figure 1. Representation of the land management system; a) during plaggen management (±1350-1900) and b) present situation (2010). Values indicate measured means (± standard errors) for total amorphous silica pools (PSi$_a$, kg SiO$_2$ ha^{-1}) in the soils.

Plaggen management for soil improvement was first introduced by Frisian farmers from about 1000 AD (*29*), and was common practice until the introduction of mineral fertilisers at the beginning of the 20th century (*30*). Since the Middle Ages, *plaggen* management replaced shifting cultivation in large parts of Germany, the Netherlands and NE Belgium (*31*, *32*). Except for herding sheep, the heathlands were used to dig up the fertile topsoil: such a topsoil slab was called a plag (plur: plaggen). Afterwards these *plaggen* were brought into the stables over winter where they became enriched with nutrients as they were mixed

with cattle dung (referred to as manure later on). The *plaggen* material consisted mostly of heather, although grass *plaggen*, forest litter or peat sods were also used. For centuries these *plaggen* were spread over croplands and pastures to improve the fertility of the sandy soil in western Europe, causing the development of a very specific soil at the infields: the Plaggic Anthrosol (*33*). This technique created a flow of nutrients from the heathlands to the arable land thereby making arable production sustainable.

A Plaggic Anthrosol has a typical, thick (>0.2m) A-horizon, anthropogenically sustained and enriched in organic carbon (>0.6% SOC). Other typical characteristics are its (loamy) sandy texture, dark grey to black colour and low base saturation (BS<50%). The application of *plaggen* stopped approximately 150-100 years ago with the introduction of mineral fertilisers but the A-horizons rich in organic carbon layers that were created over centuries still persist and these soils still store a large amount of SOC (*34*).

Materials and Methods

Study Area

In this study, a Plaggic Anthrosol profile under arable as present land use cover was compared with a reference soil profile, on which no *plaggen* addition occurred. The sample sites were located near the town Zolder (51°1'0.9"N; 5°19'5"E) in the Campine region NE Belgium. The average annual temperature in the area is 8.5-9°C and the annual precipitation is 750-800mm. The area has a flat, slightly undulating geomorphology with poor sandy Pleistocene sediments deposited during the Saalian Glaciation, and partly covered by fine-sorted cover sands during the Weichselian Glaciation. The *plaggen* management system was introduced in this region on a large scale from 1350-1500 onwards, and ended around 1900 (*35*). Historical maps confirmed that the sampled field sites, which have undergone *plaggen* management were arable parcels in 1750, while the non-plaggic profiles were typically located in heathlands. Therefore contemporary land use does not represent its historical development.

Soil Sampling and Analysis

The profiles were sampled with a guts auger down to a maximum depth of 1m, and cut every 0.05m in the field. Samples were dried at a temperature of 65°C for 48 hours, and gently homogenised with mortar and pestle. Carbon content (SOC) was measured with a vario MAX CN Macro Elemental Analyzer (Elementar Analysensysteme GmbH, Germany). The amorphous silica concentration was determined using a weak-base method originating from DeMaster (1981) (*36*). The alkaline (Na_2CO_3) extraction procedure digests various Si fractions (i.e. biogenic and pedogenic silica, absorbed silica, poorly crystalline forms) (*2*). Given their origin and the acidic conditions in our soils, poorly crystalline mineral forms such as allophane and imogolite are not important in this study. The alkali-extractable Si pool can therefore be considered as equivalent to the amorphous Si pool. We therefore refer to the extracted Si pool as the amorphous

Si pool (PSi$_a$) and to the equivalent Si concentration as the amorphous Si concentration, (CSi$_a$). The reliability of the method has been demonstrated for forested soils (*37*), arable soils (*38*) and wetland soils (*3*).

Total ASi (PSi$_{a,i}$, kg SiO$_2$ ha^{-1}) and SOC (PSOC, kg C ha^{-1}) pools were calculated based on the dry bulk density (ρ_d) and depth (d) of each segment (kg m^{-3}). We used the average bulk density (ρ_d) of the plaggic profile for the other site. This is a simplification of the reality as ρ_d varies between horizons and profiles. To incorporate the effect of spatial heterogeneity, pools were estimated using a conservative error range of ±10% (i.e. average standard deviation on bulk density). Total pools were calculated by integration of the pool over depth of the core. The maximum common depth that was reached in field sampling was 0.9m.

Results

ASi Concentrations

The average CSi$_a$ in the total soil column for the plaggic profile is 2.58±0.37 g Si kg^{-1} (see Table 1). The non-plaggic average is significantly lower: 0.78±0.68 g Si kg^{-1}.

Fig. 2 shows the actual profiles. There is a clear accumulation of CSi$_a$ in the topsoil (upper 0.3m) of the non-plaggic profile with average concentration of 1.49±0.20 g Si kg^{-1}. Below the topsoil concentrations are low (ca. 0.41 g Si kg^{-1}) with a small peak at 0.9 m. In contrast, the plaggic arable profile has a high CSi$_a$ down to a depth of 0.9 m: below this depth, the concentration drops rapidly.

SOC Concentrations

On average all SOC concentrations range between 1.20±0.89% (non-plaggic) and 1.42±0.38% (plaggic) (Table 1) and do not differ significantly. However, distribution profiles show clear SOC accumulation in the top 0.3m of the non-plaggic soil profile with average SOC concentrations of 2.30±0.21% (Fig. 2). Below the topsoil, SOC- values decrease rapidly at the non-plaggic arable site and they are low further down in the profile (generally < 0.5%). The plaggic arable profile has a slightly lower SOC content in the topsoil than the non-plaggic profile, but SOC contents in the subsoil gradually decline between 0.3 m and 0.4 m depth and remain significantly higher (ca. 1.20%) than those measured in the non-plaggic profile. SOC content drops sharply at 0.9 m, a depth which is located just below the bottom of the plaggic horizon.

The plaggic anthrosol at the arable site stores the largest amorphous silica pool (PSi$_a$): 72038±7452 kg SiO$_2$ ha^{-1} (Fig. 1). A significant difference exists with the non-plaggic arable that stores 21529±2205 kg SiO$_2$ ha^{-1}. Analogous to PSi$_a$, the plaggic arable profile stores the largest amount of organic carbon (PSOC): 185600±19200 kg C ha^{-1}. The non-plaggic arable stores 156100±16100 kg C ha^{-1}. The error term represents a 10% error to account for spatial heterogeneity of the measured bulk density (ρ_d = 1450±150 kg m^{-3}) as only data for the plaggic profile are available.

Table 1. Average amorphous silica concentration (CSi$_a$, g Si kg^{-1}) and soil organic carbon content (SOC, %) for plaggic arable (PA) profiles (±standard deviation) with median difference values of CSi$_a$ and SOC for the different profiles.

	PA	*nPA*	*Median Difference*[a]
CSi$_a$ (g Si kg^{-1})			
Total	2.58±0.37	0.78±0.68	1.83 (<.0001)
<0.3m	2.68±0.41	1.49±0.20	1.27 (0.0016)
0.3-0.6m	2.53±0.28	0.40±0.69	2.24 (0.0011)
0.6-0.9m	2.52±0.45	0.42±0.34	2.18 (0.0008)
SOC (%)			
Total	1.42±0.38	1.20±0.89	0.38 (0.1173)
<0.3m	1.85±0.11	2.30±0.21	-0.47 (0.0132)
0.3-0.6m	1.23±0.39	0.54±0.58	0.70 (0.0082)
0.6-0.9m	1.19±0.06	0.75±0.30	0.47 (0.0066)

[a] p-values of t-test are given in between brackets.

Discussion and Outlook

Arable land management always includes biomass removal, reducing organic inputs to the soil system. Inevitably this leads to a depletion of the bio-available nutrient pools. The application of *plaggen* was a low-input management strategy used to compensate for these losses. When plaggen management is applied, this results in a net nutrient and C flux from adjacent heathlands towards cultivated fields (pasture and arable) through the translocation of the organic rich top-layer, mixed with manure collected in stables. As a result of this redistribution of nutrients, relatively high food production levels could be maintained for several centuries on the agricultural fields, despite the infertile nature of the soils. Nutrient pools (PSOC and PSi$_a$) under heathland and cultivated fields have hence undergone depletion and accumulation respectively. Our comparison between soils with and without plaggen management within the Campine region suggests that this difference is persistent and that, at the present day ASi preservation is even more important than SOC preservation (+70% vs. +20%) (Figure 1).
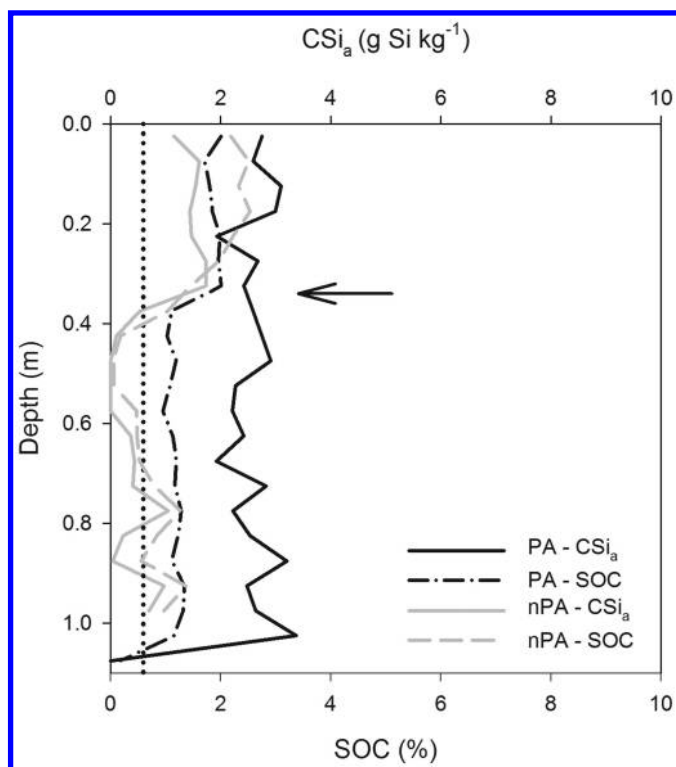
Figure 2. Amorphous silica content (solid - CSi$_a$, g Si kg^{-1}) and soil organic carbon content (dashed - SOC, %) for the plaggic arable profile (PA), non-plaggic arable profile (nPA). The dotted line indicates the reference for a plaggic horizon (> 0.6%). The arrow indicates the biological active layer (0.3m).

In the plaggic cropland soils, both SOC at depth (Median Diff: ±0.55%) and ASi concentrations (Median Diff: ±1.83 g Si kg^{-1}) are higher than in the reference profile. This confirms the biogenic origin of the higher ASi pool in *plaggen* soils. The combined effect of Si fertilisation at plaggic cultivated fields, and the depletion at the reference heathlands, at present used as arable land (non-plaggic), led to a discrepancy of 29500 kg C ha^{-1} for SOC - and 50500 kg SiO$_2$ ha^{-1} for ASi - between the plaggic and non-plaggic site. In creating this difference, the relative accumulation on the plaggic soils was much more important than the relative depletion of the non-plaggic profile, located in former heathland. Indeed, the heathland was relatively abundant as compared to the arable land in the plaggen system, with ratio's varying between ca. 20 to 1 and 6 to 1 (*39*). There were therefore relatively long time intervals between consecutive *plaggen* removals at a given heathland site, so that the vegetation and the soil organic carbon and ASi stocks could at least partly be re-established.

To determine net C and Si accumulation rates, knowledge of the plaggic horizon's age is necessary. We estimated the age of our plaggic arable profile based on the average plaggen accumulation rate of 1 mm y^{-1}, reported by Driessen and coworker (*39*), and assumed that the bottom 0.3m of the profile enriched in SOC and ASi is a mixture of the original soil's A-horizon (before plaggen management) and plaggen-manure through ploughing. These assumptions result in an age of ca. 650 years for the plaggic soil, which would place the initiation of *plaggen* management at this site at ca. 1250 CE, which corresponds reasonably well with historic information on the development of the technique. These estimates result in net C and Si accumulation rates of 45 kg C ha^{-1} y^{-1} and 77 kg SiO_2 ha^{-1} y^{-1} respectively. These net figures do not account for removal of ASi through plant uptake nor for the mineralisation of part of the SOC. Thus, actual inputs were of SOC and Si were certainly higher. This implies that, although we see a consistently high ASi in the plaggic soils, a substantial part of the added ASi was harvested, and imported into the agricultural harvest loop.

Constructing a complete C and/or Si budget is impossible with the current limited dataset. Some data on SOC losses are available: for the Belgian Campine post-plaggen- management losses were modelled (using RothC-26.3 model) to equal 228 kg C ha^{-1} y^{-1} or a total of 11400 kg C ha^{-1} ($\pm 6\%$ of the present pool) in the past 60 years (*34*). Clearly, overall losses of imported SOC over the total period of plaggen application were much more important. ASi losses were less important: this is not only reflected in the larger increase of the ASi inventory in comparison to the SOC inventory but is also suggested by the fact that ASi concentrations remain nearly constant throughout the entire depth of the plaggic horizon. This is corroborated by (1) a different relation between ASi and SOC at the plaggic and non-plaggic site, and (2) an increasing ASi/SOC ratio with increasing depth for the plaggic site (Fig. 3). Higher ASi/SOC ratio´s suggest that a significant amount of the SOC that was originally added to the plaggen soil has, in the meantime, been decomposed while most of the ASi that was imported is still present in the profile. The decomposition of SOC is to be expected: SOC turnover times in the plough layer of arable land are known to vary between 15 and ca. 200 year (*40*). This implies that, when surplus SOC is added to a soil profile a significant fraction of this SOC may be expected to be lost over the time scale considered here (ca. 1000 yr). Very little information is available concerning ASi stability in soil profiles: Clymans and coworkers (*13*) showed that forest clearing and conversion to agricultural land led to a significant reduction of the ASi pool in glacial till soils in Sweden over a centennial time scale. The first data from *plaggen* soils suggest that the ASi pool in these soils is more stable as ASi concentrations are nearly constant throughout the plaggen horizon, suggesting a relative stability of the ASi pool over a similar timescale. Long-term preservation was previously encountered in tropical forest soils (*1*). They applied - in analogy to C - a bi-compartmental model with a labile and stable pool to explain ASi distribution i.e. evolution towards stable ASi levels with increasing depth. In plaggen soils a decoupling between ASi and SOC refutes such straightforward analogy and other factors could explain the stability of ASi over the total length of the profile. Clearly, additional data are necessary to substantiate the trends observed here, but it is not unlikely that such differences in response do exist. Solubility of ASi may depend

on the type of ASi present as well as on the soil type and climatic regime. Presently available data do not allow us to quantify the effects of such factors: our study simply shows the necessity of a better understanding of ASi dynamics in different soils, under different land uses and different climatic regimes.
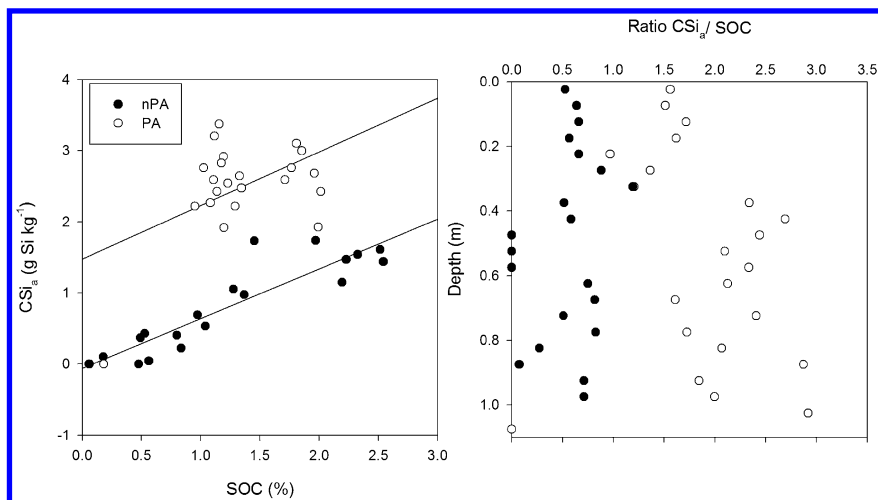

Figure 3. Relation between soil organic carbon content (SOC, %) and amorphous silica concentration (CSi$_a$,g Si kg^{-1}) (left) and, ratio between amorphous silica concentration and soil organic carbon content (right) for non-plaggic arable profile (nPA – solid) and plaggic arable profile (PA – open).

It has been suggested that reforestation and biogenic Si fertilisation (e.g. the application of crop residues) can lead to the accumulation of bio-available Si in soils (*16*, *22*, *23*). Here, we explored for the first time the potential effect of long-term Si addition on Si storage. The limited data suggest that the *plaggen* technique indeed led to ASi accumulation in arable soils, thereby confirming that human disturbance can strongly affect ASi storage within a landscape. Although based on limited data and several assumptions, our preliminary results imply that at present, most of the added ASi has remained stably stored in the soils over a centennial timescale, while mineralisation possibly led to a decrease in SOC pools. This study should be seen as a first analysis of the Si dynamics in Anthrosols and awaits validation. To consolidate our research results as well as to answer unresolved questions, e.g. the stability of ASi pools in *plaggen* soils, future research should (1) collect information on additional soil profiles, using a higher vertical resolution (2) consider different ASi pools having a different origin and solubility and (3) collect datings of *plaggen* profiles so that a more precise time frame can be set.

Acknowledgments

References

1. Alexandre, A.; Meunier, J.; Colin, F.; Koud, J. *Geochim. Cosmochim. Acta* **1997**, *61*, 677.
2. Sauer, D.; Saccone, L.; Conley, D.; Herrmann, L.; Sommer, M. *Biogeochemistry* **2006**, *80*, 89.
3. Struyf, E.; Mörth, M.; Humborg, C.; Conley, D. *J. Geophys. Res.* **2010**, *115*, G04008.
4. Gérard, F.; Mayer, K.; Hodson, M.; Ranger, J. *Geochim. Cosmochim. Acta* **2008**, *72*, 741.
5. Blecker, S. W.; McCulley, R. L.; Chadwick, O. A.; Kelly, E. F. *Global Biogeochem. Cycles* **2006**, *20*, GB3023.
6. Ronchi, B.; Clymans, W.; Barão, A.; Vandevenne, F.; Struyf, E.; Batelaan, O.; Dassargues, A.; Govers, G. *Silicon* **2013**, *5*, 115.
7. Struyf, E.; Conley, D. *Biogeochemistry* **2011**, *1*.
8. Laruelle, G. G.; Roubeix, V.; Sferratore, A.; Brodherr, B.; Ciuffa, D.; Conley, D. J.; Dürr, H. H.; Garnier, J.; Lancelot, C.; Le Thi Phuong, Q.; Meunier, J. D.; Meybeck, M.; Michalopoulos, P.; Moriceau, B.; Ní Longphuirt, S.; Loucaides, S.; Papush, L.; Presti, M.; Ragueneau, O.; Regnier, P.; Saccone, L.; Slomp, C. P.; Spiteri, C.; Van Cappellen, P. *Global Biogeochem. Cycles* **2009**, *23*, GB4031/1.
9. Bartoli, F. *Ecol. Bull.* **1983**, *35*, 469.
10. Conley, D. *Global Biogeochem. Cycles* **2002**, *16*, 1121.
11. Struyf, E.; Conley, D. *Front. Ecol. Environ.* **2009**, *7*, 88.
12. Cornelis, J.-T.; Titeux, H.; Ranger, J.; Delvaux, B. *Plant Soil* **2011**, *342*, 369.
13. Clymans, W.; Struyf, E.; Govers, G.; Vandevenne, F.; Conley, D. J. *Biogeosciences* **2011**, *8*, 2281.
14. Struyf, E.; Smis, A.; Van Damme, S.; Meire, P.; Conley, D. *Silicon* **2009**, *1*, 207.
15. Colman, S. M.; Bratton, J. F. *Geology* **2003**, *31*, 71.
16. Struyf, E.; Smis, A.; Van Damme, S.; Garnier, J.; Govers, G.; Van Wesemael, B.; Conley, D. J.; Batelaan, O.; Frot, E.; Clymans, W.; Vandevenne, F.; Lancelot, C.; Goos, P.; Meire, P. *Nat. Commun.* **2010**, *1*, 129.
17. Saccone, L.; Conley, D.; Likens, G.; Bailey, S.; Buso, D.; Johnson, C. *Soil Sci. Soc. Am. J.* **2008**, *72*, 1637.
18. Kelly, E. F. *Biogeochemistry* **1998**, *42*, 21.
19. Conley, D.; Likens, G.; Buso, D.; Saccone, L.; Bailey, S.; Johnson, C. *Global Change Biol.* **2008**, *14*, 2548.
20. Cornelis, J. T.; Delvaux, B.; Georg, R. B.; Lucas, Y.; Ranger, J.; Opfergelt, S. *Biogeosciences* **2011**, *8*, 89.

21. Smis, A.; Van Damme, S.; Struyf, E.; Clymans, W.; van Wesemael, B.; Frot, E.; Vandevenne, F.; Van Hoestenberghe; Govers, G.; Meire, P. *Biogeochemistry* **2010**.

22. Meunier, J. D.; Guntzer, F.; Kirman, S.; Keller, C. *Mineral Mag.* **2008**, *72*, 263.

23. Guntzer, F.; Keller, C.; Poulton, P.; McGrath, S.; Meunier, J.-D *PLant Soil* **2012**, *352*, 173.

24. Vandevenne, F.; Struyf, E.; Clymans, W.; Meire, P. *Front. Ecol. Environ.* **2011**.

25. Guntzer, F.; Keller, C.; Meunier, J.-D. *Agron. Sustainable Dev.* **2012**, *32*, 201.

26. Ma, J. F.; Miyake, Y.; Takahashi, E.; Datnoff, L.; Snyder, G.; Korndorfer, G. *Studies in Plant Science*; Elsevier: 2001; Vol. 8, p 17.

27. Korndörfer, G.; Lepsch I. In *Silicon in agriculture. Studies in plant species*; Datnoff, L., Snyder, G., Korndörfer, G., Eds.; Elsevier: Amsterdam, 2001; Vol. 8, p 133.

28. Webb, N. *Heathlands: a natural history of Britain's lowland heaths*; Collins: London, 1986.

29. Blume, H.-P.; Leinweber, P. *J. Plant Nutrit. Soil Sci.* **2004**, *167*, 319.

30. Simpson, I. A.; Dockrill, S. J.; Bull, I. D.; Evershed, R. P. *J. Archaeol. Sci.* **1998**, *25*, 729.

31. Pape, J. C. *Geoderma* **1970**, *4*, 229.

32. Spek, T. The age of plaggen soils. An evaluation of dating methods for plaggen soils in the Netherlands and Northern Germany. In *Proceedings of the Standing European conference for the transformation of the European rural landscape*, Brussels; Verhoeve A., Vervloet J., Eds.; 1992; p 72.

33. ISSS-ISRIC-FAO, Vol 84. *World Soil Resources Reports*; Food and Agriculture Organisation of the United Nations: Rome.

34. van Wesemael, B.; Paustian, K.; Meersmans, J.; Goidts, E.; Barancikova, G.; Easter, M. *Proc. Natl. Acad. Sci.* **2010**, *107*, 14926.

35. Schulp, C. J. E.; Verburg, P. H. *Agric., Ecosyst. Environ.* **2009**, *133*, 86.

36. DeMaster, D. *Geophys. Monogr. Ser.* **1991**, *63*, 363.

37. Saccone, L.; Conley, D.; Koning, E.; Sauer, D.; Sommer, M.; Kaczorek, D.; Blecker, S.; Kelly, E. *Eur. J. Soil Sci.* **2007**, *58*, 1446.

38. Clymans, W.; Govers, G.; Van Wesemael, B.; Meire, P.; Struyf, E. *Geoderma* **2011**, *167-68*, 228.

39. Driessen P.; Deckers J.; Spaargaren, O.; Nachtergaele, J. *Lecture notes on the major soils of the world*; World Soil Resources Report; Food and Agriculture Organisation of the United Nations: Rome, 2001.

40. Six, J.; Jastrow, J. D. In *Encyclopedia of soil science*; Marcel Dekker Inc.: New York, 2002; p 936.

Chapter 2

Sol-Gel Materials for WSUD Water Treatment Applications

Stephen R. Clarke,[*] Elda Markovic, and Kim-Anh Thi Nguyen

Mawson Institute, University of South Australia, Mawson Lakes, South Australia, 5095, Australia
[*]E-mail: stephen.clarke@unisa.edu.au

Introduction

Deltares (formerly Delft Hydraulic – Netherlands) joined forces with the National University of Singapore (NUS) to form the Singapore-Delft-Water-Alliance (SDWA) which has its operations based at NUS, in Singapore. SDWA subsequently linked with Dr Clarke's research laboratories and United Water researchers to receive an Australian Government funded ARC Linkage grant to use organosilicon and silicone modified materials for the treatment and purification of run-off storm water. This international project linked Australian, Singaporean, Dutch and French researchers, wishing to improve quality of life through the development of new water treatment technologies.

Singapore and Australia, like most nations around the globe have considerable issues with unsightly concrete drains, as shown in Figure 1. These concrete drains are used to re-direct vast quantities of excess storm water and run-off water into our lakes, seas and oceans.
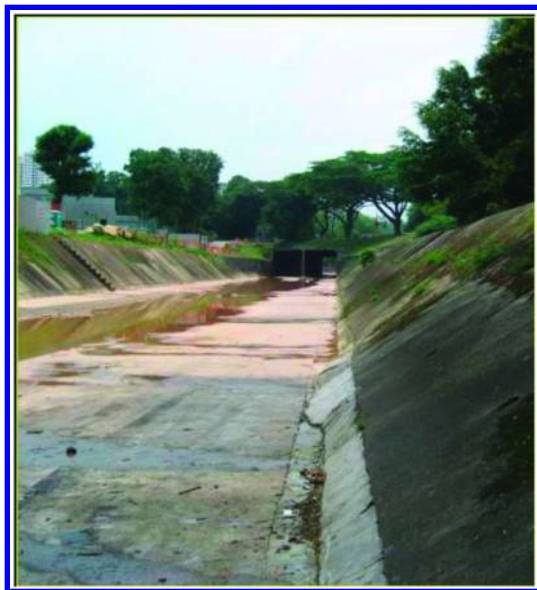
Figure 1. Concrete storm water drains used extensively in Australia, in Singapore and around the world

In times of growing water scarcity, generally attributed to climate change, it seems amazing that in many countries, including Singapore and Australia, which have major issues with water supply, that this waste storm and run-off water is rarely collected and treated for subsequent re-use.

The purpose of the research in this project was to develop organosilicon and silicon modified materials, for the treatment and purification of run-off and storm water, allowing unsightly concrete drains shown in Figure 1 to be transformed into people friendly waterways as shown in Figure 2.

The silicon polymers developed in this research allow treated waste water to be cleaned, by removing harmful dissolved inorganic and organic toxins. The organosilicon and silicone modified materials synthesised by Dr Clarke's research team (formerly at Flinders University) but now at the University of South Australia in Australia were applied to water treatment technologies developed by SDWA in Singapore, and United Water in Australia.

Figure 2. An impression of what stark concrete stormwater drains should look like using sol-gel water treatment materials.

Sol-Gel Chemistry

It was proposed for this project, from the outset, to employ organosilicon sol-gel chemistry to functionalize silica filtration media that was being used by SDWA and United Water. It was believed these materials could enhance the removal of soluble inorganic and organic toxins.Clarke's laboratories believed the science of choice to best achieve this outcome was sol-gel chemistry (*1*, *2*). The sol-gel process involves the hydrolysis and condensation reactions of the starting alkoxides as shown in Figure 3.
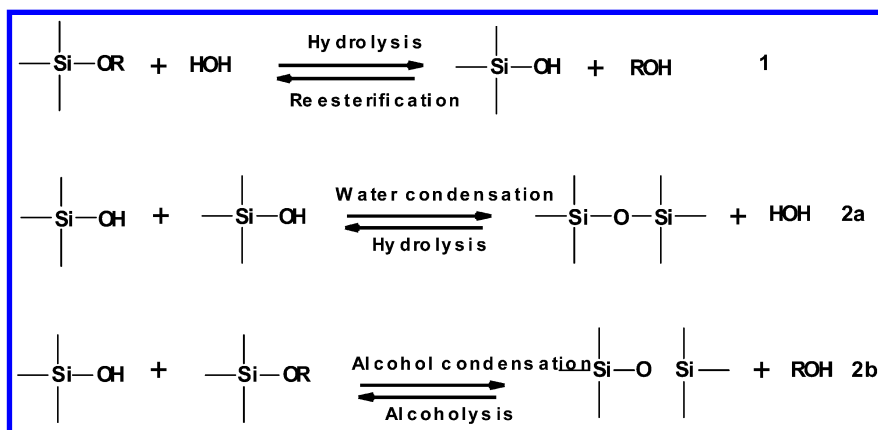

Figure 3. The general hydrolysis and condensation chemical reactions involved in the sol-gel process.

However, a number of factors affect the rate of hydrolysis and condensation deemed responsible for the properties of a particular sol-gel inorganic network such as, pH, temperature and time of reaction, reagent concentrations, nature and concentration of catalyst, H_2O/Si molar ratio (R), aging temperature and time, and drying (*3, 4*).

The sol-gel technique is a two step process that involves the formation of inorganic networks through the evolution of a colloidal suspension (sol) and gelation of the sol to form a network in a continuous liquid phase (gel) (*5*). Metal alkoxides are mostly used because they react readily with water. The most widely used metal alkoxides are the alkoxysilanes, such as tetramethoxysilane (TMOS) and tetraethoxysilane (TEOS). Other alkoxides such as aluminates, titanates, and borates are also employed in the sol-gel process, very often in mixtures with TEOS.

Using this process, it is possible to produce ceramic or glass materials in various forms; ultra-fine or spherical shaped powders, thin film coatings, ceramic fibbers, microporous inorganic membranes, monolithic ceramics and glasses, or extremely porous aerogel materials.

In general, silanol formation occurs by an hydrolysis reaction, where a water molecule replaces the alkoxide group (OR) with hydroxyl groups (OH). This is followed by subsequent condensation reactions involving either the conversion of silanol groups (Si-OH) to siloxane bonds (Si-O-Si) with water being the leaving molecule, or the reaction of a silanol with an alkoxy group and alcohol being the leaving molecule. This results in the formation of water and alcohol as by-products of the sol-gel process. In most cases, condensation starts before hydrolysis reaction is completed. However, variations in conditions such as, pH, H_2O/Si molar ratio (R), and catalyst can drive completion of hydrolysis before condensation begins (*6*).

Hydrolysis can occur without addition of an external catalyst, but it is most rapid and complete with the addition of catalyst. Mineral acids (HCl) and alkalis, such as ammonia, are most commonly used, however, other catalysts are acetic acid, KOH, amines, KF, and HF (*1*). In addition, it has been observed that the rate and extent of the hydrolysis reaction is most influenced by the strength and concentration of the acid or base catalyst. All strong acids behave similarly, whereas weaker acids require longer reaction times to achieve the same extent of reaction. Compared to acidic conditions, base hydrolysis kinetics is more strongly affected by the nature of the solvent (*7*).

Acid Catalysed Hydrolysis Mechanism

When acid is used as catalyst, protonation of an alkoxide group is a rapid first step (Figure 4). Electron density is withdrawn from the silicon atom, making it electrophilic and thus susceptible to water attack. This results in the formation of a penta-coordinate transition state with significant S_N2-type character.
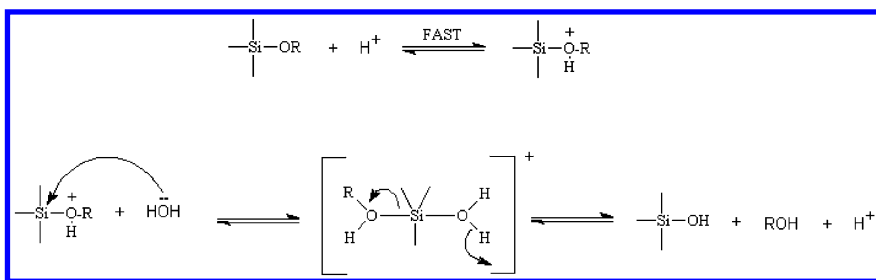
Figure 4. Acid catalysed hydrolysis mechanism

Base Catalysed Hydrolysis Mechanism

Under basic conditions, the hydrolysis reaction is first-order in base concentration (Figure 5). However, if the silane concentration is increased, the reaction changes from a first-order to a more complex second-order reaction, related to silanolate cluster formation. If weaker bases (ammonium hydroxide and pyridine) are employed, higher speeds of reaction are possible only if large concentrations are used. Compared to acidic conditions, base hydrolysis kinetics is more strongly affected by the nature of the solvent (*7*).
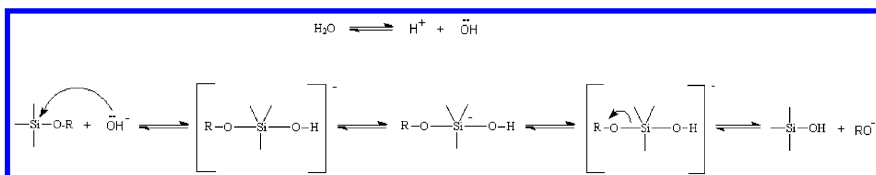

Figure 5. Base catalysed hydrolysis mechanism

Therefore, base-catalysed hydrolysis of silicon alkoxides proceeds much more slowly than acid-catalysed hydrolysis at an equivalent catalyst concentration (*7*). Under basic conditions, it is likely that water dissociates to produce hydroxyl anions in a rapid first step. The hydroxyl anion then attacks the silicon atom. Again, an S_N2-type mechanism has been proposed in which the -OH displaces -OR with inversion of the silicon tetrahedron. When the first hydrolysis reaction has occurred, the next alkoxide group is more easily removed from the monomer then the previous one and reaction proceeds stepwise (*8*).

The hydrolysis reaction has been performed with R (H_2O/Si molar ratio) ranging from 1 to over 50, depending on the desired polysilicate product, with an increase in R expected to promote the hydrolysis reaction, prior to condensation. It was found that the acid-catalysed hydrolysis of TEOS is first-order in water concentration (*7*). However, it has also been observed that under basic conditions the rate has a zero-order dependence on the water concentration. Generally, with under stoichiometric additions of water (R << 2), the alcohol producing-condensation mechanism is favoured, whereas, the water- forming condensation reaction is favoured when R = 2 (*9*). Maintaining a constant solvent:

silicate ratio, the silicate concentration is reduced, which in turn reduces the hydrolysis and condensation rates, resulting in longer gel times (*10*).

Sol-Gel Condensation Mechanism

Condensation reactions are acid and base specific, where gel times increase under more basic conditions (*11*). Catalysts dictate a specific pH which can drive the type of silica particle. Generally it is believed that the acid-catalysed condensation mechanism involves a protonated silanol species. Protonation of the silanol makes the silicon more electrophilic and thus susceptible to nucleophilic attack.The most basic silanol species (silanols contained in monomers or weakly branched oligomers) are the most likely to be protonated. Therefore, condensation reactions may occur preferentially between neutral species and protonated silanols situated on monomers, end groups of chains, etc. (*1*). Polymerisation to form siloxane bonds occurs by either an alcohol- producing or a water-producing condensation reaction. It has been shown by Engelhardt et al. (*12*) that a typical sequence of condensation products is monomer, dimer, linear trimer, cyclic trimer, cyclic tetramer, and higher order rings.This sequence of condensation requires both depolymerisation (ring opening) and the availability of monomers which are in solution equilibrium with the oligomeric species and/or are generated by depolymerisation (*1*).

The rate of ring opening polymerisations and monomer addition is dependent upon the environmental pH. For example below pH 2, the condensation rates are proportional to the proton concentration [H+]. Because the solubility of silica is quite low below pH 2, formation and aggregation of primary silica particles occur jointly, with ripening (growth of the network) contributing little to growth beyond a particle size of 2nm in diameter, thus developing exceedingly small primary particles (*1*).

Between pH=2 and pH=6 condensation rates are proportional to [-OH] concentration. Condensation preferentially occurs between more highly condensed species and those less highly condensed and somewhat neutral. Therefore the rate of dimerisation is low, however, once dimers form, they react preferentially with monomers to form trimers, which in turn react with monomers to form tetrameters. Cyclisation occurs because of the proximity of the chain ends and the substantial depletion of the monomer. Further growth occurs by addition of lower molecular weight species to more highly condensed species and aggregation of the condensed species to form chains and networks. The solubility of silica in this pH range is again low and particle growth stops when the particles reach 2-4 nm in diameter (*6*). In this pH range, condensed species are ionised and therefore, mutually repulsive. Growth occurs primarily through the addition of monomers to the more highly condensed particles rather than by particle aggregation.

Above pH=7, polymerisation occurs similarly, but due to the greater solubility of silica and the greater size dependence, particles grow in size and decrease in number as highly soluble small particles dissolve and re-precipitate on larger, less soluble particles. Growth stops when the difference in solubility between the smallest and largest particles becomes indistinguishable. This process is referred

to as Ostwald ripening. Particle size, is therefore, mainly temperature dependent, in that higher temperatures produce larger particles. Additionally, in this pH range, the growth rate depends upon the particle size distribution (*1*).

As with hydrolysis, condensation can proceed without catalyst, however, the use of acids or bases promote the rates of reaction, and are acid and base specific. In addition, it has been shown that under more basic conditions, gel times are observed to increase (*11*).

Acid-catalysed condensation involves protonation of the silanol, that makes the silicon more electrophilic and thus susceptible to nucleophilic attack. The most basic silanol species (silanols contained in monomers or weakly branched oligomers) are the most likely to be protonated. Therefore, condensation reactions may occur preferentially between neutral species and protonated silanols situated on monomers, end groups of chains, etc. (*1*).

The most widely accepted mechanism for the base-catalysed condensation reaction involves the attack of a nucleophilic deprotonated silanol on a neutral silicic acid (Figure 6) (*11*).
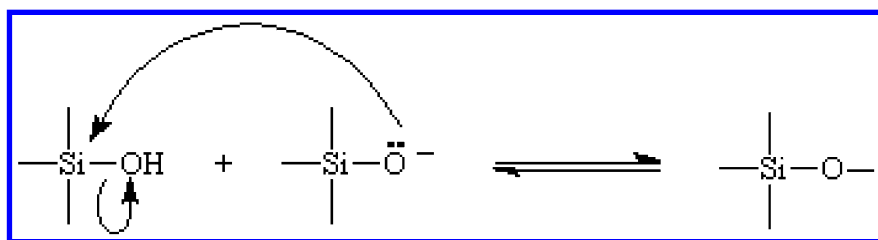

Figure 6. Base-catalysed condensation

Furthermore, it is believed that the base-catalysed condensation mechanism involves penta- or hexa-coordinated silicon intermediates or transition states, similar to that of a S_N2 type mechanism (*1*).

Sol-Gel Process, Materials and Applications

The sol-gel process is a convenient and inexpensive technique to prepare organic-inorganic hybrid coatings, having both glassy and polymeric properties by including alkyl alkoxides with one or more non-hydrolysable groups in precursor alkoxide solutions (*13, 14*). Interest in novel methods for the application of sol-gel method in coatings has increased significantly over last two decades (*15–17*).

The most utilised techniques for preparing sol-gel films has been spin-coating, dip-coating, spraying and electro-deposition (*18–20*). All these techniques use solutions containing silicon alkoxides, pre-hydrolysed monomers, or colloidal metal hydroxides as precursors that undergo further condensation to form a glassy substance at ambient temperature after a drying process. However, in many cases the created films are uneven with defects. Many of these defects can be minimised by modifying the surface of the films using silicates with various organic groups The sol-gel technique provides high-optical-quality silica matrices, functionalised

with organic molecules. This method has the potential to tailor the properties of bulk and thin film materials. The mechanism and hydrolysis of the most common precursors studied and used in the sol-gel coatings, are tetraethylorthosilicate (TEOS) and tetramethylorthosilicate (TMOS) (*21, 22*). To modify the properties of the sol-gel coatings, such as porosity, connectivity, and hydrophobicity, organically-modified silane compounds, $R_x'Si(OR)_y$ have been employed.

Sol-gel derived silica films have been extensively used for anti-glare and anti- reflectance in many optical applications including cathode ray tubes, colour monitor tubes, video display panels, solar energy, and many other applications. Until now, work has been largely devoted to improving the abrasion resistance and mechanical strength of the sol-gel derived coatings (*23, 24*). Sol-gel coating processes generally occur near ambient conditions, so it is possible to incorporate organic components into sol-gel ceramics by three different routes (*25*):

1. Surfactants as a supramolecular templates can be introduced (*26, 27*). These templates are able to self-assemble into molecular aggregates that physically assemble with silicates through Si-OH or Si-O-Si groups (*28–31*).
2. The second method is to replace one or more alkoxysilane groups of the precursor silanes with nonhydrolysable organic groups (for example by using methyltrimethoxysilane) (*32–35*).
3. The third method employs bridged silanes, as a precursor that has two trialkoxysilyl moieties joined by an organic segment (for example 1,2 bis(trimethoxysilyl) ethane) (*36, 37*).

All these methods are effective for controlling some aspect of the structure and properties of a sol-gel material. Thus, surfactant incorporation provides organic groups with long-range order. Since the interactions with material are only physical, the surfactant can be easily extracted to generate mesoporous material. Nonbridging organotrialkoxysilanes are covalently incorporated into the sol-gel network and can be used to introduce a variety of organic functionalities. But, siloxane cyclisatoin usually occurs and may limit the extent of network formation. Bridged siloxanes can overcome these limitations as they gel much more easily than trialkoxysilanes. In addition, they introduce organic components directly into the sol-gel network without blocking the accessibility of the pores that are obtained after drying (*36, 37*). Lately, there have been a number of demonstrations of combining these methods of organic modifications to create advanced materials with a combination of useful properties.

Experimental

Preliminary research was undertaken using ^{1}H-NMR to better understand acid catalysed hydrolysis of TEOS and FTIR studies were used to better understand the sol-gel condensation reaction.

¹H-NMR Studies of Acid Catalysed TEOS Hydrolysis

¹H-NMR was carried out to determine the rate of hydrolysis of TEOS using deuterated acetonitrile (d₃ - CAS No: 2206-26-0) as a solvent. 10.5ml acetonitrile, 0.2g TEOS were mixed in a glass vial, a small amount of the mixture was placed in an NMR tube and a scan taken, The mixture was then replaced in the glass vial and 2ml 0.01M HCl added and mixed. A small amount of this mixture was then used to perform more NMR; scans which were taken every 5 minutes. Peak heights versus time were plotted for the TEOS CH_2 (3.66ppm) and CH_3 (1.06ppm) hydrogens, and the ethanol CH_2 (3.28ppm) and CH_3 (0.86ppm) hydrogens. The NMR spectra were recorded on a Varian Gemini (300MHz@ 300 MHz for protons), liquid nitrogen cooled NMR spectrometer. These spectrometers use VNMR 6.1 analysis software with a Sun Workstation based on a Unix system. The residual CH_3CN peak was used as an internal reference at 1.96 ppm. 16 transients were collected for each analysis and this was used as an internal reference from which to normalize other peak areas.

FTIR Studies of Base Catalysed TMOS Hydrolysis

10ml of partially hydrolysed TMOS oligomer ($CH_3O\{Si(OCH_3)2O\}CH_3$ containing 51% silica by mass in the oligomer with an average DP of 3, a MWt approximately 600 g/mole and a liquid density of 1.18g/mL) was added to solution of 60ml ethanol, plus 1 ml water to form a silica precursor solution. This solution was applied to a glass substrate and cured overnight in a cabinet containing a concentrated ammonia vapour for 24 hours. The subsequent coating was then analysed by FTIR DRIFT. The coating was then post-cured at 80°C, 110°C, 450°C and 800°C for 60 minutes and analysed by FTIR DRIFT. The ratio of the areas under the siloxane (1003-1290 cm⁻¹) and the silanol (856-997 cm⁻¹) peaks were then used as an estimate of the condensation achieved. FTIR spectra were obtained using a Nicolet Nexus 870 spectrometer between 500 and 4000cm⁻¹ with 4cm⁻¹ resolution over 256 scans. Diffuse Reflectance Infrared Fourier Transform (DRIFT) Spectroscopy. The cured material was ground to a finely divided powder sample and set on a stage surrounded by mirrors that reflect outgoing radiation back to the sample where it is further absorbed until it eventually reaches the detector.

Results and Discussion

¹H-NMR Studies of Acid Catalysed TEOS Hydrolysis

The results shown in Figure 7, clearly show the loss of methoxy CH_2 and CH_3 form the TEOS, and the associated formation of ethanol CH_2 and CH_3 peaks in the NMR spectrum. The advantage of following the hydrolysis in this manner is that water required for the condensation can be accurately added in a stoichiometric fashion and using acetonitrile solvent instead of water or alcohols means that the equilibrium exchange effects from these solvents do not interfere with the rate of

reaction. From this work it can be seen that the condensation reaction goes to completion in around 30 minutes.
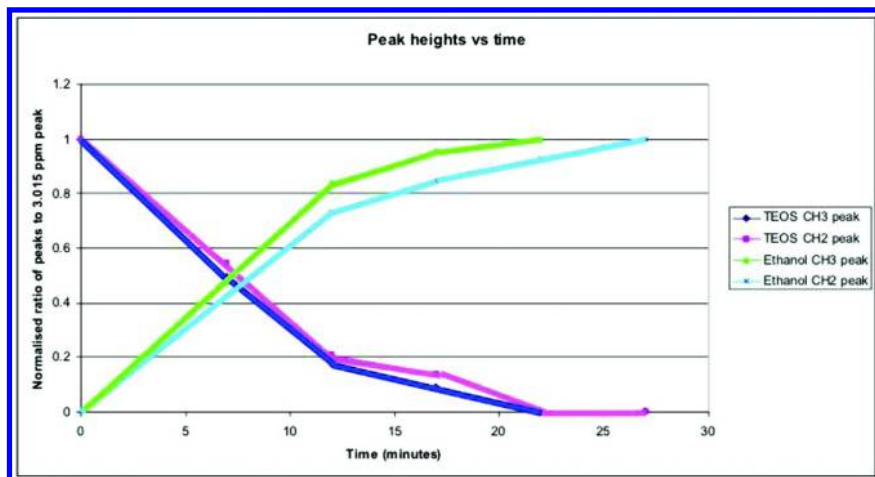

Figure 7. Acid hydrolysis of TEOS in acetonitrile

FTIR Studies of Base Catalysed TMOS Hydrolysis

In order to study cross-linking that occurred during post-curing at high temperatures the ratio of the peaks attributed to siloxane bonds formed during cross-linking versus silanol peaks was calculated.

The FTIR data shown in Table 1 clearly demonstrates the increasing degrees of cross-linking that occurs with post-curing of the TMOS sol-gel coating. Figure 8 shows the type of FTIR DRIFT spectra obtained, which is used for this analysis. The advantage of this FTIR method is that it is a relatively simple, low cost and rapid analysis technique to assess silanol conversion to siloxane bonds, compared to other techniques such as solid state ^{29}Si NMR analysis.

Using FTIR DRIFT data a shown in Figure 8 it is possible to ratio the area under the siloxane peak (1290-1002 cm^{-1}) to the silanol peak (997-856 cm^{-1}). This data has been provided in Table 1, where it was shown that the ratio of Si-O-Si/SiOH increases with increasing cure temperatures of the silica films. Thus, the silica films must be post-cured at temperatures ≥ 450 °C to obtain maximum cross-linking of the Si-OH bonds to Si-O-Si. The surface silanol groups of silica films are generally of two types:

- free silanols which have a sharp FT-IR absorption band (3750 cm-1) and,
- adjacent silanols which form hydrogen bonds between each other (*38*).

These adjacent silanols show broad absorbances at around 3600 cm^{-1}. Figure 9 shows DRIFT FT-IR of the same samples between the regions 2800 cm^{-1} to 3800 cm^{-1}.

Table 1. Siloxane and silanol peak area ratios by DRIFT analysis

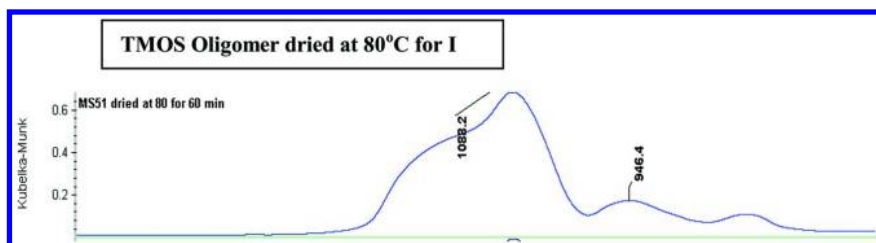| Sample	Si-O-Si (Area) 1290-1002 cm^{-1}	Si-OH (Area) 997-856 cm^{-1}	Ratio Si-O-Si : Si-OH
Cured at ambient	39.11	2.749	14.2
Dried at 80°C; 60 min	88.97	5.811	15.3
Dried at 110 °C; 60 min	132.9	6.376	20.8
Dried at 450 °C; 60 min	57.57	0.205	280.8
Dried at 800 °C; 60 min	54.59	0	

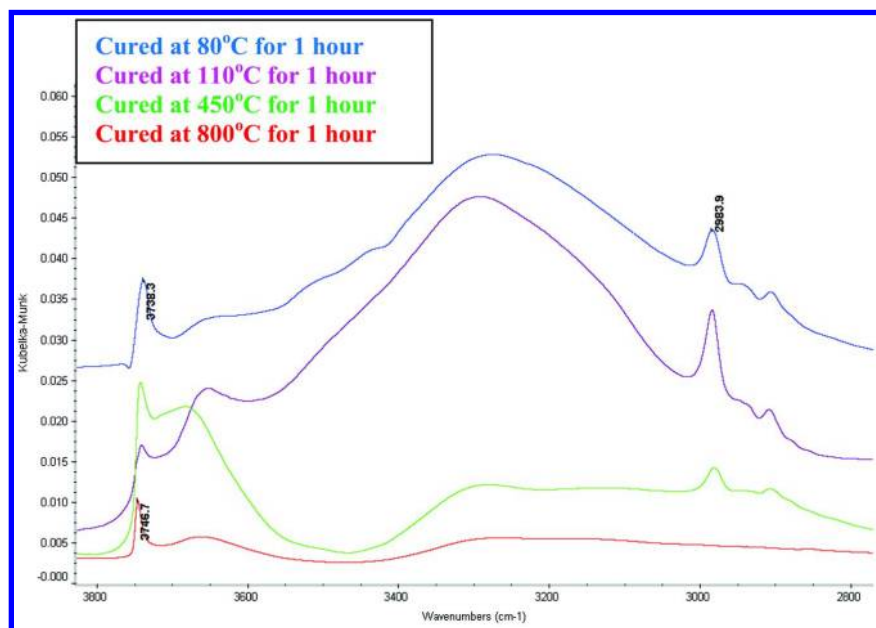*Figure 8. FTIR analysis of TMOS condensation*

Figure 9. DRIFT FT-IR of sol-gel coatings dried at 80, 110, 450 and 800°C (region 2800- 3800 cm^{-1}).

These spectra clearly demonstrate that only silanol groups left after post-cure at 800°C appear at 3740 cm⁻¹. Also bonds, due to absorbed water from the atmosphere, appear as a very broad absorbance between 3000-3600 cm⁻¹, which diminishes upon heating. When heated to very high temperatures, silica surfaces first lose physisorbed water and then additional water *via* condensation of adjacent hydroxyls. This condensation reaction is reversible up to about 400°C. (Figure 10).
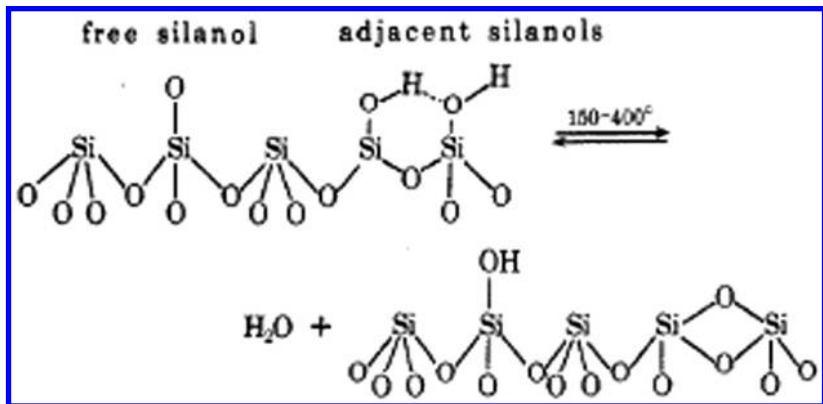
Figure 10. Condensation of SiOH at higher temperature (38)

Breakthrough Analysis of Toxic Metal Absorption

Researchers from Dr Clarke's laboratories in collaboration with University of Singapore (NUS), the Public Utilities Board (PUB-Singapore), Deltares (Holland) and United Water developed a unique sol-gel water treatment process for the removal of toxins from urban waste-water from ARC Linkage LP0777033 – "Modifying and Improving Porous Sol-Gel Materials for Water Purification". Small 2kg test-bedding, column tests on of sol-gel filter media, were carried out in Singapore. See Figures 11 to 18.

Figure 11. Dr Elda Markovic from Clarke's laboratories working in Singapore at the NUS laboratories on ARC Linkage LP0777033 project

Figure 12. Dr Clarke invited to attend the opening of the new SDWA laboratories at NUS in Singapore on 14-16 November 2010

Figure 13. Dr Kim Nguyen from Clarke's laboratories undertaking test-bed 2 kg column trials in Singapore at the NUS laboratories on ARC Linkage LP0777033 project

Figure 14. Breakthrough plots for copper (Cu^{2+}) by Deltares in Holland, on 2 kg test-bedding trials undertaken at NUS in Singapore

Figure 15. Breakthrough plots for arsenic (As^{3+}) by Deltares in Holland, on 2 kg test-bedding trials undertaken at NUS in Singapor
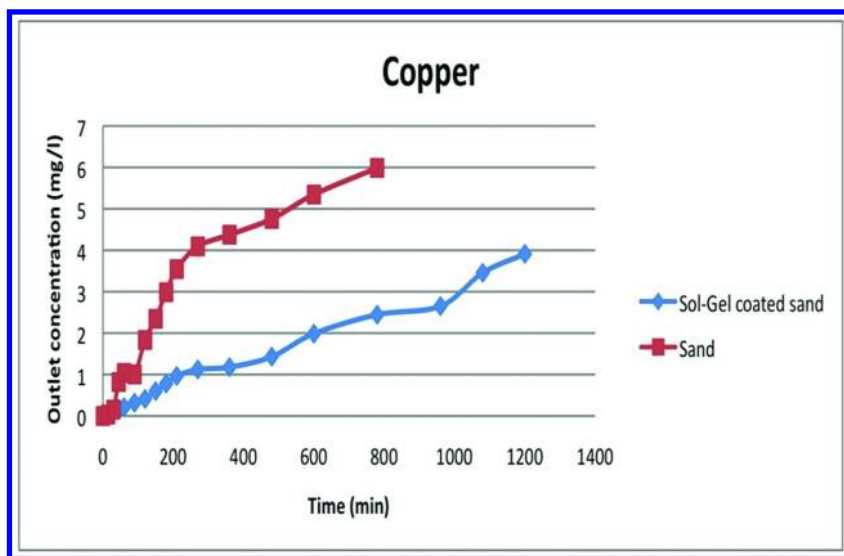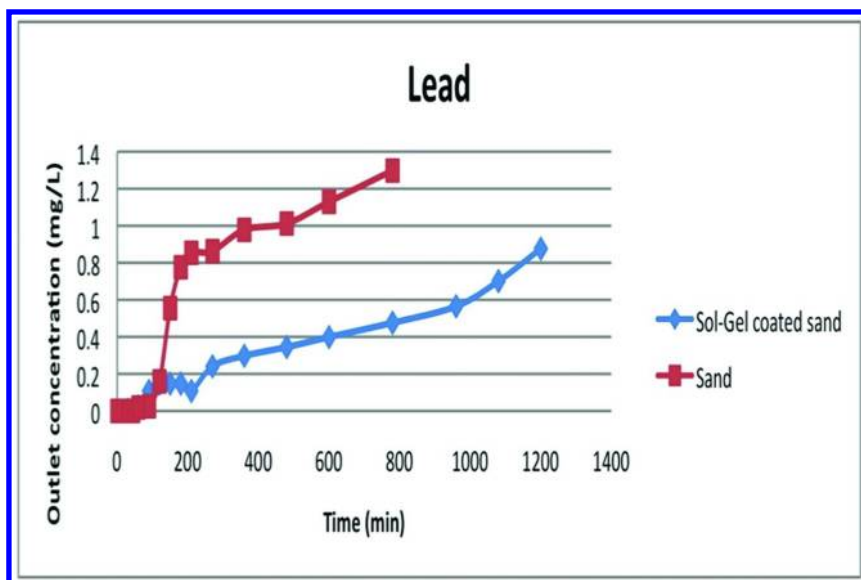
Figure 16. Breakthrough plots for lead (Pb^{2+}) by Deltares in Holland, on 2 kg test-bedding trials undertaken at NUS in Singapore
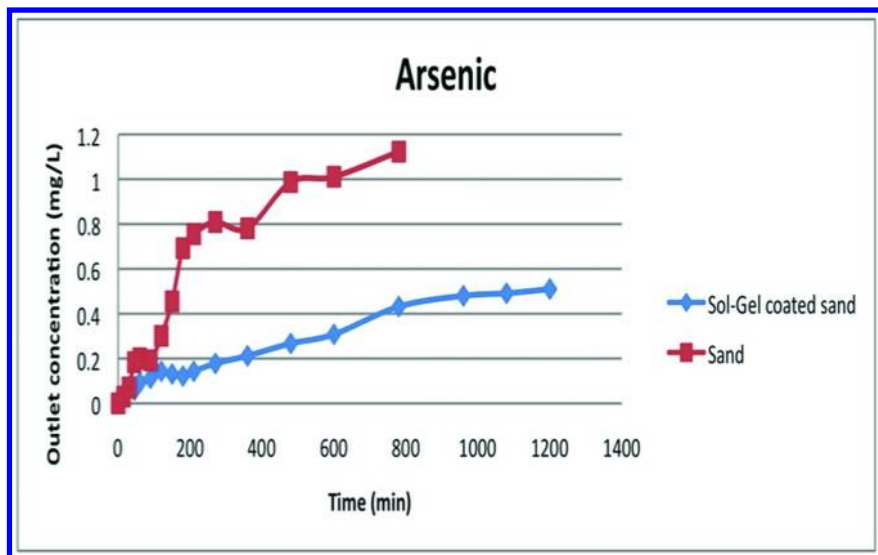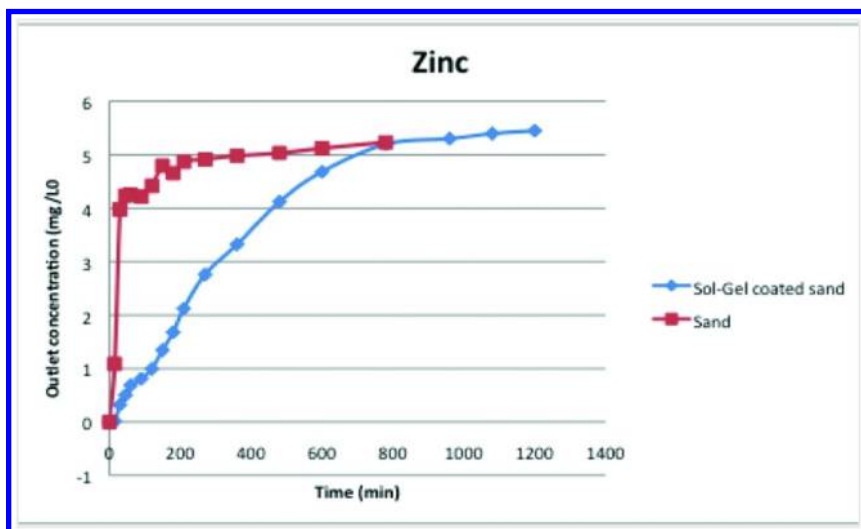

Figure 17. Breakthrough plots for zinc (Zn^{2+}) by Deltares in Holland, on 2 kg test-bedding trials undertaken at NUS in Singapore
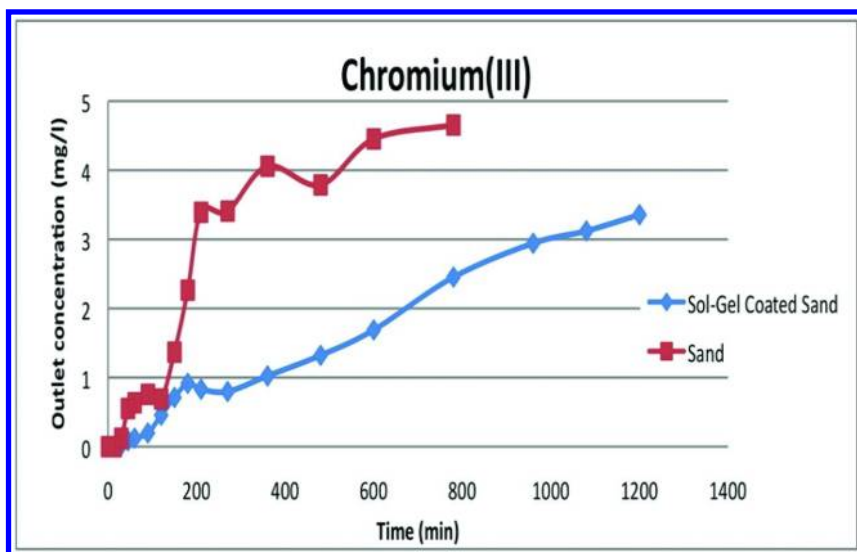
Figure 18. Breakthrough plots for chromium (Cr^{3+}) by Deltares in Holland, on 2 kg test-bedding trials undertaken at NUS in Singapore

Conclusions

This work outlines some novel NMR and FTIR analysis techniques, developed by researchers from the Clarke laboratories, that will be used in the preparation of new sol-gel technologies that will be used for the treatment of run-off, storm water by industry partners SDWA and United Water.

Acknowledgments

References

1. Brinker, C. J.; Scherer, G. W. *Sol-Gel Science: The Physics and Chemistry of Sol-Gel Processing*; Academic Press, Inc.: New York, 1990.
2. Brinker, C. J.; Scherer, G. W. *J. Non-Cryst. Solids* **1985**, *70*, 301.

3. Prassas, M.; Hench, L. L. In *Ultrastructure Processing of Ceramics, Glasses, and Composites*; Hench, L. L, Ulrich, D. R., Eds.; John Wiley & Sons: New York, 1984; pp 100−125.

4. Brinker, C. J. *J. Non-Cryst. Solids* **1988**, *100*, 31.

5. Lev, O.; Tsionsky, M.; Rabinovich, L.; Glezer, V.; Sampath, S.; Pankratov, I.; Gun, J. *Anal. Chem.* **1995**, *67* (1), 22A−30A.

6. Keefer, K. D. In *Silicon Based Polymer Science: A Comprehensive Resource*; ACS Advances in Chemistry Series No. 224; Zeigler, J. M., Fearon, F. W. G.; American Chemical Society: Washington, DC, 1990.

7. Aelion, R.; Loebel, A.; Eirich, F. *J. Am. Chem. Soc.* **1950**, *72*, 5705.

8. Kelts, L. W.; Effinger, N. J.; Melpolder, S. M. *J. Non-Cryst. Solids* **1986**, *83*, 353.

9. Assink, R. A.; Kay, B. D. *J. Non-Cryst. Solids* **1988**, *99*, 359.

10. Klein, L. C. *Annu. Rev. Mater. Sci.* **1985**, *15*, 227.

11. Iler, R. K. *The Chemistry of Silica*; Wiley: New York, 1979.

12. Engelhardt, V. Q. *Anorg. Allg. Chem.* **1977**, *418*, 43.

13. Avnir, D. *Acc. Chem. Res.* **1995**, *28*, 328.

14. Hench, L. L.; West, J. K. *Chem. Rev.* **1990**, *90*, 33.

15. Collinson, M.. M. *Crit. Rev. Anal. Chem.* **1999**, *29*, 289. Maruuszewski, K.; Strek, W.; Jasiorski, M.; Ucik, A. *Radiat. Eff. Defects Solids* **2003**, *158*, 439.

16. Caruso, R. A.; Antonietti, M. *Chem . Mater.* **2001**, *13*, 3272.

17. Schotner, G. *Chem. Mater.* **2001**, *13*, 3422.

18. Birnie, D. P. *J. Sol.-Gel Sci. Technol.* **2004**, *31*, 225. Ngyen, H.. T.; Miao, L.; Tanemara, M.; Toh, S.; Kaneko, K.; Kawasaki, M. *J. Cryst. Growth* **2004**, *271*, 245.

19. Ahmaniemi, S.; Tuominem, J.; Vippola, M.; Vuoristo, P.; Mantyla, T.; Cernuschi, F.; Gualco, C.; Bonadei, A.; Di Maggio, R. *J. Therm. Spray Technol.* **2004**, *13*, 361.

20. Walcarius, A.; Mandler, D.; Cox, J. A.; Collinson, M.; Lev, O. *J. Mater. Chem.* **2005**, *15*, 3663.

21. Schmidt, H.; Scholze, H.; Kaiser, A. *J. Non-Cryst. Solids* **1984**, *63*, 1.

22. Pouxviel, J. C.; Boilot, J. P.; Beloiel, J. C.; Lallemand, J. Y. *J. Non-Cryst. Solids* **1987**, *89*, 345.

23. Einarsrud, M. A.; Nilson, E. *J. Non-Cryst Solids* **1998**, *226*, 122.

24. Hereid, S.; Dahle, M. A.; Einarsrud, M. A. *J. Non-Cryst. Solids* **1995**, *186*, 96.

25. Tan, B.; Rankin, S. E. *J. Phys. Chem. B* **2006**, *110*, 22353.

26. Beck, J. S.; Vartuli, J. C.; Roth, W. J.; Leonowicz, M. E.; Kresge, C. T.; Schmitt, K. D.; Chu, C. T.-W.; Olson, D. H.; Sheppard, E. W.; McCullen, S. B.; Higgins, J. B.; Schlenker, J. L. *J. Am. Chem. Soc.* **1992**, *114*, 10834.

27. Kresge, C. T.; Leonowicz, M. E.; Roth, W. J.; Vartuli, J. C.; Beck, J. S. *Nature (London)* **1992**, *359*, 710.

28. Monnier, A.; Schu¨th, F.; Huo, Q.; Kumar, D.; Margolese, D.; Maxwell, R. S.; Stucky, G. D.; Krishnamurty, M.; Petroff, P.; Firouzi, A.; Janicke, M.; Chmelka, B. F. *Science* **1993**, *261*, 1299–1303.

29. Huo, Q.; Margolese, D. I.; Stucky, G. D. *Chem. Mater.* **1996**, *8*, 1147.

30. Ying, J. Y.; Mehnert, C. P.; Wong, M. S. *Angew. Chem., Int. Ed.* **1999**, *38*, 56–77.
31. Dabbs, D. M.; Aksay, I. A. *Annu. Rev. Phys. Chem.* **2000**, *51*, 601–622.
32. Novak, B. M. *Adv. Mater.* **1993**, *5*, 422–433.
33. Baney, R. H.; Itoh, M.; Sakakibara, A.; Suzuki, T. *Chem. Rev.* **1995**, *95*, 1409.
34. Zhang, Z.; Tanigami, Y.; Terai, R. *J. Non-Cryst. Solids* **1995**, *189*, 212.
35. Judeinstein, P.; Sanchez, C. *J. Mater. Chem.* **1996**, *6*, 511.
36. Loy, D. A.; Shea, K. *J. Chem. Rev.* **1995**, *95*, 1431.
37. Shea, K. J.; Loy, D. A. *Chem. Mater.* **2001**, *13*, 3306.
38. Azrek, R. G.; Angell, C. L. *J. Phys. Chem.* **1973**, *77*, 3048.

Chapter 3

Preparation of Epoxy-Functional Silicones Using Sol-Gel Chemistry

James V. Crivello*

Department of Chemistry and Chemical Biology, Rensselaer Polytechnic Institute, Troy, New York 12180, USA
***E-mail: crivej@rpi.edu**

A series of novel epoxy-silicone oligomers based on α-epoxy-ω-trimethoxysilanes were prepared by a controlled sol-gel method employing a solid phase macrorecticular weakly acidic ion exchange resin as a catalyst. Hydrolysis of the trialkoxysilane functional groups and subsequent condensation of the silanol groups formed takes place to produce oligomers bearing pendant epoxy functional groups with a predominantly linear structure. The reaction can be carried to high conversions and high molecular weights without side reactions involving the epoxy groups. Using this approach, a series of reactive epoxy siloxane oligomers with controlled molecular weights were prepared and their photoinitiated cationic ring-opening polymerizations studied. Oligomers bearing pendant epoxycyclohexyl groups were especially reactive under these conditions and these materials were evaluated in such applications as coatings, photoresists and as photopolymers for use in the stereolithographic construction of 3D objects.

Introduction

The main focus of research in this laboratory over the past two decades has been on various aspects of photoinitiated cationic polymerizations (*1*). Due to their growing academic and commercial importance, a topic of special interest has been an investigation of the photoinitiated cationic ring-opening polymerizations of epoxy monomers and epoxy functional oligomers (*2*). In Scheme 1 is

shown a general mechanism that has been proposed for these polymerization reactions illustrated using a diaryliodonium salt as the cationic photoinitiator. The photoinduced fragmentation of diaryliodonium salts bearing anions (MtX_n^-) with low nucleophilic character yields a variety of highly reactive species among which are radicals, cation radicals and cations. Subsequent interaction of those species with water, alcohol and other proton donors present in the monomer yields a strong protonic acid. Ring-opening polymerization ensues by first, protonation of the epoxide monomer followed by repeated attack of the monomer on the activated oxonium ion chain end that results in polymer chain growth.
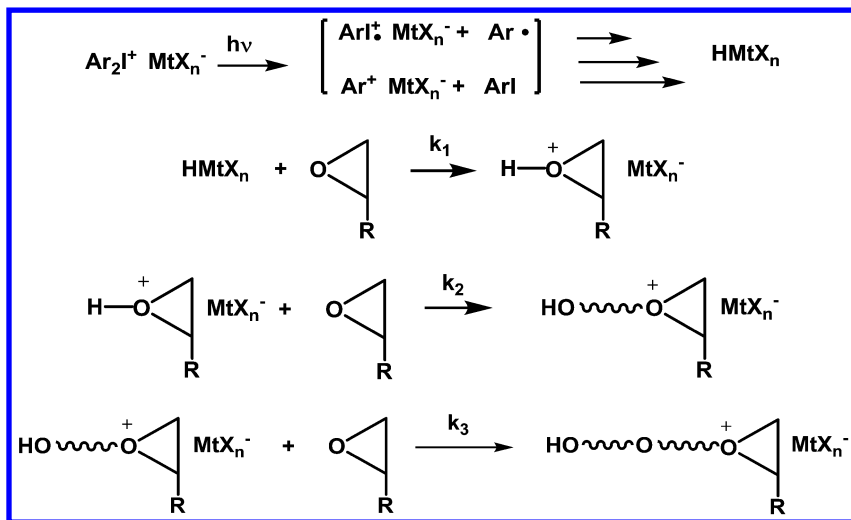
Scheme 1. Mechanism for the photoinitiated cationic polymerization of epoxy monomers.

Of considerable importance to our ongoing work in the area of photoinitiated cationic ring-opening polymerizations (CROP) is an understanding of structure-reactivity relationships of the epoxy monomers. There is little information in the literature available on this topic. Accordingly, we have undertaken these studies in this laboratory (*3*, *4*). The results showed that a wide range of reactivity in CROP is exhibited by various epoxy monomers. The most reactive monomers are those that possess the highest ring strain within the oxirane functional group and, in addition, possess no other nucleophilic groups such as ethers, ketones or esters. Further investigations showed that epoxy monomers bearing siloxane groups are highly reactive in CROP and this was ascribed to the fact that although siloxanes are analogous to carbon-based ethers, the siloxane oxygen is non-nucleophilic since the lone pairs of electrons on oxygen occupy p orbitals that interact with the 3d orbitals of the neighboring silicon atoms resulting in d_π–p_π bonding (*5*). In the following sections, several methods will be described that were used to prepare a variety of epoxy-silicone monomers and functional oligomers, focusing especially on sol- gel methods.

Results and Discussion

Hydrosilation Methods for the Synthesis of Epoxy-Silicones
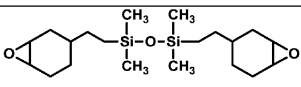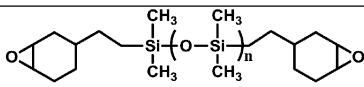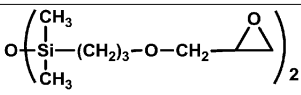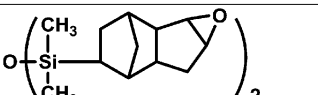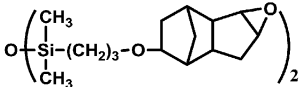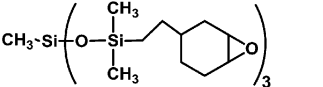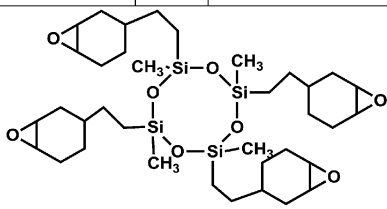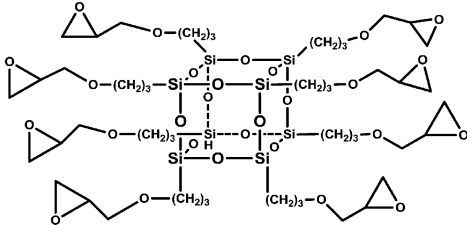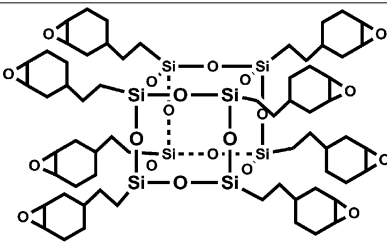
With the above described structure reactivity relationship information in hand, we began to investigate various mthods for the preparation of novel epoxy-silcone monomers and reactive oligomers. We observed that the platinum or rhodium catalyzed hydrosilation reaction was especially useful tool with which to construct novel epoxy-silicone monomers or employed to functionalize existing poly(siloxane) polymers (*6*, *7*). For example, the now commercially available photocurable epoxy-silicone release agents are prepared by the hydrosilation of terminal and pendant Si-H functional poly(dimethylsiloxanes) with 4-vinylcyclohexane-1,2-oxide as shown in Scheme 2. Photoinitiated CROP is carried out using a diaryliodonium salt (bis(4-dodecylphenyl)iodonium hexafluoroantimonate) (*8*) that was specially designed to be compatible with these polymers. The reactivity of these systems is outstanding and the commercial lines that apply and UV cure the release coatings on paper and plastic films currently operate at speeds in excess of 300 m/min.
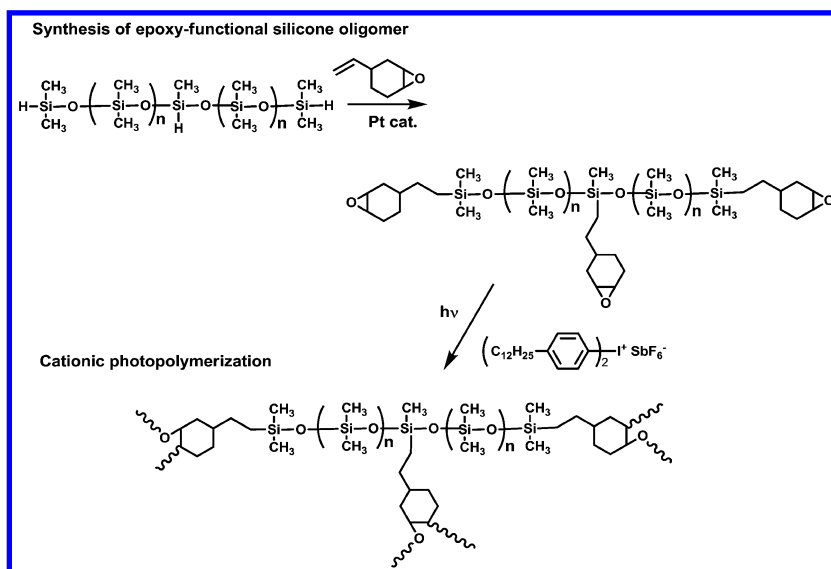
Scheme 2. Preparation of epoxy-functional poly(dimethyldiloxane oligomers)

Similarly, the condensans of di-, and tri- Si-H functional siloxane substrates with various unsaturated epoxides were carried out to prepare a wide assortment of linear, branched and cyclic monomers (*9–11*). Given in Table 1 are a sampling of the structures of a representative number of those monomers. Octafunctional epoxy-silsesquioxane monomers were prepared by Selinger and Laine (*12*) and in our laboratory (*13*) using this same general synthetic approach. As observed previously, those monomers bearing the highly strained epoxycyclohexylgroup or the epoxydicyclopentadienyl moieties display the highest reactivity in photoinitiated CROP.

Table 1. Structures of Epoxy-Silicone Monomers Prepared by Hydrosilation Methods

Structure	Ref.	Structure	Ref.
	9, 10		9, 10
	10		11
	11		10
			10
			12
			13

Concurrent Acid Catalyzed Alkoxysilane Condensation and Epoxide CROP

It occurred to us that it might be possible to conduct sol-gel condensation reactions in the presence of catalytic amounts of photogenerated acids derived from the UV irradiation of typical onium salts such as diaryliodonium and triarylsulfonium salts that are used as cationic photoinitiators. Indeed, we observed that the UV irradiation of solutions of those latter photosensitive salts in triethylorthosilicate (TEOS) results in the formation of a hard brittle glass-like gels. The sol-gel process involves a complex series of alkoxysilane hydrolysis and silanol condensation reactions that are summarized as shown in Scheme 3. Characteristically, the overall process is rather slow, requiring the absorption of water from the atmosphere and volatilization of the alcohol that is formed.
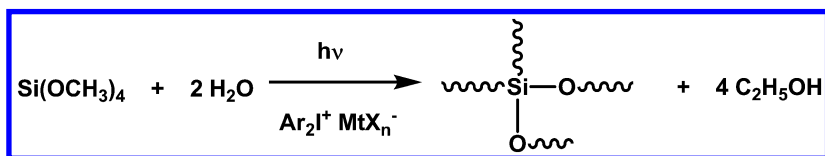
Scheme 3. Photoinduced sol-gel condensation of TEOS in the presence of (4-n-octyloxyphenyl)phenyliodonium hexafluoroantimonate as a photoacid generator.

The initial success of our photoinitiated sol-gel polymerizations suggested that this reaction could be applied to a wide variety of substituted and non-substituted alkoxy silanes. Of particular interest was the possible concurrent polymerization of alkoxysilanes bearing epoxy functional groups. Specifically, 3-glycidoxypropyltrimethoxysilane, **I**, and [2-(3,4-epoxycyclohexylethyl)]-trimethoxysilane, **II,** are commonly used glass-epoxy coupling agents and were readily available as potentially interesting dual reactivity monomers.
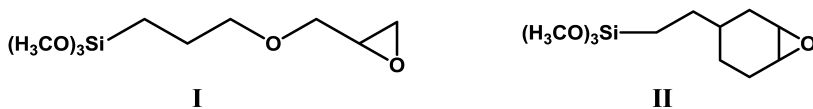
These two compounds are prepared respectively by the reaction of trimethoxysilane with allyl glycidyl ether and 4-vinylcyclohexane-1,2-oxide. UV irradiation of **I** and **II** in the presence of a typical strong acid generating onium salts results in the formation of colorless, hard and brittle glass-like solids. Real-time IR studies of the progress of the two reactions showed that the epoxide CROP was much faster than the sol-gel condensation reaction of the alkoxysilane portion of the molecule (*14*). However, on standing in the dark at room temperature, the reaction continues until a substantial portion of the methoxysilane groups are converted to polysiloxane linkages and a highly crosslinked matrix is formed. A general reaction for the photopolymerization of **II** is depicted in Scheme 4. Other mono- and multifunctional epoxide monomers can also be incorporated along with **I** and **II** to further modify the properties of the final products. Croutxé-Barghorn and her coworkers (*15, 16*) confirmed these

initial results and provided extensive and definitive solid-state ^{13}C and ^{29}Si NMR evidence for the proposed structure of these hybrid materials. In addition, they have further investigated their use in a wide assortment of potential applications including: abrasion resistant coatings for plastics, the fabrication of microlens and optical waveguides.
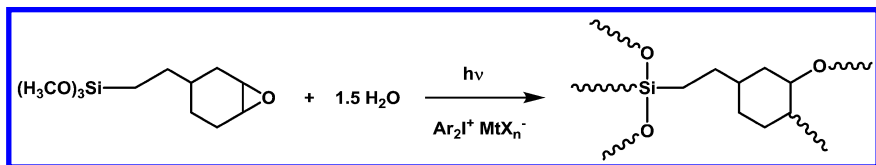
*Scheme 4. Photopolymerization of **II***

Application of Sol-Gel Chemistry to the Preparation of Epoxy Functional Silicone Oligomers

As described above, the use of concurrent photoinduced sol-gel condensation and CROP is a straightforward and convenient method for the preparation of interesting hybrid organic-inorganic matricies. However, it does have certain drawbacks that limit its use. Among these is the very slow rates of the sol-gel hydrolysis and condensation that make it incompatible with high speed coating applications. In addition, during sol-gel condensations, a large portion of the original mass of the starting material is lost as the alcohol is volatilized after it is liberated from the alkoxy silane by hydrolysis. This results in appreciable dimensional shrinkage and the consequent introduction of a high level of stress in the final crosslinked matrix. For this reason, sol-gel reactions are purposefully conducted at controlled slow rates to avoid the formation cracks and other defects.

In order to circumvent these difficulties, it was decided to discard the concurrent sol-gel and CROP approach and pursue a different synthetic strategy. Instead, we proposed, as a first step, to carry out a controlled sol-gel condensation with hybrid monomers such as **I** and **II** that would essentially provide isolable, high molecular weight siloxane oligomers bearing epoxy functional groups. In this scheme, the chemical and mechanical problems associated with the loss in mass of the alcohol during cure would no longer be significant issues. In a second step, the epoxy functional siloxane oligomers would subsequently be subjected to photoinitiated CROP in the presence of onium salt photoacid generators. Crucial to the success of the above-described proposed scheme is to identify a catalyst that would provide the selective hydrolysis and condensation of alkoxysilanes without simultaneously ring- opening the epoxy groups or interfering with their subsequent photoinitiated CROP. In addition, since **I** and **II** are trialkoxysilanes, their complete hydrolysis during the sol-gel condensation would result in insoluble, infusible crosslinked materials that would be worthless as photocurable materials. Fortunately, the rates of hydrolysis for the alkoxy groups of a trialkoxysilane proceed progressively slower as each alkoxygroup is removed from the silicon center. Further, the condensation of each of the silanol groups formed proceeds at its own rate (*17*). For all these reasons, a

prospective catalyst must provide a high degree of control over the hydrolysis and condensation reactions and preferably be quantitatively removed once the desired extent of reaction is reached to stop further sol-gel reaction from reaching the gel point.

These goals were realized through the discovery that weakly acidic macroreticular ion-exchange resins function as selective sol-gel hydrolysis and condensation catalysts (*18*, *19*). Applications of such catalysts in sol-gel chemistry had not previously been described in the literature. However, they appear to be nearly ideal for this purpose and to afford the desired high degree of control that was sought over the complex series of sol-gel reactions. A number of these resins are available from commercial sources as crosslinked beads and several were screened as potential sol-gel catalysts. As a result of the screening studies, three ion-exchange resins; Amberlyst A-27, Amberlite IRA-400 and Amberlite IRA-904 (Rohm and Haas, Sigma-Aldrich) were identified as useful catalysts. All three resins have similar structures, **III**, and display comparable catalytic reactivity. The resins are derived by functionalizing crosslinked chloromethylated poly(styrene) with trimethyl amine to provide the corresponding polymeric quaternary ammonium chlorides. They differ from one another with respect to their crosslink density, porosity and ion-exchange capacity.

III
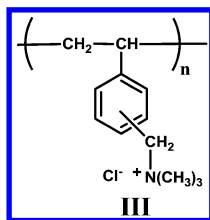
A typical laboratory procedure for conducting sol-gel chemistry in the presence of **III** as a catalyst consists of heating 8 mmol **II** in the presence of 1.5 equivalents of deionized water, 0.5 g of 2-propanol and 80 mg of Amberlyte IRA-904 resin at 45 °C for 9 hours. The reaction was followed by periodically taking samples, diluting with 0.5 g 2-propanol, filtering to remove the catalyst beads and evaporating the solvent. The resulting colorless, viscous liquid oligomer was analyzed using GPC, IR and ^{29}Si and ^{1}H-NMR spectroscopy. Over the course of the reaction time, GPC analysis shows a shift to higher molecular weight reaction products. At the same time, ^{1}H-NMR spectroscopy shows a 78-82% loss of the methoxy groups attached to silicon while retaining the characteristic protons at $\delta = 3.1$ ppm corresponding to the epoxycyclohexyl groups. Likewise, the sol-gel condensation of **I** containing a glycidyl ether epoxide group was successfully carried out to yield an oligomeric silicone epoxide.

It is interesting to note that despite the presence of sufficient water to hydrolyze all three methoxy groups of the starting materials, that colorless soluble oligomers were obtained in all cases. This, together with evidence from the ^{1}H-NMR analysis, would tend to suggest that the hydrolysis proceeds in a discrete stepwise manner such that the last of the three methoxy groups is quite resistant to hydrolysis and, therefore, is largely preserved in the product. In addition, it further suggests that the structure of the oligomer is chiefly linear

with some branched, cyclic and, perhaps, also cage siloxane groups also present. This is in accord with previous work (*20*) in this field in which the hydrolysis of alkoxysilanes is known to yield similar products. Accordingly, a proposed structure of the oligomer derived from **II** as a substrate that incorporates these structural features is shown in **IV**.

IV
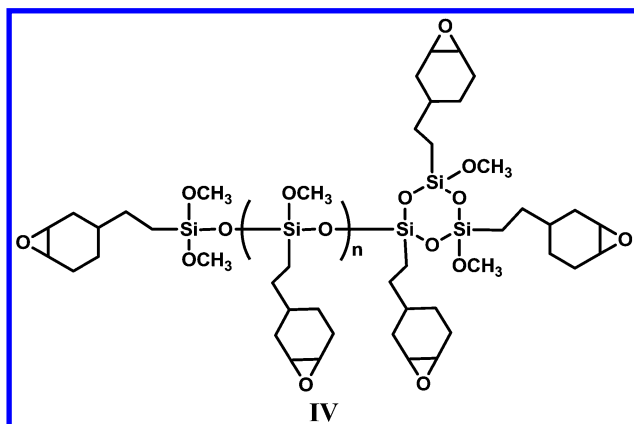
Successful optimization of reaction conditions was carried out. The reaction times were shortened by carrying out the reaction at reflux in 1-propanol. Subsequent scale-up of these sol-gel reactions in 25 and 50 gallon stainless steel reactors was achieved that provided a series of oligomers on a multi-killogram basis with different molecular weights, epoxide contents and viscosities. In this way, oligomers with up to an average of eleven epoxycyclohexyl groups per molecule were obtained. Gelled products were not obtained. The catalysts were easily separated from the reaction product by a simple filtration and could be recycled. Along with oligomers from the sol-gel condensation of monomers **I** and **II**, it was found that cocondensation could be carried out with a variety of alkyltrialkoxysilanes and dialkyldialkoxysilanes. In addition, several additional epoxides with different siloxane spacers interposed between the trialkoxysilyl group and the epoxide group were also prepared and successfully subjected to the solid-phase catalyzed sol-gel condensation (*21*). Shown in Scheme 5 is a two-step, one-pot synthetic method that was used for the preparation of a series of α-epoxy−ω-trimethoxysilanes, **V**. The rhodium catalyzed regioselective monohydrosilation of the starting terminal di-Si-H functional silane can be carried to high conversion (>95%) at 60 °C in 4 hours. Addition of vinyltrimethoxysilane followed by increasing the temperature to 60 °C for 6 hours results in the formation of the desired products, **V**, in nearly quantitative yields.
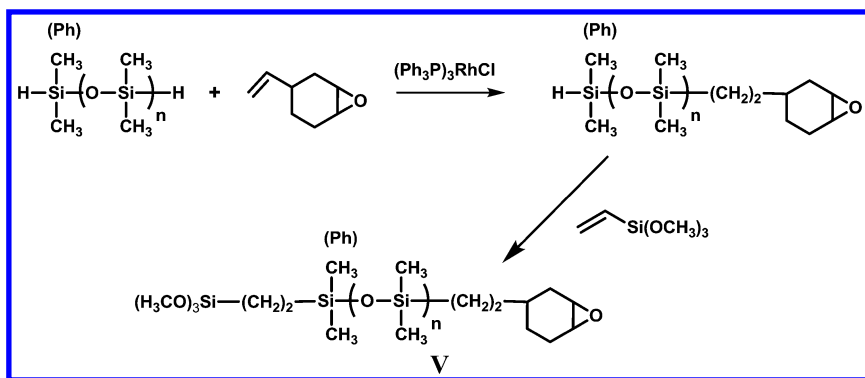
Scheme 5. Preparation of α-epoxycyclohexylethyl-ω-trimethoxysilanes (n = 0, 1, 2, 3)

These starting material variations permit the sol-gel synthesis of a wide range of epoxy functional reactive oligomers with tailored mechanical properties and reactivities in photoinitiated CROP. Studies of the diaryliodonium and triarylsulfonium salt photoinitiated CROP of the multifunctional epoxysiloxane oligomers showed that they displayed reactivities that parallel those of simple mono- or diepoxy monomers. Thus, oligomers bearing epoxycyclohexyl functional groups display the highest reactivity, compared to their less reactive analogs with glycidyl ether epoxy groups. For the sake of brevity this article will focus primarily upon oligomers such as **IV** bearing pendant epoxycyclohexyl groups that display high orders of reactivity as well as other interesting and rather unique properties. Since these oligomers do not contain aromatic or other conjugated groups, they are transparent at UV wavelengths down to 180 nm and, therefore, well suited to photoinitiated CROP using diaryliodonium and triarylsulfonium salt cationic photoinitiators. Depicted in Figure 1 is a real-time FT-IR study of the photopolymerization of a **IV** oligomer that confirms the high reactivity of these compounds. In this case, the diaryliodonium salt **VI** having the structure shown below was used. Due to the high epoxide functionality of this oligomer, gelation occurs at low epoxide conversion during the photopolymerization. For this reason, the highest rate is also obtained at low conversions. Once gelation takes place, the rate of the further epoxide conversion slows markedly due to restricted mobility of the remaining functional groups within the solid matrix.
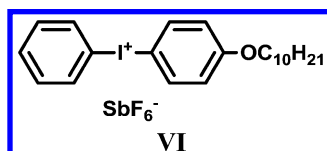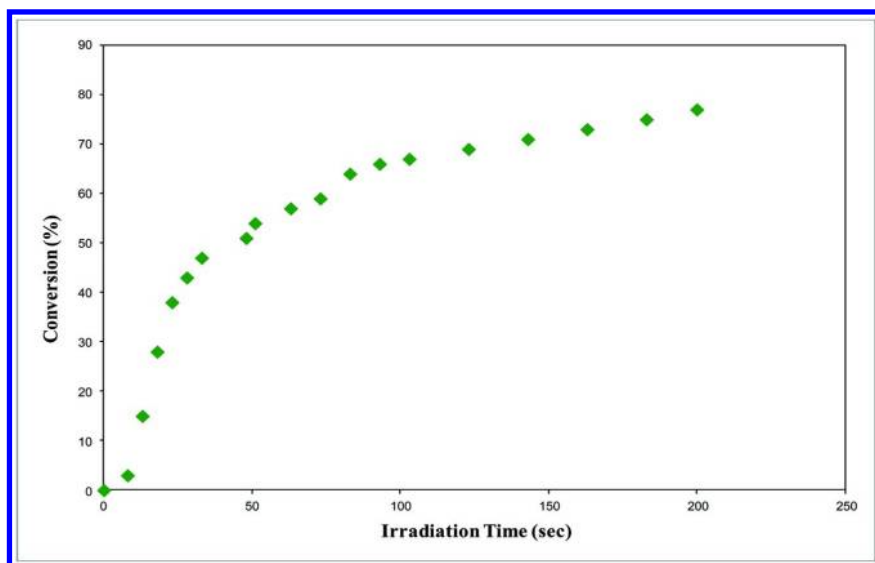
*Figure 1. Real time FT-IR study of the photoinitiated CROP of **IV** using 2.0 mol% of (4-n-decyloxyphenyl)phenyliodonium hexafluoroantimonate (**VI**) as photoinitiator.*

Despite many attempts, we were unable to measure the glass transition temperature for this photocrosslinked polymer using differential scanning calorimetry. No transition corresponding to a T_g was observed below 225 °C. The thermogravimetric analysis (TGA) scan conducted in nitrogen at a heating rate of 20 °C/min is shown in Figure 2. The UV cured oligomers display excellent thermal stability with the onset of thermal decomposition at approximately 350-400 °C. It is notable that a high char yield is obtained. Pyrolysis of photocured macroporous beads of **IV** at 800 °C in air results in the formation of replicas of the beads consisting essentially of pure silica (*22*). Photopolymerized epoxy-silicone resins were also found to possess excellent resistance to atomic oxygen which makes them potential candidates for aerospace uses in low earth orbit (*23*). In contrast, under the same conditions most organic polymers are extensively eroded by atomic oxygen. Presumably, the surfaces of epoxy silicone resins are rapidly oxidized under these conditions to form a thin, protective layer of silicon dioxide that resists further attack by this aggressive oxidant.

In Table 2 are listed the values for various electrical and mechanical properties determined on standard films and tensile bars of UV cured **IV** oligomers produced by photoinitiated CROP. Particularly interesting are the excellent dielectric strength, low coefficient of thermal expansion and low water uptake that make them particularly well suited for semiconductor insulation and encapsulation.
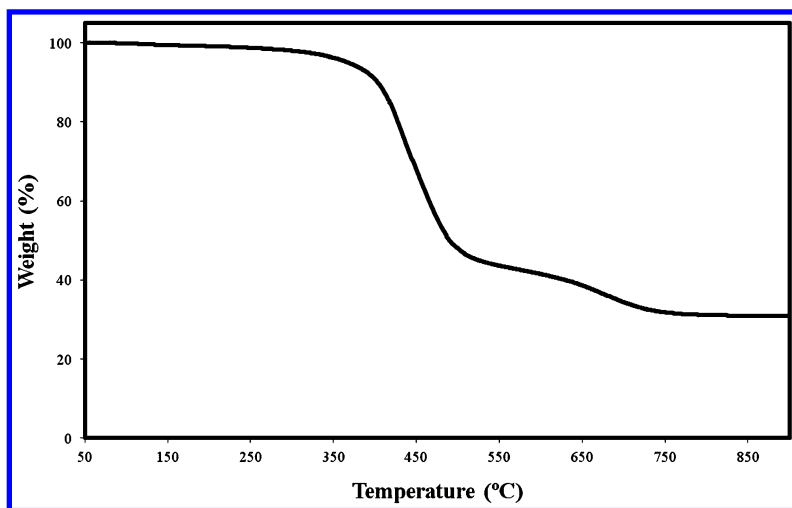
*Figure 2. TGA of **IV** carried out in nitrogen at 20 °C/min.*

Table 2. Electrical and physical properties of photopolymerized epoxy-silicone IV

Property	*Value*
Dielectric constant	2.8
Leakage current density	10^{-9} A/cm^2 (5 MV/cm)
Dielectric strength	> 5 MV/cm
Thermal stability	>350 °C
Young's modulus	5 GPa
Coefficient of therm expansion	52 ppm/°C
Water uptake	< 0.2% at 85 °C/85% RH

The ability to pattern epoxy-silicone oligomers and to use them as negative working photoresists make them interesting candidates for photolithographic applications. Employing high molecular weight (approx. 20,000 g/mol) **IV** polymer, conventional projection imaging using 365 nm UV light followed by development in acetone was used to produce images with 2 μm lines with 5 μm spaces (*24*). Nanoimprint lithography has been receiving a great deal of attention as an unconventional patterning method that has the capability of replicating the very fine features of a mold in a thin layer film of a liquid photoresist that is hardened with UV light (*25*). Lu et al. (*26*) reported that they were able to produce sub-100 nm nanostructures by nanoimprint lithography employing a low molecular weight version of **IV** in combination with a diaryliodonium salt as a cationic photoinitiator.

A very different potential application for epoxysilicone oligomers is in the fabrication of three dimensional (3D) polymer objects using stereolithography (*27*). This technology employs CAD-CAM engineering design as a first step to create a 3D computer image of an object that is to be translated into a corresponding 3D solid plastic object. The computer image is next mathematically cut into thin slices and each slice is then written onto the surface of a liquid photopolymer using a highly focused laser. The laser irradiation rapidly causes the photopolymer to harden in the exposed regions. The first image is written onto a movable stage submerged just below the surface of the liquid photopolymer bath and after it is written, the stage is lowered into the bath by an increment equal to the thickness of the next layer to be written. The photopolymer flows over the first layer and the second layer is written on the top of the first. This process is repeated until the entire solid object is written. Then, the stage is raised out of the bath revealing the entire solid plastic object. Fluid epoxy-silicone oligomers are attractive as photopolymers for stereolithography because of their excellent photosensitivity and the excellent mechanical properties that are obtained in the resultant 3D object. Particularly important is the low volume shrinkage that takes place during the photoinitiated CROP of these materials that affords 3D objects with excellent fidelity, low shrinkage and low distortion. Shown in Figure 3 is an example 3D objects produced by stereolithography using epoxy-silicones as photopolymers.
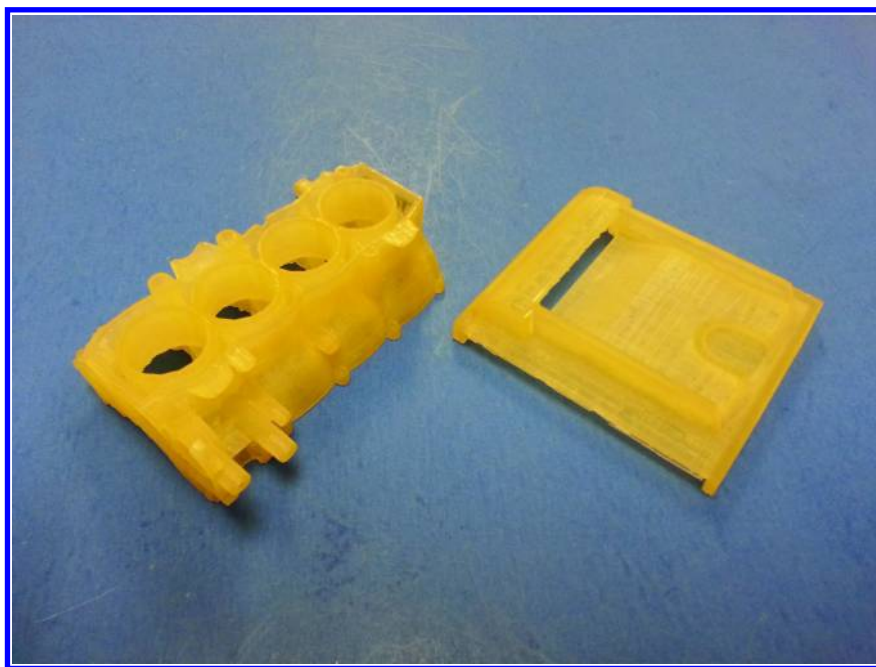
Figure 3. Examples of 3D prototypes constructed from epoxy-silicones using stereolithography

Conclusions

The development of a novel, efficient and versatile sol-gel method for the synthesis of multifunctional epoxy-silicone oligomers offers the possibility to make these materials available in substantial quantities from readily available starting materials. Recent efforts have carried this work beyond the laboratory and have shown that a wide range of materials with different reactivities can be prepared using this method. Photoinitiated CROP of the epoxy-silicone oligomers proceeds rapidly to give materials with excellent thermal, electrical and mechanical properties. Future efforts in this laboratory will focus on finding additional unique applications for the use of these materials.

References

1. Crivello, J. V. Photopolymerization. In *Polymer Science: A Comprehensive Reference*; Matyjaszewski, K., Möller, M., Eds.; Vol. 4; Elsevier: Amsterdam, 2012; p 919.
2. Crivello, J. V. Photo and Thermal Catalysts For Cationic Polymerization. In *Ring-Opening Polymerization*; Brunelle, D. J., Ed.; Hanser: Munich, 1993; p 157.
3. Crivello, J. V.; Varlemann, U. *J. Polym. Sci., Part A: Polym. Chem.* **1995**, *33* (14), 2463.
4. Bulut, U.; Crivello, J. V. *Macromolecules* **2005**, *38* (9), 3584.
5. Voronkov, M. G.; Mileshkevich, V. P.; Yuzhelevskii, Yu. A. *The Siloxane Bond*; Consultants Bureau: New York, 1978; p 9.
6. Crivello, J. V.; Lee, J. L. *PMSE Prepr.* **1989**, *60*, 217.
7. Eckbberg, R. P. U.S. Patent 4,977,198, Dec. 11, 1990, to G.E. Corp.
8. Eckberg, R. P.; LaRochelle, R. W. U.S. Patent 4,279,717, Jul. 21, 1981, to G.E. Corp.
9. Crivello, J. V., Lee, J. L. *Proceedings of the Radtech '90 North America Conference*, Chicago, March 25, 1990; p 432.
10. Crivello, J. V.; Lee, J. L. *J. Polym. Sci., Part A: Polym. Chem.* **1990**, *28*, 479.
11. Crivello, J. V.; Song, S. *J. Polym. Sci., Part A: Polym. Chem.* **1999**, *37* (16), 3427.
12. Selinger, A.; Laine, R. M. *Chem. Mater.* **1996**, *8*, 1592.
13. Crivello, J. V.; Malik, R. *J. Polym. Sci., Part A: Polym. Chem.* **1996**, *35*, 407.
14. Crivello, J. V.; Bi, D.; Lu, Y. *Macromol. Symp.* **1995**, *95*, 79.
15. Chemtob, A.; Versace, D.-L.; Belon, C.; Croutxé-Barghorn, C.; Rigolet, R. *Macromolecules* **2008**, *41*, 7390.
16. Belon, C.; Chemtob, A.; Croutxé-Barghorn, C.; Rigolet, S.; Schmitt, M.; Bistac, S.; Le Houérou, V.; Gauthier, C. *Polym. Int.* **2010**, *591*, 1175.
17. Loy, D.; Shea, K. *J. Chem. Rev.* **1995**, *95*, 1431.
18. Crivello, J. V. U.S. Patent 6,391,999 B1, May 21, 2002, to Rensselaer Polytechnic Institute.
19. Crivello, J. V.; Mao, Z. *Chem. Mater.* **1997**, *9*, 1554.

20. Matějka, L.; Pleštil, J.; Dušek, K. *J. Non-Cryst. Solids* **1998**, *226*, 114.
21. Crivello, J. V.; Song, K. Y.; Ghoshal, R. *Chem. Mater.* **2001**, *13*, 1932.
22. Falk, B.; Crivello, J. V. *Chem. Mater.* **2004**, *16*, 5033.
23. Connell, J. W.; Crivello, J. V.; Bi, D. *J. Appl. Polym. Sci.* **1995**, *57*, 1251.
24. Wang, P.-I.; Nalamasu, O.; Ghoshal, R.; Ghoshal, R.; Schaper, C. D.; Li, A.; Lu, T.-M. *J. Vac. Soc. Technol. B* **2008**, *26* (1), 244.
25. Krauss, P. R.; Chou, S. Y. *J. Vac. Sci. Technol. B* **1995**, *13*, 850.
26. Ye, D.; Wang, P.-I.; Ye, A.; Ou, Y.; Ghoshal, R.; Ghoshal, R.; Lu, T.-M. *Microelectron. Eng.* **2010**, *87*, 2411.
27. Hull, C. W. U.S. Patent 4,575,330, March 11, 1986, to UVP, Inc.

Chapter 4

3-Methacryloxypropyltrimethoxysilane

Michael J. Owen*

Michigan Molecular Institute, Midland, Michigan 48640
E-mail: michaelowen01@chartermi.net

The silane 3-methacryloxypropyltrimethoxysilane is one of the oldest and still one of the most important coupling agents available for improving the practical adhesion of polymers to minerals. It has also featured strongly in research and development studies establishing the dominance of the chemical bonding theory as the primary mechanistic explanation of silane coupling agent effectiveness. This aspect of 3-methacryloxypropyltrimethoxysilane studies is summarized in this review. Its surface energy and water wettability are also discussed and compared with those of related polymers. These physical properties ought to be of some importance in adhesion enhancement but evidently they are less significant than the chemical reactivity of the silane.

Introduction

The term silicone is not a precise one. It is commonly used to describe polymers based on a silicon-oxygen (siloxane) backbone with organic groups attached directly to silicon atoms. Some might argue that such a definition excludes trialkoxysilanes of the type commonly used as coupling agents. Typically, their generic structure is $XRSi(OR^1)_3$ and they are derived from trichlorosilane ($SiHCl_3$) obtainable in very low yield (<1%) as a by-product of the Rochow-Muller direct process. The X moiety is designed to react with the organic resin phase and the OR^1 moiety with the glass or other inorganic material surface. As groups that react readily with resins tend to cause the silane to be unstable if directly attached to silicon, a bridging group R is usually required. The most familiar X groups include vinyl, chloropropyl, epoxy, methacrylate, amine, and mercapto. The OR^1 alkoxy group is usually methoxy or ethoxy, and the bridging group R is, most commonly, either ethylene or propylene although silanes with

shorter (methylene) or longer hydrocarbon links are commercially available. The nature of the X group definitely qualifies such silanes for consideration as silicones but what of the siloxane requirement?

As Matisons explains (*1*) "it is important to note that such silanes are usually applied from aqueous solution where both hydrolysis and condensation of the silane coupling agent occur resulting in the formation of oligomeric siloxane materials". Indeed, since the aqueous solutions are generally prepared some time in advance of fabrication of the composite it must be that it is such siloxane oligomers that are applied to the glass or other substrate and not unreacted silanes. Thus, both as materials in their own right and because of their important role in silicone-containing hybrid materials such silanes certainly have a place in the present volume. Silane coupling agents have been available for over sixty years according to Plueddemann (*2*), having been found to improve adhesion between the glass and the resin in fiberglass-reinforced organic resins following a "confidential" report to the Naval Bureau of Ordnance by Ralph K. Witt et al. of Johns Hopkins University where allyltriethoxysilane gave twice the strength of composites compared to when the glass was treated with ethyltrichlorosilane.

Over the years, the variety of organic X functionalities introduced into these reactive silanes, and the number of inorganic hydroxylated substrates they have been applied to, have increased markedly, some suppliers offering close to 200 different silanes. Expectedly, this reflects the growing interest in other areas of surface modification beyond their application as coupling agents in mineral- filled organic resin composites. In 1991, Plueddemann (*3*) recognized a variety of different uses, including hydrophobing agents, chromatography, soil treatment for water harvesting, detergents, immobilized metal complex catalysts, antimicrobials, coated metal oxide electrodes and immobilized enzymes. Current areas of high interest include uses in medical materials, nanocomposites, and self-assembled monolayers. Today's global market for silane coupling agents is of the order of one billion dollars comprising about one tenth of the total silicone market. Such a significant size and age of this field has inevitably produced a very large scientific literature. In order to illustrate some key aspects of silane coupling agent behavior and properties we have chosen to review just one outstanding example, 3-methacryloxypropyltrimethoxysilane. This silane is also known as γ-methacryloxypropyltrimethoxysilane or 3-(trimethoxysilyl)propyl methacrylate and commercially as A 174 or Z-6030 silane (CAS number 2530-85-0).

Coupling Agent Effectiveness

Silane coupling agents of this type were first disclosed in a patent by Plueddemann and Clark in 1966 (*4*) and 3-methacryloxypropyltrimethoxysilane has continued as one of the industry standards for fiberglass-filled unsaturated polyesters to this day, although it no longer has the predominant position it once held. According to Matisons (*5*) it maintains a significant use within this treated glass fiber market although over 60% is now held by 3-glycidoxypropyltrialkoxysilane. Table 1 lists some simple properties of 3-

methacryloxypropyltrimethoxysilane, those that are typically quoted by the many suppliers of this coupling agent. There is general agreement amongst them with the exception of the flash point where a considerable range is evident. This silane is a colorless transparent liquid that is soluble in a variety of solvents including methanol, ethanol, isopropanol, acetone, benzene, toluene and xylene. Obviously, it reacts with water and remains soluble after hydrolysis provided the pH is acidic (~ 4.0). Surfaces can typically be treated with 0.5% (v/v) concentration in ethanol or pH 3.5 water.

Table 2 illustrates the improvement in flexural strength reported by Plueddemann (*2*) that a 2% loading of 3-methacryloxypropyltrimethoxysilane confers on a polyester glass laminate. This silane performed the best of the nine methacrylate-containing compounds evaluated. Also included in the table are the other two silicon-containing compounds investigated – note that they are not conventional silane coupling agents but rather on complete hydrolysis will be orthosilicates ($SiO_{4/2}$ structures). It is the retention of the strength after exposure to boiling water that is the most significant aspect of these data. It translates into longevity in aqueous environments at ambient temperatures. For example, in his article "Built to Last: the Lifetime of Fiberglass Boats", Green (*6*) gives an assessment of US Coast Guard fiberglass composite patrol boats after 20 years service. He reports a +3% increase in tensile strength, +0.08% increase in compressive strength, +13% increase in flexural strength and -6% decrease in shear strength. These are relatively modest changes that, if anything, suggest a tightening of the composite network rather than any water-induced breakdown.

Table 3, taken from a compilation by Walker (*7*) shows the improvement in bond strength to metals of epoxide and polyurethane coatings provided by 3-methacryloxypropyltrimethoxysilane. Adhesion was measured by direct pull-off in an Instron Universal Testing Machine The data shown are for the silane coupling agent used as a primer pre-treatment but Walker also reported beneficial improvements when incorporated as additives in the coatings. He examined several other silane coupling agents and investigated other variables such as the effect of humidity and water immersion. More details are available in (*7*). His general conclusion was that silanes have great utility in polymer technologies where improved dry bond strength is desirable or retention of bond strength in an aqueous environment is important; a conclusion as true today as it was 20 years ago.

Mechanistic Studies

The chemical bonding theory is the most frequently invoked explanation offered for the effectiveness of silane coupling agents and 3-methacryloxypropyltrimethoxysilane has featured in some significant mechanistic studies to establish reactivity to both the inorganic and organic phases although not to the extent that other silane coupling agents have, particularly various amino-functional ones. There is considerable information on the bonding of 3-methacryloxypropyltrimethoxysilane to a variety of inorganic substrates

including, for example, glass, silica, alumina, lead and titanium. The classic proof of substrate reactivity came just a year after the publication of the original Plueddemann and Clark patent. Johannson and co-workers (*8*, *9*) studied the adsorption on E-glass and Aerosil surfaces of two silane coupling agents, 3-methacryloxypropyl-trimethoxysilane and 3-(2,3-epoxypropoxy)propyl trimethoxysilane. The results of tracer studies and electron photomicrography of the fiber surfaces showed that the coupling agents formed continuous films on E-glass surfaces with covalent bonding occurring at the interface. When exposed to boiling water failure did not occur at the glass-coupling agent interface but by attack on the glass substrate itself. E-glass rovings were treated with untagged 1% solutions of 3-methacryloxypropyltrimethoxysilane. C^{14} labeled methyl methacrylate and untagged styrene were then coupled to the treated rovings and extracted for 24 hours in refluxing tetrahydrofuran with several solvent changes. Initial coverage of the methyl methacrylate/styrene copolymer was 0.224 g/g of glass and there was still 0.016 g/g after the tetrahydrofuran extraction. Since the resin copolymer is completely soluble in tetrahydrofuran this result is also suggestive of coupling agent/resin bonding.

More recently, Garbassi and co-workers (*10*) have used x-ray photoelectron spectroscopy (XPS) and static secondary ion mass spectrometry (SSIMS) to quantitatively and qualitatively assess the bonding of 3-methacryloxy propyltrimethoxysilane to E glass, alumina and quartz. Miller and Ishida (*11*) used diffuse reflectance Fourier transform infrared (FTIR) to demonstrate covalent interfacial bonding between 3-methacryloylpropyltrimethoxysilane and lead oxide. An antisymmetric stretching vibration near 965 wavenumbers was attributed to a Pb-O-Si plumbosiloxane unit. This assignment was confirmed by repetitive independent experiments, control experiments and model compound studies. Matinlinna and co-workers (*12*) used FTIR and XPS to characterize the surface of titanium treated with a mixture of allyltrimethoxysilane and 3-methacryloxypropyltrimethoxysilane. In particular, the FTIR studies suggested the existence of Si-O-Ti bonds. Most recently,Wu et al. (*13*) prepared 3-methoxypropyltrimethoxysilane grafted silica hybrid nanoparticles by surface-initiated atom transfer radical polymerization. Their successful preparation was confirmed by FTIR, nuclear magnetic resonance (NMR), gel permeation chromatography (GPC), XPS, atomic force microscopy (AFM) and scanning electron microscopy (SEM).

Information on the reactivity of 3-methacryloylpropyltrimethoxysilane with the organic phase is somewhat sparser. It was firmly established in 1979 by Ishida and Koenig (*14*) using FTIR. They studied a high surface area silica that had been treated with 3-methacryloxypropyltrimethoxysilane and then mixed with styrene. After polymerization of the styrene the vinyl group signal disappeared indicating copolymerization and establishing that the coupling agent/matrix interface was covalently bonded. There have also been a number of studies using techniques such as XPS, SIMS and sum frequency generation vibrational spectroscopy (SFG) establishing the formation of an interpenetrating silsesquioxane network of a polymerized silane into the organic phase but, unfortunately, such studies have focused on amino- and epoxy-functional silanes and have not yet encompassed methacryloxy-functional silanes.

Table 1. Typical properties of 3-methacryloxypropyltrimethoxysilane

Property	Value
Specific gravity	1.045 g/cc at 25°C
Kinematic viscosity	2.50 cSt (RT)
Molecular weight	248.35
Boiling point	190°C
Flash point	92 – 138°C
Refractive index	1.431

Table 2. Flexural strengths of polyester glass laminates

Coupling agent	Flexural strength (MPa) Dry	Flexural strength (MPa) Wet (2 h boil)
No additive	386	240
$CH_2=C(Me)COO(CH_2)_3Si(OMe)_3$	633	588
$CH_2=C(Me)COOCH_2CHClCH_2OSiCl_3$	622	539
$CH_2=C(Me)COO(CH_2)_2OSi(OMe)_3$	347	232

Surface Tension Considerations

Interfacial contact and development of attractive forces across the interface are commonly considered prerequisites for subsequent good adhesion so the surfaces of substrates and the effect on these surfaces by any applied coupling agent is expected to play an important role in the adhesion at that interface. Because of the polar nature of most inorganic substrates, wetting of glasses, metal oxides, etc. is usually not a problem for aqueous or alcoholic solutions of coupling agents. However, a problem can be presented in the wetting of such treatments by the organic matrix if the organic component of the coupling agent furnishes a relatively low-surface-energy, difficult-to-wet surface.

Table 4 shows the values of the surface tension of solid films of 3-methacryloxypropyltrimethoxysilane obtained by two commonly-used but different contact angle approaches. The critical surface tension of wetting (γ_C), pioneered by Zisman and co-workers ([20]), is obtained from a plot of the cosine of the contact angles of liquid drops placed on a polymer surface against their liquid surface tension. The intercept of this line with the surface tension axis at $\cos\theta = 0$ is γ_C. The solid surface tension (γ_S) is derived from the method of Owens and Wendt ([19]) and Kaelble and co-workers ([21]) (Equation 1) where γ_S is the sum of the dispersion force component of surface tension, γ^d, and the polar component, γ^p, and the subscripts LV and SV refer to the liquid/vapor and solid/vapor interfaces, respectively:

$$\gamma_{LV}(1 + \cos\theta) = 2(\gamma_{LV}{}^d\gamma_{SV}{}^d)^{0.5} + 2(\gamma_{LV}{}^p\gamma_{SV}{}^p)^{0.5} \qquad (1)$$

Also included in the table are comparative values for the only common polyester reported in the literature, polyethyleneterephthalate, and poly(methyl methacrylate).

Precise comparisons of these data are unwarranted because of procedural differences such as, for example, in choice of contact angle test liquids, differing degrees of roughness of the samples, substrate type and treatment, deposition procedure, use and type of catalyst, and relative humidity. Both Lee's (*15*) and Sacher's (*17*) data for 3-methacryloxypropyltrimethoxysilane are for treated clean glass slides. However, not all their contact angle test liquids were the same. Both used water, glycerol and ethylene glycol; but Lee also used some polyglycols whereas Sacher used formamide and tricresyl phosphate. Another difference was the use of glacial acetic acid by Lee to catalyze silane hydrolysis. The γ_S of Lee and Sacher appear to be in reasonable agreement, however, this is not really the case. Their γ^d and γ^p components are quite different, 14.1 mN/m and 22.6 mN/m, respectively, for Lee, compared to 26.1 mN/m and 12.8 mN/m, respectively, for Sacher. Note also that although Sacher declined to report a critical surface tension of wetting value for the silane, citing excessive scattering of the data, he did provide a Zisman plot suggesting a value of 30 +/- 5 mN/m.

With regard to the low critical surface tension of wetting value of 16-17 mN/m by Browne and Throckmorton (*16*), this measurement is not for smooth glass slides but is for E-glass filaments where the silane was applied from aqueous solution followed by mild heating. This surprisingly low value is likely to be an artifact of roughness.

Comparison with the polyester polymer data in Table 4 is further complicated because the range of difunctional acids and alcohols that the polymer chemist can use to synthesize a polyester with specific properties is quite considerable. Certainly most of the resins used in composites are more likely to be based on intermediates such as maleic anhydride rather than terephthalic acid. Nevertheless, in the absence of a better comparison it does appear that the 3-methacryloxypropyltrimethoxysilane coupling agent film has a lower surface tension than this particular polyester. Since improved wetting is a desirable first step in developing improved adhesion this is a somewhat surprising observation. Note also the similarity of the advancing water contact angles for the three materials listed in Table 4 (see Table 5).

Plueddemann's comment (*24*) on these surface tension data was that the generally poor agreement "suggests that a rather broad range of surface tensions may be obtained with any silane, depending on the method of application, degree of silanol condensation etc.". He also noted that "it was somewhat disconcerting, however, to discover that the proven silane coupling agents most commonly used in the reinforced plastics industry led to critical surface tensions of less than 35. The best coupling agent for polyester resins (a methacrylate ester-functional silane) imparted a critical surface tension of only 28". He went on to state that "reactivity of the silane in copolymerization is obviously of much greater significance than polarity or wettability of the treated glass surface".

Table 3. Effect of silane coupling agent on coating bond strength

Substrate	Coating	Cleaning technique	Bond strength (MPa)	Area detached (%)
Mild steel	Epoxide	Degrease	28	20
Mild steel	Epoxide	Degrease	21 (no primer)	30-40 (no primer)
Mild steel	Epoxide	Grit blast	32	10
Mild steel	Epoxide	Grit blast	28 (no primer)	20 (no primer)
Aluminum	Epoxide	Degrease	31	20
Aluminum	Epoxide	Degrease	23 (no primer)	40-60 (no primer)
Aluminum	Epoxide	Grit blast	36	10
Aluminum	Epoxide	Grit blast	33 (no primer)	20 (no primer)
Mild steel	Polyurethane	Degrease	29	10-20
Mild steel	Polyurethane	Degrease	18 (no primer)	100 (no primer)
Mild Steel	Polyurethane	Grit blast	36	0-20
Mild steel	Polyurethane	Grit blast	34 (no primer)	10-40 (no primer)
Aluminum	Polyurethane	Degrease	31	0-60
Aluminum	Polyurethane	Degrease	13 (no primer)	100 (no primer)
Aluminum	Polyurethane	Grit blast	34	10
Aluminum	Polyurethane	Grit blast	28 (no primer)	10-30 (no primer)

Table 4. Comparison of surface tension data

Polymer	γ_C (mN/m)	[Ref.]	γ_S mN/m	[Ref.]
3-methacryloxypropyltrimethoxysilane	28, 16-17	(15, 16)	36.7	(15)
3-methacryloxypropyltrimethoxysilane	-	-	38.9	(17)
Polyethyleneterephthalate	43	(18)	47.3	(19)
Poly(methyl methacrylate)	39	(20)	40.2	(19)

Table 5. Comparison of water contact angle data

Polymer	θ_{WATER} (°)	Ref.
3-methacryloxypropyltrimethoxysilane	70, 75	(22, 23)
Polyethyleneterephthalate	76	(19)
Poly(methyl methacrylate)	80	(20)

We concur with these assertions. In any case, although the contact angle of a polyester resin on a silane-treated glass may not be zero it is likely to be quite small, well less than 90° thus offering a state of partial rather than complete wettability. There is a deal of difference between the wetting of a bunch of fibers with agitation as opposed to the placing of a drop on a smooth surface. The wetting of a fibrous mat is more akin to the effect of surface roughening where if the intrinsic contact angle is less than 90° roughening will enhance wetting whereas if it is greater than 90° roughening will enhance non-wetting (hence the superhydrophobic "lotus effect"). There would seem to be little difficulty during the preparation of glass fiber-reinforced compositions for reactive entities such as the methacryloxy groups on the silane treated glass and those in the resin to come together and covalently bond.

Moreover, there are other possible complications with interpreting the data presented in Table 4. Implicit in the preceding discussion is the assumption that since the methoxy groups interact with the substrate, it is the organic functionality that presents itself to the air and is probed by the contact angle test liquids. Nevertheless, this need not always be the case. Fowkes and co-workers (25), employing angle-resolved XPS and zeta potential measurements, found that both the methacryloxy-functional group of 3-methacryloxypropyl trimethoxysilane and the amino functional group of 3-aminopropyl trimethoxysilane were oriented towards the surface of a magnesium aluminum silicate glass powder. Wu et al. (13) included contact angle studies in their arsenal of surface characterization techniques of silane-treated silica hybrid nanoparticles and concluded that their surface energy reaches as low as 6.1 mNm. This seems only possible if aliphatic fluorocarbon-based entities are involved and can possibly be explained by roughness factors although nanoscale roughness as demonstrated by the SEM and AFM studies is not usually a major complicating factor as it is with microroughness. Whatever the reasons there are still reservations concerning the 3-methacryloxypropyltrimethoxysilane surface tension data presented in Table 4 and a new study using surfaces of proven surface composition would be welcome. The Johnson, Kendall and Roberts (JKR) (26) contact mechanics approach for determining surface energy involves no uncertainties as to choice of contact angle test liquids and interpretive equations. Chaudhury (27) has used this approach to determine the surface energy of plasma-oxidized poydimethylsiloxane elastomer surfaces treated with organofunctional trichlorosilanes including those with polar functionalities such as $-CO_2CH_3$. Perhaps a similar study using alkoxysilanes such as 3-methacryloxypropyltrimethoxysilane might be possible.

Concluding Comments

This silane continues to be a compound of great scientific interest. A Google Scholar search yields over 3,000 hits for the year 2012 alone. It is still widely used in established applications such as glass fiber reinforcement, other filler treatments, improvement of mechanical and electrical properties of electrical wire and cable, and in adhesives and coatings. However, one is struck by the number of studies in other areas as diverse as dental bases where 3-methacryloxypropyltrimethoxysilane is the most commonly used coupling agent (for example, see (*11*, *28*)), novel nanocomposites (*29*), and non-siliceous substrates (*30*). Silanes are known to form Si-O-M oxane bonds with surfaces containing the elements Si, Fe, Cr, Al, Zr, Pb, Sn, Ni and Ti but a much wider range of substrates is under investigation including C (coal, carbon nanotubes), CuS, Co-Cr alloys, Zn, B, Fe, and cellulosic microfibrils to give a few examples.

Acknowledgments

References

1. Matisons, J. G. In *Silicone Surface Science*; Owen, M. J., Dvornic, P. R., Eds.; Springer: Dordrecht, The Netherlands, 2012; Chapter 10.
2. Plueddemann, E. P. *Silane Coupling Agents*, 2nd ed.; Plenum Press: New York, 1991; Chapter 1.
3. Plueddemann, E. P. *Silane Coupling Agents*, 2nd ed.; Plenum Press: New York, 1991; Chapter 8.
4. Plueddemann, E. P.; Clark, H. A. U.S. Patent 3,258,477, 1966.
5. Matisons, J. G. In *Silanes and Other Coupling Agents*; Mittal, K. L., Ed.; VSP/Brill: Leiden, 2009; Vol. 5, p 3.
6. Green, E. *Composites Manufacturing* **2006** (Oct), 28.
7. Walker, P. In *Silanes and Other Coupling Agents*; Mittal, K. L., Ed.; VSP: Utrecht, The Netherlands, 1992; Page 21.
8. Johannson, O. K.; Stark, F. O.; Vogel, G. E.; Fleischmann, R. M. *J. Compos. Mater.* **1967**, *1*, 278.
9. Johannson, O. K.; Stark, F. O.; Vogel, G. E.; Lacefield, R. M.; Baney, R. H.; Flaningam, O. L. *Interfaces in Composites*; ASTM STP 452; American Society for Testing and Materials: 1969; p 168.
10. Garbassi, F.; Occhiello, E.; Bastioli, C.; Romano, G. *J. Colloid Interface Sci.* **1987**, *117*, 258.
11. Miller, J. D.; Ishida, H. In *Silanes Surfaces and Interfaces*; Leyden, D. E., Ed.; Gordon and Breach Science Publishers: New York, 1986; p 525.
12. Matinlinna, J. P.; Laajalehto, K.; Lassila, L. V. J.; Yli-Urpo, A.; Vallittu, P. K. In *Silanes and Other Couping Agents*; Mittal, K. L., Ed.; CRC Press: 2004; Vol. 3, p 21.

13. Wu, J.-R.; Lai, G.-Q.; Yu, H.-J.; Luo, Z.-H. *J. Appl. Polym. Sci.* **2012**, *124*, 3821.

14. Ishida, H.; Koenig, J. L. *J. Polym. Sci., Polym. Chem. Ed.* **1979**, *17*, 615.

15. Lee, L.-H. In *Adhesion Science and Technology*; Plenum: New York, 1975; Vol. 9B, p 647.

16. Browne, M. F.; Throckmorton, P. E. *SPI Reinforced Plastics Div. 20th Anniv. Tech. Conf.*; Chicago, 1965; p 1-15-A.

17. Sacher, E. In *Symposium on Silylated Surfaces*; Leyden, D. E., Collins, W., Eds.; Gordon and Breach: London, 1980; p 347.

18. Ellison, A. H.; Zisman, W. A. *J. Phys. Chem.* **1954**, *58*, 503.

19. Owens, D. K.; Wendt, R. C. *J. Appl. Polym. Sci.* **1969**, *13*, 1741.

20. Jarvis, N. L.; Fox, R. B.; Zisman, W. A. In *Contact Angle Wettability and Adhesion*; Advances In Chemistry Series No. 43; American Chemical Society: Washington, DC, 1964; p 317.

21. Kaelble, D. H.; Dynes, P. J.; Cirlin, E. H. *J. Adhes.* **1974**, *6*, 23.

22. Arkles, B.; Pan, Y.; Kim, Y. M. In *Silanes and Other Coupling Agents*; Mittal, K. L., Ed.; VSP/Brill: Leiden, 2009; Vol. 5, p 53.

23. Mansur, A. A. P.; Nascimento, O. L.; Vasconcelos, W. L.; Mansur, H. S. *Mater. Res.* **2008**, *11* (3), 293.

24. Plueddemann, E. P. *Silane Coupling Agents*, 2nd ed.; Plenum Press: New York, 1991; Chapter 4.

25. Fowkes, F.; Dwight, D.; Manson, J.; Lloyd, T. *Mater. Res. Soc. Symp. Proc.* **1988**, *119*, 223.

26. Johnson, K. L.; Kendall, K.; Roberts, A. D. *Proc. R. Soc. London, Ser. A* **1971**, 324–301.

27. Chaudhury, M. K. *J. Adhes. Sci. Technol.* **1993**, *7*, 669.

28. Chaijareenont, P.; Takahashi, H.; Nishiyama, N.; Arksornnukit, M. *Dent. Mater. J.* **2012**, *31*, 623.

29. Yu, Z.-Q.; You, S.-L.; Baier, H. *Polym. Compos.* **2012**, *33*, 1516.

30. Cheng, G.; Yu, X.; Tang, Z. *Adv. Mater. Res.* **2012**, *538−541*, 2246.

31. Plueddemann, E. P.; Clark, H. A.; Nelson, L. E.; Hoffman, K. R. *Mod. Plast.* **1962**, *39* (12), 135.

Chapter 5

Living Polymerization Routes to Siloxane Macromers and Higher Order Silicone Structures

Jonathan Goff,* Edward Kimble, and Barry Arkles

Gelest, Inc., 11 East Steel Road, Morrisville, Pennsylvania 19067
***E-mail: jgoff@gelest.com**

This report describes the synthesis, characterization and physical properties of symmetric silicone macromers, as well as new dual functional macromers, with both asymmetric and symmetric structures. Higher order silicone structures are introduced as convergent-branched silicones synthesized using hydride functional silicone macromer building blocks linked to a cyclic siloxane core. Silicone chain length, endgroup functionality and number of chains attached to the core have been studied to elucidate the physical properties of these higher order silicone structures.

Introduction

Functional siloxane polymers, commonly referred to as reactive silicones, constitute a large class of reactive materials. Siloxanes with vinyl, silanol and hydride substitution have the broadest utilization, serving as the basis for the majority of elastomeric silicone products (*1*). Functional siloxanes combined with organic monomers form "hybrid" polymers, which, while demonstrating utility, have comparatively limited commercial application (*2*). Most siloxane polymers are prepared by ring-opening polymerization with broad molecular weight distributions, which curtail their ability to act as precise structural elements. An alternative is to employ silicone macromers prepared by controlled "living" anionic ring-opening polymerization (AROP). Silicone macromers are defined as silicon containing species with a single functional polymerizeable group, which, although used as monomers, have sufficiently hig molecular weight and internal monomer units to be considered polymeric (*3*).

Monomer requirements for 'living' polymerization technique are more restrictive than standard acid/base catalyzed ring-opening polymerizations, requiring a cyclic siloxane with ring strain. Cyclic trimer monomers, such a hexamethylcyclotrisiloxane (D3), are commonly used. A lithium reagent is used to generate a lithium siloxanolate *in situ* and a polar aprotic solvent is used to form a lose ion pair between the siloxanolate and the lithium counter ion allow for propagation of the siloxane chains. The conditions and time scale of the 'living' AROP must be carefully considered to ensure that the propagation of the polymer chains occurs preferentially over chain scrambling and backbiting reactions. An endcapper is used to react with the siloxanolate once the monomer is consumed to add functionality. Siloxanes made from living polymerizations are reported to have PDIs close to unity. In addition to homopolymer silicones, the AROP technique can produce random or block copolymer structures depending on monomer choice and order of addition to the polymerization (*4*, *5*).

Traditional asymmetric silicone macromers with a single functional group synthesized by living polymerizations afford many desirable properties, including, narrow molecular weight distribution, high oxygen permeability, increased polarity and available reactive functionality. They can serve as precise structural elements to prepare hybrid copolymers. The methacrylate functional silicone macromers first reported nearly 25 years ago are representative of the typical structure (*6*):
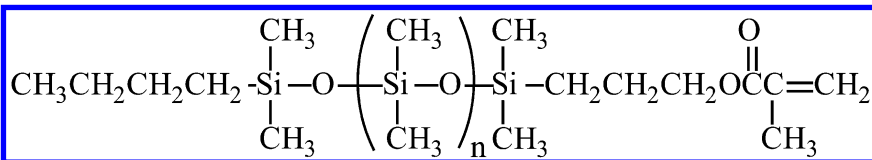

As depicted, the structure indicates the α-butydimethylsiloxy termination derived from the lithium butyldimethylsilanolate initiator, the repeating dimethylsiloxane unit derived from the ring-opening polymerization of the ring-strained hexamethylcyclotrisiloxane and the omega termination or "capping" functionality derived from methacryloxypropyldimethylchlorosilane.

Methacrylate functional macromers have been commercialized in pigment dispersion, adhesive release, controlled atmosphere food packaging and contact lens applications (*7–11*). To date, however, the utilization of silicone macromers has been limited primarily by economic, but also by structural and compositional considerations. Objectives for silicone macromer design include increasing their solubility range in organic monomers/solvents, retention of desirable siloxane properties without domain formation and improvement of economics (*3*).
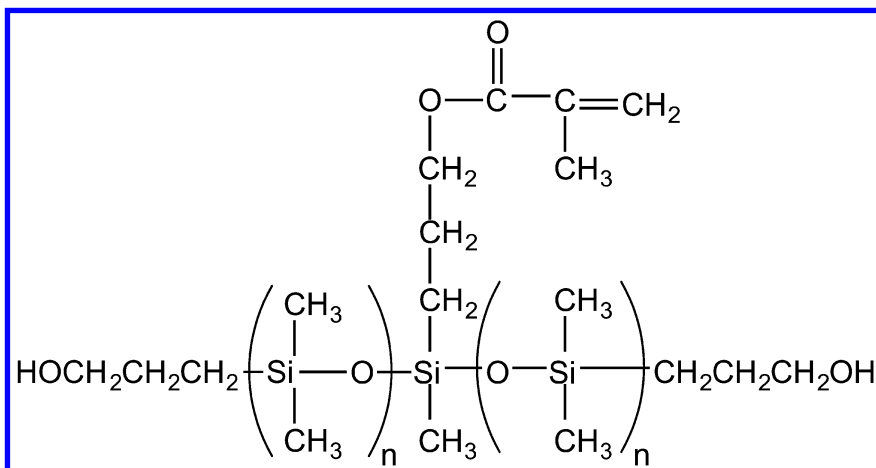
Silicone macromers with symmetric architectures can be readily formed via the anionic ring-opening polymerization of a cyclic trisiloxane and subsequent coupling with a functional dihalogen substituted silane reagent (*3*, *12*).
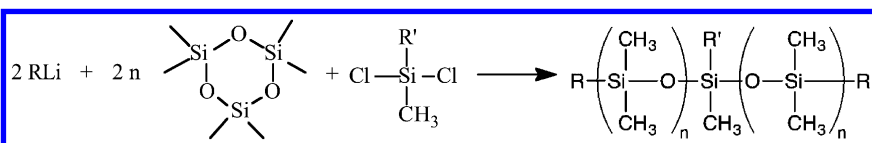
Symmetric macromers, for example, can contain a pendant methacrylate group bisecting the polydimethylsiloxane backbone.
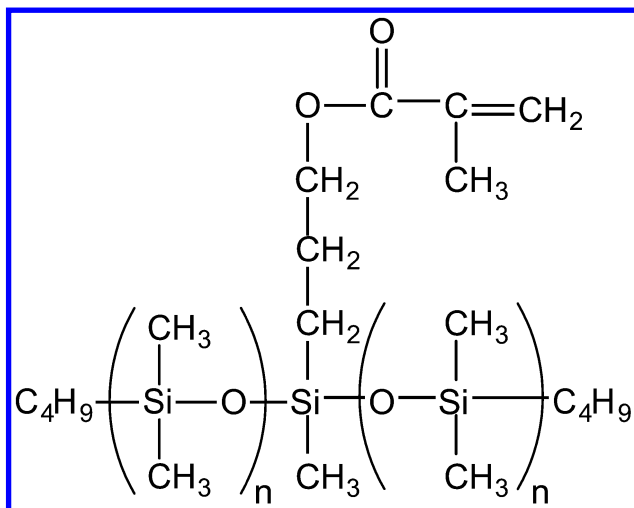
A second class of functionality can be introduced into macromers by using novel initiators, yielding telechelic polymers in which the second functional class, for example hydroxyl, is at the telechelic polymer termini, which are equidistant from the first functional class (*12*).

This report describes the synthesis, characterization and physical properties of symmetric silicone macromers, as well as new dual functional macromers, with both asymmetric and symmetric structures. Higher order silicone structures are introduced as convergent-branched silicones synthesized using hydride functional silicone macromer building blocks linked to a cyclic siloxane core. Silicone chain length, endgroup functionality and number of chains attached to the core have been studied to elucidate the physical properties of these higher order silicone structures.

Experimental

Materials

Hexamethylcyclotrisiloxane (D_3, 98%), (3,3,3-trifluoropropyl)methylcyclo-trisiloxane (97%), dimethylchlorosilane (97%), methyldichlorosilane (97%), trichlorosilane (97%), methacryloxypropyldimethylchlorosilane (95%, inhibited with MEHQ), methacryloxypropylmethyldichlorosilane (95%, inhibited with MEHQ), methacryloxypropyltrichlorosilane (95%, inhibited with MEHQ), platinum-divinyl tetramethyldisiloxane catalyst (Karstedt catalyst, 2.2 wt% Pt), 1,3,5,7-tetravinyl-1,3,5,7-tetramethylcyclotetrasiloxane (D_4vinyl, 97%), 3-methoxypropyl lithium (1.3 M in hexanes) and 3-(t-butyldimethylsiloxy)-1-propyl lithium (1.0 M in cyclohexane) were obtained from Gelest and used as received. n-Butyl lithium (2.6 M in hexanes, Chemetall-Foote), tetrahydrofuran (THF, HPLC grade, J.T. Baker), hexanes (Ashland Chemical), glacial acetic acid (Quaker City), and ethanol (Quaker City) were used without further purification.

Synthesis of Methacrylate Functional Asymmetric Silicone Macromers

An exemplary synthesis of a 1,000 g mol^{-1} monomethacryloxypropyl terminated poly(dimethylsiloxane) asymmetric macromer (MCR-M11) is provided. In the case of a 1,000 g mol^{-1} monomethacryloxypropyl terminated poly(trifluoropropylmethylsiloxane) (MFR-M15) synthesis, (3,3,3-trifluoropropyl)methylcyclotrisiloxane is substituted for hexamethyl-cyclotrisiloxane (D_3). Other molecular weight asymmetric silicone macromers can be synthesized in an analogous manner by adjusting monomer to initiator ratios to control polymer chain length. D_3 (250 g, 1.12 mol) and hexanes (230 mL) were added to a 1 L round bottom flask containing a magnetic stir bar. The flask was purged with nitrogen and the reaction mixture was stirred at room temperature until the D_3 monomer was dissolved. n-Butyllithium (2.6 M, 96.0 mL, 0.250 mol) was added to the reaction flask via addition funnel and the solution was stirred for 1 h, followed by the addition of THF (100 mL) to the solution as polymerization promoter. Upon ~95% conversion of monomer (3 h), the polymer was terminated with a slight excess of methacryloxypropyldimethylchlorosilane (55.2 g, 0.250 mol). The solution was stirred overnight and washed three times with deionized water. The organic layer was dried with MgSO$_4$ and concentrated under vacuum at 80 °C. The resulting MCR-M11 macromer was characterized using ^{1}H NMR and GPC.

Synthesis of Methacrylate Functional Symmetric Silicone Macromers

An exemplary synthesis of a 1,000 g mol^{-1} bis(n-butyl terminated poly-[dimethylsiloxane])methylmethacryloxypropylsilane symmetric macromer (MCS-M11) is provided. In the case of a 1,000 g mol^{-1} bis(n-butyl terminated polytrifluoropropylmethylsiloxane)methylmethacryloxypropylsilane (MFS-M15) synthesis, (3,3,3-trifluoropropyl)methylcyclotrisiloxane is substituted for D_3. Following a living anionic ring opening polymerization procedure previously described for MCR-M11, D_3 (125 g, 0.562 mol) dissolved in

hexanes (224 mL) was initiated with n-butyllithium (2.6 M, 96.0 mL, 0.250 mol) followed by addition of THF (110 mL) to promote propagation of the silicone chains. At 95% consumption of the D_3 monomer (3 h) the lithium siloxanolate chain ends were coupled using a stoichiometric amount of methacryloxypropylmethyldichlorosilane (30.1 g, 0.125 mol). The solution was stirred overnight and washed three times with deionized water (3 X 200 mL). The organic layer was dried with $MgSO_4$ and concentrated under vacuum at 80 °C. The resulting MCS-M11 macromer was characterized using ^{1}H NMR and GPC.

Synthesis of Methacrylate Functional T-Structure Silicone Macromers

A 1,000 g mol^{-1} tris(n-butyl terminated poly[dimethylsiloxane])-methacryloxypropylsilane (MCT-M11) was synthesized using a D_3 anionic ring opening polymerization procedure similar to the synthesis of MCR-M11 and MCS-M11. Once the propagating silicone chains reached the desired length, a stoichiometric amount of methacryloxypropyltrichlorosilane was added to the reaction mixture to couple the lithium siloxanolate chain endgroups. The MCT-M11 was worked up as previously described and characterized using ^{1}H NMR and GPC.

Synthesis of Dual Functional Silicone Macromers

Anionic lithium initiator alternatives to n-butylithium were investigated, including methoxypropyllithium and 3-(t-butyldimethylsiloxy)-1-propyl lithium, for the purpose of introducing hydrophilic chain endgroups in the silicone macromer structure. The synthesis of a targeted 1,000 g mol^{-1} bis(hydroxypropyl terminated poly[dimethylsiloxane])methacryloxypropylmethylsilane (MCS-MC12) is provided. D_3 (85.0 g, 0.382 mol) was dissolved in hexanes (90 mL) in a 1 L roundbottom flask containing a magnetic stir bar with nitrogen purge. The polymerization was initiated with the addition of the silylated or "blocked" initiator, 3-(t-butyldimethylsiloxy)-1-propyl lithium, (1.0 M, 382 mL, 0.382 mol) via addition funnel and the solution was allowed to stir for 1 h. THF (92 mL) was added to the reaction mixture to promote the propagation of the silicone chain ends. Methacryloxypropylmethyldichlorosilane (46.1 g, 0.191 mol) was added to the reaction mixture after 2 h to couple the lithium siloxanolate chain endgroups. The solution was stirred overnight and washed three times with deionized water (3 X 200 mL). The organic layer was dried with $MgSO_4$ and concentrated under vacuum at 80 °C. The resulting macromer precursor was characterized using ^{1}H NMR and GPC.

The t-butyldimethylsiloxylpropyl endgroups were deblocked using mildly acidic deprotection conditions to form a hydroxypropyl terminated symmetric silicone macromer. MCS-MC12 precursor (70.0 g, 0.073 mol) containing protected hydroxyl groups was dissolved in ethanol (160 mL) in a 500 mL roundbottom flask containing a magnetic stir bar. 10 mL of a 67 wt% aqueous acetic acid solution was added to the reaction mixture. The solution was stirred under nitrogen for 24 h. Water (140 mL) was added to the stirring solution followed by addition of hexanes (200 mL). The solution was allowed to stir for

15 minutes and was transferred to a 1 L separatory funnel. The organic layer was collected and washed with a 5 wt% aqueous sodium bicarbonate solution (200 mL) until the pH was neutral. The organic layer was dried with $NaSO_4$ and concentrated under vacuum at 100 °C with a dry air sparge. Deprotection of the MCS- MC12 endgroups was quantified using various spectral techniques.

Methoxypropyllithium was used as the initiator in a similar procedure to yield monomethoxypropyl-, monomethacryloxypropyl- terminated poly(dimethylsiloxane) (MCR-ME11) and bis(methoxypropyl-terminated poly[dimethylsiloxane])methacryloxypropylmethylsilane (MCS-ME11).

Synthesis of Hydride Functional Branched Silicone Precursors

Asymmetric, symmetric and T structure silicones containing hydride functionality were synthesized using living anionic ring opening polymerization techniques. A characteristic procedure for the synthesis of a 900 g mol^{-1} hydride functional asymmetric silicone is provided. D_3 (200.0 g, 0.900 mol) and hexanes (205 mL) were charged to a 1 L round bottom flask containing a magnetic stir bar. The mixture was stirred for 1 h under nitrogen. n-Butyl lithium (2.6 M, 103.0 mL, 0.270 mol) was charged to the flask via addition funnel and the mixture was stirred for 1 h. THF (90 mL) was added to the flask and the polymerization was monitored during the propagation step. At 95% consumption of D_3 (4 h) an excess of dimethylchlorosilane (27.0 g, 0.285 mol) was added to the solution. The solution was stirred overnight and washed three times with deionized water (3 X 200 mL). The organic layer was dried with $MgSO_4$ and concentrated under vacuum at 80 °C. The resulting precursor to convergent-branched silicone structures (MCR-H07) was characterized using ^{1}H NMR and GPC.

Convergent Branched Silicone Synthesis

A characteristic procedure for the synthesis of a MCR-H07 (α-monobutyl, ω-monohydride terminated polydimethylsiloxne DP=10) convergent-branched silicone is provided. 1,3,5,7-tetravinyl-1,3,5,7-tetramethylcyclotetrasiloxane (D_4vinyl) (43.40 g, 0.126 mol) and 2.4 g of platinum-divinyl tetramethyldisiloxane catalyst in xylene (2.2 wt% Pt) were charged to a 1 L roundbottom flask containing a magnetic stir bar. The reaction mixture was heated to 90 °C under nitrogen with stirring. A 900 g mol^{-1} hydride functional asymmetric silicone (450 g, 0.50 mol) was added over 2 h to the reaction mixture via addition funnel. The flask temperature was increased to 110 °C and the reaction mixture was allowed to stir for an additional 3 h while monitoring reaction progress by FTIR. The reaction was heated under vacuum at 110 °C for 1 h and filtered over celite. The product was characterized by ^{1}H NMR and GPC.

Characterization

^{1}H NMR spectral analyses of compounds were performed on a 400MHz Jeol NMR using CDCl$_3$ as solvent. A Thermo Nicolet Avatar 360 was used for FTIR

measurements. Viscosities were measured using a Brookfield Viscometer Model DV-II+ at 25.0 °C.

A Viscotek GPC Max VE2001 with a TDA 301 detector equipped with a Viscotek LT5000L mixed medium organic column was used for gel permeation chromatography (GPC) analyses. GPC data were collected in THF at 35 °C. Data were analyzed with a refractive index detector using a calibration made with polystyrene standards. Thermogravimetric Analysis (TGA) of the macromers was performed using a TA Instruments TGA Q50. Samples were equilibrated at 25 °C and the temperature was ramped at 10 °C min-1 to 700 °C in both nitrogen and air atmospheres.

Rheological measurements were carried out using a TA Instruments AR2000 equipped with a TA Instruments Environmental Test Chamber at 25 °C using 40 mm stainless steel parallel plates. Samples were analyzed using a steady state flow experiment, where viscosity was measured as a function of shear rate (0.01-500 s-1).

Results and Discussion

Description of Polymer Designations

In order to provide a concise description of the macromer systems discussed, the following designation was adopted: The first two letters MC indicate macromer M structure with a C conventional dimethylsiloxane repeat unit. The third letter indicates whether it is asymmetric R, symmetric S or T for "T-structure." Functionality and viscosity of the macromer are indicated after a hyphen as follows: 1) letters indicate functionality where M is methacrylate, H is hydride, C is carbinol, V is vinyl, E is methoxy; and 2) numbers are the viscosity ranges of the macromer in powers of 10 followed by the first significant figure. For example MCR-H25 indicates a macromer, an asymmetric architecture with hydride functionality and a viscosity of 10^2 x 5 or 500 cSt. For branched silicones the core or hub is designated, followed by the number of branchpoints or spokes at the hub and the DP of the spokes. These designations are provide a facile method of discussing comparative structures, but are not intended to be detailed descriptions of the polymer structures.

Methacrylate Functional Silicone Macromers

The synthesis of methacrylate functional silicone macromers requires a well-defined polymerization approach. Macromolecular design objectives for silicone macromers include increasing their solubility in polar monomers or solvents, retention of desirable siloxane properties and improvement of economics (*3*, *12*). Due to the lack of controlled chain length and inability to have a single functional group on a silicone, chain growth equilibration polymerizations of silicones are unsuitable for the synthesis of silicone macromers. Chain growth equilibration polymerization of cyclic siloxanes is widely used approach for the synthesis of functional silicones in industry (*13*). This approach utilizes a disiloxane endcapper reagent and an acid or base catalyst with no restrictions

on the ring size of the cyclic siloxane monomer. Silicone polymer growth is achieved by the insertion of the monomer into an active chain center, leading to an equilibrium consisting of approximately 85% functional silicone and a remainder of cyclics and oligomeric siloxanes (Scheme 1). Functional silicones synthesized via this polymerization technique have broad molecular weight distributions with a polydispersity index (PDI) typically ≥ 2.
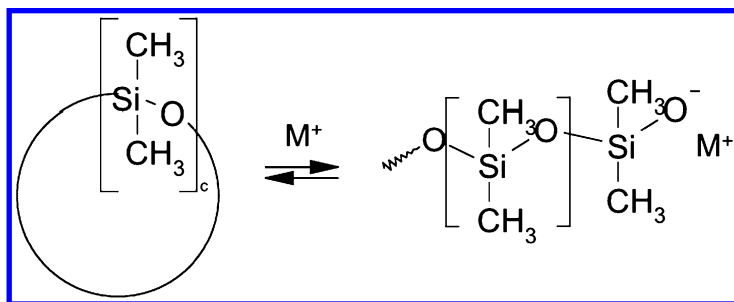
Scheme 1. Base catalyzed chain growth equilibration of cyclic siloxanes. [c = 3, 4, 5, 6, etc.; M⁺ = Na⁺, K⁺, Cs⁺, R₄N⁺, etc.]

Silicones derived from chain growth equilibration techniques are limited by the polymer architectures achievable using a disiloxane endcapper. Acrylate functional silicones synthesized by chain growth equilibrations (e.g. bis(methacryloxypropyl) terminated polydimethylsiloxane and bis(acryloxy-hydroxypropoxypropyl) terminated polydimethylsiloxane) have a telechelic structure, which does not fit the definition of a macromer structure (Figure 1).
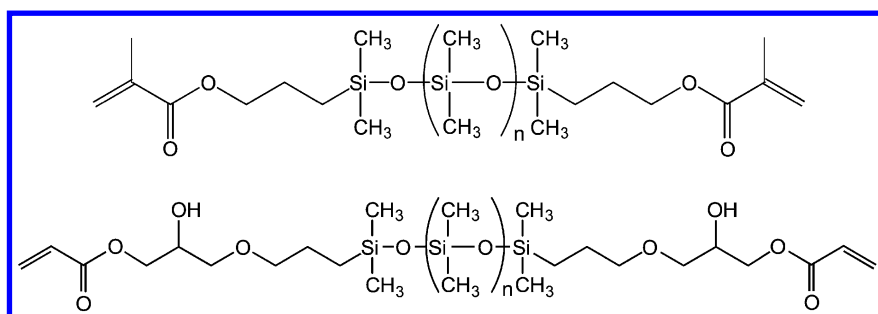

Figure 1. Acrylate functional silicone telechelic structures synthesized by chain growth equilibration techniques. Bis(methacryloxypropyl) terminated PDMS (top) and bis(acryloxyhydroxypropoxypropyl) terminated PDMS (bottom).

The limitations of the chain growth approach led to investigation of other polymerization techniques. Living anionic ring opening (AROP) polymerization techniques were found to be suitable for the synthesis of methacrylate functional

silicone macromers with different architectures. This approach uses an alkyl lithium reagent as an initiator, a cyclic siloxane monomer with ring strain, such as D_3, and a polar aprotic solvent to drive propagation of the siloxane chains (Scheme 2) (*13–16*). A combination of monomers may be used to produce block copolymers from the living AROP approach (*4*). Molecular weight was controlled by adjusting the monomer to initiator ratios, leading to controlled silicone chain lengths with PDIs near unity. Equimolar amount of chlorosilane to lithium siloxanolate was used to obtain the targeted methacrylate functional silicone macromer architectures and reduce the high molecular weight methacrylate impurities associated with the addition of excess chlorosilane.
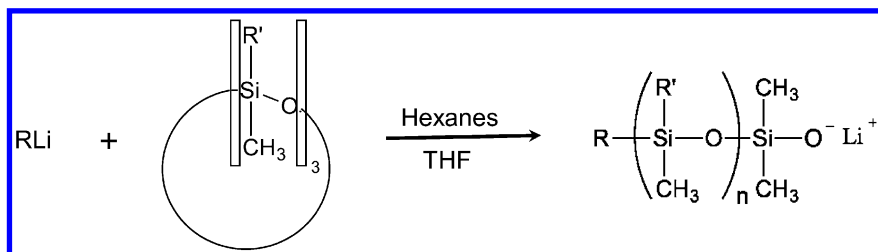
Scheme 2. AROP of cyclic trisiloxanes yields propagating silicone chains with 'living' lithium siloxanolate chain ends. Use of a functional chlorosilane (e.g. methacryloxypropyldimethylchlorosilane) to endcap the chain ends yields a silicone macromer structure. [R = CH₃-, n-butyl-, C₄H₉Si(CH₃)₂O(CH₂)₃-, CH₃O(CH₂)₃- ; R' = CH₃-, CF₃(CH₂)₂-]

The simplest methacrylate functional silicone macromer, MCR-M11, is a well- defined polymer with a single functional group, asymmetric architecture and a controlled branch length. Silicone macromers have four main components that can be altered to yield materials with different bulk properties and functionalities: 1) initiator selection, 2) polymer backbone structure, 3) endgroup functionality and 4) molecular weight of the macromer. In the initial investigation into methacrylate functional silicone macromers, endgroup functionality and number of siloxane units (DP=10) were held constant. Polymer backbone structure modification of asymmetric silicone macromers utilized trifluropropyltrimethylcyclotrisiloxane monomer, introducing a polar 3,3,3-trifluoropropyl side group on each repeat unit in the polymer backbone. The resulting macromer, MFR-M15, had an increased polarity, decreased refractive index (RI) and a decreased solubility in hydrocarbon solvents due to the influence of the trifluoropropyl groups. Main chain structure modification addresses the silicone macromer objective of increased solubility ranges, but the reduction of siloxane domain formation objective is unaddressed. Domain formation is associated with polymer block size. To achieve a reduction in block size while maintaining siloxane content, silicone macromer architecture modifications were investigated in conjunction with main chain and initiator modifications.

Modifying the silicone macromer to have a symmetric architecture with central methacrylate functionality and dimethylsiloxane (MCS-M11) or

trifluoropropylmethylsiloxane (MFS-M15) backbone units decreased the relative block size of the siloxane compared to asymmetric macromers of similar molecular weight (~1,000 g mol^{-1}). Structural analysis of the symmetric silicone macromers by ^{1}H NMR revealed a 2:1 stoichiometry between the n-butyl endgroups and the central methacryloxypropyl group, indicating a well-defined architecture (Figure 2).

The macromolecular design approach utilized for methacrylate functional silicone macromers allows for a maximum of three silicone pendant chains per methacrylate functional group. A 1,000 g mol^{-1} T-structure silicone macromer (MCT-M11) architecture further reduces the relative siloxane block size compared to their asymmetric and symmetric counterparts. At high molecular weights, the economics are favorable for T-structures, however, the economics of producing such materials at low molecular weights are unfavorable due to the required stoichiometry of three moles of initiator to produce one mole of macromer. Figure 3 illustrates the different methacrylate functional silicone macromer architectures synthesized.

In addition to silicone backbone and architecture modification, the initiator can be modified to add reactive or polar chain endgroups to the macromers. Polar functionalities are of specific interest for the methacrylate functional silicone macromers, leading to research effort to develop novel living AROP initiators. 3-Methoxypropyl lithium and 3-(t-butyldimethylsiloxy)-1-propyl lithium were investigated for the methacrylate functional silicone macromer series, leading to methoxypropyl and hydroxypropyl chain endgroups respectively (*3*, *12*). Symmetric silicone macromers with polar chain endgroups, such as MCS-MC12 and MCS-ME11, combine reduced siloxane block size with the presence of hydrophilic endgroups to help achieve the objective of increased macromer solubility in polar solvents or monomers.

Table 1 shows the characterization data for the series of DP=10 methacrylate functional silicone macromers synthesized via living AROP techniques. NMR and GPC analysis showed good agreement between molecular weights with monomodal peaks and low molecular weight distributions (PDI), indicating precise control over the design of silicone macromer architecture and chain length to obtain desired properties.

The effect of backbone and architecture macromer modification on solubility in dimethylacrylamide (DMA) and hydroxyethylmethacrylate (HEMA) is illustrated in Table 2. MCS-M11 has increased solubility in the polar monomers compared to the asymmetric MCR-M11. The decreased siloxane block size reduces the tendency towards phase separation, leading to an increased solubility in polar monomers. Introducing methoxypropyl endgroups in an asymmetric architecture (MCR-ME11) also increased the solubility of the macromer in polar monomers. The contribution of a polar endgroup did not modify the solubility profile of the macromer as significantly as the reduced block size of the symmetric architecture. Backbone modification of the symmetric macromer to contain trifluoropropyl pendant groups also had a drastic effect on solubility, leading to complete miscibility of MFS-M15 in DMA and a doubling of solubility in HEMA compared to MCR-M11.
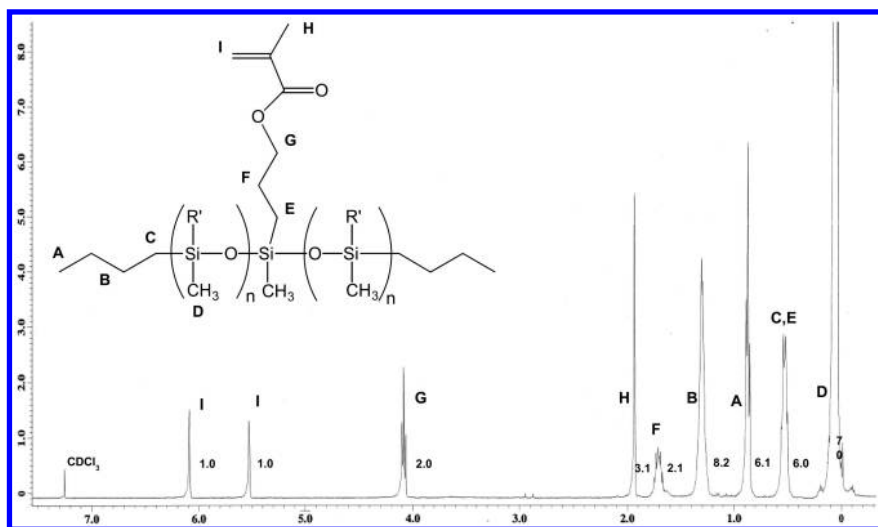
Figure 2. ¹H NMR analysis of MCS-M11 synthesized via living anionic ring opening polymerization shows a well-defined structure with no impurities.

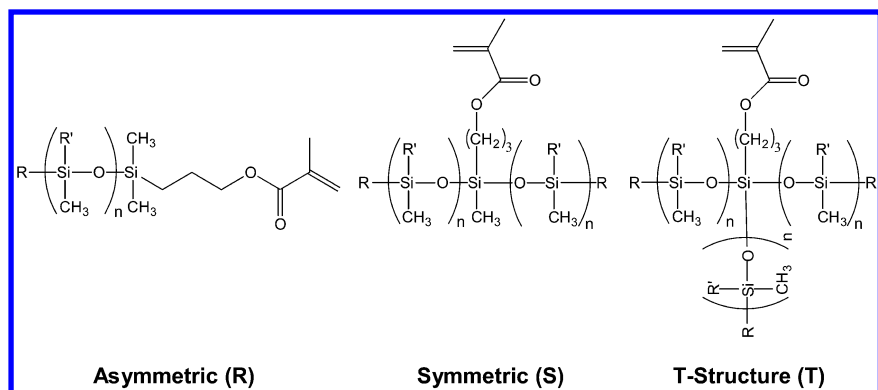**Asymmetric (R)**   **Symmetric (S)**   **T-Structure (T)**

Figure 3. Asymmetric (MCR-M11/MFR-M15/MCR-ME11), Symmetric (MCS-M11/MFS- M11/MCS-MC12/MCS-ME11), and T Structure (MCT-M11) Silicone Macromer Structures. [R = CH₃-, n-butyl-, HO(CH₂)₃-, CH₃O(CH₂)₃-; R' = CH₃-, CF₃(CH₂)₂-]

Table 1. Characterization data of methacrylate functional silicone macromers.

Methacrylate Functional Silicone Macromer ($D_p \sim 10$)	Chain Endgroup	Backbone Structure	M_n GPC (g mol^{-1})	Reported PDI[a]	Viscosity (cSt)
MCR-M11 (asymmetric)	n-butyl	$Si(CH_3)_2O$	1050	1.3	11
MFR-M15 (asymmetric)	n-butyl	$Si(CF_3[CH_2]_2Me)O$	1300	1.2	55
MCR-ME11 (asymmetric)	methoxypropyl	$Si(CH_3)_2O$	900	1.2	13
MCS-M11 (symmetric)	n-butyl	$Si(CH_3)_2O$	1250	1.2	9
MFS-M15 (symmetric)	n-butyl	$Si(CF_3[CH_2]_2Me)O$	970	1.2	44
MCS-ME11 (symmetric)	methoxypropyl	$Si(CH_3)_2O$	840	1.2	9
MCS-MC12 (symmetric)	hydroxypropyl	$Si(CH_3)_2O$	1100	1.3	17
MCT-M11 (T-structure)	n-butyl	$Si(CH_3)_2O$	990	1.4	9

[a] PDIs from GPC are reported without deconvoluting macromer peak from solvent and low MW (e.g. inhibitor) interference.

Table 2. Solubility study of macromers with polar monomers and water.

Macromer	Solubility in DMA (wt%)	Solubility in HEMA (wt%)	H₂O Haze Point (ppm)
MCR-M11	4	1	1500
MCS-M11	8	2	3500
MCR-ME11	5	2	3000
MFS-M15	100	2	9000

Comparing the solubility of the macromers in water, a trend similar to the solubility in polar monomers was observed (Table 2). The reported haze points of the macromer in water increased when architecture, chain endgroup and backbone modifications were introduced in the silicone macromer structure. A combination of these modifications could be employed to further improve the solubility range of the silicone macromers.

Hydride Functional Silicone Macromers

Living AROP macromolecular design approach can produce macromer building blocks for higher order silicone structures. From this perspective, hydride functional silicone macromers can be viewed as the simplest structural element of a branched silicone structure (Figure 4). Convergent-branched silicones were synthesized by linking the hydride functional silicone macromers to a cyclic siloxane core via hydrosilylation chemistry.
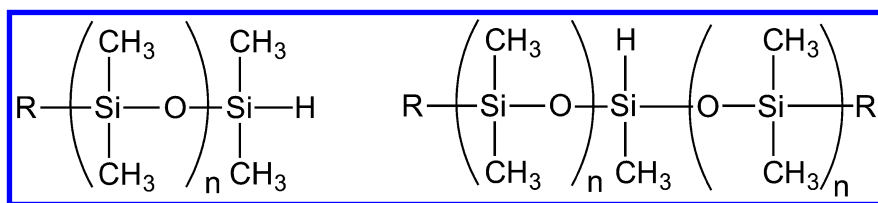

Figure 4. Asymmetric (MCR-H; left) and symmetric (MCS-H; right) hydride functional silicone macromers. [R = CH₃-, n-butyl-, C₄H₉Si(CH₃)₂O(CH₂)₃-, CH₂=CH-]

Degree of branching in the higher order silicone structures can be controlled by modifying the architecture of the hydride functional silicone macromer (asymmetric vs. symmetric). Convergent higher order silicone structures can be generated utilizing D₄vinyl as the cyclic siloxane as a core and reacting with a macromer (Figure 5). Reacting an asymmetric monohydride functional macromer, which can be visualized as possessing a single siloxane pendant, generates a structure with four monospokes. Reacting a symmetric monohydride functional macromer, which can be visualized as possessing two siloxane pendants, generates a structure with four dispokes. T-structure hydride functional

silicone macromers, which would in principle lead to a trispoke structure, were investigated, but was abandoned for economic reasons and the inability to quantitatively hydrosilylate the macromer onto the cyclic siloxane core.
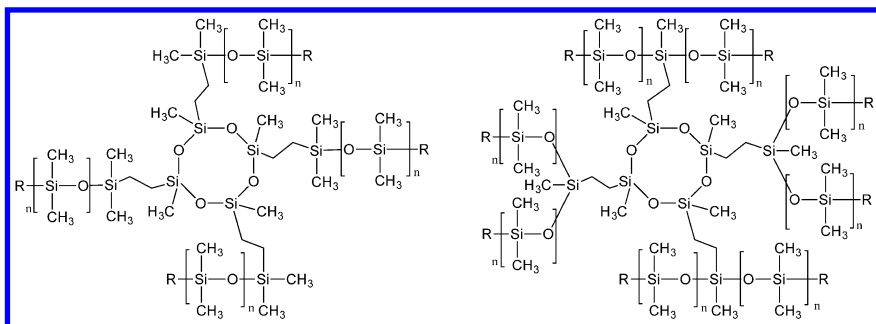

Figure 5. Monospoke (left) and dispoke (right) convergent-branched silicones with a D$_4$Vinyl hub. [R = CH$_3$-, n-butyl-, HO(CH$_2$)$_3$-, CH$_3$O(CH$_2$)$_3$-]

Previously described initiator modification techniques were employed to synthesize dual functional silicones with functional endgroups (e.g. protected siloxylpropyl or vinyl) (*12*, *17*). A series of hydride functional silicones were synthesized for use as precursors for convergent-branched silicone structures (Table 3). The number of D units per siloxane block was held constant between asymmetric and symmetric architectures to allow for direct comparison of branching effects between the higher order silicone structures. Good molecular weight agreement was observed between GPC, NMR and our targeted molecular weights. Low PDIs are indicative of controlled living polymerization technique. The recorded viscosities of the hydride functional silicone macromers were typical of silicones of their respective MWs.

Convergent Branched Silicones

Assembled silicone macromer structures attached to metal oxide cores have been reported in literature (*18*, *19*). A similar approach with hydride functional silicone macromers would allow access to convergent, branched architectures with a variety of cores (*20*). Higher order silicones were synthesized by attaching the hydride functional silicone building blocks to a cyclic siloxane core (D$_4$Vinyl) in a convergent approach using hydrosilylation chemistry. The structure of the convergent-branched silicones can be tailored for number of branches and functionality on the branch termini via design of the hydride functional silicone macromer precursors (Figure 5). Deblocking the t-butyldimethylsiloxypropyl endgroups of the precursor macromer under acidic conditions after the hydrosilylation step revealed hydroxypropyl termination on the branch termini.

Table 3. Characterization data of hydride functional silicone precursors for branched silicone structures.

Hydride Functional Silicone Macromer	Chain Endgroup	# D Units/PDMS Block	Targeted MW (g mol⁻¹)	Mn GPC (g mol⁻¹)	PDI	Viscosity (cSt)
MCR-H07 (asymmetric)	n-butyl	10	900	1090	1.2	7
MCR-H11 (asymmetric)	n-butyl	20	1,560	1,530	1.3	13
MCR-H14 (asymmetric)	n-butyl	50	3,800	4,080	1.2	43
MCR-HC12 (asymmetric)	siloxypropyl	20	1,640	1,850	1.3	17
MCS-H14 (symmetric)	n-butyl	20	3,140	3,220	1.2	44
MCS-H21 (symmetric)	n-butyl	50	7,600	8,200	1.2	104
MCS-HC14 (symmetric)	siloxypropyl	20	3,300	3,700	1.3	45

Table 4. Characterization data of the convergent branched silicones.

Convergent Branched Silicone (D₄Vinyl Hub)	Chain Endgroup	# D Units/Branch	Targeted MW (g mol⁻¹)	M_n GPC (g mol⁻¹)	PDI	Viscosity (cSt)
MCR-H07 (monospoke)	n-butyl	10	4,700	4,400	1.4	37
MCR-H11 (monospoke)	n-butyl	20	6,400	6,050	1.4	66
MCR-H14 (monospoke)	n-butyl	50	16,700	16,900	1.7	236
MCR-HC12 (monospoke)	hydroxypropyl	20	8,000	9,850	2.5	165
MCS-H14 (dispoke)	n-butyl	20	12,500	10,500	1.4	91
MCS-H21 (dispoke)	n-butyl	50	33,500	33,400	1.8	329
MCS-HC14 (dispoke)	hydroxypropyl	20	16,300	11,400	2.8	400

Molecular weight characterization and solubility properties of these materials were studied. Molecular weight characterization showed good agreement with the theoretical MW (Table 4). The PDI of the higher order silicones increased from the precursor monohydride functional macromers. The observed broadening of molecular weight distribution increased with molecular weight and number of the silicone branches in the assembled higher order structure. The broadening of the molecular weight distribution is attributable to the efficiency of hydrosilylation of the precursors onto the D_4Vinyl hub.

Solubility of water in the branched structures, while retaining the core silicone properties, can be increased with hydrophilic termination of the silicone branches (Table 5). The solubility differences between n-butyl terminated silicones and hydroxypropyl silicones were studied. In the case of monospoke DP=20 branched materials, the solubility of water was doubled from butyl to hydroxypropyl termination. The observed increase in solubility of water was not as dramatic for the dispoke branched materials. It was observed that the hydroxypropyl terminated materials had significantly greater ability to disperse in aqueous phases.

Table 5. Solubility study of higher order silicones with water.

Convergent Branched Silicone (D₄Vinyl Hub)	Chain Endgroup	# D Units/ Branch	H₂O Haze Point (ppm)
MCR-H11 (monospoke)	n-butyl	20	300
MCR-HC12 (monospoke)	hydroxypropyl	20	600
MCS-H14 (dispoke)	n-butyl	20	290
MCS-HC14 (dispoke)	hydroxypropyl	20	530

Rheological studies were performed on higher order and linear, chain growth equilibration silicones to highlight the differences in behavior. Comparing the viscosity as a function of shear rate, a shear-thinning region of non-Newtonian behavior was observed for all convergent-branched silicones. The curves reached a Newtonian plane at higher shear rates. The viscosity at specific shear rates increased with MW and number of spokes extending from the core. The predicted behavior of these materials, like dendrimers, should be Newtonian (*20*). However, little difference in rheological behavior is observed between these convergent-branched silicones and linear silicones for the lower molecular weight materials (Figure 6). This corresponds to theoretical models where the reptation component is reduced and the gyration component is maintained (*21*).

Deviation in rheological behavior was observed between the higher molecular weight (33,000 g mol⁻¹) dispoke branched silicone and linear silicone (40,000 g mol⁻¹) (Figure 7). An explanation for this phenomenon is that silicone chains begin to entangle at higher molecular weights. The 33,000 g mol⁻¹ dispoke branched silicone contains relatively short DP=50 pendants and will not chain entangle.
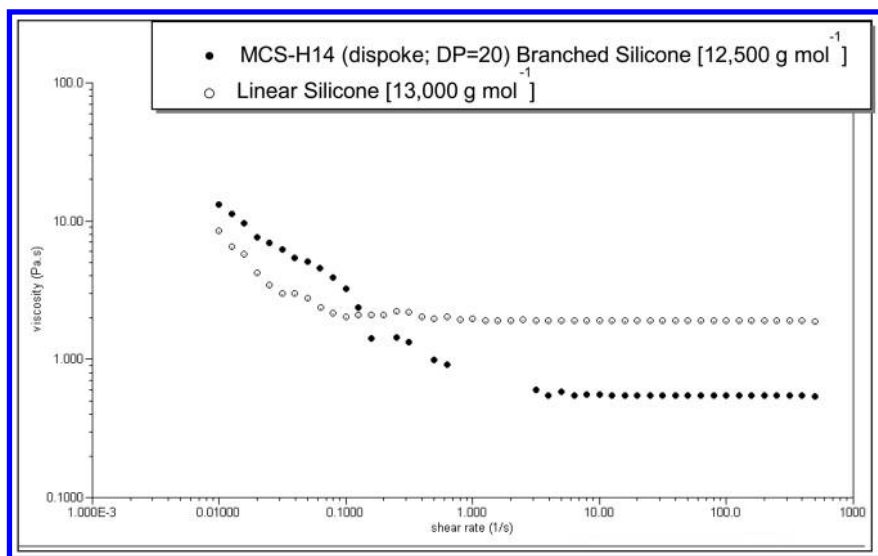
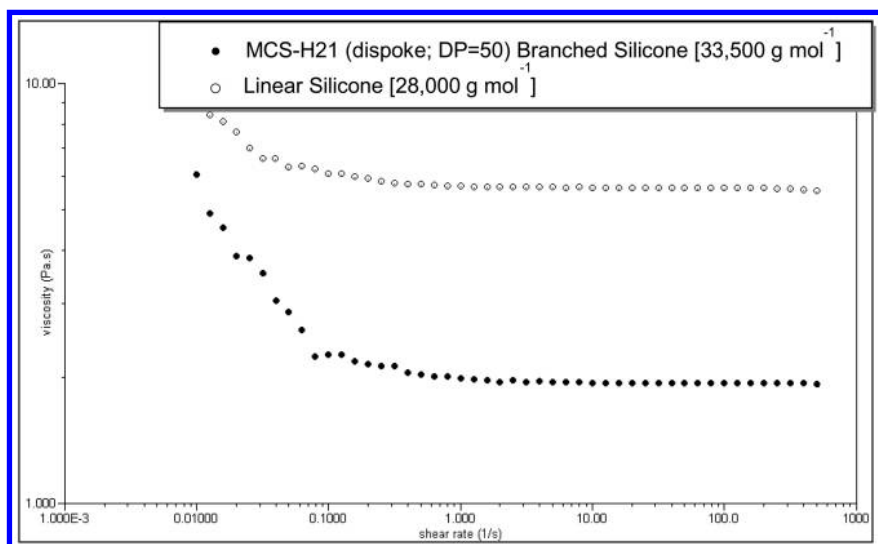*Figure 6. Rheological comparison of lower molecular weight branched silicone and linear silicone materials.*

Figure 7. Rheological comparison of higher molecular weight branched silicone and linear silicone materials.

Conclusions

The structures of silicone macromers have been significantly elaborated. By utilization of a "coupling" rather than "capping" approach to living polymerization, symmetric and T-structures are readily available. The interruption the dimethylsiloxane backbone at a central point formed during the coupling reaction reduces the opportunity for domain formation and phase separation compared to asymmetric monomers of equivalent molecular weight. Utilization of polar and blocked initiators can further modify compatibility with organic monomers. The revealed deblocked initiator segments provide access to dual-functional siloxanes. These materials have telechelic functionality with a different central functionality, allowing them to behave as building blocks for higher order structures, for example convergent-branched silicones with cyclic siloxane cores.

References

1. Noll, W. *Chemistry and Technology of Silicones*; Academic: 1968.
2. Arkles, B. Commercial hybrid organic-inorganic polymers. In *Organosilicon Chemistry: Molecules to Materials*; Auner, N., Weiss, J., Eds.; Wiley-VCH Verlag GmbH: 2000; Vol. IV, pp 592−612.
3. Kimble, E.; Arkles, B.; Cameron, R. Symmetric silicone macromers. *Polym. Prepr. (Am. Chem. Soc., Div. Polym. Chem.)* **2009**, *50* (2), 859–860.
4. Noshay, A.; McGrath, J. E. *Block Copolymers. Overview and Critical Survey*; Academic Press: 1977; 516 pp.
5. Bostick, E. E. *Synthesis and properties of siloxane block polymers*; Plenum: 1970; pp 237−247.
6. Anderson, R.; Arkles, B. C.; Larson, G. L. *Silicon Compounds Register & Review* **1987**, *4*, 271.
7. Sun, J. X.; Beach, B. B. Chemically Prepared Toner and process therefor. U.S. Patent 6,991,884 B2, 2006.
8. Vanderlaan, D. G.; Turner, D. C.; Hargiss, M. V.; Maiden, A. C.; Love, R. N.; Ford, J. D.; Molock, F. F.; Seteffen, R. B.; Hill, G. A.; Alli, A.; Enns, J. B.; McCabe, K. P. Soft Contact Lenses. U.S. Patent 6,943,203 B2, 2005.
9. Hayama, K.; Narazaki, K.; Kawagucchi, S. Hair-care products containing copolymers. U.S. Patent 5,480,634, 1996.
10. Hayama, K.; Narazaki, K.; Kawaguchi, S. Polymer for hair-care products. U.S. Patent 5,166,276, 1992.
11. Clemens, L.; Kanter, S.; Mazurek, M. Polysiloxane-grafted copolymer release coating sheets and adhesive tapes. U.S. Patent 4,728,571, 1988.
12. Arkles, B. C.; Kimble, E. Low molecular weight siloxanes with one functional group. US7799888, 2010.
13. Chojnowski, J. Kinetically controlled siloxane ring-opening polymerization. *J. Inorg. Organomet. Polym.* **1991**, *1* (3), 299–323.
14. Frye, C. L.; Salinger, R. M.; Fearon, F. W. G.; Klosowski, J. M.; DeYoung, T. Reactions of organolithium reagents with siloxane substrates. *J. Org. Chem.* **1970**, *35* (5), 1308–1314.

15. Bostick, E. E. Polysiloxane block copolymers with ordered structures. US3378521A, 1968.
16. Bostick, E. E. Polysiloxane block copolymers. US3337497, 1967.
17. Arkles, B. C.; Goff, J. D. *Dual functional linear polysiloxanes, Step-growth polymers derived therefrom, and method of preparation thereof*. U.S. Patent Appl. 20130041098, February 14, 2013.
18. Miles, W. C.; Goff, J. D.; Huffstetler, P. P.; Mefford, O. T.; Riffle, J. S.; Davis, R. M. The design of well-defined PDMS-Magnetite complexes. *Polymer* **2010**, *51* (2), 482–491.
19. Wilson, K. S.; Goff, J. D.; Riffle, J. S.; Harris, L. A.; St, P. T. G. Polydimethylsiloxane-magnetite nanoparticle complexes and dispersions in polysiloxane carrier fluids. *Polym. Adv. Technol.* **2005**, *16* (2−3), 200–211.
20. Dvornic, P. R.; Owen, M. J. The role of silicon in dendritic polymer chemistry. *Adv. Silicon Sci.* **2009**, *2*, 1–20 (Silicon-Containing Dendritic Polymers).
21. Bosko, J. T.; Todd, B. D.; Sadus, R. J. Viscoelastic properties of dendrimers in the melt from nonequilibrium molecular dynamics. *J. Chem. Phys.* **2004**, *121* (23), 12050–12059.

<div align="center">

Chapter 6

Synthesis, Characterization, and Properties of New Fluorosilicone Block Copolymers

A Study of the Synthesis and Properties of Perfluorcyclobutyl (PFCB) Aryl Ether Modified Siloxane Block Polymers

</div>

<div align="center">

Olawale Lawal, Sharon C. Kettwich, and Scott T. Iacono[*]

Department of Chemistry and Chemistry Research Center, United States Air Force Academy, 2355 Fairchild Drive, Suite 2N225, Colorado Springs, Colorado 80840, USA
[*]E-mail: scott.iacono@usafa.edu

</div>

In this work, perfluorocyclobutyl (PFCB) aryl ether block dimethylsiloxane polymers were prepared via the step-growth addition polymerization of discreetly sized PFCB prepolymers and carbinol (hydroxyl) terminated silicones. These hybrid fluorosilicone polymer systems displayed high thermal stability, are entirely amorphous, and solution processable producing transparent films with high optical clarity. The synthesis, characterization, thermal analyses, and current scope of hybrid PFCB aryl ether polymer systems are discussed.

<div align="center">

Introduction

</div>

In contrast to hydroalkenes, the relief of orbital angular strain of fluorinated terminal alkenes produces highly electrophilic systems (*1*). Spanning several decades, nucleophile addition to fluorinated alkenes has matured in the area of organofluorine chemistry. For commercial practice, phenols and amines are used to crosslink unsaturated fluoropolymers and are of major importance in the fluoroelastomer industry (*2*). Feiring et al. has developed one of the earlier reported step-growth polymerization based on this transformation in order to produce an alternative route toward aliphatic perfluoropolyethers (PFPEs) that exhibit exceptional thermal and chemical resistance (*3*, *4*). The utility of this polymerization methodology was further expanded to include amorphous

fluoropolymers and liquid crystalline polymers (*5*, *6*). Utilizing this scheme showed a key important feature of chain extending fluorinated alkenes in that this eliminated high pressures, temperatures, or gaseous starting materials, which is benificial to commercial preparation. The preliminary work by Feiring et al. presents an opportunity for preparing partially fluorinated poly(ether)s with an aromatic polymer backbone that could not be achieved from typical PFPE synthesis.

Aryl trifluorovinyl ethers (TFVE) are a class of fluorinated alkenes that are synthesized from readily available phenolic precursors including mono-, di-, and trisphenols. Two general linear polymerization routes using difunctional aryl TFVE have been employed in order to prepare tailorable advanced materials and are illustrated in Figure 1. In one instance, aryl TFVEs undergo condensate-free, thermal [2 + 2] cyclodimerization (*7*) to afford the corresponding chain-extended perfluorocyclobutyl (PFCB) aryl ether polymers (*8*). Due to the stereorandom nature of the PFCB linkage, these high molecular weight systems are often amorphous and solution processable affording optically transparent films. On the other hand, base-catalyzed step-growth polymerization of aryl TFVEs with bisphenols afford fluorinated arylene vinylene ether (FAVE) polymers (*9*). The resulting polymers possess 1,2-difluoroethylene ($Z = CF=CF$) or 1,2,2-hydrofluoroethane ($Z = CHFCF_2$) enchainment depending on the nature of the base. These polymers can be modularly tailored by functionalization of the aryl group (the functional spacer) for applications including thermally crosslinkable fluoroelastomer additives (*10*, *11*), proton exchange membranes (PEMs) for hydrogen-based fuel cells (*12*), polymer light emitting diodes (PLEDs) (*13*), and chemical sensors (*14*, *15*). The work herein entails the expansion of FAVE polymer systems with the first preparation of silicone block PFCB aryl ether copolymers. While the first report of tetramethyldisiloxane PFCB aryl ether polymer produced solution processable thermoplastic and high thermally stable thermosets (*16*), the ability to introduce varying lengths of silicone segments still remains limited. The complimentary thermal and chemical resistant properties of silicones and partially fluorinated PFCB aryl ether polymers would afford a new class of thermoplastic fluorosilicones for optically transparent membrane applications.
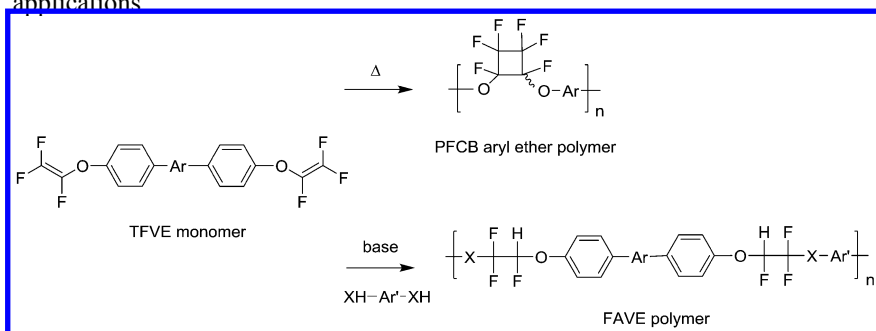

Figure 1. Aryl TFVE ether undergo thermal [2+2] cyclopolymerization to afford PFCB aryl ether polymers (top) or the base-promoted polymerization of dinucleophiles to produce FAVE polymers.

Experimental

Materials

Solvents were obtained from commercial suppliers and used as received unless otherwise noted. Perfluorocyclobutyl (PFCB) aryl ether prepolymers **PFCB8K** and **PFCB16K** were purchased from Tetramer Technologies, LLC., Pendleton, SC and distributed through Oakwood Chemicals, Inc. Carbinol (hydroxyl) terminated poly(dimethylsiloxane) (**CS1K**) were acquired from Gelest, Inc (cataloged as DMS-C15). Anhydrous *N,N*-dimethylfomamide (DMF) was further dried by storage over anhydrous, powdered MgSO4 under nitrogen atmosphere.

General Procedures

All reactions were carried out under a nitrogen atmosphere. Flasks and syringes were oven dried at 100 °C and allowed to cool in a desiccator prior to use. ^{19}F NMR and ^{1}H NMR data were obtained on a Varian AS400 NMR, and chemical shifts were reported in part per million (δ ppm). ^{19}F NMR was referenced to CFCl3 and ^{1}H NMR was referenced to tetramethyl silane at 0.0 ppm. Gel permeation chromatography (GPC) data was collected using polystyrene as a standard (Polymer Labs Rascal PS-2) on a PL-GPC-220 with RI detection for samples in THF. GPC samples were eluted in series through Polymer Labs PLGel 5 mm Mixed-D and Mixed-E columns at 35 °C. Differential scanning calorimetry (DSC) data was obtained on a TA Q100 in nitrogen from the head space on a liquid N2 tank that passes through Dry-rite before entering the sample chamber. Samples (ca. 5 mg) are sealed in aluminum hermetic pan with an empty sealed hermetic pan serving as the reference. Samples are heated from −40 °C to 200 °C at a rate of 10 °C/min and then cooled down to 20 °C, three times. Thermal transitions were reported on the third heating cycle. Thermal gravimetric analysis (TGA) data was collected on a TA Q500 heated from room temperature to 900 °C with a ramp rate of 20 °C/min in N2 using a platinum crucible.

CS1K-*b*-PFCB8K

Carbinol silane **CS1K** (254 mg, 0.254 mmol, M_n ~ 1000), PFCB aryl ether prepolymer **PFCB8K** (2.02 g, 0.253 mmol, M_n ~ 8000), and Cs2CO3 (53.4 mg, 0.164 mmol) in a minimal amount DMF (~ 3 mL) was placed in a preheated silicon oil bath at 80 °C. After 8 d, the solution contents were then precipitated into cold MeOH, filtered under vacuum, and washed with copious amounts of MeOH. The solid polymer was then dried in a vacuum oven at 60 °C for an additional 24 h to afford the titled polymer as a white powdery solid (2.3 g, 86%). ^{19}F NMR (CDCl3, 400 MHz) δ −78.6 (s, (−CHFC*F*2−), −123.5−(−126.7) (m, cyclobutyl-*F*6) −141.5 (broad d, (−CH*F*CF2−); ^{1}H NMR (CDCl3, 400 MHz) δ 7.92−6.90 (m), 5.80 (broad dt, −C*H*FCF2−), 4.00−3.45 (m), 0.51−0.49 (m) 0.10−0.00 (m).

CS1K-*b*-PFCB16K

Carbinol silane *CS1K* (0.072 mg, 0.072 mmol, $M_n \sim 1000$), PFCB prepolymer **PFCB16K** (1.01 g, 0.063 mmol, $M_n \sim 16000$), and Cs_2CO_3 (52.6 mg, 0.162 mmol) in a minimal amount DMF (~ 3 mL) was placed in a preheated silicon oil bath at 80 °C. After 8 d, the solution contents were then precipitated into cold MeOH, filtered under vacuum, and washed with copious amounts of MeOH. The solid polymer was then dried in a vacuum oven at 60 °C for an additional 24 h to afford the titled polymer as a pale white, fibrous solid (614 mg, 38%). ^{19}F NMR (CDCl₃, 400MHz) δ −82.4 (s, −CHFCF_2−), −128.7−(−131.9) (m, cyclobutyl-F_6) −140.7 (broad d, (−CHFCF₂−); ^{1}H NMR (CDCl₃, 400 MHz) δ 7.91−6.92 (m), 5.79 (broad dt, −CHFCF₂−), 3.98−3.45 (m), 0.51−0.49 (m) 0.12−0.00 (m).

Results and Discussion

The preparation of siloxane segmented PFCB aryl ether block copolymers was carried out employing carbinol (hydroxyl) terminated polydimethylsiloxanes and PFCB oligomers under base-catalysed conditions shown in Figure 2. Carbinol (−CH₂OH) silanes were chosen in this study as opposed to the more accessible and nucleophilic silanol (−R₂SiOH) terminated siloxanes because the resulting addition to aryl TFVE affords an unstable silyl ether −R₂*Si−O−CF₂*CFH−O−Ar− readily susceptible to rearrangement−disproportionation to the thermodynamically favoured Si−F and acyl fluoride. The carbinol siloxanes obtained from commercial sources with varying number-average molecular weight (M_n) included 1000 (**CS1K**), 5000 (**CS5K**), and 10000 (**CS10K**). PFCB aryl ether prepolymers used in this study include those with M_n of 8000 (**PFCB8K**) and 16000 (**PFCB16K**) possessing reactive aryl TFVEs.

Figure 2. Base-promoted polymerization of carbinol silicones and PFCB aryl ether prepolymers affording block copolymers via 1,2,2-hydrofluoroethane enchainment.

Initial step-growth polymerization was carried out in a 1:1 molar ratio of **CS1K** and **PFCB8K** using catalytic Cs_2CO_3 (50 mol %) in a minimal amount of DMF at 80 °C in order to prepare **CS1K-*b*-PFCB8K** block copolymer. The block copolymer was purified from repeated precipitations in cold MeOH from THF and produced optically transparent spin cast films. The addition of the carbinol to the aryl TFVE ($-O-CF=CF_2$) affording the anchoring hydro-1,2,2- fluoroethane ($-O-CHFCF_2-O-$) was monitored by ^{19}F NMR and full conversation was achieved after 5−8 days. Figure 3 illustrates an example ^{19}F NMR of the conversion from the AMX *dd*-pattern from the aryl TFVE to broadened signals at –82.4 ppm ($-CHFCF_2-$) and −140.7 ppm ($-CHFCF_2-$) with the PFCB ring intact with a range of multiplicity at −128.7−(−131.9). These results are consistent with small molecule model studies on the investigation of the addition mechanism (*17*). ^{1}H NMR showed further evidence of dimethylsiloxane segment incorporation with the presence of a broadened *dt*- pattern at 5.8 ppm indicative of the fluoroalkene addition with the dihydroxylterminated siloxane producing the hydro-1,2,2-fluoroethane ($-O-CHFCF_2-O-$) (Figure 4).
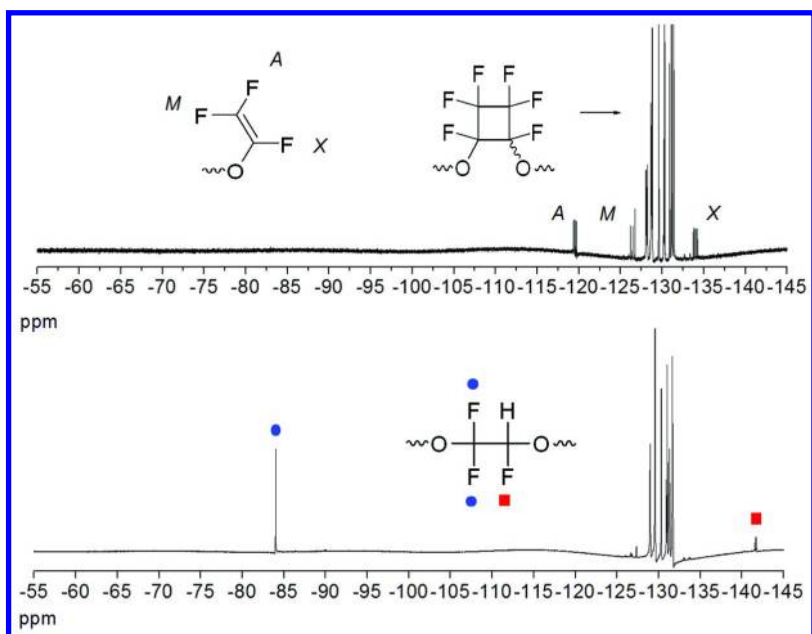
*Figure 3. ^{19}F NMR illustrating conversion of the aryl TFVE from **PFCB8K** to 1,2,2-hydrofluoroethane via addition of the hydroxyl terminated silane affording **CS1K-b-PFCB8K** polymer.*
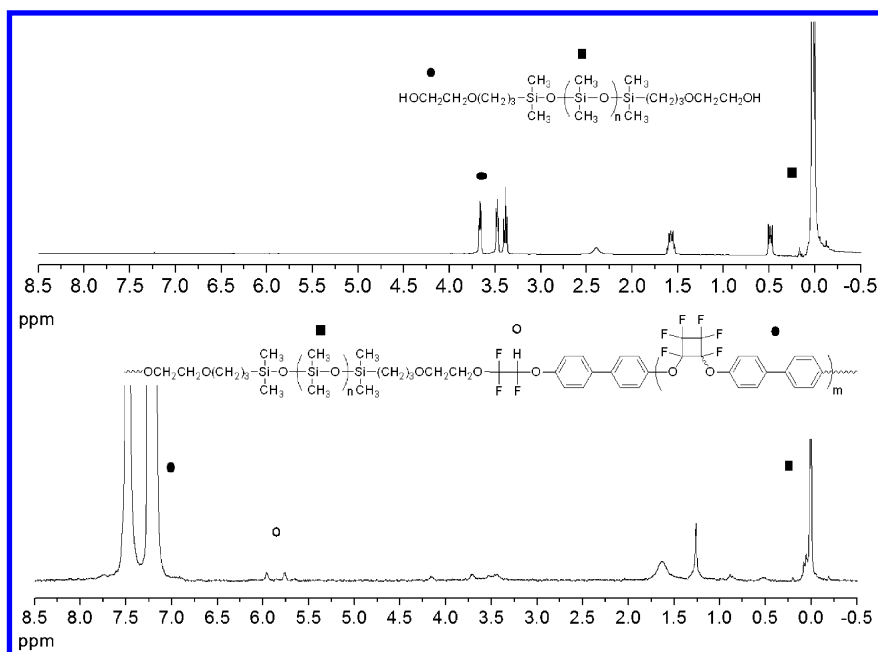
*Figure 4. ¹H NMR of **CS1K** (top) and segmented polymer **CS1K-b-PFCB8K** (bottom).*

This optimized methodology was employed for the attempted preparation of the larger PFCB aryl ether block copolymer **CS1K-b-PFCB16K** as well as subsequent siloxane-extended copolymers **CS5K-b-PFCB8K**, **CS5K-b-PFCB16K**, **CS10K-b-PFCB8K**, and **CS10K-b-PFCB16K**. All purified block copolymers indicated quantitative conversion of the aryl TFVE end groups based on ¹⁹F NMR. However, ¹H NMR indicated less than 10 mol % incorporation of the polydimethylsiloxane segments for attempted **CS5K** and **CS10K** addition based on peak integration of the repeat unit of the biphenyl (7.0−8.6 ppm) compared with dimethylsiloxane (0.0−0.5 ppm). This observation indicated carbinol siloxane chain segment is limited the **CS1K** and the higher molecular weight **CS** may indicate a presence of cyclics as the kinetically favoured outcome. Control experiments whereby Cs₂CO₃ and **CS5K** and **CS10K** were heated at 80 °C in DMF for 48 h without PFCB aryl ether prepolymer showed no evidence of degradation to smaller oligomers by GPC analysis. Therefore, the remainder of this study will focus on block copolymers **CS1K-b-PFCB8K** and **CS1K-b-PFCB16K,** which provided suitable free-standing films for thermal analysis.

Selected properties for **CS1K**, PFCB aryl ether prepolymers, and the corresponding copolymers **CS1K-b-PFCB8K** and **CS1K-b-PFCB16K** are shown in Table 1. Initially, GPC analysis was invoked in order to determine the molecular weights of the block copolymers. However, GPC analysis of the carbinol polydimethylsiloxanes showed a large disparity of M_n values

compared with commercially published values. ^{1}H NMR proved to be a more reliable technique for measurement of the molecular weight; calculated M_n based on end group analysis was comparable with published values from the supplier. Advancement of molecular weight was observed for the prepared block copolymers **CS1K-*b*-PFCB8K** and **CS1K-*b*-PFCB16K** producing a M_n of 13000 and 33300, respectively. In both cases, the PFCB aryl ether block is nearly doubled on average with a predominant architecture of polydimethylsiloxane ether enchainment. DSC analysis revealed an entirely amorphous material and showed a substantial increase in the glass transition temperature (T_g) for block the **CS1K-*b*-PFCB8K** systems by 21 °C. A negligible increase was observed for **CS1K-*b*-PFCB16K** indicating the biphenyl segment influences the bulk mechanical properties. TGA analysis of the both block copolymers in N_2 did not show evidence of degradation (T_d) before onset occurred at ca. 470 °C with char yields at ca. 40%, typical of PFCB aryl ether chain extended systems.

Table 1. Selected Properties of Silicone-Segmented PFCB Aryl Ether Polymers

polymer	M_n	T_g (°C)[c]	T_d (°C)[d]	char (%)[e]
CS1K	1300[a]	−	277	2
PFCB8K	8000[b]	96	477	40
PFCB16K	16000[b]	138	478	40
CS1K-*b*-PFCB8K	13000[a]	117	485	43
CS1K-*b*-PFCB16K	33300[a]	141	472	45

[a] ^{1}H NMR end group analysis. [b] ^{19}F NMR end group analysis. [c] DSC (10 °C/min) −40 °C to 200 °C in N_2 from third scan. [d] TGA onset at 20 °C/min in N_2. [e] TGA after 900 °C in N_2.

Conclusions

A new class of fluorosilicone has been prepared via the block copolymerization of a carbinol (hydroxyl) terminated polydimethylsiloxane with PFCB aryl ether prepolymers of varying chain lengths. This approach mirrors a well-established methodology whereby facile dinucleophile addition to highly fluorinated alkenes, in this case, bistrifluorovinyl aryl ethers, produce chain extended systems. These block copolymers produce optically transparent, processable films and possess high thermal stability. Although larger dimethylsiloxane segments could not be anchored stoichiometrically with the PFCB aryl ether prepolymers via conditions optimized for FAVE polymer systems, this work provided insight to other possible architectures. Work is on-going for the preparation of aryl TFVE end-capped polydialkyl/arylsiloxanes from the corresponding carbinol siloxane that can undergo further thermally-promoted chain extension to via PFCB linkages.

Acknowledgments

We acknowledge the Defense Threat Reduction Agency (DTRA) under the Service Academy Research Initiative for financial support.

References

1. Chambers, R. D. In *Synthetic Fluorine Chemistry*; Olah, G. A.; Chambers, R. D.; Prakash, G. K. S., Ed.; John Wiley & Sons, Inc.: New York, 1992, p 359.
2. Schmiegel, W. W. *Angew. Makromol. Chem.* **1979**, *76/77*, 39.
3. Hung, M.-H.; Farnham, W. B.; Feiring, A. E.; Rozen, S. *J. Am. Chem. Soc.* **1993**, *115*, 8954.
4. Feiring, A. E.; Rozen, S.; Wonchoba, E. R. *J. Fluorine Chem.* **1998**, *89*, 31.
5. Yang, Z. Y.; Feiring, A. E.; Smart, B. E. *J. Am. Chem. Soc.* **1994**, *116*, 4135.
6. Rodenhouse, R.; Percec, V.; Feiring, A. E. *J. Polym. Sci., Part C: Polym. Lett.* **1990**, *28*, 345.
7. Spraul, B. K.; Suresh, S.; Jin, J.; Smith, D. W., Jr. *J. Am. Chem. Soc.* **2006**, *128*, 7055.
8. Iacono, S. T.; Budy, S. M.; Jin, J.; Smith, D. W., Jr. *J. Polym. Sci., Part A: Polym. Chem.* **2007**, *45*, 5705.
9. Kettwich, S. C.; Lund, B. R.; Smith, D.W., Jr.; Iacono, S. T. In *Advances in Fluorine-Containing Polymers*; American Chemical Society: 2012; Vol. 1106, p 9.
10. Iacono, S. T.; Budy, S. M.; Ewald, D.; Smith, D. W., Jr. *Chem. Commun.* **2006**, 4844.
11. Tackett, K. N.; Iacono, S. T.; Smith, D. W., Jr. *Polym. Prepr.* **2008**, *49*, 801.
12. Iacono, S. T.; Ewald, D.; Sankhe, A.; Rettenbacher, A.; Smith, D. W., Jr. *High Perform. Polym.* **2007**, 581.
13. Iacono, S. T.; Budy, S. M.; Moody, J. D.; Smith, R. C.; Smith, D. W., Jr. *Macromolecues* **2008**, *41*, 7490.
14. He, S.; Iacono, S. T.; Budy, S. M.; Dennis, A. E.; Smith, D. W., Jr.; Smith, R. C. *J. Mater. Chem.* **2008**, *18*, 1970.
15. Gilliard, R. J., Jr.; Iacono, S. T.; Budy, S. M.; Moody, J. D.; Smith, D. W., Jr.; Smith, R. C. *Sens. Actuators, B* **2009**, *143*, 1.
16. Smith, D. W., Jr.; Babb, D. A. *Macrmolecules* **1996**, *29*, 852.
17. Moody, J. D.; VanDerveer, D.; Smith, D. W., Jr; Iacono, S. T. *Org. Biomol. Chem.* **2011**, *9*, 4842.

Chapter 7

Silicone Macroinitiator in the Atom Transfer Radical Polymerization of Styrene and Vinyl Acetate: Synthesis and Characterization of Novel Thermoreversible Block Copolymers

Sahar Amiri* and Mohammad Ali Semsarzadeh

Polymer Group, Department of Chemical Engineering, University of Tarbiat Modares, Tehran, P.O. Box: 14155/143, Iran
*E-mail: amiri_s@modares.ac.ir

Organic-inorganic block copolymers have been synthesized *via* atom transfer radical polymerization (ATRP) of styrene (St), methyl methacrylate (MMA), methyl acrylate (MA) and vinyl acetate (VAc) monomers at 60°C using CuCl/ N,N,N′,N″,N″-pentamethyldiethylenetriamine (PMDETA) as a catalyst system initiated from bromoalkyl-terminated poly(dimethylsiloxane) (Br-PDMS-Br) macroinitiator. Well-defined poly(styrene-b-methyl methacrylate-b-vinyl acetate-b-dimethylsiloxane-b-vinyl acetate-b-methyl methacrylate-b-styrene) (PSt-b- PMMA-b-PVAc-b-PDMS-b-PVAc-b-PMMA-b-PSt) and poly(styrene-b-methyl acrylate-b- vinyl acetate-b-dimethylsiloxane-b-vinyl acetate-b-methyl acrylate-b- styrene) (PSt-b-PMA-b-PVAc-b-PDMS-b-PVAc-b-PMA-b-PSt) were successfully synthesized through ATRP. The novel block copolymers were characterized using nuclear magnetic resonance spectroscopy (¹H-NMR), differential scanning calorimetry (DSC) and gel permeation chromatography (GPC). The resulting block copolymers were reacted with γ-cyclodextrin in a controlled radical polymerization with Co(acac)₂/DMF as a catalyst/ligand complex. The novel supramolecular block coplymers can undergo a temperature-induced reversible transition upon heating-cooling of the copolymer complex from white complex at 22°C to green complex in 55°C which was characterized with XRD and

^{1}H-NMR. The XRD showed a change in the percent crystalinity of the copolymers with changing the temperature.

Introduction

Recent developments in controlled radical polymerization (CRP) techniques in polymer synthesis allow versatile molecular designs for supramolecular architecture having novel functional materials. Atom transfer radical polymerization (ATRP), reversible addition fragmentation chain transfer (RAFT) polymerization and nitroxide-mediated radical polymerization techniques have been utilized to develop well-defined functional polymers (*1*, *2*). Of all the inorganic polymers studied, polysiloxanes have been the most widely exploited. Particularly, poly(dimethylsiloxane) (PDMS) is used in materials for its hydrophobic, highly flexible, high oxygen permeability, biocompatibility, selective gas permeability and heat transfer properties. However, since PDMS is a fluid at room temperature, the homopolymer lacks dimensional stability (*3*, *4*). In an effort to produce materials composed of silicones with more desirable mechanical properties, block, graft, and network copolymers containing PDMS segments have been examined. In block copolymers with different monomers, the morphology of the polymer chain is influenced not only by the overall molecular weight and the mole fraction of each block, but also by the sequence of the blocks with different properties, applications, and functionality such as methylacrylate, methyl methacrylate, styrene and vinyl acetate as monomers (*5–7*). There have been few reports on inclusion complexes formed from block copolymers and cyclodextrins. Due to their unique structures and properties, polyrotaxanes represent an important addition to the repertoire of polymer architectures. Recently, the supramolecular assemblies of rotaxane type received a renewed interest, analogous to the one on noncovalent interactions in biological and stimuli-sensitive systems. Such complexes provide interesting structures and properties since CDs could preferentially thread onto one of the blocks (*8–10*). Systems of these novel complexes can have applications in areas such as drug delivery, sensors, separations, and membranes (*4*, *8–10*).

A series of polyrotaxane-based block copolymers comprising γ-cyclodextrin threaded onto PDMS as a central block and PVAc, PMMA, PMA and styrene as outer blocks as end-stoppers were prepared via ATRP (*4*, *11*). The structure of the resultant copolymers was characterized in detail by ^{1}H-NMR, GPC and DSC. The results of the current research uncovered block copolymers containing Br- PDMS-Br macroinitiator. The findings suggest that the reaction condition changes the crystalline structure. This work aims to prepare polyrotaxane based on PSt-PMMA-b-PVAc-b-PDMS-b-PVAc-b-PMMA-b-PSt and PSt-PMA-b-PVAc-b-PDMS-b-PVAc-b-PMA-b-PSt in addition to compare the effect of various monomers on the synthesized block copolymers (*5–7*). It seems that no other report can be found in the literature on the application of Br-PDMS-Br macroinitiators for synthesis new polyrotaxane based on new block copolymers making stimuli-sensitive systems (*4*, *11*).

This chapter reports a supramolecular polymeric host-guest system consisting of PVAc, PMA, PMMA and PSt initiated with bis(boromoalkyl)-terminated PDMS in an aqueous solution. This interesting host-guest system exhibited a dual thermoresponse behavior due to three existing kinds of thermoresponsive segments, PDMS and cyclodextrin (*11*). In other words, this polymeric host- guest system was able to form DCABACD type supramolecular block copolymers via inclusion complexation in aqueous solution (*5–7*). This block copolymer revealed a thermosensitive micelle formation behavior in the solid state (*12–17*). As temperature increased, the polyrotaxane based block copolymer chains were dehydrated while the color of complex was changed from white to green through hydrophobic-hydrophobic interactions (*4, 18*). The complex is colorless; however the presence of catalyst, like CuCl-ligand turns the block copolymer green. In this work we have removed the catalyst impurities of PSt-b-PMMA-b-PVAc-b-PDMS-b-PVAc-b-PMMA-b-PSt and PSt-b-PMA-b-PVAc-b-PDMS-b-PVAc-b-PMA-b-PSt rotaxane by alumina column. Further increase of the temperature caused the phase transition related to PDMS to occur on the corona of noncovalently connected micelles. Therefore, the micelles were destabilized which resulted in micelle aggregation and precipitation. The supramolecular system presented here is rather different from the reported systems. This work has formed dual thermoresponsive pentablock copolymers in order to propose a novel supramolecular approach in designing and constructing the noncovalently connected polymeric micelles with modifiable properties.

Results and Discussion

PDMS Macroinitiator (Br-PDMS-Br)

^{1}H-NMR of the functionalized PDMS was used to verify the quantitative modification of the end groups to the terminal bromine (Scheme 1). The volatiles were removed under vacuum from the final product. GPC analysis showed M_n=14800 g mol^{-1}, with a MWD=1.93, maximum yield determined gravimetrically is 82%. ^{1}H-NMR (CDCl$_3$) indicated δ=0.0-0.3 ppm for protons of the methyl groups of -Si(CH$_3$)$_2$O, δ=2.0 ppm for the methylene group next to the bromide (*6, 10, 11*).
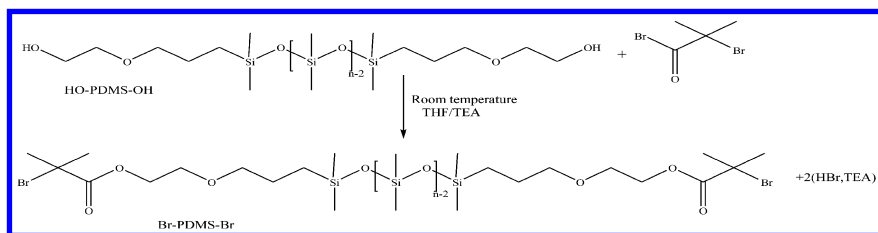
Scheme 1. Reaction scheme for the synthesis of bis(2-bromoisobutyrate)-terminated PDMS macroinitiator using bis(hydroxyalkyl)-terminated PDMS (10).

First-order kinetic polymerization plots of St, MA, MMA and PVAc initiated by Br-PDMS-Br macroinitiator are shown in Figure 1. The linear fit indicated that the concentration of propagating radical species is constant and radical termination reactions are not significant over time scale of the reaction. It was found that the molecular weights increase almost linearly with conversion, indicating that the number of chains was constant and the chain transfer reactions were rather negligible (*4–7*). Thus from Figure 1, one may conclude that the polymerization was controlled and had a narrow molecular weight distribution (see Table 1).
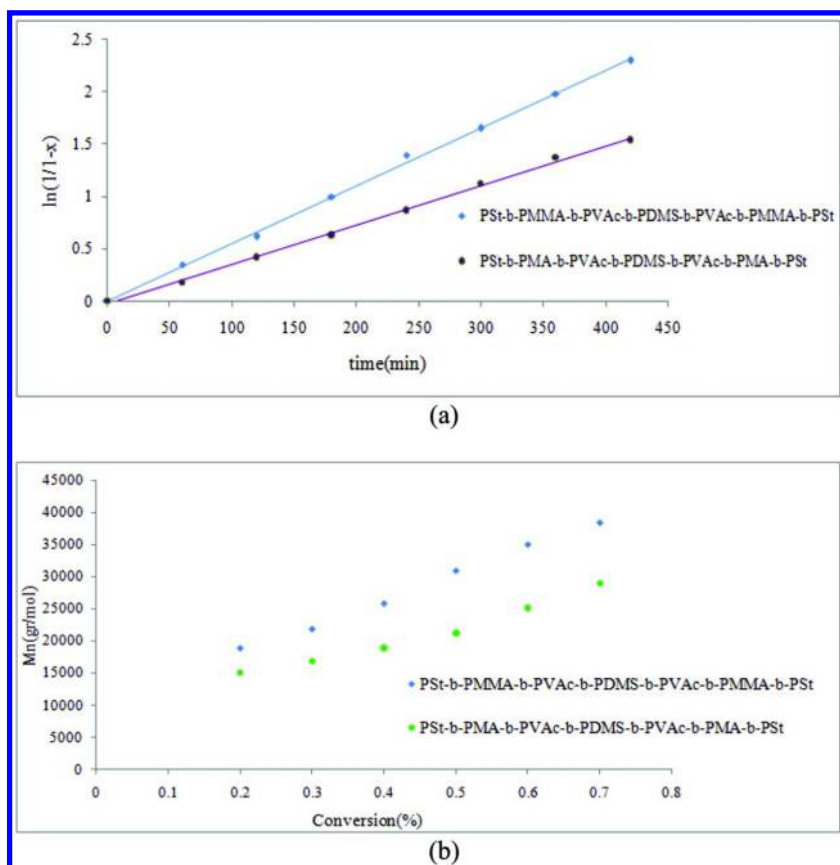
Figure 1. (a) Time dependence of ln[M]$_0$/[M] (M: monomer); (b) dependence of the block copolymer M$_n$ on the conversion for the ATRP of St, MA, MMA and PVAc with Br-PDMS-Br macroinitiator at 60°C

Table 1. Results obtained from GPC analysis for PSt-b-PMMA-b-PVAc-b-PDMS-b-PVAc-b-PMMA-b-PSt and PSt-b-PMA-b-PVAc-b-PDMS-b-PVAc-b- PMA-b-PSt block copolymers

(Co)Polymer	$X(\%)^a$	$M_{n,GPC}$ $(gmol^{-1})$	PDI
Br-PDMS-Br	87	14800	1.93
PSt-b-PMMA-b-PVAc-b-PDMS-b-PVAc-b-PMMA-b-PSt	75	38500	1.36
PSt-b-PMA-b-PVAc-b-PDMS-b-PVAc-b-PMA-b-PSt	54	28900	1.45

[a] Final conversion measured by gravimetric method.

GPC traces for the progress of ATRP reaction of PVAc, PSt, PMA and PMMA initiated with Br-PDMS-Br macroinitiator is represented in Figure 2 (see Table 1). The growing peak of block copolymers remained monomodal throughout the reaction, indicating that all the unreacted attachable initiators have been removed prior to polymerization (*4–7*).
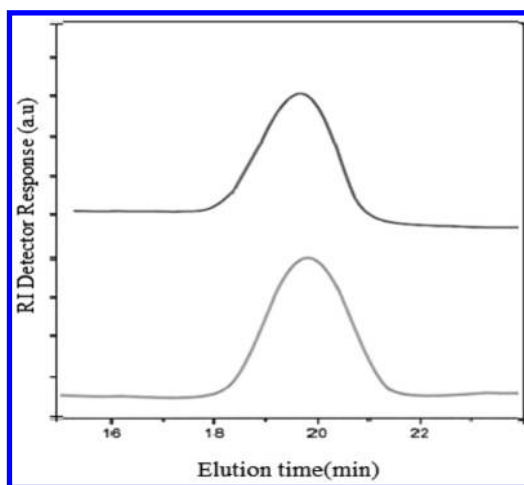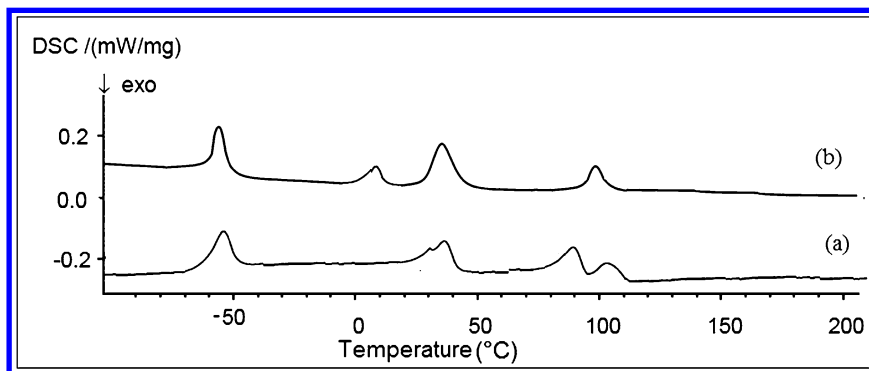

Figure 2. GPC traces for the (a) PSt-b-PMMA-b-PVAc-b-PDMS-b-PVAc-b-PMMA-b-PSt and (b) PSt-b-PMA-b-PVAc-b-PDMS-b-PVAc-b-PMA-b-PSt block copolymers initiated with PDMS macroinitiator and MMA, MA,VAc and St as monomers at 60°C for 6 hours

¹H-NMR spectra of the PSt-b-PMMA-b-PVAc-b-PDMS-b-PVAc-b-PMMA-b- PSt and PSt-b-PMA-b-PVAc-b-PDMS-b-PVAc-b-PMA-b-PSt block copolymers have been demonstrated in Figure 3. All the signals of the ¹H-NMR spectra were assigned to their corresponding monomers and it can be declared that the synthesis of block copolymers have proceeded successfully (4–7, 11). The ¹H- NMR of block copolymers showed a signal at 0.0-0.2 ppm associated with the CH₃-Si methyl protons of PDMS along with the signals at 2.1-2.3 ppm and 6.6-7.1 ppm corresponded to the OCOCH₃ group from the PVAc segment and PSt segment, respectively. Signals at 0.8-1.0 ppm, 1.9-2.1 ppm and 3.6 ppm corresponded to the CH₃, CH₂ and COOCH₃ groups from the PMMA and PMA segment (6, 7, 11). Therefore, it is possible to synthesize the novel PDMS-based block copolymers *via* ATRP of monomers such as vinyl acetate, methyl methacrylate, methyl acrylate and styrene in the presence of bis(haloalkyl)-terminated PDMS macroinitiator (10, 11). The well-define microstructure can be used in macromolecular design of the block copolymer, assuming one can increase the mole ratio of the monomer or used different molecular weight of the PDMS macroinitiator in the structure (5, 6).
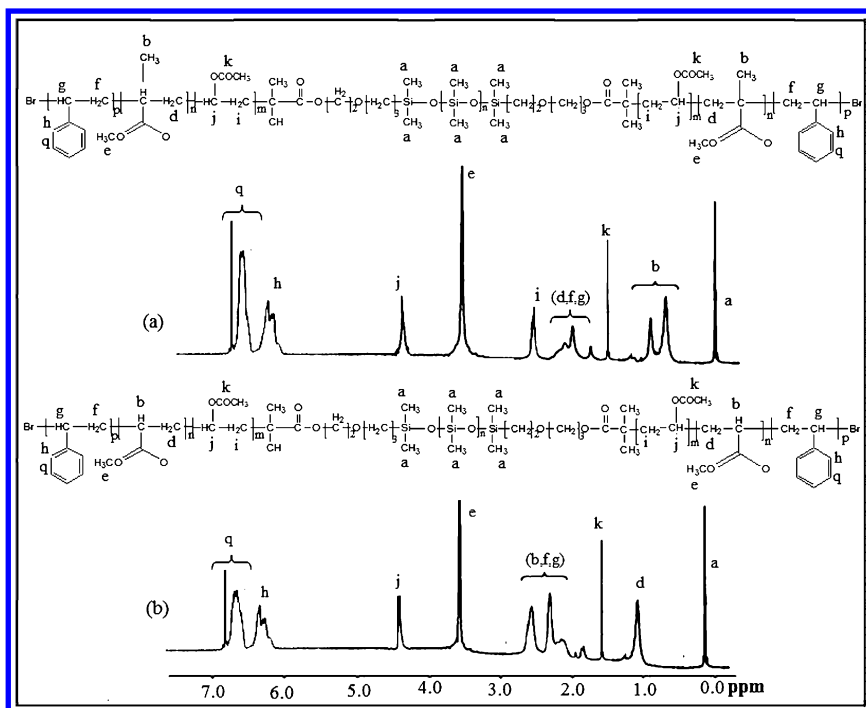
Figure 3. ¹H-NMR traces for the PSt-b-PMMA-b-PVAc-b-PDMS-b-PVAc-b-PMMA-b-PSt and PSt-b-PMMA-b-PVAc-b-PDMS-b-PVAc-b-PMMA-b-PSt block copolymers initiated with PDMS macroinitiator and MMA,MA,St and VAc as monomers at 60°C

The ratio of sequence lengths of PVAc and PDMS was 2.08, PMA and PDMS was 2.18, PSt and PDMS was 2.38 and for PMMA to PDMS was 2.34, so block copolymers of PSt-b-PMMA-b-PVAc-b-PDMS-b-PVAc-b-PMMA-b-PSt and PSt-b-PMA-b-PVAc-b-PDMS-b-PVAc-b-PMA-b-PSt were synthesized. Therefore, it is possible to synthesize the PDMS-based block copolymers via ATRP of monomers such as vinyl acetate, methyl acrylate, methyl methacrylate and styrene in the presence of bis(haloalkyl)-terminated PDMS macroinitiator (*4–6*).

DSC thermograms of PDMS-based block copolymers are depicted in Figure 4 for temperature range -100°C to +200°C. Glass transition temperature (T_g) of PDMS is expected to be about -120°C, thus it is observed in Figure 6 at -60°C. PMMA, PMA, PVAc and PSt segments exhibited T_g values of 90,5, 40 and 105°C (*4–6*, *11*), respectively for the corresponding block copolymers. Considering the DSC results, one can conclude that PDMS-based penta-block copolymers have been synthesized successfully.

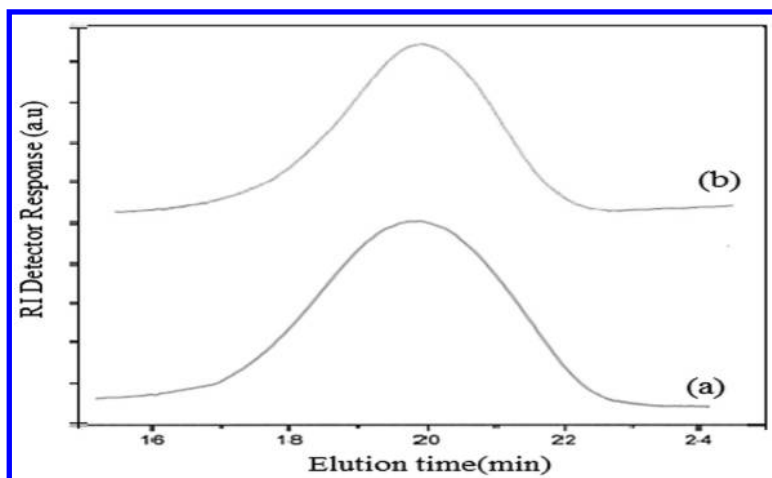*Figure 4. DSC thermograms for the (a) PSt-b-PMMA-b-PVAc-b-PDMS-b-PVAc-b-PMMA-b-PSt and (b) PSt-b-PMA-b-PVAc-b-PDMS-b-PVAc-b-PMA-b-PSt block copolymers initiated with Br-PDMS-Br macroinitiator and MMA, MA,VAc and St as monomers at 60°C for 6 hours*

Preparation and Characterization of Polyrotaxane-Based Block Copolymers

The synthesized block copolymers were reacted with γ-cyclodextrin. First-order kinetic polymerization plots of PSt-b-PMMA-b-PVAc-b-PDMS-b-PVAc-b-PMMA-b-PSt and PSt-b-PMA-b-PVAc-b-PDMS-b-PVAc-b-PMA-b-PSt polyrotaxanes are shown in Figure 5. The linear fit indicated that the concentration of propagating radical species is constant and radical termination reactions are not significant over the time scale of the reaction. It was found that the molecular weights increase almost linearly with conversion, indicating that the number of chains was constant and the chain transfer reactions were rather negligible (*4–7*).
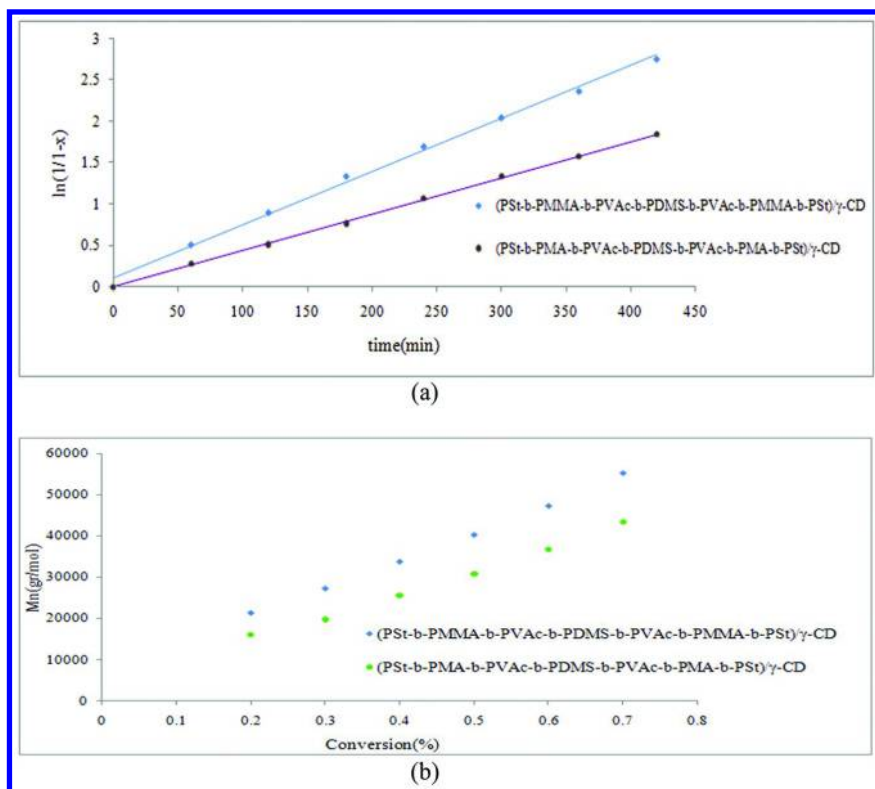
Figure 5. (a) Time dependence of ln[M]$_0$/[M] (M: monomer); (b) dependence of the block copolymer M_n on the conversion for the ATRP of St, MA, MMA and PVAc with Br-PDMS-Br macroinitiator at 60°C

GPC is an effective analytical technique to discover the structure of polyrotaxanes. If polyrotaxanes are not efficiently end-capped, dethreading of CDs will produce multiple GPC peaks. The GPC curves of polyrotaxanes-based block copolymers (PSt-b-PMMA-b-PVAc-b-PDMS-b-PVAc-b-PMMA-b-PSt and PSt-b-PMA-b-PVAc-b-PDMS-b-PVAc-b-PMA-b-PSt polyrotaxane) are depicted in Figure 6. (see Table 2). A nearly symmetrical and unimodal peak with a relatively low polydispersity index of 1.24-1.53 can be clearly observed in Figure 6. From Table 2 and M_n of PSt-b-PMMA-b-PVAc-b-PDMS-b-PVAc-b-PMMA-b-PSt (38500) and PSt-b-PMMA-b-PVAc-b-PDMS-b-PVAc-b-PMA-b-PSt (28900) and M_n γ-CD (1270), number of CDs capped in polyrotaxane can be calculated which is shown in Table 2 (*4*).

Figure 6. GPC of (a) PSt-b-PMMA-b-PVAc-b-PDMS-b-PVAc-b-PMMA-b-PSt and (b) PSt-b-PMA-b-PVAc-b-PDMS-b-PVAc-b-PMA-b-PSt initiated with Br-PDMS-Br at 60°C in 6 hours

Table 2. Results obtained from GPC and ¹H-NMR Analyses for PSt-b-PMMA- b-PVAc-b-PDMS-b-PVAc-b-PMMA-b-PSt and PSt-b-PMA-b-PVAc-b-PDMS- b-PVAc-b-PMA-b-PSt block copolymers

(Co)Polymer	$X(\%)^a$	$M_{n,GPC}$ $(gmol^{-1})$	PDI	CD number
(PSt-b-PMMA-b-PVAc-b-PDMS-b-PVAc-b-PMMA-b-PSt)/γ-CD	67	55264	1.21	13
(PSt-b-PMA-b-PVAc-b-PDMS-b-PVAc-b-PMA-b-PSt)/γ-CD	51	43505	1.34	11

[a] Final conversion measured by gravimetric method.

DSC thermograms of polyrotaxane based block copolymers over the temperature range of -100°C to +350°C are depicted in Figure 7. The glass transition temperature (T_g) of PDMS has been reported to be about -120°C. PVAc, PMMA, PMA and PSt segments in the corresponding block copolymers exhibited T_g values of 32, 90, 5 and 80°C, respectively which can be observed in the Figure 7 (*4–7, 11*). The DSC plot of γ-CD revealed two endothermic peaks one at temperature range of 100-110°C due to the loss of water and another one near 330°C which corresponds to the γ-CD fusion, although they are not observed in Figure 7. These results were characteristic of the microphase separated morphology of the polyrotaxanes. It can judge that polyrotaxanes based block copolymers have been synthesized successfully by taking into account the DSC results (*4, 9–11, 17, 18*). The thermo-responsiveness of the pentablock copolymers was investigated with ¹H-NMR in CDCl₃ and XRD at 22°C and 55°C.
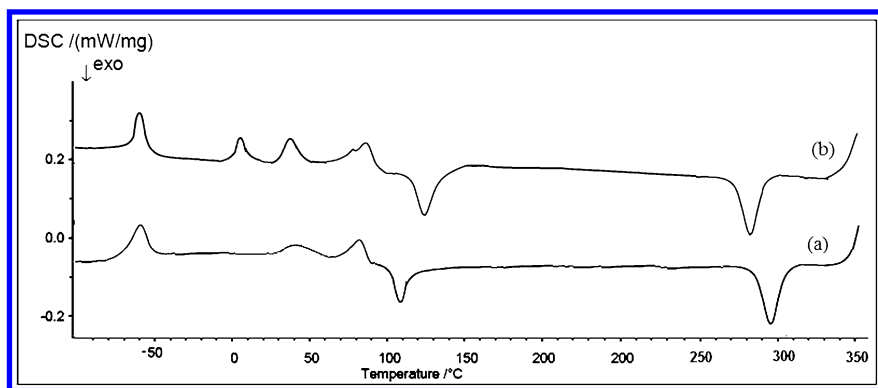
Figure 7. DSC thermograms for the polyrotaxane based on (a) PSt-b-PMMA-b-PVAc-b-PDMS-b-PVAc-b-PMMA-b-PSt and (b) PSt-b-PMA-b-PVAc-b-PDMS-b-PVAc-b-PMA-b-PSt block copolymers at 60°C for 6 hours

^{1}H-NMR and XRD spectra obtained for the PSt-b-PMMA-b-PVAc-b-PDMS-b- PVAc-b-PMMA-b-PSt and PSt-b-PMA-b-PVAc-b-PDMS-b-PVAc-b-PMA-b-PSt based polyrotaxane in thermal cycle from 22°C to 55°C (Figures 8-11). All signals of the ^{1}H-NMR spectra were assigned to their corresponding monomers and it can be declared that the synthesis of new polyrotaxane based block copolymers have proceeded successfully (*4*, *11*, *17*).

The ^{1}H-NMR of the polyrotaxane showed a signal at 0.0-0.2 ppm associated with the CH_3-Si methyl protons of PDMS in addition to some other signals at 2.1-2.3 ppm and 6.6-7.1 ppm corresponding to the $OCOCH_3$ group from the PVAc segment and PSt segment, respectively. Signals at 0.8-1.0 ppm, 1.9-2.1 ppm and 3.6 ppm corresponded to the CH_3, CH_2 and $COOCH_3$ groups from the PMMA and PMA segment. The signals observed at about 4.5 ppm were attributed to the OH of the CDs segment (*4*, *11*). The interaction of cyclodextrin with aromatic end groups of the block copolymer, indicated in peaks around 6.0-8.0 ppm shows a temperature dependency. The peaks shift during the temperature cycle from 55°C to 22°C indicates a temperature induced effect on the complex in a reversible process that dislocates cyclodextrin from the end group of the block copolymer (*4*). Figure 8 shows the ^{1}H-NMR spectra obtained for the PSt-b-PMMA-b-PVAc-b-PDMS-b-PVAc-b-PMMA-b-PSt at 22°C (see Fig. 8-a), temperature increased to 55°C (see Fig. 8-b) and temperature decreased from 55°C to 22°C (see Fig. 8-c).
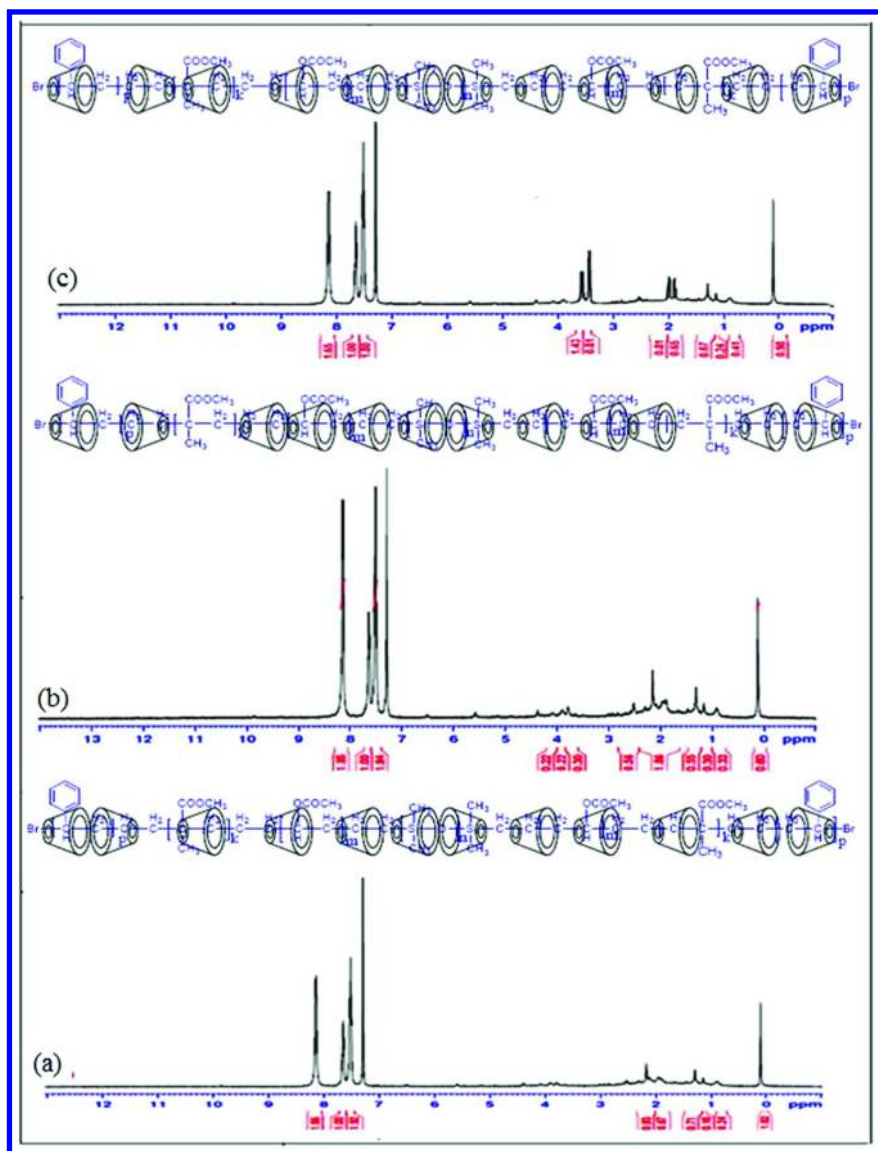
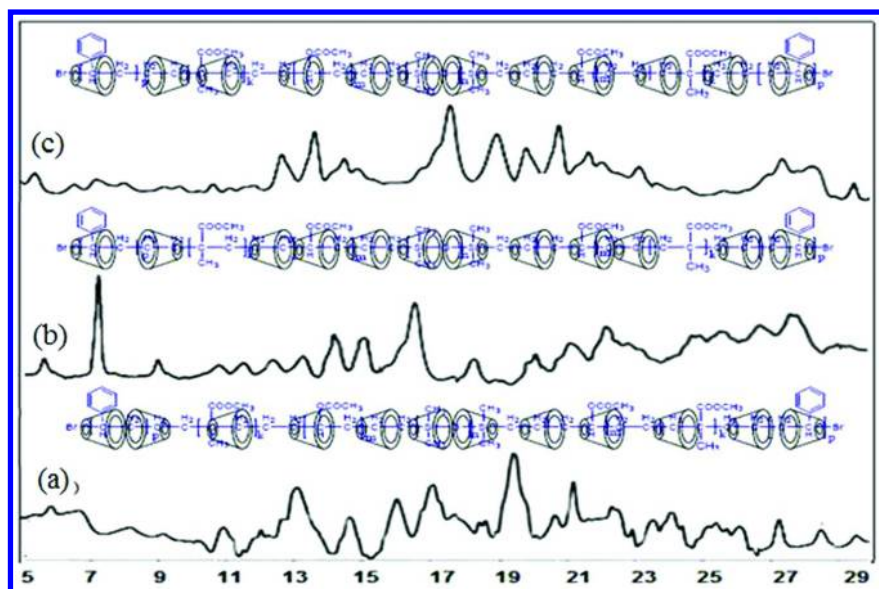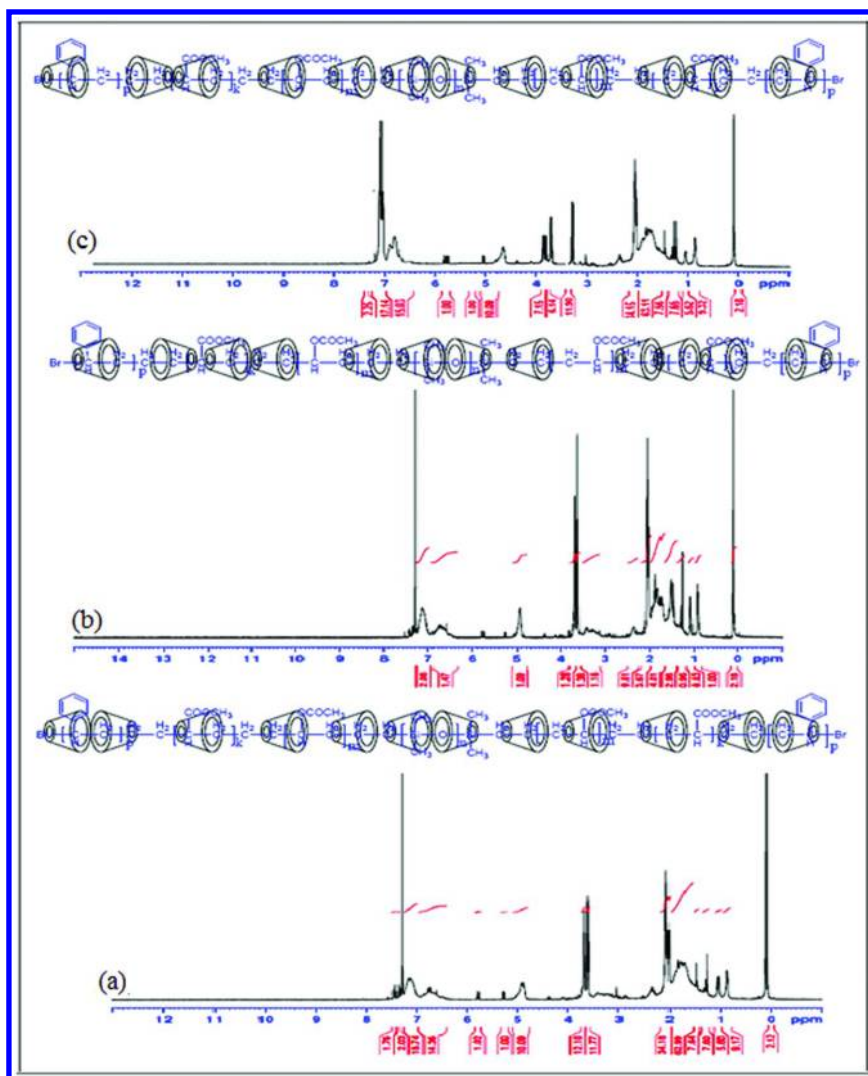*Figure 8. ¹H-NMR of the thermoreversible polyrotaxane of PSt-b-PMMA-b-PVAc-b-PDMS-b-PVAc-b-PMMA-b-PSt block copolymers at (a) 22°C, (b) 55°C and (c) 22°C*

The integral of the peaks associated with protons adjacent to the methyl methacrylate (2.0-2.5 ppm) were observed to decrease which integral of the peaks associated with protons adjacent to the vinyl acetate (1.2-2.1 ppm) were observed to increase with increasing temperature from 22°C to 55°C relative to the integral of the protons in the PDMS (see Fig. 8-b). This reflects the mobility of the γ-cyclodextrin in the block copolymer structure, upon decreasing temperature to 22°C, integral of the peaks associated with protons adjacent to the vinyl acetate the copolymer undergo decrease to reach initial integral (see Figure 8-c) (*4*).

Figure 9 shows the XRD spectra obtained for the PSt-b-PMMA-b-PVAc-b-PDMS-b-PVAc-b-PMMA-b-PSt at 22°C (see Fig. 9-a), temperature increased to 55°C (see Fig. 9-b) and temperature decreased from 55°C to 22°C (see Fig. 99-c). Characteristic peaks of PDMS occurring at $2\theta=8,13,18$, characteristic peaks of PVAc occurring at $2\theta=13$, characteristic peaks of PMMA occurring at $2\theta=16-18$ and characteristic peaks of PSt occurring at $2\theta=8,11,12,14, 6-17,25-29$. At 22°C, the percent crystalinity of PVAc and PMMA is 11 and 28%, respectively (see Fig. 9-a).
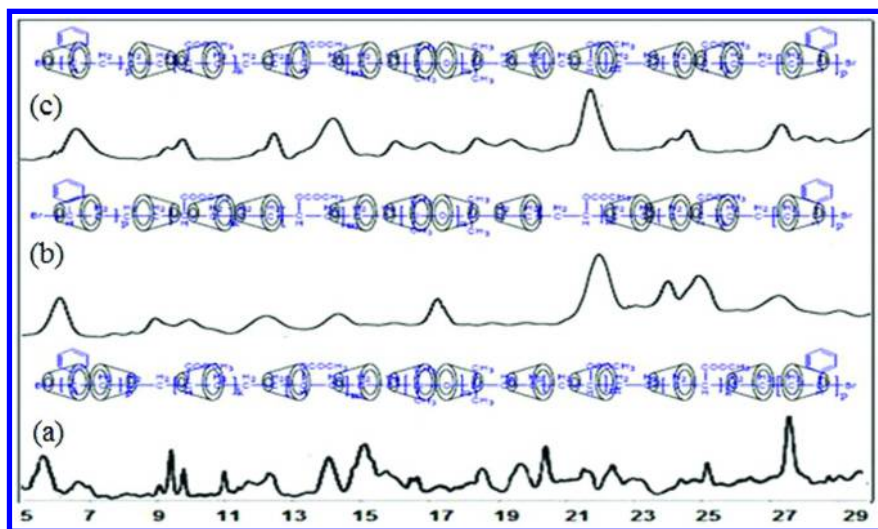

Figure 9. XRD of the thermoreversible polyrotaxane of PSt-b-PMMA-b-PVAc-b-PDMS-b-PVAc-b-PMMA-b-PSt block copolymers at (a) 22°C, (b) 55°C and (c) 22°C

By increasing temperature from 22°C to 55°C, percent crystallinity of PVAc and PMMA becomes 24 and 16% respectively (Fig. 9-b), which indicated migration of the CD from PMMA to PVAc. By decreasing the temperature from 55°C to 22°C, the percent crystalinity of the PVAc and PMMA becomes 13 and 26%, respectively (Fig. 9-c), which indicates migration of the CD from PVAc to PMMA (*4*).

Figure 10. ¹H-NMR of thermoreversible polyrotaxane of PSt-b-PMA-b-PVAc-b-PDMS-b-PVAc-b-PMA-b-PSt block copolymers at (a) 22°C, (b) 55°C and (c) 22°C

Figure 10 shows the ¹H-NMR spectra obtained for the PSt-b-PMA-b-PVAc-b-PDMS-b-PVAc-b-PMA-b-PSt at 22°C (Fig. 10-a), temperature increased to 55°C (Fig. 10-b) and temperature decreased from 55°C to 22°C (Fig. 10-c). The integral of the peaks associated with protons adjacent to the styrene and vinyl acetate (6.5-7 ppm and 1.2-2.1 ppm, respectively) were observed to increase with increasing temperature from 22°C to 55°C which integral of the peaks associated with protons adjacent to the methyl acrylate (3.5-3.6 ppm) were observed to decrease, relative to the integral of the protons in the PMDS (see Fig. 8-b). This

reflects the mobility of the γ-cyclodextrin in the block copolymer structure, upon decreasing temperature to 22°C, integral of the peaks associated with protons adjacent to the styrene and vinyl acetate the copolymers undergo decrease and integral of the peaks associated with protons adjacent to the methyl acrylate undergo increase to reach initial integral (Figure 8-c) (*4*).

Figure 11 shows the XRD scan obtained for the PSt-b-PMA-b-PVAc-b-PDMS-b-PVAc-b-PMA-b-PSt at 22°C (Fig. 11-a), temperature increased to 55°C (Fig. 11-b) and temperature decreased from 55°C to 22°C (Fig. 11-c). Characteristic peaks of PDMS occurring at 2θ=8,13,18, characteristic peaks of PVAc occurring at 2θ=13, characteristic peaks of PMA occurring at 2θ=21-23 and characteristic peaks of PSt occurring at 2θ=8,11,12,14, 6-17,25-29. At 22°C, crystalinity percent of PVAc and PSt is 18 and 16% respectively (Fig. 11-a). By increasing temperature from 22°C to 55°C, crystalinity percent of PVAc and PSt becomes 6 and 10% respectively (Fig. 11-b), which indicated migration of CD from PVAc and PSt to PMA. By decreasing temperature from 55°C to 22°C, crystalinity percent of PVAc and PSt becomes 16 and 11% respectively (see Fig. 11-c), which indicated migration of CD from PMA to PSt and PVAc (*4*).

Figure 11. XRD of thermoreversible polyrotaxane of PSt-b-PMA-b-PVAc-b-PDMS-b-PVAc-b-PMA-b-PSt block copolymers at (a) 22°C, (b) 55°C and (c) 22°C

Conclusions

The unique temperature-dependent polyrotaxanes were successfully synthesized *via* ATRP of MA, MMA, St and PVAc using CuCl/PMDETA as a catalyst system at 60°C and Br-PDMS-Br as macroinitiator. The results in this study strongly supported our assumption that the control of temperature can induce the block-selective inclusion complexation to form the polyrotaxanes,

where γ-CD could be threaded exclusively on the middle PDMS block. These polyrotaxanes are of major interest because of their possibility to form amphiphilic block copolymers of PSt-b-PMMA-b-PVAc-b-PDMS-b-PVAc-b-PMMA-b-PSt and PSt-b-PMA-b-PVAc-b-PDMS-b-PVAc-b-PMA-b-PSt by hydrolysis of the PVAc blocks. ^{1}H-NMR was utilized to analyze the microstructure of the block copolymers as well as the number of PSt, PMA, PMMA, Br-PDMS-Br and PVAc units in the block copolymer. The narrow dispersity indices from GPC of the synthesized block copolymers produced a lower PDI block copolymer due to the living/controlled characteristic of the reaction. The obtained results showed that ATRP of MA, MMA, St and PVAc initiated with inclusion complex of Br-PDMS-Br and the presence of PVAc occurs with well-controlled compositions and molecular weights as well as narrow dispersity indices. Furthermore, the DSC results uncovered the fact that Br-PDMS-Br based block copolymers have been synthesized successfully.

References

1. Matyjaszewski, K. *Prog. Polym. Sci.* **2005**, *30*, 858.
2. Braunecker, W. A.; Matyjaszewski, K. *Prog. Polym. Sci.* **2007**, *32*, 93.
3. Debuigne, A.; Caille, J. R.; Jerome, R. *Macromolecules* **2005**, *38*, 5452.
4. Semsarzadeh, M. A.; Amiri, S. *J. Incl. Phenom. Macrocycl. Chem.* **2013**, DOI: 10.1007/s10847-013-0330-1.
5. Semsarzadeh, M. A; Amiri, S. *J. Inorg. Organomet. Polym.* **2013**, *23*, 432.
6. Semsarzadeh, M. A; Amiri, S. *J. Inorg. Organomet. Polym.* **2013**, *23*, 553.
7. Semsarzadeh, M. A.; Abdollahi, M. *J. Appl. Polym. Sci.* **2012**, *123*, 2423.
8. Okumura, H.; Kawaguchi, Y.; Harada, A. *Macromolecules* **2001**, *36*, 6422.
9. Okumura, H.; Kawaguchi, Y.; Harada, A. *Macromolecules* **2003**, *36*, 6422.
10. Storsberg, A; Helmut, R *Macromol. Rapid Commun.* **2000**, *21*, 1342–1346.
11. Semsarzadeh, M. A.; Amiri, S. *Silicon* **2012**, *4*, 151.
12. Ivaylo, D.; Barbara, T.; Andrzej, D.; Christo, B. T. *Prog. Polym. Sci.* **2007**, *32*, 1275.
13. Yu-Cai, W.; Ling-Yan, T.; Yang, L.; Jun, W. *Biomacromolecules* **2009**, *10*, 66.
14. Giancarlo, M.; Marco, D.; Vittorio, C. *J. Polym. Sci., Part A: Polym. Chem.* **2008**, *46*, 4830.
15. Neeraj, K.; Majeti, N. V. R.; Domba, A. *J. Adv. Drug Delivery Rev.* **2001**, *53*, 23.
16. Choi, H. S.; Kontani, K.; Huh, K. M.; Sasaki, S.; Ooya, T.; Lee, W. K.; Yui, N. *Macromol. Biosci.* **2002**, *2*, 298.
17. Fujita, H.; Ooya, T.; Yui, N. *Macromol. Chem. Phys.* **1999**, *200*, 706.
18. Semsarzadeh, M. A.; Amiri, S. *Bull. Mater. Sci.* **2012**, accepted for publication.

Chapter 8

Silicone Macroinitiator in the Atom Transfer Radical Polymerization of Methyl Methacrylate and Vinyl Acetate: Synthesis and Characterization of Pentablock Copolymers

Sahar Amiri* and Mohammad Ali Semsarzadeh

Polymer Group, Department of Chemical Engineering, University of Tarbiat Modares, Tehran, P.O. Box: 14155/143, Iran
*E-mail: amiri_s@modares.ac.ir

Poly(dimethylsiloxane) (PDMS) based pentablock copolymers have been synthesized *via* atom transfer radical polymerization (ATRP) of methyl methacrylate (MMA) and vinyl acetate (VAc) telomer at 60°C in the presence of CuCl/PMDETA as the catalyst system. The vinyl acetate telomer was prepared from controlled radical telomerization using $Co(acac)_2$/DMF and had a PDI ≈ 1.3. Poly(vinyl acetate-b-methyl methacrylate-b-dimethylsiloxane-b-methyl methacrylate-b-vinyl acetate) (PMMA-b-PVAc-b-PDMS-b-PVAc-b-PMMA) pentabloblock copolymers provided a method to design the block copolymer with PDMS segments and thus allowing for the adjustments to the flexibility by the PDMS content and a large effect of the softening point (T_g), or rigidity from the methyl methacrylate monomer from the higher melting temperature (T_m). The penta-block copolymers were characterized by ^{1}H-NMR, DSC and GPC. Meanwhile, the number-average molecular weights as determined from the ^{1}H-NMR spectra were in very good agreement with the theoretically calculated values. It can be concluded from the ^{1}H-NMR and DSC data that the pentablock copolymers of PMMA-b-PVAc-b-PDMS-b-PVAc-b-PMMA consisting of a PDMS center block and PMMA and PVAc terminal blocks were synthesized. The reactivity ratio for VAc and MMA monomer pairs was calculated from Mayo-Lewis

(r_{MMA} =0.733, r_{VAc} =0.196), Kelen-Todous (r_{MMA} = 0.760, r_{VAc} =0.211) and Finemann-Rose (r_{MMA} = 0.736, r_{VAc}=0.180).

Introduction

Polydimethylsiloxane (PDMS) is undoubtedly the most widely used silicone, which is characterized by a unique combination of properties such as low surface tension, low glass transition temperature, high permeability to gas, and excellent weather resistance. Its wide range of applications such as polyurethane foam stabilization, release coatings, and pressure-sensitive adhesives illustrates the versatility of this inorganic polymer (*1–4*). In order to produce silicone-based materials with more desirable mechanical properties, block, graft, and network copolymers containing PDMS segments have been investigated (*5*, *6*). Earlier we have reported the synthesis of silicone block copolymers with acrylate (*6*), and styrene (*7*).

We would like to report here the effect of vinyl acetate microstructures from a controlled radical telomerization of $Co(acac)_2$/DMF catalyst complex as monomer in the synthesis of a pentablock copolymer with PDMS and PMMA (*8–11*). In this work we are reporting the ATRP of poly(dimethylsiloxane) macroinitiator used in the synthesis of methyl methacrylate monomer and vinyl acetate telomers from controlled radical telomerization. The ^{1}H-NMR study of the microstructure of the telomers indicated that the sequential arrangement of CH_2 and CH groups in the telomer depends on the $Co(acac)_2$ and is different in radical and controlled radical telomerization (*8*, *10*). $Co(acac)_2$ provides the new syndiotactic route to make a telomer with controlled chain structures in the synthesis of macroinitiators used in ATRP (*8*, *10*). The final pentablock copolymers of PMMA-b-PVAc-b-PDMS-b-PVAc-b-PMMA have been characterized and the well-define microstructure of the copolymer is reported. The presence of PMMA in the block copolymer can increase the rigidity of the chain and it can be used in the macromolecular design of silicone based copolymers. Thermal properties of the pentablock copolymer indicated the low glass transition temperature of PDMS block at -100°C, PVAc at 45°C and PMMA at 89°C, making well-define thermal transitions, characterization of the pentablock microstructure of PMMA-b-PVAc-b-PDMS-b-PVAc-b-PMMA microstructure with specific units (*10*). The DP_n of specific units calculated from ^{1}H-NMR were in good agreement with the GPC data and can be used in the macromolecular design of the pentablock copolymer to adjust the glass transition dependence on the degree of flexibility of the PDMS or the PMMA units to adjust the rigidity of the copolymer (*10*, *11*).

Results and Discussion

PDMS Macroinitiator (Br-PDMS-Br)

^{1}H-NMR of the functionalized PDMS was used to verify the quantitative modification of the end groups to the terminal bromine atoms (Scheme 1). The volatiles were removed under vacuum from the final product. GPC analysis showed a M_n=14800 g mol^{-1}, with a MWD=1.93, maximum yield determined

gravimetrically is 82%. ^{1}H-NMR (in CDCl$_3$) indicated a δ=0.0-0.3 ppm for the protons of the methyl groups of -Si(CH$_3$)$_2$O, δ=2.0 ppm for the methylene group next to the bromide (*6, 10, 11*).
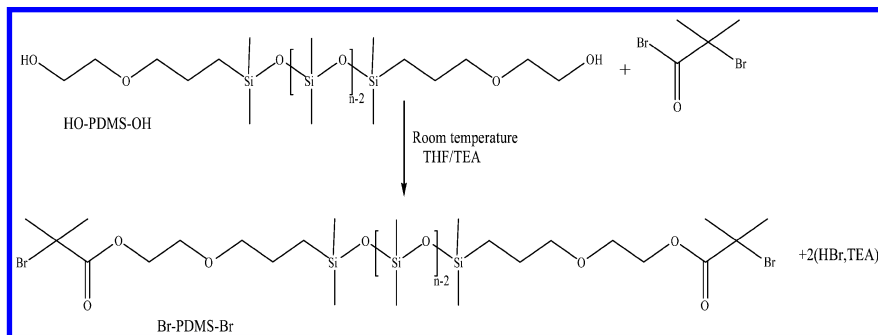
Scheme 1. Reaction scheme for the synthesis of bis(2-bromoisobutyrate)-terminated PDMS macroinitiator using bis(hydroxyalkyl)-terminated PDMS (5, 6)

PVAc Telomers from Radical and Controlled Radical Telomerization

A three-neck round-bottom flask equipped with a condenser and a magnetic stirrer was charged with VAc/CHCl$_3$/AIBN/DMF/Co(acac)$_2$ in the concentration ratios of (1/1/0.01/0.01/0.05 and 1/1/0.01/0.01/0.0). The flask was immersed at 60°C in an oil bath to initiate the reaction. The reaction was terminated after 6 hours by removing the flask from the bath with unconverted monomer and chloroform being evaporated at room temperature. THF was then added to the product and refluxed for 2 hours in order to decompose traces of the residual unreacted initiator. Finally, THF was evaporated and the polymer was dried under vacuum at 50°C to constant weight. The final yield was 81 and 68 % respectively for the controlled radical and the radical telomerization (see Scheme 2) (*8*).
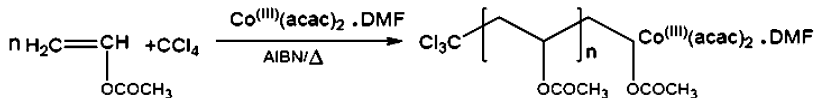
Scheme 2. Mechanism of the controlled telomerization of vinyl acetate with Co(acac)$_2$/DMF

Figure 1 illustrates the ^{1}H-NMR spectra of PVAc telomers obtained from controlled radical telomerization and radical telomeization. Peaks of methylene protons in neighborhood of CCl$_3$ (a) appear at 2.7-2.8. The methine protons of the first VAc unit (b) made a small peak at about 3.9 ppm. The peak at about 4.6-4.8 ppm was related to the methine proton from repeating VAc units in backbone of the polymer as well as the telomer molecules which are higher in radical

telomerization than controlled telomerization, telomers with CCl₃ α-end group's increases in radical telomerization (*8, 10, 11*).
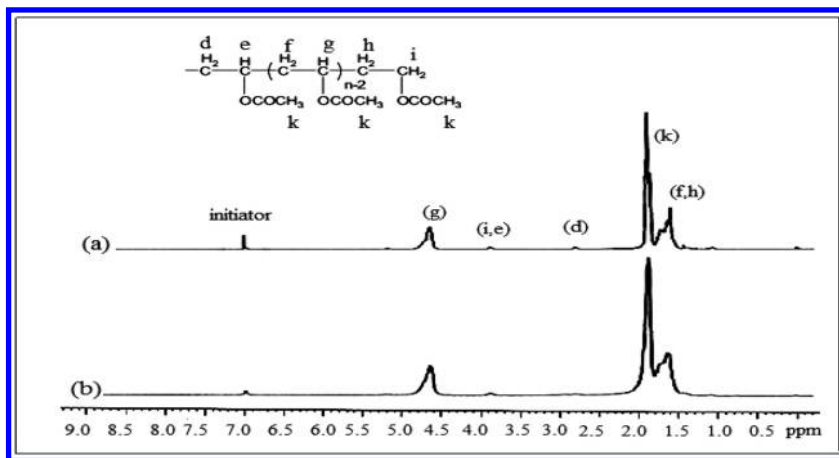
Figure 1. ¹H-NMR of the PVAc telomers from (a) the controlled radical telomerization and (b) the radical telomerization at 60°C

A presentation of the data calculated from ¹H-NMR and GPC of the controlled telomerization and the radical telomerization for 6 h at 60°C is summarized in Table 1. The methyl group of the acetate is revealed at 4.5 ppm (g). Protons of the methylene for repeating units (f) and end of chains (h) make broad signals at 1.6 to about 1.8 ppm (*8*). The AIBN peak at 7.0 ppm is small and negligible for radical telomerization but is significant for controlled radical telomerization, this indicated that the active site is a complex of Co(acac)₂/DMF.

Table 1. Data calculated from the ¹H-NMR of the controlled radical and radical telomerization of VAc at 60°C for 5 h with AIBN as initiator (*8*)

Polymer	$CDCl_3(cc)$	DP_n	Telomer%	$M_{n(HNMR)}$	$M_{n(GPC)}$	$PDI_{(GPC)}$
PVAc telomer[a]	4.6	34.09	76.85	3775	4139.2	1.65
PVAc telomer[b]	4.6	29.5	55.5	3135.14	3300	1.8

[a] Controlled radical telomerization in the presence of Co(acac)₂/DMF [b] Radical telomerization

First-order kinetic polymerization plots of PMMA and PVAc initiated by PDMS macroinitiator are shown in Figure 2-a. The linear fit indicated that concentration of propagating radical species is constant and radical termination reactions are not significant on the time scale of the reaction. Within the bounds of experimental error, the first-order correlations were essentially linear, as required for a living polymerization.
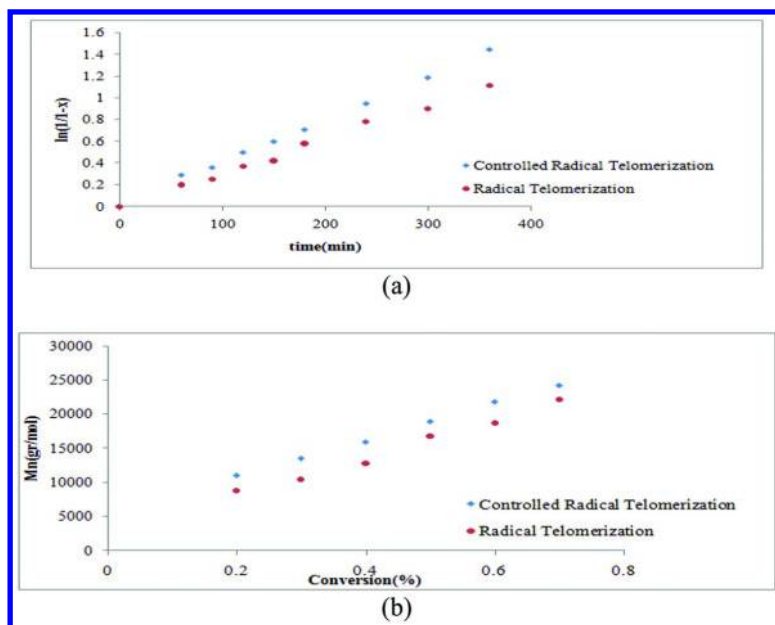
Figure 2. (a) First-order kinetic plot and (b) dependence of the polyvinyl acetate M_n on the monomer conversion for the ATRP of PMMA and PVAc with PDMS macroinitiator from (blue diamond) controlled radical telomerization and (red circle) radical telomerization at 60°C

The plot of number-average molecular weight, M_n, dependence on conversion in this polymerization is shown in Figure 2-b. A linear increase of M_n versus monomer conversion was observed indicating that the number of chains is strongly controlled and remained constant during the reaction. Since the molecular weight distribution remained low during the polymerization, nearly all the chains were expected to have been started and grown simultaneously during an equilibrium step (*10*). Figures 2-a and 2-b, demonstrated that the reaction was controllable and there is good agreement between the theoretical and experimental molecular weight results from GPC (Table 2) (*10*).

^{1}H-NMR spectra of the PMMA-b-PVAc-b-PDMS-b-PVAc-b-PMMA pentablock copolymer have been presented in Figure 3. All signals of the ^{1}H-NMR spectra were assigned to their corresponding monomers and it can be declared that the synthesis of the pentablock copolymers proceeded successfully (*10*, *11*).

(Co)Polymer	(%)X[a]	$M_{n,theory}$ (g mol^{-1})[d]	$M_{n,GPC}$ (g mol^{-1})	PDI
Br-PDMS-Br	87	14282	14800	1.93
PMMA-b-PVAc-b-PDMS-b-PVAc-b-PMMA[b]	91	23600	24200	1.21
PMMA-b-PVAc-b-PDMS-b-PVAc-b-PMMA[c]	83	21800	22100	1.35

[a] Final conversion measured by a gravimetric method.   [b] PVAc from controlled radical
telomerization   [c] PVAc from radical telomerization   [d] $M_{n,theory} = M_{n,Macroinitiator} + ([M]_{PDMS}/[M]_{Macroinitiator}) \times M_{n,PDMS} \times Conversion$
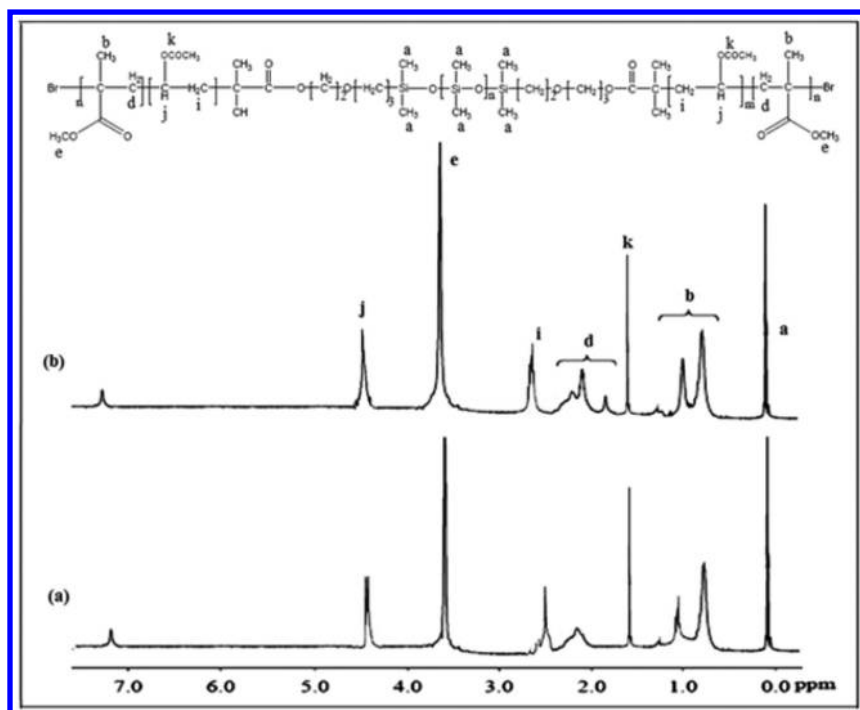
*Figure 3. ^{1}H-NMR traces for the PMMA-b-PVAc-b-PDMS-b-PVAc-b-PMMA
pentablock copolymers copolymers initiated with PDMS macroinitiator and
MMA and VAc as monomers which vinyl acetate synthesized from (a) radical
telomerizatin, (b) controlled radical telomerization and at 60°C for 6 hours*

The ^{1}H-NMR of pentablock showed a signal at 0.0-0.2 ppm associated
with the CH$_3$-Si methyl protons of PDMS along with the signals at 2.1-2.3 ppm
corresponded to OCOCH$_3$ group from the PVAc segment. Signals at 0.8-1.0 ppm,
1.9-2.1 ppm and 3.6 ppm corresponded to CH$_3$, CH$_2$ and COOCH$_3$ group from
the PMMA segment. Therefore, it is possible to synthesize the PDMS-based
pentablock copolymers via ATRP of monomers such as vinyl acetate and methyl

methacrylate in the presence of bis(haloalkyl)-terminated PDMS macroinitiator (*10*, *11*). The well-define microstructure can be used in the macromolecular design of the pentablock copolymer, assuming one can increase the mole ratio of the monomer or used different molecular weight of the VAc telomer or PDMS macroinitiator in the structure (*10*).

The reactivity ratio parameters for Kelen-Tüdös method and Fineman-Ross methods were calculated. The values of r_1 and r_2 which were estimated for MMA and VAc monomer pairs from Mayo-Lewis (r_{MMA} =0.733, r_{VAc} =0.196), Kelen-Todous (r_{MMA} = 0.760, r_{VAc} =0.211) and Finemann-Rose (r_{MMA} = 0.736, r_{VAc}=0.180) indicates that the growing radicals tend to addition to MMA monomer. The ratio of sequence lengths of PVAc and PDMS was 2.11 and for PMMA to PDMS was 2.41, so pentablock copolymers of PMMA-b-PVAc-b-PDMS-b-PVAc-b-PMMA were synthesized. Therefore, it is possible to synthesize the PDMS-based pentablock copolymers via ATRP of monomers such as vinyl acetate and methyl metacrylate in the presence of bis(haloalkyl)-terminated PDMS macroinitiator (*10*, *11*). DSC thermograms of PDMS-based block copolymers are depicted in Figure 4 for the temperature range of -100°C to +200°C. The glass transition temperature (T_g) of PDMS is expected to be about -120°C, thus it is observed in Figure 6 at -59°C (*6*, *10*). PVAc and PMMA segments exhibited T_g values of 40 and 89°C (*8*, *10*), respectively for the corresponding block copolymers. Considering the DSC results, one can conclude that PDMS-based penta-block copolymers have been synthesized successfully.
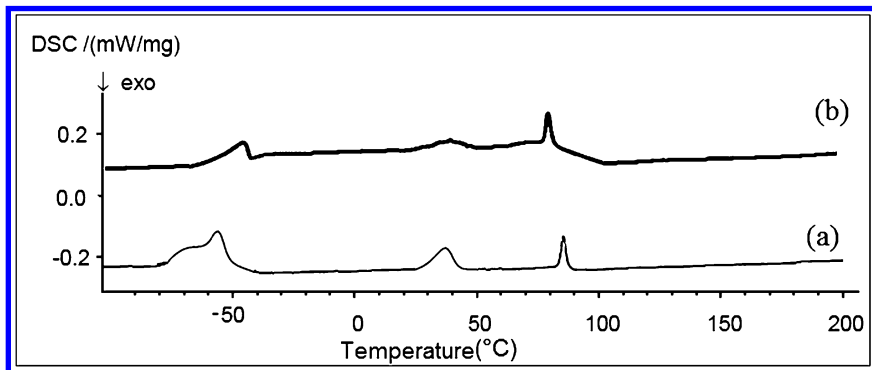
Figure 4. DSC thermograms for the PMMA-b-PVAc-b-PDMS-b-PVAc-b-PMMA pentablock copolymers initiated with PDMS macroinitiator and using MMA and VAc as monomers in which the vinyl acetate was synthesized from (a) radical telomerizatin (b) controlled radical telomerization at 60°C for 6 hours

Conclusions

Poly(dimethylsiloxane)(PDMS)-based pentablock copolymers were successfully synthesized *via* ATRP of PMMA and PVAc telomers in the presence of CuCl/PMDETA as a catalyst system at 60°C. The copolymers are of major interest because of the possibility of preparing amphiphilic pentablock copolymers

PMMA-b-PVAc-b-PDMS-b-PVAc-b-PMMA by hydrolysis of the PVAc blocks. ^{1}H-NMR was used to analyze the microstructure of the pentablock copolymers with number of PMMA, PDMS and PVAc units in the block copolymer. There was very good agreement between the number-average molecular weight determined from the ^{1}H-NMR spectra and that calculated theoretically. The narrow dispersity indices from the GPC of the synthesized pentablock copolymers yielded a lower PDI block copolymer indicating the living/controlled characteristic of the reaction. The results showed that ATRP of methyl methacrylate and vinyl acetate telomer from controlled radical telomerization proceeds with a well-controlled microstructure and narrower distribution than for radical telomerization.

References

1. Matyjaszewski, K.; Xia, K. *J. Chem. Rev.* **2001**, *101*, 2921.
2. Ibrahim, K. A.; Al-Muhtaseb, A. H. J. *Polym. Int.* **2009**, *58*, 927.
3. Wang, T. L.; Liu, Y. Z.; Jeng, B. C.; Cai, Y. C. *J. Polym. Res.* **2005**, *12*, 65.
4. Paik, H. J.; Teodorescu, M.; Xia, J.; Matyjaszewski, K. *Macromolecules* **1999**, *32*, 7023.
5. Brown, D. A.; Price, G. *J. Polym.* **2001**, *42*, 4767.
6. Semsarzadeh, M. A.; Abdollahi, M. *J. Appl. Polym. Sci.* **2012**, *123*, 2423.
7. Semsarzadeh, M. A; Amiri, S. *J. Inorg. Organomet. Polym.* **2013**, *23*, 553.
8. Semsarzadeh, M. A; Amiri, S. *J. Polym. Res.* **2012**, *19*, 9891.
9. Semsarzadeh, M. A.; Abdollahi, M. *J. Appl. Polym. Sci.* **2009**, *114*, 2509.
10. Semsarzadeh, M. A; Amiri, S. *J. Inorg. Organomet. Polym.* **2013**, *23*, 432–438.
11. Semsarzadeh, M. A.; Amiri, S. *J. Chem. Sci.* **2012**, *124*, 521–527.

Chapter 9

Organic Surface Modifications on Silicone Elastomers: Impact on Moisture Vapor Permeability and Surface Energy Dynamics

Rashi Grewal and Julie A. Willoughby*

Fiber and Polymer Science Program, College of Textiles, North Carolina State University, 2401 Research Drive Raleigh, North Carolina 27695-8301
*E-mail: jacrowe@ncsu.edu

The purpose of this study was to observe the effects of organic surface modifications on silicone elastomers with respect to moisture vapor permeability properties as a function of both grafted moiety functionality and packing density. We utilized chemical vapor deposition and mechanical manipulation of the elastomer to deposit (tridecafluoro-1,1,2,2-tetrahydrooctyl)trichlorosilane and 3-aminopropyltrimethoxysilane. As expected, the chemical vapor deposition of both species altered the chemistry of the elastomer surface to more hydrophobic for the fluorinated silane and more hydrophilic for the amino - terminated silane in the absence of mechanical elongation during the modification. As previously demonstrated, increasing the packing density of the silanes by increasing the degree of tension on the substrate during activiation and deposition, resulted in an increase in the contact angle of water. This turned out to be true even for the hydrophilic species. In all modified samples, the moisture vapor permeability (MVP) decreased by about 50% and is attributed to the ultraviolet/ ozone activation step that created a silica-like layer. Despite the reduction in MVP, the modified elastomer films are still considered to have a high moisture vapor permeability on the order of $5 \cdot 10^{-1}$ g·mm/m²·hr·kPa.

Introduction

Silicone elastomers are used in a wide array of applications, including cosmetics, bakeware, automotives, and medical devices. Their high permeability, durability, and non-toxicity make them a great material for such uses. Silicone elastomers are known to be very breathable and permeable to many gases including oxygen, carbon dioxide, methanol, toluene, and of course water vapor (*1*). Its high permeability is due to its high free volume between polymer chains; allowing facile diffusion of small molecules (*2*). Its high permeability of water vapor can be an issue when used as encapsulants for light emitting devices where moisture transport through the encapsulant prematurely degrades the device's function; warranting further modification to the encapsulant to prevent moisture egress, yet not impact the desirable optical properties of silicone elastomers (*3, 4*). On the opposite end of the spectrum, medical products, such as wound care coverings require high moisture permeability and high occlusive characteristics for optimum function.

Previous work to modify the permeability of silicone elastomers involved various methods, including surface treatments. The purpose of one such study was to make inherently hydrophobic polydimethylsiloxane (PDMS) more hydrophilic in order to make it more usable for biomedical applications. PDMS films were compared to PDMS-co-poly(ethylene glycol) (PEG) films. Water sorption increased for these films with increasing hydrophilic ethylenoxy content (up to 6% weight/weight), with a maximum increase of nearly 100% compared to plain PDMS. Contact angles also decreased significantly, from 110° for plain PDMS with no ethylenoxy content, to 40° for PDMS/PEG copolymer with 6% ethylenoxy conent. Drug-release experiments were also performed with these films by loading them with a hydrophilic drug, theophylline. It was observed that the copolymer films had a higher release of theophylline, and at more controlled rate, than the homopolymer films (*5*).

In another study, copolymer films of PDMS and polyether urethane were created in order to have an encapsulant material with low water permeability and high elasticity. Increasing PDMS content of the copolymer resulted in a decrease in water absorption, with % absorption at 37°C decreasing from 3% for pure polyether urethane to 1% for a PDMS:polyether urethane ratio of 50:1. Liquid water permeability at 37°C decreased from 7mg/cm^2 for pure polyether urethane to 5mg/cm^2 for all copolymer ratios of 2:1, 10:1, and 50:1. These are not significant differences. The same was true for water vapor transmission rate at 25°C; after a week, the vapor transmission was the lowest for pure polyether urethane (35 mg/cm^2) and only increased slightly for the various ratios. The highest transmission was for pure PDMS (50 mg/cm^2), which was the only one with a noticeably different transmission rate (*6*).

When designing multidirectional breathable materials, composite structure of films, fibers, clays are often utilized for enhancement in structural integrity, lower over-all cost, and multi-functionality that may be a bulk property imparted from one of the composite components or a surface modification to any given layer. Figure 1 shows the concept of an silicone elastomer wound care dressing, in which one side is liquid repellent due to densely packed silane alkanes and the inherent

chemical structure of poly(dimethylsiloxane) (PDMS) and the other side allows the transport of bodily fluids such as sweat or wound exudate. The moisture vapor transport rate of PDMS was determined by our laboratory to be 25.47g/m²·hr for a 0.22mm thick film. This is a comparable rate of the moisture transport through human skin, thus a good skin mimic with respect to breathability (*7*). In addition, the amino- terminated silane moieties that are grafted to the outermost surface of the silicone could further facilitate moisture vapor transport due to its polar nature. In an actual clinical setting, a more absorbent layer between the skin and protective silicone covering would be necessary.
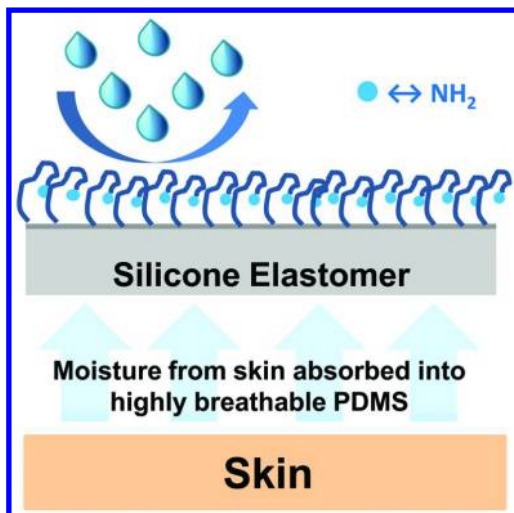
Figure 1. Basic schematic of a modified elastomeric wound covering comprising a breathable silicone elastomer that has been modified with amino-terminated silane moieties to facilitate wicking of excess moisture from skin through film.

It is well known that the methyl groups of PDMS make it hydrophobic; rendering its surface liquid repellant and resistant to further modification. In many cases, this inert surface is not desirable, requiring subsequent engineering design to such surfaces. While resultant surface stability and dynamics of modified silicone elastomers have been previously studied (*8–12*), to our knowledge there has not been a systematic evaluation of the resultant barrier properties of the modified substrates. The main goal of this work was to determine how chemical vapor deposition (CVD) of polar and non- polar silane moieties on silicone elastomers impacts moisture vapor transport and surface chemistry of the modified substrates. The two central questions of the study were 1) "Does modifying the surface of a highly permeable elastomeric film by nano- scale organic species result in a change in the substrate barrier properties?" and 2) "If the deposited chemical species are packed more closely together, will there be a further change in barrier properties?" Figure 2 illustrates the potential influence of packing density of grafted moieties could have on moisture vapor permeability. In addition, for this study, both hydrophobic and hydrophilic species are grafted

onto silicone films to determine surface and barrier properties as a function of the terminal moiety chemistry and grafted packing density.

Figure 2. At normal packing density, the silane molecules allow moisture vapor to pass through at their normal rate. If the hydrophobic moieties are densely packed on the elastomeric substrate, there could be a possibility of reduced moisture transmission.

In order to create densely packed moieties on a silicone elastomer, we utilized the technique coined "mechanically-assembled monolayers" by Genzer et al (*8*). They showed that the high elasticity of the PDMS backbone enabled them to elongate a crosslinked silicone film prior to chemical vapor deposition of fluorinated alkanes (-$(CH_2)_2C_6F_{13}$). After release of the elongation, a stable superhydrophobic surface on the PDMS film was realized. This technique allows for the control of the packing density of hydrophobic molecules that have been grafted onto the surface of the film as the elongation increases, the grafting density of deposited moieties increases.

Experimental

Materials

Sylgard® 184 PDMS elastomeric kit was obtained from Dow Corning. Throughout this paper, it will be referred to simply as PDMS. Fluoro-octyl trichlorosilane (-$(CH_2)_2C_6F_{13}$, product #SIT8174.0) came from Gelest, Inc. and amino-propyl trimethoxysilane (-$C_3H_6NH_2$, CAS# 13822-56-5) came from Sigma Aldrich. Toluene (histology grade 99.5%) and paraffin oil also came from Sigma Aldrich.

Methods

Preparation of PDMS Films

A Sylgard® 184 PDMS elastomeric kit was used for substrate formation for chemical vapor deposition. A 10g:1g ratio of Sylgard® 184 base to crosslinker was mixed thoroughly for about 1 minute. The mixture was then de-aired and cast on a non-adhering substrate, LDPE coated paperboard. The mixture was drawn-down with a #8 Mayer rod and cured at 70°C for 24 hours on a level oven rack. After curing, 2.5 x 2 square inch rectangles were cut and placed in a large covered toluene bath for extraction of impurities. Toluene was changed three times at 24 hour intervals. Once extraction was complete, the films were allowed to air-dry overnight, and then the individual films were placed in Petri dishes and locked in a dry desiccant chamber to keep out moisture.

Chemical Vapor Deposition and Mechanically-Assisted Monolayers

The protocol to create "mechanically-assisted monolayers" (MAMs) on silicone elastomers used in this study is depicted in Figure 3 and described elsewhere in detail (*8*). Briefly, a PDMS film is clamped onto a mechanical stretcher. The end screw of the stretcher is turned to allow the film to elongate the desired percentage of its original length. While elongated, the film is exposed to UV/Ozone (UV/O) where the methyl groups on the siloxane backbone are cleaved with ozone to form polar species such as carbonyl, hydroxyl, and carboxy groups but as demonstrated by others the majority of the formed surface bound groups are –OH terminated (*13*). The hydroxy-funtional film allows for the condensation of hydrolyzed $C_6F_{13}(CH_2)_2SiCl_3$ to covalently bond with the elastomer substrate. After deposition, the film is contracted back to its original length.
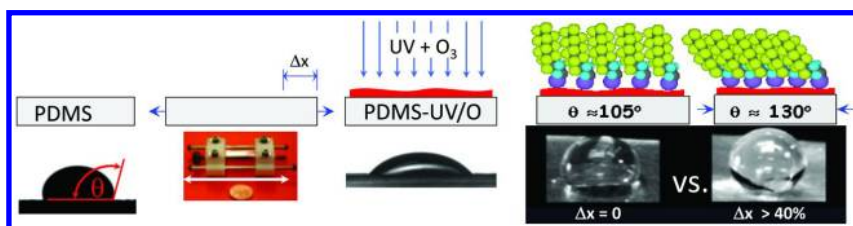
Figure 3. Illustration of mechanically assisted monolayers (MAMs) to increased packing density of a self-assembled monolayer by elongating the substrate during ultraviolet/ ozone activiation and chemical vapor deposition. The microscope images of the water droplets with contact angles correspond to substrates processed without mechanically stretching the sample (or 0% elongation) versus when the substrate is stretched to 40% elongation. Adapted from reference (8).

The grafting reaction itself is a two-step condensation reaction: 1) $C_6F_{13}(CH_2)_2SiCl_3$ molecules are vaporized to the activated PDMS film via a pressure gradient. Of the utmost importance is to have the deposition chamber at a sufficient humidity (ca. 65%) to intiate the hydrolysis reaction of the C_6F_{13}-$(CH_2)_2$- terminated chlorosilane. The next step is where 2) silane molecules, now with –OH terminated groups, to condense with the surface bound –OH groups of the UV/O activated PDMS film (see Figure 4) (*8*).
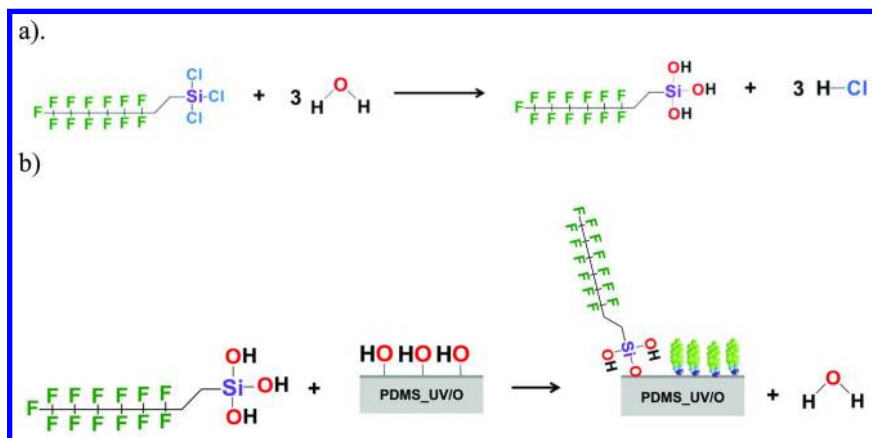
Figure 4. Two-step condensation reaction for grafting of silane to PDMS where a) the chlorosilane is hydrolyzed by reacting with ambient humidity and b) the condensation between the hydrolyzed silane and the polar groups imparted on PDMS by ultraviolet/ ozone (UV/O) exposure (–OH groups are depicted for simplicity).

To create a range of functionalized elastomeric substrates, the extracted films were taken from the desiccant chamber and 1) elongated to 0%, 25%, or 50% of the original length. Next, the films were 2) activated to created hydrophilic moieties for subsequent grafting. For 0% elongation, the PDMS film was simply placed onto the rack of the UV/O oven. For the 25% and 50% elongated samples, the film was placed lengthwise onto a mechanical stretcher, i.e., 2.5 inches along the length of the stretcher such that 2 inches were in the elongation region. For 25% elongation, the film length increased from 2 inches to 2.5 inches, and for the 50% sample, the length increased from 2 inches to 3 inches. While elongated, the film was placed in the UV/O oven (UV/OCS T10X10/0ES) for 60 minutes. A set of UV/O-only treated films was created for comparison against further silane-modified treatment. Finally, 3) the samples were subjected to chemical vapor deposition for two hours with either (tridecafluoro-1,1,2,2-tetrahydrooctyl)trichlorosilane (denoted as PDMS-$(CH_2)_2C_6F_{13}$) or 3-aminopropyltrimethoxysilane (denoted as PDMS-$C_3H_6NH_2$).

Figure 5 shows the vapor deposition for both $-(CH_2)_2C_6F_{13}$ and $-C_3H_6NH_2$. For $-(CH_2)_2C_6F_{13}$; prior to introducing the activated substrate to the chemical vapor deposition (CVD) chamber, a water source was placed into the chamber to insure a humidity of ca. 65% (step 1). Concurrently, a fresh silane/paraffin oil mixture was prepared. The paraffin oil served to control the diffusion rate of the silane (*14*). A 1:1 weight ratio mix of paraffin oil and silane was added to an Erlenmeyer flask comprising a valve stopper. The contained mixture was gently rotated for about 5 seconds before being placed in an oven to be heated at 85°C for 10 minutes.

1. **Humidify chamber**
2. **Create negative pressure gradient**
3. **Deposit heated silane**
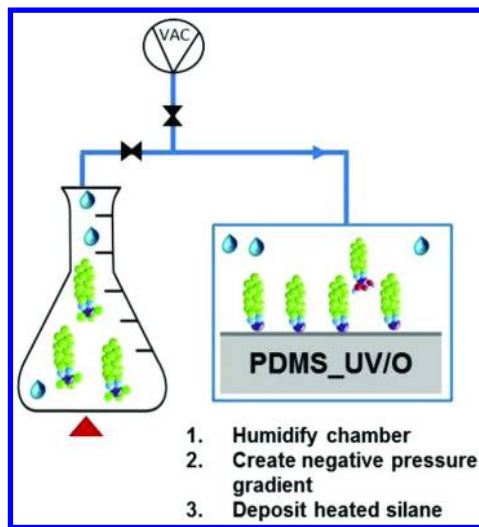
Figure 5. Chemical vapor deposition procedure for $-(CH_2)_2C_6F_{13}$ and $-C_3H_6NH_2$ terminated silanes.

Upon completion of UV/O exposure and heating the silane mixture, the water source was removed from the CVD chamber, and the PDMS film put in its place. Vacuum was then pulled on the chamber, to which the silane flask was then hooked up (step 2). At this point the valve of the stopper was opened, allowing the silane to flow into the chamber and deposit for 2 hours onto the film (step 3). After 2 hours of deposition, the stopper valve was again closed, shutting off the flow and ending the experiment. The flask was disconnected from the chamber, the films were released from the tension mode and stored in a Petri dish in the desiccator.

For $-C_3H_6NH_2$, the same procedure was followed, except the humidity of the chamber was 67%, toluene was used instead of paraffin oil in order facilitate vaporization (*15*, *16*) and the mixture was heated at 100°C. Also, in the first step of the condensation grafting reaction, methanol versus HCl is given off as a by-product, since $-C_3H_6NH_2$ has methoxy reactive groups.

Surface Chemistry and Stability

Fourier Transform Infrared in the Attenuated Total Reflectance Mode

FTIR-attenuated total reflectance (ATR) was used to verify deposition. An Excalibur FTS 3000MX spectrometer was used; 64 scans were taken for each sample. In order to assess completion of the silane reaction, the UV/O-only-treated samples were used as the background for silylated samples. The ZnSe crystal was cleaned with ethanol and air background taken before every sample to ensure no contamination of the sample spectrum. Samples were compared for a difference in the spectrum based on UV/O treatment only versus silylation. This was done by observing any changes in the broad peak from 3500 to 3300cm^{-1}, which is the frequency range for –OH vibrations as well as amino- containing groups.

Contact Angle Measurements

In order to determine that the deposition modification correlated with those of previous literature (*8*), water contact angle measurements were performed. The contact angle (sessile drop technique) experiments were performed with deionized water (bulk resistivity 14 MΩ·cm) using a DataPhysics OCA goniometer equipped with a high speed camera (30 frames/second). The film was placed onto the stage between the camera and the light source. All surface activity was conducted and monitored via the imaging software used for the instrument. A 50 µL syringe filled with deionized water was held in place above the film, with drop size of 5µLs pumped out at 2µL/s. The outer diameter of the needle was 0.18 micrometers. Upon the drop's contact onto the film and release from the syringe needle, a video of the drop was recorded for 30 seconds. From this video, the baseline of the drop's position on the film was located and a plot obtained for the calculation of the contact angle.

Contact angle measurements were also recorded at elevated temperature (25°C and 37°C) and humidity (15% and 85%). The drop volume during this period varied from 1-5µLs thus we conducted measurements at ambient conditions to ensure that contact angle was not effected by the size of the drop, consistent with others' observations (*17–19*).

Moisture Vapor Permeability (MVP)

The desiccant method of ASTM E96 was implemented for this study (*20*). As described elsewhere (*21*), a Mason jar filled with 100g of blue indicating silica gel desiccant constituted the apparatus. A round metal shim was hot-glued onto the mouth of the jar. The film was sandwiched between two foil discs, one with a larger punched hole (1.5" diameter) than the other (1" diameter) and trimmed around the edge. The sandwich was sealed onto the shim. Once assembled, the apparatus was measured for its initial mass, then placed inside the humidity chamber (ESPEC

BTL-433) at 38°C and 90% RH and monitored daily for moisture pickup for up to 10 days.

Results and Discussion

Confirmation of Surface Modifications

In order to determine if the CVD modification was successful, we employed FTIR-ATR spectroscopy and contact angle techniques for surface characterization. The FTIR-ATR spectra for PDMS (Sylgard® 184), the UV/O activated substrate (PDMS-UV/O), and the subsequent CVD modified substrate (either PDMS with $-(CH_2)_2C_6F_{13}$ or $-C_3H_6NH_2$, the nonpolar and polar components, respectively) are shown in Figure 6. While the broad $-SiOH$ peak region from 3000-3500 cm^{-1}, did show sufficient activation by UV/O as compared to the native PDMS, the change in this same region after CVD treatment was not clearly apparent. In addition, the $-NH_2$ groups only have weak vibration frequencies in FTIR and the fluorine groups are not detectable. Further analysis with X-ray photoelectron spectroscopy was performed to confirm the presence of fluorine and nitrogen.
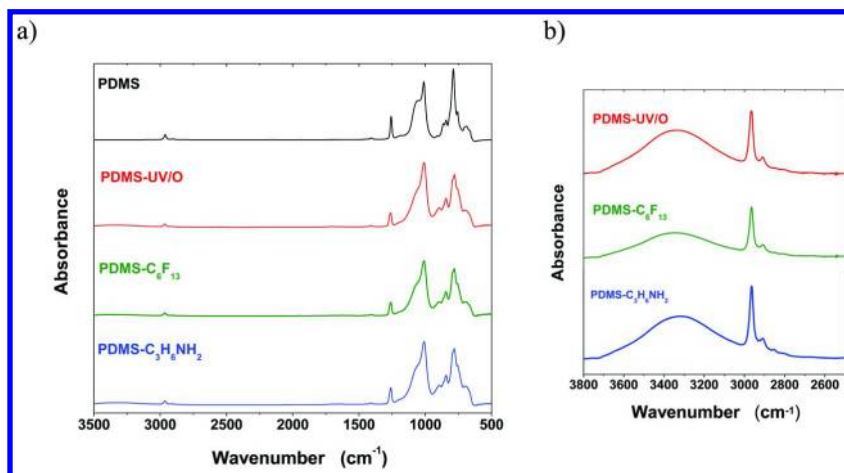
Figure 6. FTIR spectra: a) FTIR spectra of PDMS and the various treated samples. At 1000cm^{-1} there is a shift in the peaks that are Si-O and Si-CH$_3$. b) Hone-in between 3600 and 3000cm^{-1} shows that there is a peak due to the presence of –OH from UV/O treatment. Treatment with $-(CH_2)_2C_6F_{13}$ apparently gives a greater reduction in this peak than does $-C_3H_6NH_2$, due to $– NH_2$ appearing in the same region, but this is not quantifiable.

Figure 7 shows the XPS spectra of untreated PDMS and CVD-modified PDMS films at two conditions: 1) the fluorinated silane deposited when the PDMS was activated and modified under a 50% elongation and 2) the amino-terminated silane deposited without tension on the PDMS film. It is apparent in Figure 7 that a high packing density for fluorine molecules was deposited onto the

film with a silicon:fluorine peak area ratio of 1.1 as compared to not detectible in the virgin sample. Correspondingly, the silicon:nitrogen peak area ratio of 12.95 corresponds to less 3-aminopropyltrimethoxysilane deposited in the unelongated state (see Figure 7c). Nonetheless, nitrogen was still detectable as compared to not present in the virgin sample. Our findings are consistent with previous studies of varying the degree of elongation of PDMS elastomers for CVD of fluorinated alkane chains (*8*).
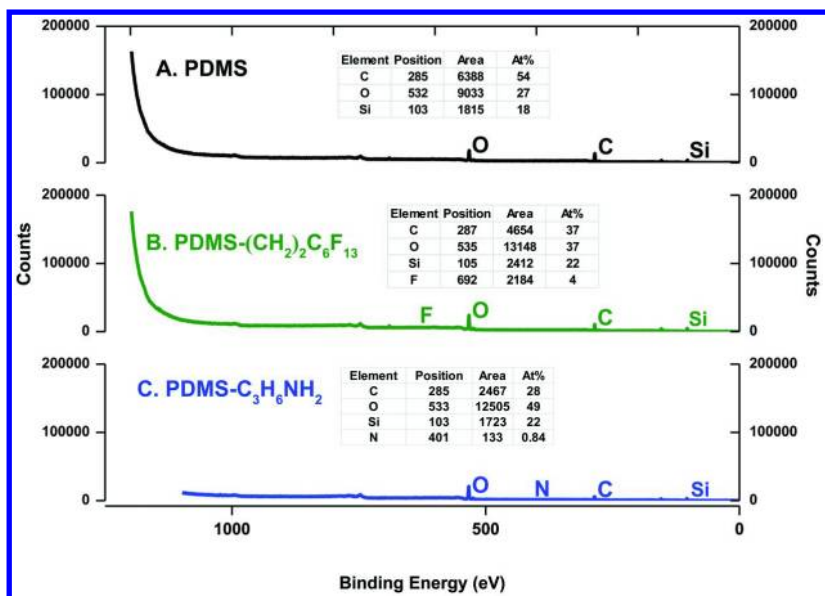
Figure 7. XPS data comparing: A. PDMS untreated, B. –(CH₂)₂C₆F₁₃-treated, and C. -C₃H₆NH₂-treated films. Fluorine (F) and nitrogen (N) are present in the corresponding treated samples as compared to being non-detectable in the virgin PDMS sample.

Contact angle of water is frequently used to characterize surface chemistry of polymer films. Whitesides et al. also demonstrated the surface sensitivity of the technique where an ether group contributing to surface polarity was not detectable there were more than four methylene groups between the air- substrate interface and the ether group. While contact angles for gold surfaces with monolayers of $HS(CH_2)_{16}O(CH_2)_{n\geq4}CH_3$, were identical to the C21 alkane thiol, deeper surface probing with XPS and external reflection infrared spectroscopy confirmed the presence of ether groups. This verified that surface "deep" ethers have little impact on the surface contact angle making it a sensitive technique to study surface chemistry dynamics (*22*). Broadly speaking, a value of less than 90° is deemed a hydrophilic surface and a value greater than 90° is deemed a hydrophobic surface. PDMS is clearly hydrophobic and based on prior studies (*8*) it was expected that as the percent elongation of the silicone elastomer prior to activation and CVD modification with fluorinated moieties increased, so would

the contact angle of the modified surface. Figure 8 illustrates our contact angles obtained as a function of the elongation during modification with -$(CH_2)_2C_6F_{13}$. In addition, we show that even the aminopropyl counterpart of the fluorinated silane showed the same increase in contact angle due to the apparent increase in packing density and possible chain orientation of the grafted molecules (see Figure 8b).
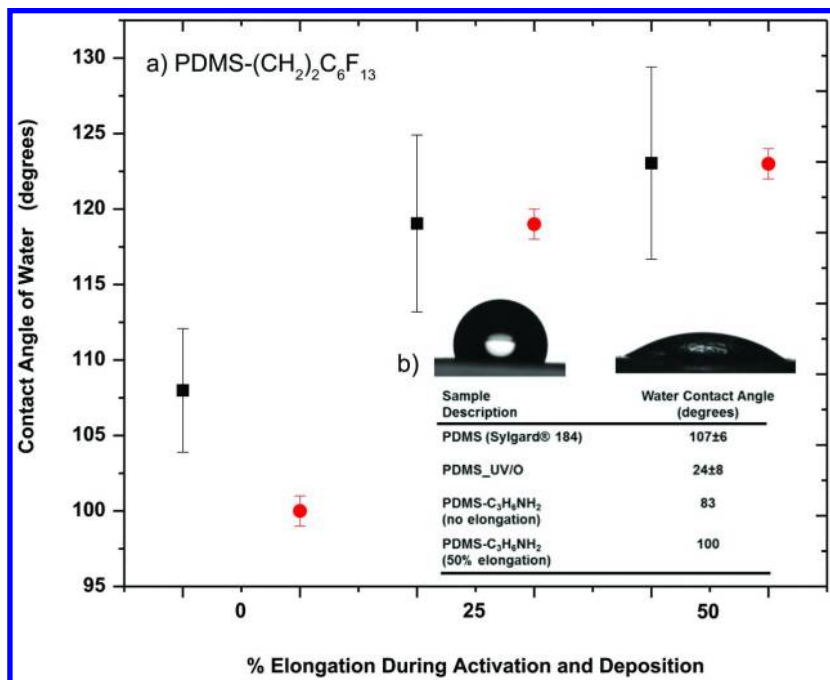
Figure 8. Contact angle of water for a) the fluorinated trichlorosilane modified substrate (PDMS-$(CH_2)_2C_6F_{13}$)) as a function of % elongation during surface modification for our work (black squares) and previous work (red circles) (8), and b) optical microscopy images and contact angle of water data for virgin PDMS (Sylgard® 184), activated PDMS (PDMS-UV/O), and aminopropyltrimethoxysilane modified substrates (PDMS-$C_3H_6NH_2$) at 0% and 50%, elongations. Of notable interest is that even the substrate modified with the polar amino- group experiences an increase in hydrophobicity with increasing packing density of the grafted molecules.

Moisture Vapor Transport through Surface-Modified Silicone Elastomers

Figure 9 compares the moisture vapor permeability (MVP) for CVD-treated elastomer samples. It is evident that while MVP does not seem to correspond with the degree of packing density, there was an overall MVP reduction of 50% with the surface treatment. The greatest contributing factor was the UV/O exposure for decreasing the substrate MVP. This decrease is due to the densification of

PDMS, which creates a silicate glass-like layer (*13*). This rigid, crystalline layer, being more solid-like, slows diffusion, thus more impermeable to vapor than the flexible PDMS polymer chains. Of noteworthy consideration is that MVP reduced by the same magnitude with both hydrophobic and hydrophilic moieties. It appears that the amino end-groups and fluorinated chains have no differing effect on permeability. This can be advantageous when modifying polymer surfaces for different applications requiring either hydrophilic or hydrophobic surface chemistries yet still maintaining the inherent breathability of PDMS.
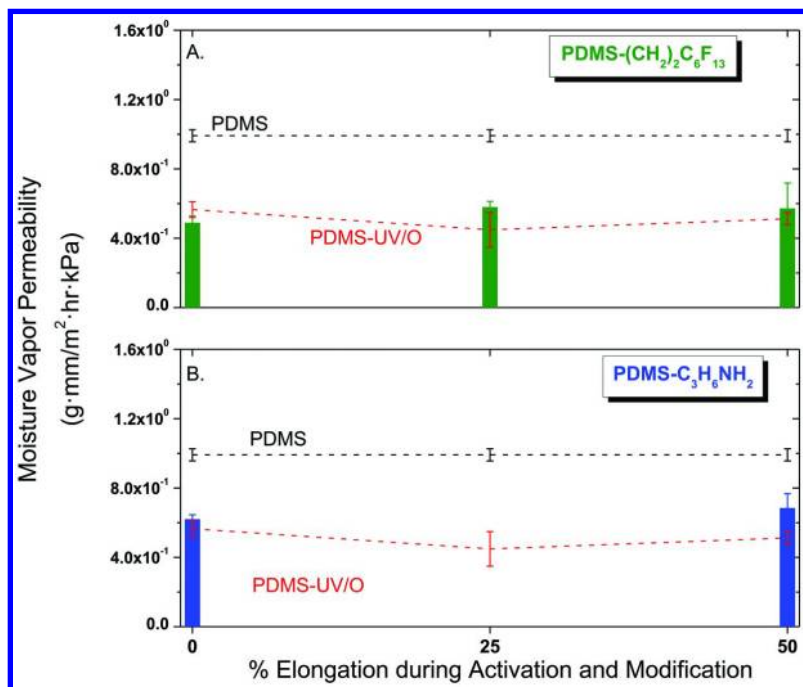
Figure 9. Moisture vapor permeability of untreated PDMS and treated counterparts. UV/O treatment is significant in reducing permeability by about 50%. There is no further decrease in MVP by modification with A. -$(CH_2)_2C_6F_{13}$, or B. -$C_3H_6NH_2$ silanes, which have no difference in permeability despite being of different polarities. There is also no difference in permeability based on the degree of elongation during modification of the PDMS film, implying that increased packing density does not further reduce permeability.

Surface Dynamics of Modified Silicone Elastomers

Amino-Terminated Moieties Grafted onto Sylgard® 184

The silicone elastomer modified with the chemical deposition of 3-aminopropyltrimethoxysilane (-$C_3H_6NH_2$) demonstrated interesting surface dynamic behavior that could be advantageous when designing materials with

adaptable properties. Since the films were stored in a dry desiccator, they became hydrophobic over time, including the PDMS–$C_3H_6NH_2$ films that were not elongated prior to modification. After storage in the arid environment for 2 weeks, the sample was placed into water for one hour and surface dried prior to measuring the contact angle. For the unelongated PDMS–$C_3H_6NH_2$ specimen, the surface returned from a hydrophobic state to a mildly hydrophilic state upon the change in its environmental conditions (see Figure 10).
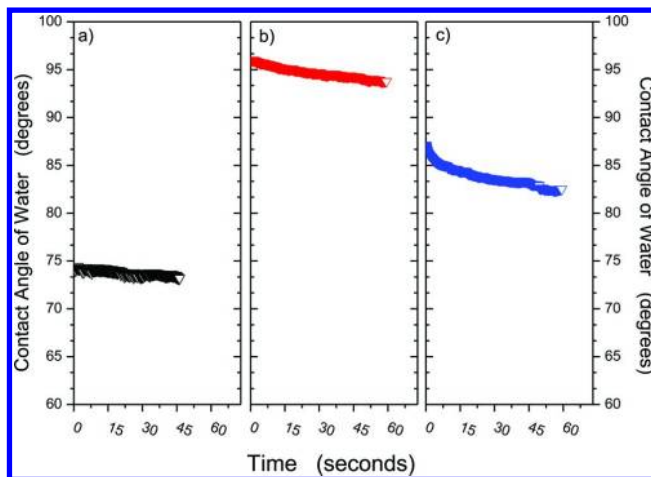
Figure 10. PDMS modified with –$C_3H_6NH_2$ without elongation during activation and CVD where a) is the contact angle measured immediately following deposition (hydrophilic), b) is the contact angle measured 2 weeks after the sample had been stored in desiccator (hydrophobic), and c) is the contact angle measured after 2 weeks in desiccator and 1 hour in water. It has become mildly hydrophilic again, although not to its original value.

However, after another month in storage, the film had become hydrophobic again, and did not convert back to hydrophilic after placement in water. XPS was done again, to detect whether or not nitrogen was still present. Figure 11 compares the XPS results as a function of time for the modified film. While nitrogen is still detected over time, the amount is decreased. The oxygen to carbon ratio has also changed; it became lower over time as carbon content increased. This would likely be due to the adventitious carbon that deposits on a film over time.

For the 50% elongated films, there was no change in behavior based on wet or dry conditions, and in fact surface hydrophobicity increased. Contact angles are shown in Table 1. XPS was also done on a 50% elongated film with no detectable nitrogen at the time of testing (see Figure 11). It should be noted that XPS was done on this film after several months, thus the results could be due to aging effects as noted in the 0% elongation PDMS-$C_3H_6NH_2$ film.
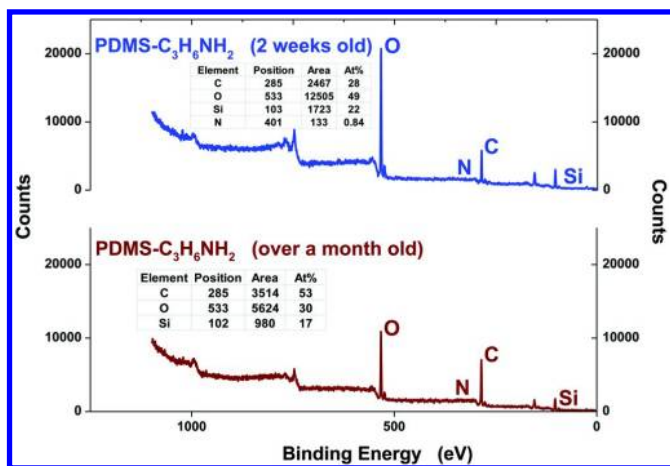
Figure 11. XPS analysis of 0% elongated treated film over time (stored in a desicator). After 2 weeks from modification, there is nitrogen (N) present, but in very low amounts. After one month of aging, nitrogen has become even more difficult to detect. The oxygen to carbon (O: C) ratio has changed over time, implying an increase in adventitious carbon depositing onto the film.

Table 1. Contact angle data before and after water immersion for PDMS-$C_3H_6NH_2$ at 50% elongation during activation and deposition.

Sample Age and Environmental Exposure	*Contact Angle (degrees)*
Immediately following CVD Treatment	100.32 +/- 4.09
After Several Months in Desiccator	120.57 +/ -4.45
After Several Months in Desiccator + Water Immersion	120.36 +/- 1.12

In-Situ Environmental Variations during Contact Angle Measurements

As the permeability data was obtained, the question of surface stability arose. The main question here was "How is surface stability affected by the packing density of the deposited species?" This in turn gave way to a more specific question appropriate for barrier materials: "Do the surface dynamics for the modified elastomers change under the tropical test conditions of the MVTR measurement?" A drop of 2-3μL was lowered onto the film surface and contact angle measured under varying relative humidity (15 and 85%) and temperature (25 and 38°C).

Figures 12 and 13 depict the interaction of the surface chemistry of PDMS and its silane-treated counterparts with the environment, at varying conditions. Figure 12 compares PDMS with PDMS-$C_3H_6NH_2$ at 15% (left column) and 85% (right column) relative humidity. The non-elongated silane was only a day old thus

still hydrophilic. The 50% elongated sample remained hydrophobic throughout all conditions. Figure 13 compares PDMS with PDMS-$(CH_2)_2C_6F_{13}$. There is little difference in contact angle behavior for either silane based on relative humidity; at 38°C, however, there is a greater change in contact angle at both humidities than at room temperature.

Other studies varying humidity and temperature concurs with our polymer surface behavior. In one study, the contact angle of hydrophobized sand increased dramatically as relative humidity was increased at several points from 33 to 94%. It was explained here that this may occur because the water vapor from humidity adsorbed onto the few remaining high-energy points on the largely hydrophobic surface. They would thus be more attracted to each other than the surface, hence driving down the surface energy, and in turn increasing the hydrophobicity, or contact angle (*23*). Similar results were obtained in another study where three different conditions were used: dry, still air, and vapor-saturated environment. The latter gave the highest contact angles that were also the most stable over the course of several minutes.
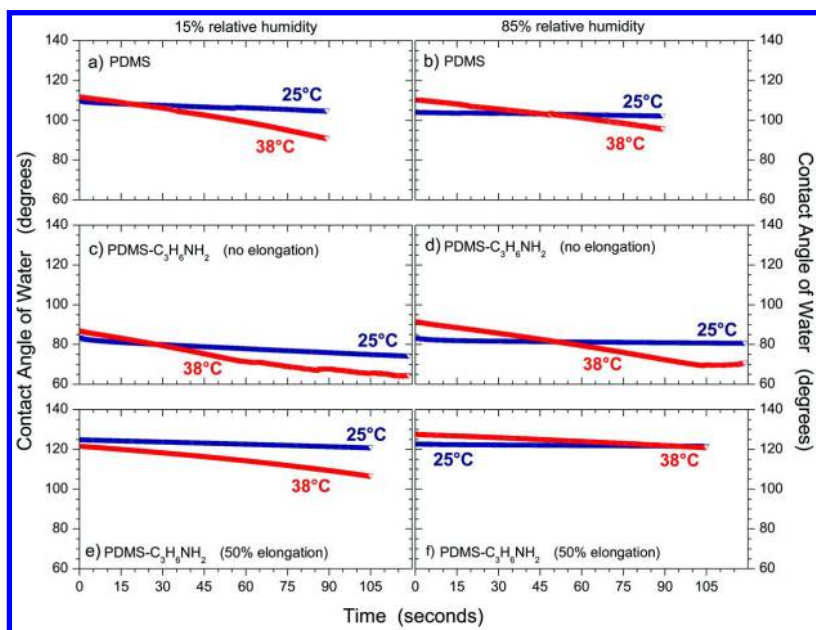
Figure 12. Contact angles by varying relative humidity and temperature for a) PDMS at 15% relative humidity, b) PDMS at 85% relative humidity, c) PDMS-C₃H₆NH₂ (no elongation) at 15% relative humidity, d) PDMS-C₃H₆NH₂ (no elongation) at 85% relative humidity, e) PDMS-C₃H₆NH₂ (50% elongation) at 15% relative humidity, and f) PDMS-C₃H₆NH₂ (50% elongation) at 85% relative humidity. The non-elongated sample was tested one day after modification, thus hydrophilic as noted in Figure 10, compared to the 50% elongated sample that remained hydrophobic regardless of the environmental condition. Note that the constant slope is likely due to water evaporation over time.
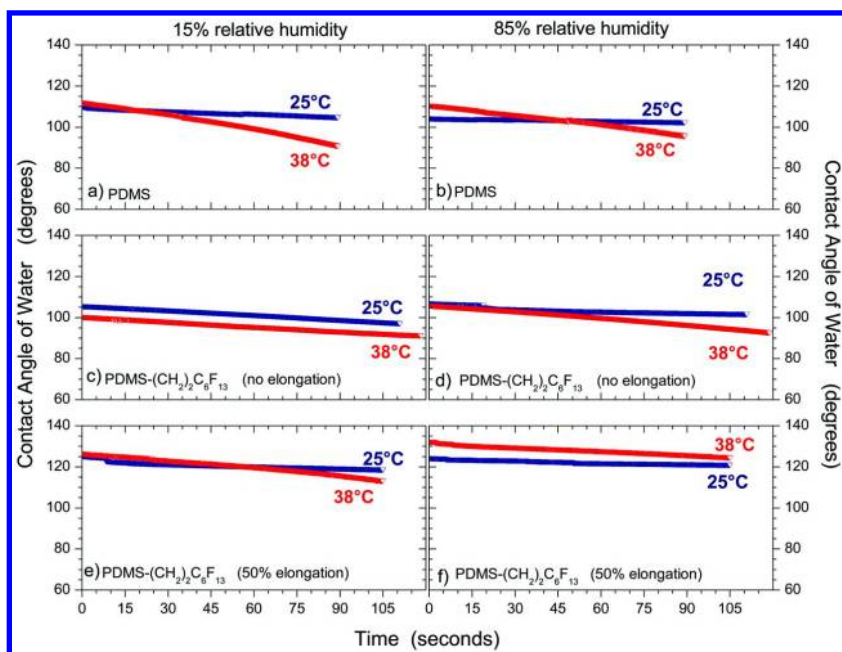
Figure 13. Contact angles by varying relative humidity and temperature for a) PDMS at 15% relative humidity, b) PDMS at 85% relative humidity, c) PDMS-$(CH_2)_2C_6F_{13}$ (no elongation) at 15% relative humidity, d) PDMS-$(CH_2)_2C_6F_{13}$ (no elongation) at 85% relative humidity, e) PDMS-$(CH_2)_2C_6F_{13}$ (50% elongation) at 15% relative humidity, and f) PDMS-$(CH_2)_2C_6F_{13}$ (50% elongation) at 85% relative humidity. There is no difference based on humidity, and a slight increase in hydrophobicity at higher temperature. Note that the constant slope is likely due to water evaporation over time.

Temperature-dependence of contact angles has also been studied for elastomers and polymer-water interfaces (*24*, *25*). It has been observed that for butyl rubber and silicone fluids, as temperature increases, contact angle increases (*26*). In one report, it was said that the hydrophobic phase of the polymer-water interface dominates the temperature-dependence of contact angle, while the hydrophilic phase dominates the interfacial properties (*27*). Ferguson and coworkers demonstrated the reconstruction differences between amorphous or crystalline polymers utilizing chemically oxidized semi-crystalline and completely amorphous poly(butadiene) films (*25*). While initially hydrophilic (θ_{water} < 60°) the oxidized surfaces would reconstruct to a hydrophobic state (≈90°) after remaining in ambient conditions. Rearrangement of hydrophilic groups occurred when the oxidized films were exposed to water reaching original water contact angle values after 6 hours (*28*, *29*). Enthalpy- driven equilibrium involves hydrogen bonding, Lewis acid-base interactions and van der Waals forces between the hydroxyl and carboxylic acid moieties along the polymer

chain. However, upon heating the oxidized films in water, the water contacting side became hydrophobic. This switch from hydrophilic to hydrophobic triggered by heat was attributed to an entropy change, rather than enthalpy, in the system. This allowed surface chains to assume their random coil conformations thereby pulling out the hydrophilic moieties from the surface to the bulk.

Finally, Figure 14 compares the films of the two silanes at 15% relative humidity and 25°C, after several months. The key observation is that for PDMS-$C_3H_6NH_2$, there is a greater increase in contact angle with increased packing density. For both silanes, regardless of polarity, the contact angle is the same for substrates modified during the 50% elongation mode. For PDMS-$C_3H_6NH_2$, this is likely due to surface rearrangement over time.
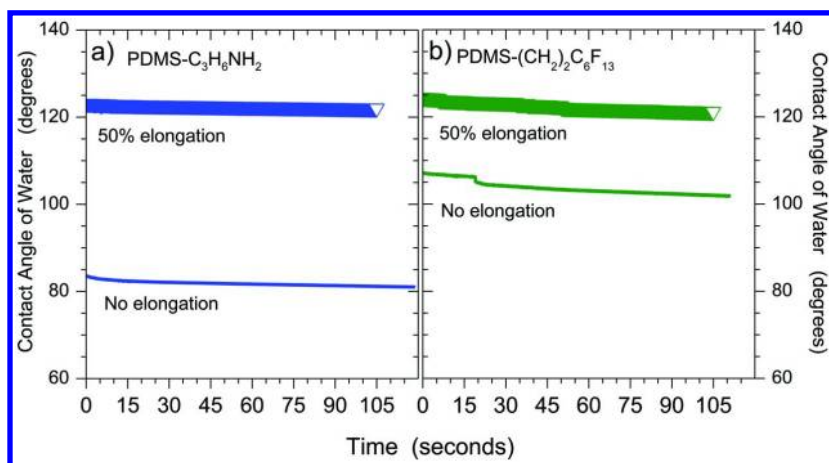
Figure 14. Contact angles at 15% relative humidity and 25°C for a) PDMS-$C_3H_6NH_2$ (no elongation and 50% elongation), b) PDMS-$(CH_2)_2C_6F_{13}$ (no elongation and 50% elongation). There is a greater difference in contact angle for PDMS–$C_3H_6NH_2$ with increased packing density, and for both silanes (regardless of polarity), contact angles are essentially matched after several months for the samples modified at 50% elongation.

Conclusions

We have shown that polar and non-polar moieties grafted onto silicone elastomers at various packing densities do not impact moisture vapor transport properties. Essentially, only the activation step to create the silica-like surface for subsequent condensation with the hydrolyzed silanes causes a change in the permeation of moisture vapor through the elastomer. This nanoscale layer (ca. 260 nm in thickness) reduces the moisture vapor permeability by 50% of its original value. Due to polydimethylsiloxane's inherently high MVP, the reduction attributed to the ultraviolet/ ozone activation step is not significant for most applications. As expected, the increased packing density of fluorinated silanes resulted in a more hydrophobic and stable surface; consistent with previous

results. Interestingly, at high packing densities the grafting of amino- terminated silanes also created the same level of hydrophocity as its fluorinated counterpart. Contact angle testing of the substrates at elevated temperature and humidity showed moderate surface rearrangement of the hydrophobic species for the substrates subjected to the higher strain during modification, or higher packing density, regardless of silane functionality.

Acknowledgments

References

1. Metz, S. J. Water Vapor and Gas Transport through Polymeric Membranes. Ph.D. Dissertation, University of Twente, Belgium, January 14, 1975.
2. Van Reeth, I.; Wilson, A. Understanding Factors Which Influence Permeability of Silicones and Their Derivatives. *Cosmetics and Toiletries*; Personal Care Group, Dow Corning Europe: Brussels, Belgium, July 1994.
3. Biebuyck, H.; Haskal, E. Siloxane and siloxane derivatives as encapsulants for organic light emitting devices. U.S. Patent 5855994.
4. Ariga, K.; Hill, J. P.; Ji, Q. Layer-by-layer assembly as a versatile bottom-up nanofabrication technique for exploratory research and realistic application. *Phys. Chem. Chem. Phys.* **2007**, *9*, 2319–2340.
5. Soulas, D. N.; Sanopoulou, M.; Papadokostaki, K. G. Hydrophilic modification of silicone elastomer films: Thermal, mechanical and theophylline permeability properties. *Mater. Sci. Eng. C* **2013**, *33*, 2122.
6. Roohpour, N.; Wasikiewicz, J. M.; Paul, D.; Vadgama, P.; Rehman, I. U. Synthesis and characterisation of enhanced barrier polyurethane for encapsulation of implantable medical devices. *J. Mater. Sci.: Mater. Med.* **2009**, *20*, 1803–1814.
7. Sussman, C.; Bates-Jensen, B. *Wound Care: A Collaborative Practice Manual for Health Professionals*; Lippincott Williams & Wilkins: Baltimore, MD, 2007.
8. Genzer, J.; Efimenko, K. Creating Long-Lived Superhydrophobic Polymer Surfaces Through Mechanically Assembled Monolayers. *Science* **2000**, 2130–2133.
9. Efimenko, K.; Crowe, J. A.; Manias, E.; Schwark, D. W.; Fischer, D. A.; Genzer, J. Rapid formation of soft hydrophilic silicone elastomer surfaces. *Polymer* **2005**, *46*, 9329–9341.

10. Crowe, J. A.; Genzer, J. Creating responsive surfaces with tailored wettability switching kinetics and reconstruction reversibility. *J. Am. Chem. Soc.* **2005**, *127*, 17610–17611.

11. Crowe, J. A.; Efimenko, K.; Genzer, J. Manipulating Siloxane Surfaces: Obtaining the Desired Surface Function via Engineering Design. *Sci. Technol. Silicones Silicone-Modified Mater.* **2007**, *964*, 222–255.

12. Crowe-Willoughby, J. A.; Genzer, J. Formation and Properties of Responsive Siloxane-Based Polymeric Surfaces with Tunable Surface Reconstruction Kinetics. *Adv. Funct. Mater.* **2009**, *19*, 460–469.

13. Ouyang, M.; Yuan, C.; Muisener, R. J.; Boulares, A.; Koberstein, J. T. Conversion of Some Siloxane Polymers to Silicon Oxide by UV/Ozone Photochemical Processes. *Chem. Mater.* **2000**, *12*, 1591–1596.

14. Genzer, J.; Efimenko, K.; Fischer, D. A. Formation mechanisms and properties of semifluorinated molecular gradients on silica surfaces. *Langmuir* **2006**, *22*, 8532–8541.

15. Wang, W.; Vaughn, M. W. Morphology and Amine Accessibility of (3-Aminopropyl) Triethoxysilane Films on Glass Surfaces. *Scanning* **2008**, *30*, 65–77.

16. Glass, N. R.; Tjeung, R.; Chan, P.; Yeo, L. Y.; Friend, J. R. Organosilane deposition for microfluidic applications. *Biomicrofluidics* **2011**, *5*, 36501.

17. First Ten Angstroms. Influence of Drop's Volume on Contact Angle. http://www.firsttenangstroms.com/pdfdocs/DropVolumeAndCA.pdf (accessed Jan 2013).

18. Huff, J. W.; Egan, D. J.; Katich, M. J. Parameter and environmental influences on rigid contact lens wettability. *Am. J. Optom. Physiol. Opt.* **1988**, *65* (9), 717–721.

19. Ponter, A. B.; Yekta-Fard, M. The influence of environment on the drop size and contact angle relationship. *Colloid Polym. Sci.* **1985**, *263*, 673–681.

20. ASTM E96: *Standard Test Methods for Water Vapor Transmission of Materials*.

21. Grewal, R.; Sweesy, W.; Jur, J.; Willoughby, J. In *Moisture Vapor Barrier Properties of Biopolymers for Packaging Materials*; Liebner, F., Rosenau, T., Eds.; Functional Materials from Renewable Sources; American Chemical Society: Washington, DC, 2012; Vol. 1107, pp 271−296.

22. Bain, C. D.; Whitesides, G. M. Depth Sensitivity of Wetting: Monolayers of ω-Mercapto Ethers on Gold. *J. Am. Chem. Soc.* **1988**, *110*, 5897–5898.

23. Leelamanie, D. A. L.; Karube, J.; Yoshida, A. Relative humidity effects on contact angle and water drop penetration time of hydrophobized fine sand. *Soil Sci. Plant Nutrit.* **2008**, *54*, 695–700.

24. Khongtong, S.; Ferguson, G. S. Integration of bulk and interfacial properties in a polymeric system: Rubber elasticity at a polybutadienen/water interface. *J. Am. Chem. Soc.* **2001**, *123*, 3588.

25. Carey, D. H.; Ferguson, G. S. A smart surface: Entropic control of composition at a polymer/water interface. *J. Am. Chem. Soc.* **1996**, *118*, 9780.

26. Budziak, C.; Varghabutler, E.; Neumann, A. Temperature Dependence of Contact Angles on Elastomers. *J. Appl. Polym. Sci.* **1991**, *42*, 1959–1964.

27. Yuk, S. H.; Jhon, M. S. Temperature dependence of the contact angle at the polymer-water interface. *J. Colloid Interface Sci.* **1987**, *116*, 25–29.
28. Carey, D.; Grunzinger, S.; Ferguson, G. Entropically influenced reconstruction at the PBD-ox/water interface: The role of physical cross-linking and rubber elasticity. *Macromolecules* **2000**, *33*, 8802–8812.
29. Carey, D. H.; Ferguson, G. S. Synthesis and Characterization of Surface-Functionalized 1,2-Polybutadiene Bearing Hydroxyl or Carboxylic-Acid Groups. *Macromolecules* **1994**, *27*, 7254.

NMR Investigations of Network Formation and Motional Dynamics in Well-Defined Model Poly(dimethylsiloxane) Elastomers

James P. Lewicki,* Stephen J. Harley, Jasmine A. Finnie, Michael Ashmore, Crystal Bell, and Robert S. Maxwell

Lawrence Livermore National Laboratory, 7000 East Ave., Livermore, California 94550
*E-mail: lewicki1@llnl.gov

In this work, results of a study to optimize the structure of a series of model PDMS networks are reported. The study utilized [1]H Magic Angle Spinning (MAS), Magic Sandwich Echo (MSE) NMR methods and equilibrium solvent uptake analysis. The influence of inter-crosslink molar mass, vinyl to silane ratio and Pt chelation effects on the dynamics of network formation have been studied using low field NMR methodologies in real time. These comparatively simple solid-state NMR methodologies can be used to study the dynamics of network formation and the relationship between the chemical identity of key structural components and the final network structure of a silicone elastomer.

Introduction

Crosslinked Poly(dimethylsiloxane) (PDMS), elastomeric networks are an academically and technologically relevant sub-group of polysiloxane based materials, having wide-spread application in a large number of diverse technological, commercial and research areas (*1–4*). Simple end-linked, unfilled, condensation, addition or peroxy- cured PDMS networks typically exhibit poor mechanical properties and are of limited use as engineering elastomers (*5*). It is understood that in order to obtain the desired combinations of mechanical, physical and chemical properties for a specific real world application, the silicone formulation must, in fact, be comprised of complex multi-component systems

- incorporating multi-modal distributions of chain lengths, varied crosslink topologies/densities, chemically modified free chain ends, non-stoichiometric excesses of reactive moieties, and often large volume fractions of a variety of reactive and/or passive filler materials. The extensive modification process often results in a material with empirically tuned physical properties but is characterized by a highly complex and often poorly defined network structure (see Figure 1).
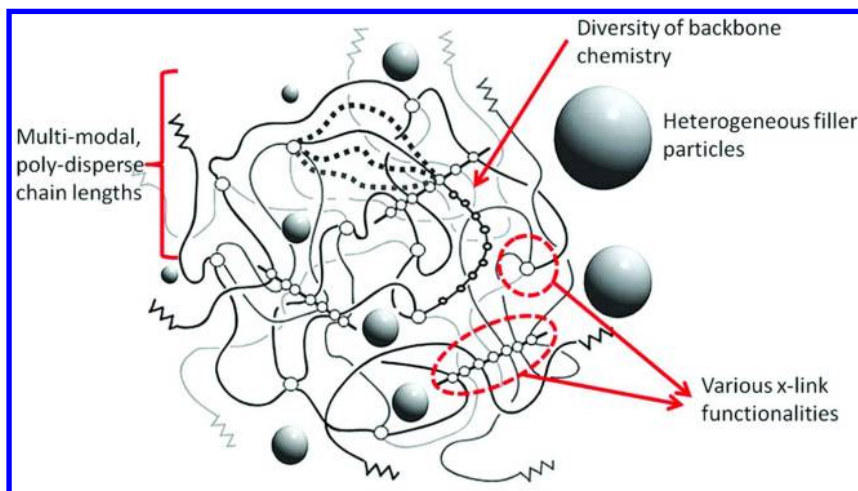
Figure 1. Illustration of the main contributory factors that define the complex structural architecture of an engineering silicone elastomer.

The physical, chemical properties and hence the performance of a silicone elastomer are governed by this underlying network structure. Therefore, in order to make accurate assessments and predictions of a materials performance and lifetime over a broad range of environmental conditions and to design materials with better defined, enhanced chemical and physical properties (*6, 7*), we must improve our understanding of the relationship between the underlying network architecture and macro-scale materials behavior.

In the past there has been a reliance on purely empirical additive methodologies in defining structure-property relationships in silicone elastomers for the prediction of materials performance (*8–10*). And beyond the most coarse grain information, the specifics of the network architecture have historically been largely ignored.

Today, there is a need to move beyond basic bulk and qualitative approaches and attempt to build a firm analytical model that links complex structural architectures over a broad range of size scales, which may be used for predicting materials performance and lifetimes. The practical realization of this goal requires a multi-scale effort encompassing the study of both model and commercial materials, using a broad range of interrogative analytical methodologies (*11–13*),

computational modeling (*14, 15*) and long term aging studies for model validation (*16*). In this article, we focus on analytical approaches towards the development of well-defined model network materials for the study of structure-property relationships in silicone systems.

Analytical Methodologies for the Analysis of Intractable Silicone Networks

Silicone elastomers are chemically crosslinked networks with an effective infinite molecular weight and are as such, insoluble. Furthermore, the high filler loadings and crosslink-densities - typically encountered in the majority of silicone engineering elastomers - render these networks intractable with respect to many commonly employed polymer characterization techniques. Consequently, high-fidelity structural information may only be accessed through means of solid-state spectroscopies or destructive analysis methods and is often non-trivial to obtain. In spite of this intractability, much progress has been made towards understanding structure-property relationships in complex siloxanes over the last three decades. Notably, Mark et al. have made extensive study of the association between network functionality, modality, filler content and the bulk mechanical/rheological properties of model silicone networks (*17–19*). Clarson et al. have studied modification of silicone based materials with a range of fillers and other physical property modifiers in great depth (*20*). Notably, Cohen-Addad made early use of solid and solution state NMR methodologies for the study of the properties of silicone melts, gels and silica-silicone systems (*21*).

Destructive, non-spectroscopic methods are also available that may be developed to probe network structure in intractable silicone networks. A worthy example is Thermal Analysis (A thorough review of which has been published by Wunderlich (*22*)). Thermal analysis techniques such as Pyrolytic analysis and gravimetry have been used extensively for the analysis of 'unknown' polymeric materials for many years (*23–26*). The temperature at which a polymeric material degrades, the mechanism and the products of the thermal degradation are all a function of its underlying chemical structure and even physical morphology. Different polymeric materials can therefore be 'fingerprinted' by their thermal or thermo-oxidative degradation behavior. It is now becoming apparent that the same holds true for silicone based materials (*11*).

While there does indeed exist a range of approaches for the in-depth investigation of structure and properties of complex silicones, it is perhaps Nuclear Magnetic Resonance (NMR) that is uniquely suited in its ability as a family of techniques to probe the structure and properties of silicones: from an atomistic-molecular scale (high resolution chemical shift dependence), in terms of their dynamic physical structure (relaxometry) and at a micro/macroscopic scale (magnetic resonance imaging (MRI)). Over the last 2 decades solid-state Nuclear Magnetic Resonance (NMR) in particular has been shown extensively (*12, 27, 28*) to be a powerful tool for directly elucidating the chemical identity and network architecture of complex engineering siloxanes. Cohen-Addad (*29, 30*), Charlesby (*31, 32*), Saalwächter (*33, 34*), Maxwell (*35*) and others have made extensive use of solid-state NMR both as a method of determining the chemical

content/makeup of the polymer backbone in commercial silicone formulations and as a tool for probing segmental dynamics of silicone networks in the solid state by utilizing spin echo and novel multiple quantum NMR methodologies (*13*, *36*).

In this paper, a range of methodologies are applied to the analytical optimization, determination of cure kinetics and final network structure in model, end-linked addition cured PDMS networks. By utilizing a range of solid state NMR methodologies in combination with equilibrium solvent uptake measurements, the influence of inter-chain molar mass, functional group stoichiometry and concentration on both the dynamic cure behavior and final structure of a series of well-defined model networks have been investigated. The results of these studies yield new insight into the complexities of addition cured silicone networks and will aid in the development of a multi-scaled approach towards the predictive modeling of silicone lifetimes and behavior.

Experimental

Materials

All Poly(dimethylsiloxane) (PDMS) polymers, tetrakis-dimethyl-methoxysilane (TKSIL) crosslinker, Platinum di-vinyl-methylsiloxane catalyst used in this study were obtained from Gelest Inc.

Synthesis of Model Networks

End-linked, tetra-functionally crosslinked 'model' networks were synthesized via a organoplatinum mediated hydrosilation reaction between vinyl terminated poly(dimethylsiloxane) (PDMS) and a organo-tetra-silane crosslinker to form network elastomers with average inter-crosslink chain lengths of 6, 28 and 115.5 kg mol^{-1}. Each model system was formulated in the following manner: 55 Grams of a given vinyl terminated PDMS (6, 28 or 115.5 kg mol^{-1}) was combined with a quantity of TKSIL crosslinker corresponding to a silane to vinyl ratio of 0.5:1 to 4:1 in the presence of 40 ppm of a Pt di-vinyl-methyl-siloxane complex and mixed for 30 seconds using a Flactek^{tm} Speedmixer off-axis centrifugal mixer at a rate of 2500 rpm. The mixed resin was then poured into a 6 by 6 inch by 2 mm deep ASTM D3182 mold and allowed to cure for 12 hours at room temperature. The formed elastomer was subsequently removed from the mold and post-cured for an additional 24 hours at 80°C under vacuum. One inch square samples were cut from the original sheet, swollen in 500 ml of spectroscopy grade toluene for 12 hours to remove any unreacted material or small molecule impurities and then re-dried under vacuum at 80°C for a further 24 hours. This process was repeated for each chain length and silane ratio variant to yield a matrix of 45 systems - details of which are given in Table 1.

Table 1. Model end-linked PDMS synthesized networks

Sample code	Molar mass PDMS /gmol^{-1}	Silane to Vinyl ratio	Physical State	Sample code	Molar mass PDMS /gmol^{-1}	Silane to Vinyl ratio	Physical State
11_A	6000	0.5	No gel	13_K	28,000	3	Stiff gel
11_B	6000	0.75	Partial gel	13_L	28,000	3.25	Partial gel
11_C	6000	1	Partial gel	13_M	28,000	3.5	Partial gel
11_D	6000	1.25	Gel	13_N	28,000	3.75	Partial gel
11_E	6000	1.5	Gel	13_O	28,000	4	Partial gel
11_F	6000	1.75	Stiff gel	17_A	115,000	0.5	Partial gel
11_G	6000	2	Gel	17_B	115,000	0.75	Partial gel
11_H	6000	2.25	Partial gel	17_C	115,000	1	Partial gel
11_I	6000	2.5	Partial gel	17_D	115,000	1.25	Gel
11_J	6000	2.75	Partial gel	17_E	115,000	1.5	Gel
11_K	6000	3	Partial gel	17_F	115,000	1.75	Stiff gel
11_L	6000	3.25	Partial gel	17_G	115,000	2	Stiff gel
11_M	6000	3.5	Partial gel	17_H	115,000	2.25	Gel
11_N	6000	3.75	No gel	17_I	115,000	2.5	Gel
11_O	6000	4	No gel	17_J	115,000	2.75	Gel
13_A	28,000	0.5	No gel	17_K	115,000	3	Gel
13_B	28,000	0.75	No gel	17_L	115,000	3.25	Gel
13_C	28,000	1	Partial gel	17_M	115,000	3.5	Partial gel
13_D	28,000	1.25	Partial gel	17_N	115,000	3.75	Partial gel
13_E	28,000	1.5	Gel	17_O	115,000	4	Partial gel
13_F	28,000	1.75	Stiff gel	-	-	-	-
13_G	28,000	2	Stiff gel	-	-	-	-
13_H	28,000	2.25	Gel	-	-	-	-
13_I	28,000	2.5	Gel	-	-	-	-
13_J	28,000	2.75	Stiff gel	-	-	-	-

NMR Analysis

High-Field Magic Angle Spinning (MAS) NMR experiments were performed on a Bruker Avance spectrometer operating with a proton Larmor frequency of 400.13 MHz, using a Bruker MAS probe configured for 4 mm (o.d.) rotors. ~500 mg Samples were powdered and packed into silicon nitride rotors. Samples were spun at 15 kHz and ninety degree pulse lengths of τ_p = 8 μs and recycle delays of 1.4 seconds were used. The spectra were referenced with respect to tetramethylsilane (0 ppm).

Low-field solid-state NMR studies were performed on a Bruker Minispec™ spectrometer at 37±0.1°C under static conditions. Ninety degree pulse lengths of τ_p = 2.25 μs and recycle delays of 15 seconds were used. Highly rigid domains relax

more rapidly than the dead time of the probe. Therefore, to regain information that may be lost during this time, a special form of refocusing sequence known as the Magic Sandwich Echo (MSE) (*37*) was employed. With MSE, near quantitative refocusing of fast relaxing components is achieved where subsequent application of a Carr-Purcell-Meiboom-Gill (CPMG) train removes the effects of magnetic field inhomogeneities (*38*). This technique is highly effective at obtaining free induction decays (FIDs) that are representative of large distributions of relaxation times.

The application of the MSE yields an FID that is a superposition of decaying exponentials whose amplitudes and time constants are representative of unique molecular motion distributions within the material. However, the extraction of this information is mathematically non-trivial (*39*, *40*). Direct non-linear regression to an unknown sum of exponentials is possible yet impractical as it requires a priori knowledge of the relaxation behavior of the material of study. Ideally, a mathematical transform is sought to de-convolute the time domain data into a spectral domain - much akin to a fast Fourier transform. Such a spectral function can only be found upon solution of the Laplace integral equation (*41*) which is part of a more general class of Fredholm integral equations. Many algorithms exist to accomplish this transformation (including the fast Tikhonov regularization routines, CONTIN (*42*) and FTIKREG (*43*) that only vary in the method used to find the criteria for the regularization parameter.

In this work, all data was processed using the FTIKREG routine. It is important to note that the solution to the Laplace integral equation may depend continuously on the data (*44*) and may not be unique. To assure confidence in the obtained spectral function, samples were run in the spectrometer a total of three times in random order.

Equilibrium Solvent Uptake Analysis

Equilibrium solvent uptake analyses of the samples were performed using a 5:6 v/v toluene/acetone mixture at 29.5 °C as the swelling medium which provides theta conditions for the polymer chains. Samples of ~25 mg mass were swollen under these conditions for 48 h and triplicate samples of each system were swollen for statistical accuracy. The swollen samples were surface dried then weighed using a sensitive microbalance (Mettler Toledo) to an accuracy of $\pm 5 \times 10^{-7}$ grams. After measurement, the networks were un-swollen gradually in methanol then dried in a vacuum oven overnight at 80 °C. The samples were weighed again and these values were used to calculate both the mass of solvent uptake per gram for each sample and fraction soluble material extracted during the swelling process.

The average inter-crosslink chain density $<M_x>$ was calculated from these data using the Flory-Hugins relationship (*45*) under equilibrium conditions, given in Equation 1.

$$< M_x >= \frac{-\rho_{poly} V_{m,solv}(c^{\frac{1}{3}}-\frac{c}{2})}{[\ln(1-c)+c+\chi c^2]} \qquad \textit{Equation 1}$$

Where ρ_{poly}= the density of the pure polymer, ρ_{solv} = solvent density $V_{m,solv}$= the molar volume of the solvent and χ = the chi parameter of the solvent (0.5 for a theta solvent). 'C' = the relative concentration and is given by Equation 2.

$$c = \frac{W_0}{\rho_{poly}V} \qquad \text{\textit{Equation 2}}$$

Where W_0=the initial polymer mass and V = volume of swollen polymer.

Results and Discussion

Optimization of Model Networks

Organoplatinum complexes such as Karstedt's catalyst are an effective and well established class of homogenous catalysts for hydrosilylation reactions (*46*). With Karstedt's catalysts and related variants, Pt(0) is chelated by bridged vinyl-siloxane ligands. The active complex, during a hydrosilation process relies on the transfer of the silane to the Pt(0) center followed by a subsequent change in the ligand complexion number and complexation with a the double bond of interest which is turn, activated towards addition of ~Si-H to form the addition product as shown in Figure 2.
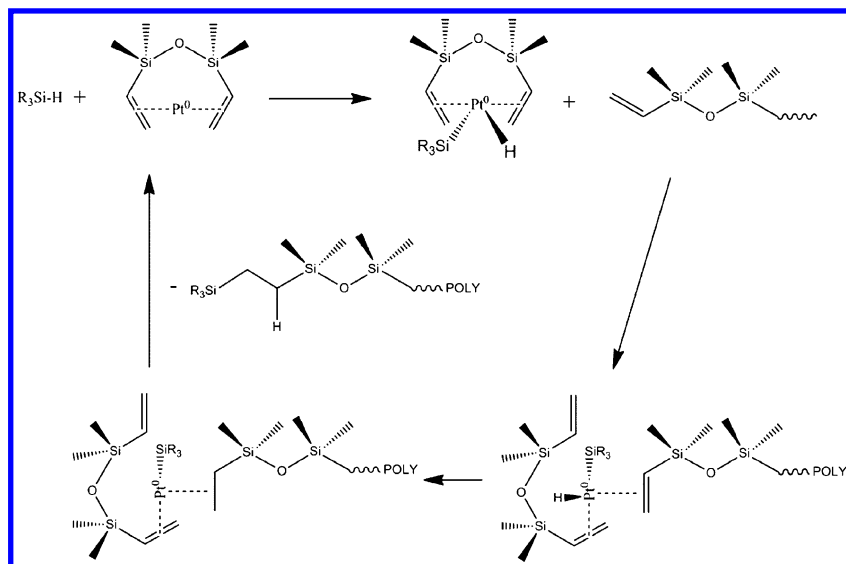
Figure 2. A basic, generalized scheme for the Pt mediated hydrosilation of a vinyl end-group on a PDMS polymer chain. Pt(0) is stabilized in a chelated state through complexation with a vinyl silane. Addition proceeds though a multi-stage mechanism involving 1) hydrogen transfer to the Pt center, 2) complexation with a vinyl and a n-1 reduction in ligand number of the Pt complex, 3) silane addition to the double bond and 4) regeneration of the original Pt complex.

Vinyl terminated PDMS resins can therefore be readily crosslinked in the presence of low levels of a Pt(0) organoplatinum complex (1-50 ppm). And although such organoplatinum complexes are considered to be highly active for room temperature vulcanization processes, these reactions are also highly temperature dependent. Furthermore, during network formation, they do not always proceed stoichiometrically with respect to vinyl-silane ratio. When attempting to form 'model' materials with idealized network structures it is therefore important to take into account these features of Pt mediated hydrosilylation. To that end, a simple tetra-functional end-linked network architecture has been selected, based on a TKSIL silane cross-linker and three different molar mass bis-vinyl terminated PDMS polymers of molar mass 6, 28 and 115.5 kg Mol-1 – representing network chain lengths below, above and very highly above the critical chain entanglement length of PDMS (~12 kg mol^{-1}) - named Models 11, 13 and 17 respectively. In order to experimentally determine the optimum silane:vinyl ratio for each model system, a series of variants of each was formulated with a varying silane:vinyl ratio - from 0.5:1 to 4:1 (see Table 1). Equilibrium solvent uptake measurements were carried out on each variant, their x-link densities and percentage sol-fractions were determined. The results of which are shown in Figures 3-5.

From the data shown in Figures 3-5 it can be observed that irrespective of chain length, Models 11-13 reach a maximum crosslink density at a silane to vinyl molar ratio of ~1.75:1. Therefore it appears that in order to achieve close to full conversion and maximum network density in this class of end-linked network, a moderate silane excess is required. This ratio may at first appear counter intuitive, however if we consider that there are 4 moles of silane per TKSIL molecule and 2 moles of vinyl per PDMS chain, then the stoichiometric (1:1) level of silane, numerically provides only ½ the number of TKSIL molecules to PDMS chains. However, at a 1.75:1 molar ratio there is almost a 1:1 numerical balance of TKSIL to polymer molecules and from the solvent uptake data it appears that having near to 1:1 molar balance between TKSIL and PDMS molecules, rather than a stoichiometric balance between silane and vinyl groups is essential for the formation of a fully dense network. This silane rich, non-stoichiometric environment is illustrated graphically in Figure 6.

Solvent uptake measurements provide evidence that the network formation process(es) taking place in these model systems are somewhat more complex than would at first be expected. The fact that a 1:1 silane to vinyl ratio does not result in the formation of a fully dense 'ideal' network structure even when driven thermally by an aggressive post-cure, suggests that other factors such as chain-end mobility, local spatial availability of reactive groups and catalyst immobilization/deactivation may influencing the ability of the precursors to form an ideal network structure. With these considerations in mind, we have employed solid-state NMR methodologies to attempt to further investigate the processes of network formation in each class of model system both as a function of silane:vinyl ratio and in real time.
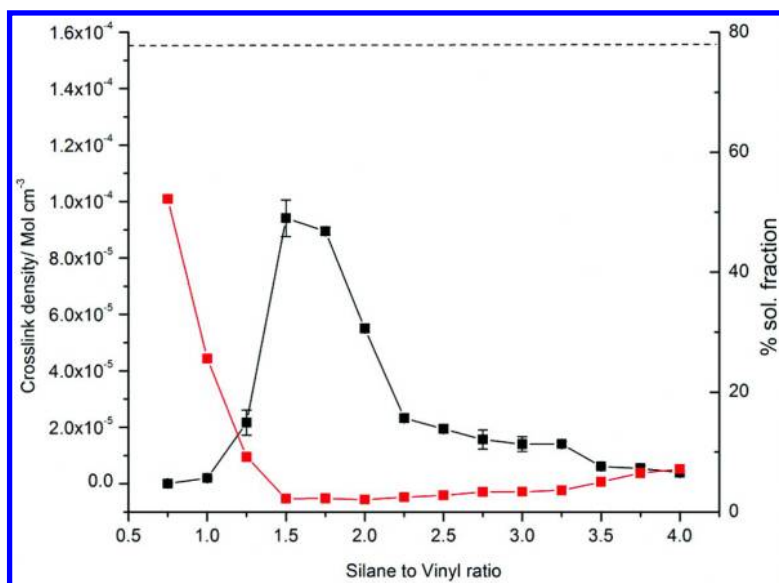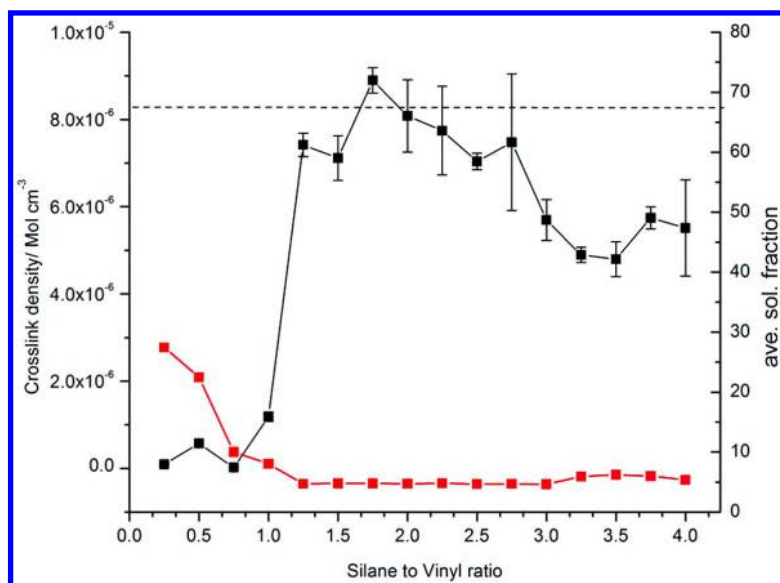
*Figure 3. Equilibrium solvent uptake data for 'Model 11' with a silane ratio
varied from 0.75 to 4. Left axis depicts crosslink density as a function of
silane:vinyl ratio (black line), right axis the % extracted sol. fraction as a
function of silane:vinyl ratio (red line). The dashed horizontal line represents the
theoretical maximun crosslink density achievable from the complete conversion
of a 6 kg mol^{-1} tetra-functional end-linked network. Note that the maximum
experimental crosslink density is somewhat lower than the theoretical value for
Model 11 and that this value and the minimum sol. fraction value correspond to
a silane:vinyl ratio of ~1.75:1.*

In theory, the progress of the network formation reaction can be followed
through direct NMR observations of the relative populations of silane and vinyl
functional groups. Solution state experiments are not suited to the analysis of
systems which undergo a melt to solid transition and are therefore subject to
excessive line broadening and the loss of chemical shift resolution (*47*) as the
reaction proceeds. Relatively simple solid state experiments, however, can be
employed to negate these difficulties. Magic Angle Spinning (MAS) NMR is one
such method which has been employed here and shown in Figure 7 is a [1]H-MAS
NMR spectrum of Model 11-C.
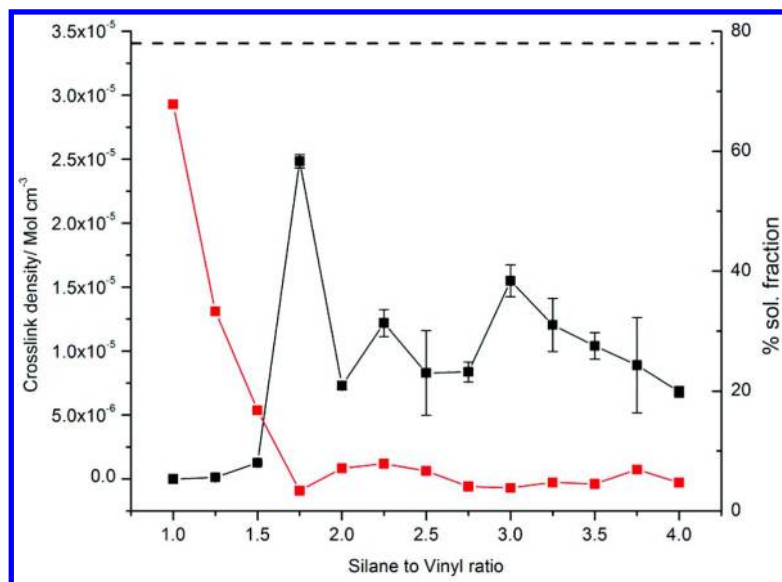
Figure 4. Equilibrium solvent uptake data for 'Model 13' with a silane ratio varied from 1 to 4. Left axis depicts crosslink density as a function of silane:vinyl ratio (black line), right axis the % extracted sol. fraction as a function of silane:vinyl ratio (red line). The dashed horizontal line represents the theoretical maximum crosslink density. Note again that the maximum experimental crosslink density is somewhat lower than the theoretical value for Model 13 and that this value and the minimum sol. fraction value correspond to a silane:vinyl ratio of 1.75:1.

The ^{1}H NMR spectrum of Model 11-C (Figure 7) clearly shows that despite 11-C having a 1:1 silane to vinyl ratio and having undergone an extensive post-cure, it has an excess of vinyl groups present in the matrix and no detectable silane signal. This both aggress with the solvent uptake data and physical appearance of the material, showing it to be a partially crosslinked gel. These data demonstrate that the silane addition reaction does not proceed quantitatively within these matrices.

While [1]H-MAS of the model systems can clearly resolve distinct chemical moieties within the crosslinked polymer matrix and has demonstrated that networks formed from 1:1 silane:vinyl ratio precursors actuality retain a significant vinyl excess, such direct detect methods are limited in sensitivity by the typical detection limits of NMR (>100's of mMolar) and the comparatively low abundance of protons corresponding to functional end groups of interest. Direct ^{1}H MAS methods are therefore generally capable of detecting comparatively large excesses of functional groups, and are not generally effective at following network reactions at high conversion levels.

Figure 5. Equilibrium solvent uptake data for 'Model 17' with a silane ratio varied from 0.25 to 4. Left axis depicts crosslink density as a function of silane:vinyl ratio (black line), right axis % extracted sol. fraction as a function of silane:vinyl ratio (red line). The dashed horizontal line represents the theoretical maximum crosslink density. In contrast to Models 11 and & 13, the maximum experimental crosslink density is marginally higher than the theoretical value for Model 17. The % extractables are also correspondingly lower due to the decreased mass fraction of crosslinker present, however once again the maximum experimental crosslink density value corresponds to a silane:vinyl ratio of 1.75:1.

Given the limitations of chemical shift resolved end-group analysis at low concentrations and high conversion levels, it is NMR relaxometry methodologies which have been utilized for the further study of network ideality and for real-time analysis of network formation in the model materials. Such methods - which measure characteristic relaxation times of observed nuclei [the spin lattice relaxation time (T_1), the transverse relaxation time (T_2), the residual dipolar coupling constant ($D_{<res>}$), etc (*48*)] related to the mobility of that nuclear spin population of interest - do not provide direct chemical speciation within a network but can yield effective information on the motional dynamics of a network elastomer (*36*). These methods have also been used to distinguish discrete populations of nuclei in differing motional environments (*49*).
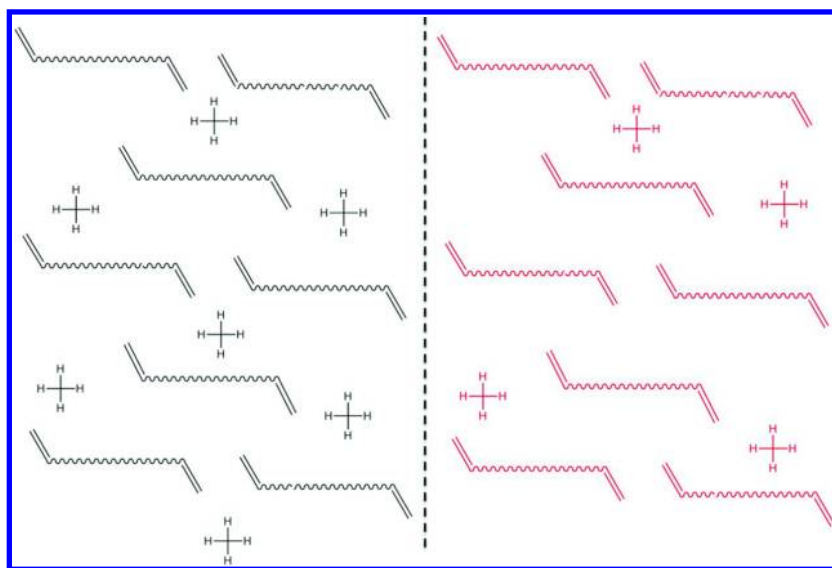
Figure 6. Illustration of the numerical difference between (left) a near to 1:1 Molar ratio of crosslinker molecules to polymer chains - as is the case with the optimized model networks and (right) a 1:1 molar ratio of silane to vinyl groups – which would be obtained from a stoichiometric calculation. Although a gross simplification of the network formation chemistry, this illustration highlights the fact that a ~1:1 ratio of x-linker to polymer is required per unit volume for the formation of a fully dense network.

For the analysis of the model silicone networks discussed here, comparatively simple and rapid low-field relaxometry techniques have been employed. These techniques are reliant on the re-focusing and measurement of ^1H T_2 values using a Magic Sandwich Echo (MSE) pulse sequence (see Experimental section) optimized for the model silicone networks. Our initial study using MSE, attempted to relate distributions of T_2 times to network ideality as a function of silane:vinyl ratio, the results of which are given in Figure 8.

The example shown in Figure 8 demonstrates that the MSE technique can distinguish distinct populations of system protons within the model networks which have characteristic T_2 relaxation times. Given that T_2 can be broadly related to mobility (T_2 μ 'proton mobility') within these networks, we can consider these populations to be representative of fractions of the polymeric system within different motional domains. What is significant is that the average relaxation times of these groups vary as a function of the network stoichiometry: at low and high silane ratios, components 'A' and 'B' have distinct distributions of relaxation times; however, as the stoichiometry approaches a ratio of 1.75:1 these distinct populations converge. These data demonstrate that on either side of the conversion curve, the networks are heterogeneous in their motional dynamics and have distributions of both comparatively 'rigid' gel type structure (A) and liquid like components (B) additionally, as these systems approach the fully

dense 'ideal' network structure both of these components become less mobile and eventually become indistinguishable – an indication that a homogenous network structure has been approached.

Real-Time Analysis of Network Formation in Optimized Systems

Through the combination of equilibrium solvent uptake and NMR analysis of the model network formulations, it has been determined that the network structure of each given system reaches an optimum in terms of crosslink density and network homogeneity at a silane to vinyl ratio of 1.75:1- irrespective of the molar mass of the PDMS precursors. The dynamics of the network formation processes during the curing of these optimized systems (hereafter referred to as Models 11, 13 and 17) have been investigated using ^{1}H MSE NMR. For each given 'optimized' model variant, the curing behavior has been studied in real time and in-situ. 2 Gram batches of Models 11, 13 and 17 were formulated in 10mm NMR tubes and allowed to cure at 37 °C within the Spectrometer. During this time, MSE relaxometry measurements were made at regular intervals in order to track the change in T_2 for each system as a function of cure time. The extracted T_2 distributions for Model 13 as a function of cure time are shown in Figure 9. Shown in Figure 10 is a plot of the amplitude of each relaxation curve as a function of cure time.
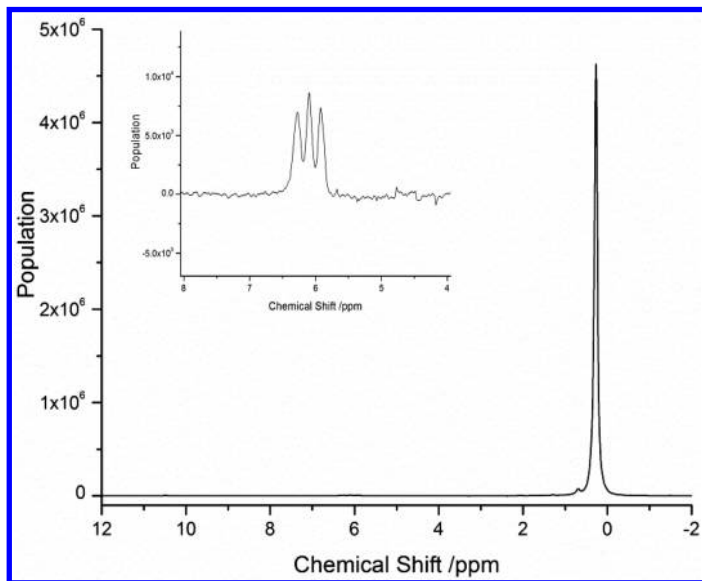
Figure 7. ^{1}H MAS NMR spectrum of a fully cured sample of Model 11-C. The main peak at 0.26ppm corresponds to the methyl protons of the PDMS backbone. Shown (inset) at 7.1ppm is the comparatively weak proton resonance from the residual vinyl end groups of model 11-C. Note that greater than 99% of the ^{1}H signal is resultant from the abundant methyl backbone protons. No silane peak was observed.
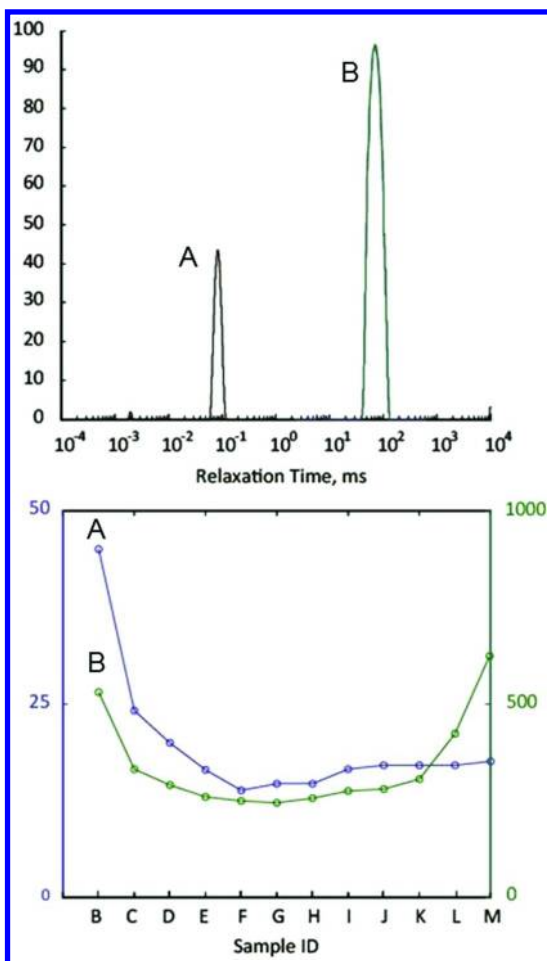
Figure 8. ¹H MSE NMR analysis of Models 13-B to 13-M. The upper plot shows the derived populations of protons having distinct relaxation times in this example, Sample 13-M. Two populations of protons having distinct relaxation times are considered which have been be related to system protons with differing mobilities, marked A and B. In the lower plot, the average T₂ values of these populations are plotted for systems 13-B to M, corresponding to silane:vinyl ratios of 0.75-3.5:1. Note that a convergence in relaxation times is observed around the 1.75:1 ratio.

The NMR analysis of the curing of Model 13 (Figures 9&10) clearly shows that the optimized system behaves in a manner consistent with the formation of a typical end-linked network. The cure rate is non-linear and decreases as a function of total cure time – owing to the decreasing availability of reactive functional groups and increasing viscosity as the network approaches high conversion levels. The appearance of a small yet distinct slowly relaxing component at long cure times has been attributed to the rapid motions of excess crosslinker and solvent

species expelled from the network as it undergoes densification on curing. In general, from these data we can conclude that the 28 kg mol^{-1} model network formation process is similar in its cure kinetics to that of a typical thermoset network polymerization processes. If the starting molar mass of the PDMS resin is however increased significantly, with a corresponding decrease in the number of moles per unit volume of reactive groups (as is the case with Model 17) a differing cure behavior is observed. Shown in Figures 11 & 12 are the extracted T_2 distributions for the optimized Model 17 and the amplitude of each relaxation curve as a function of cure time respectively.

In Model 17 the intercrosslink chain lengths are significantly greater than Model 13 and as such the initial melt viscosity of the formulation is much greater than that of Model 13. It also follows that the relative concentration of functional reactive groups is significantly lower with respect to Model 13. The practical consequence of these factors are that although the reaction proceeds, the cure time is greatly retarded and full conversion is only obtained at 37°C after ~4000 minutes. The results in Figure 12 also clearly show that the overall network formation process no longer follows a simple exponential rate law and at these high viscosities and low functional group concentrations. Instead, the silane addition network forming reaction follows a complex, higher order kinetic rate law. Simply increasing the molar mass of the linear precursor has a significant impact on the complexity of the network formation process.
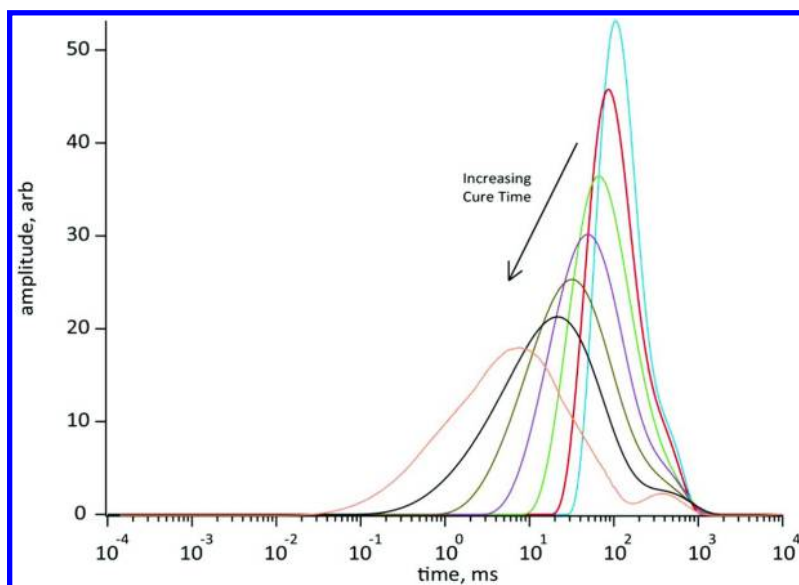
Figure 9. Derived T_2 distributions for optimized Model 13 as a function of cure time (0 – 40 min., 37°C). With increasing cure time, there is a progressive decrease in the amplitude and a broadening of the T_2 distribution, indicative of increasing motional constraint within the system as the system cures. Note that at long cure times, a highly mobile, slow relaxing component manifests itself.
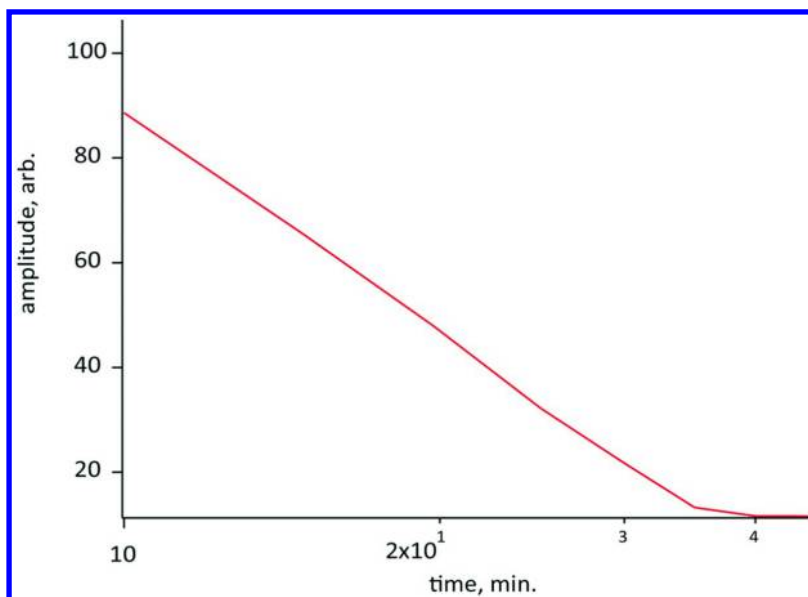
Figure 10. Derived relaxation amplitude as a function of cure time for the optimized Model 13. Note the decrease in amplitude of the relaxation curve follows a simple exponential decay process –consistent with the kinetics of a typical network formation process, the rate of which decreases exponentially as 100% conversion is approached.

At the other extreme lies Model 11, which has an average intercrosslink molar mass of ~6 kg mol^{-1} and correspondingly the highest relative concentration of vinyl groups of all three systems. Surprisingly, Model 11 did not achieve a full cure at room temperature. The optimized system was observed to partially gel at room temperature within ~2 minutes of the addition of the catalyst but was not observed to proceed further. Even samples left at room temperature for >1 month remained a partial gel and did not fully cure. Model 11 only achieves full network density after post-curing at elevated temperatures. As such, MSE analysis of the 'real-time' curing of Model 11 does not show any progressive trend in the amplitude of the measured T_2 distribution curves (see Figure 13) but instead shows evidence of the progressive in-growth of a very fast relaxing component (only partially captured in the NMR experiment – we will return to this later) as a function of cure time.

The fact that Model 11 does not cure at moderate temperatures is significant. The comparatively high concentrations of reactive functional groups and low starting viscosities should lend themselves to a rapid cure. And indeed, the systems are observed to gel in less than 2 minutes. The reaction, however, did not proceed further at room temperature and required treatment at 80°C for

extended time periods to drive the network formation process to completion. It is suggested that this anomalous cure behavior is a consequence of the inhibition of the Pt catalyst complex by the vinyl groups in the system. As discussed earlier, the catalyst consists of a stable complex between Pt(0) and a di-vinyl siloxane. The mechanism involves silane transfer to the Pt complex followed by ligand exchange with the polymer double bond, activation of that bond and the subsequent addition of the silane (see Figure 2). In both Models 13 and 17 the chain lengths are such that the probability of the Pt complex associating with more than 1 vinyl group is low. However in Model 11 the chances of the Pt(0) complex associating with more than one vinyl at a given time is greatly increased. It is proposed that if the Pt complex does indeed associate with more than one vinyl group, it forms secondary complexes which are stable and have reduced activity towards silane transfer. Increasing the temperature will either increase the exchange rate or simply disrupt the complexation (dependent on the nature of the complex formed) but in either case serves to activate the system once more to silane transfer and vinyl addition. This is illustrated in Figure 14.
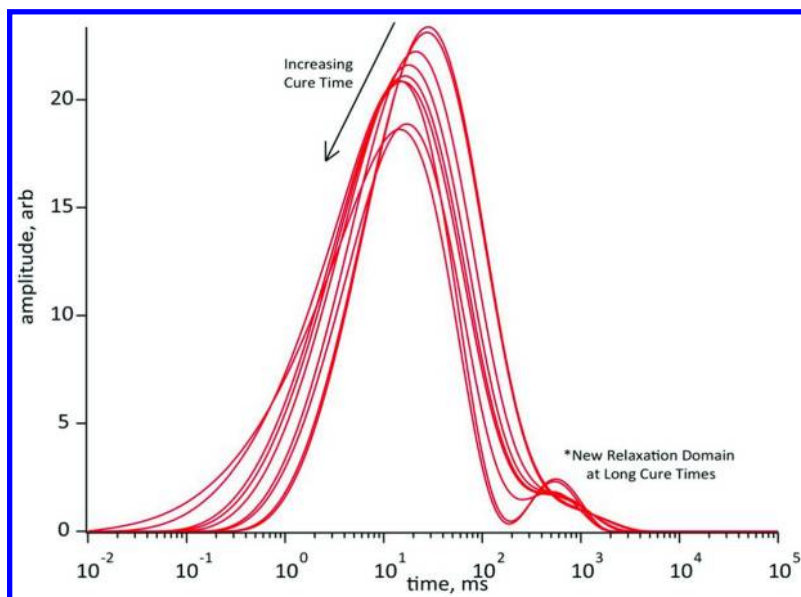
Figure 11. Derived T_2 distributions for optimized Model 17 as a function of cure time (0 – 4000 min., 37°C). In contrast with Model 13, the cure time of Model 17 is increased by 3 orders of magnitude and the distribution cures do not exhibit the same simple trend as a function of cure time. Note that at long cure times, there is once again a mobile, slow relaxing component present.
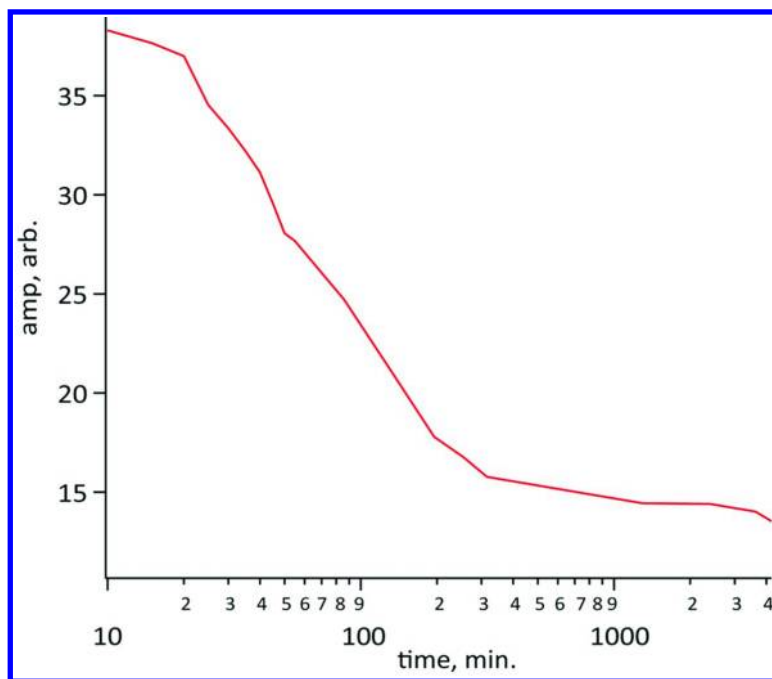
Figure 12. Derived relaxation amplitude as a function of cure time for the optimized Model 17. In this case at high initial molar masses, the decrease in amplitude of the relaxation curve does not follow a simple exponential decay process and the kinetics of the network forming process instead follow a higher order model.

The origin of the fast relaxing component is a matter of some speculation, as noted in the discussion - was only partially observed and is therefore not fully captured in the data analysis. However, the consistent trend as a function of measurement time and the exceedingly short T_2 values suggest either the formation of a highly rigid crystalline component (which is unlikely in these systems) or the paramagnetic interaction of a metallic species such as Pt(IV) with the polymer system. A color change was also observed to accompany this in-growth process in Model 11 and over time the sample changed from clear to a deep orange-yellow color, which is consistent with the presence of Pt(II) or Pt(IV) complexes. It is therefore possible that this observed process is a consequence of destabilization or other alteration of the catalyst complex within this system and indeed there is precedent for such processes in the literature (*46*, *50*). However, in the absence of more data, these observations must remain a somewhat speculative if not interesting aspect of this study and a subject of further work.
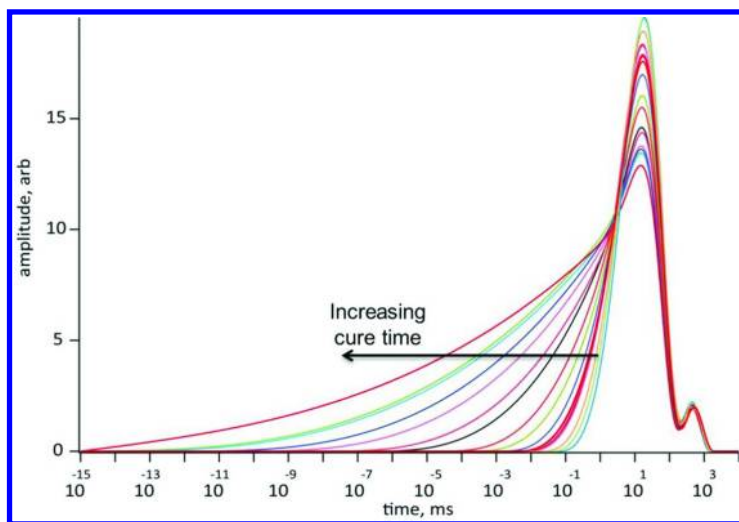
Figure 13. Derived T₂ distributions for optimized Model 11 as a function of 'cure' time (0 – 2600 min., 37°C). In stark contrast with Models 13 & 17, this low molar mass system effectively does not cure at room temperature. The system rapidly gels (not captured in this experiment) but will proceed no further at 37°C. The only clear trend is the progressive in-growth of a very fast relaxing component that was only partially captured in this experiment and as such manifests itself in this fit as a tail towards the left of the plot and not a true distribution.
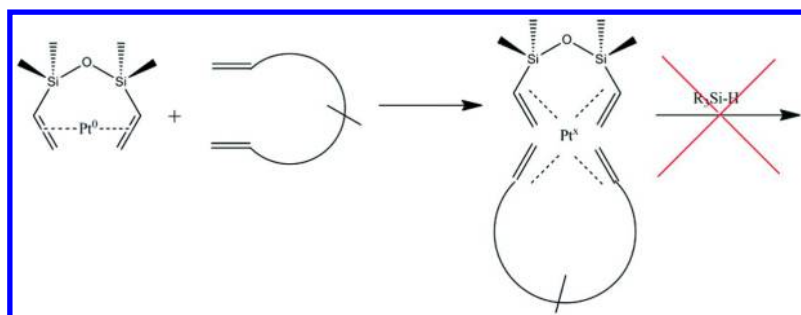
Figure 14. Proposed mechanism of Pt catalyst complex inactivation by an oligomeric vinyl terminated silicone

Conclusions

In this work it has been demonstrated that even comparatively 'simple' end-linked silane-vinyl addition cured PDMS networks have complex and non-ideal network formation chemistries that are governed by a range of factors including local availability of reactive functionalities, precursor molar mass, catalyst inhibition and complexation effects. NMR has been demonstrated to be a highly effective, informative and versatile tool for the analysis of both static network structure and real time measurements of network formation processes. The results of this study have highlighted the underlying complexity of these widely used addition cure chemistries in simple siloxane architectures and these data demonstrate that in this class of system, a silane excess is required for the formation of a fully dense and homogenous network structure. This study has also shown that network formation processes in these systems are not solely governed by functional group concentration, species diffusion and mobility – but by a complex and not fully understood series of interactions between the platinum catalyst and the vinyl groups of the polymer system itself.

Acknowledgments

References

1. Arkles, B. *Chemtech* **1983**, *13*, 542.
2. Clarson, S. J.; Owen, M. J.; Smith, S. D. *Abstr. Pap. Am. Chem. Soc.* **2009**, *238*.
3. Liu, C. *Advanced Materials* **2007**, *19*, 3783.
4. Yoda, R. *J. Biomater. Sci., Polym. Ed.* **1998**, *9*, 561.
5. Mark, J. E.; Allcock, H. R.; West, R. *Inorganic Polymers*; Oxford University Press: New York, 2005.
6. Chien, A.; Maxwell, R.; Chambers, D.; Balazs, B.; LeMay, J. *Radiat. Phys. Chem.* **2000**, *59*, 493.
7. Lewicki, J. P.; Maxwell, R. S.; Patel, M.; Herberg, J. L.; Swain, A. C.; Liggat, J. J.; Pethrick, R. A. *Macromolecules* **2008**, *41*, 9179.
8. Traeger, R. K.; Castongu, T. *J. Appl. Polym. Sci.* **1966**, *10*, 535.
9. Hadjoudj, A.; David, J. C.; Vergnaud, J. M. *Thermochim. Acta* **1986**, *101*, 347.
10. Bajaj, P.; Babu, G. N.; Khanna, D. N.; Varshney, S. K. *J. Appl. Polym. Sci.* **1979**, *23*, 3505.
11. Lewicki, J. P.; Albo, R. L. F.; Alviso, C. T.; Maxwell, R. S. *J. Anal. Appl. Pyrol.* **2013**, *99*, 85.
12. Mayer, B. P.; Lewicki, J. P.; Weisgraber, T. H.; Small, W.; Chinn, S. C.; Maxwell, R. S. *Macromolecules* **2011**, *44*, 8106.
13. Maxwell, R. S.; Chinn, S. C.; Alviso, C. T.; Harvey, C. A.; Giuliani, J. R.; Wilson, T. S.; Cohenour, R. *Polym. Degrad. Stab.* **2009**, *94*, 456.

14. Weisgraber, T. H.; Gee, R. H.; Maiti, A.; Clague, D. S.; Chinn, S.; Maxwell, R. S. *Polymer* **2009**, *50*, 5613.
15. Dinh, L. N.; Mayer, B. P.; Maiti, A.; Chinn, S. C.; Maxwell, R. S. *J. Appl. Phys.* **2011**, *109*, 094905 .
16. Chinn, S. C.; Alviso, C. T.; Berman, E. S. F.; Harvey, C. A.; Maxwell, R. S.; Wilson, T. S.; Cohenour, R.; Saalwachter, K.; Chasse, W. *J. Phys. Chem. B* **2010**, *114*, 9729.
17. Mark, J. E. *Br. Polym. J.* **1985**, *17*, 144.
18. Mark, J. E.; Pan, S. J. *Makromol. Chem., Rapid Commun.* **1982**, *3*, 681.
19. Llorente, M. A.; Andrady, A. L.; Mark, J. E. *J. Polym. Sci., Part B: Polym. Phys.* **1981**, *19*, 621.
20. *Synthesis and properties of silicones and silicone modified materials*; Clarson, S. J., Fitzgerald, J. J., Owen, M. J., Smith, S. D., Van Dyke, M. E., Eds.; American Chemical Society: 2007.
21. Cohen-Addad, J. P. *Siloxane Polymers*; Prentice Hall: Englewood Cliffs, NJ, 1993.
22. Wunderlich, B. *Thermal Analysis of Polymeric Materials*; Springer Publishing: New York, 2005.
23. *Differential scanning calorimetry—fourier transform IR spectroscopy and thermogravimetric analysis—fourier transform IR spectroscopy to differentiate between very similar polymer materials*; Provder, T., Urban, M. W., Barth, H. G., Eds.; American Chemical Society: 1994.
24. Ettre, K.; Varadi, P. F. *Anal. Chem.* **1962**, *34*, 752.
25. Ke, B. *J. Polym. Sci., Part A: Gen. Pap.* **1963**, *1*, 1453.
26. Patel, M.; Chinn, S.; Maxwell, R. S.; Wilson, T. S.; Birdsell, S. A. *Polym. Degrad. Stab.* **2010**, *95*, 2499.
27. Kimmich, R.; Fatkullin, N. In *NMr - 3D Analysis - Photopolymerization*; Advances in Polymer Science; Springer: 2004, Vol. 170, p 1.
28. Spiess, H. W. *Macromolecules* **2010**, *43*, 5479.
29. Cohenaddad, J. P.; Viallat, A. *Polymer* **1986**, *27*, 1855.
30. Ebengou, R. H.; Cohenaddad, J. P. *Polymer* **1994**, *35*, 2962.
31. Folland, R.; Charlesby, A. *Radiat. Phys. Chem.* **1977**, *10*, 61.
32. Folland, R.; Charlesby, A. *Int. J.r Radiat. Phys. Chem.* **1976**, *8*, 555.
33. Chasse, W.; Lang, M.; Sommer, J. U.; Saalwachter, K. *Macromolecules* **2012**, *45*, 899.
34. Saalwachter, K.; Ziegler, P.; Spyckerelle, O.; Haidar, B.; Vidal, A.; Sommer, J. U. *J. Chem. Phys.* **2003**, *119*, 3468.
35. Maxwell, R. S.; Chinn, S. C.; Solyom, D.; Cohenour, R. *Macromolecules* **2005**, *38*, 7026.
36. Saalwachter, K. *Prog. Nucl. Magn. Reson. Spectrosc.* **2007**, *51*, 1.
37. Maus, A.; Hertlein, C.; Saalwachter, K. *Macromol. Chem. Phys.* **2006**, *207*, 1150.
38. Carr, H. Y.; Purcell, E. M. *Phys. Rev.* **1954**, *94*, 630.
39. Addad, J. P. C. *Prog. Nucl. Magn. Reson. Spectrosc.* **1993**, *25*, 1.
40. Mayer, B. P.; Chinn, S. C.; Maxwell, R. S.; Reimer, J. A. *Chem. Eng. Sci.* **2009**, *64*, 4684.
41. Theocaris, P. S.; Ioakimidis, N. I. *Q. Appl. Math.* **1977**, *35*, 173.

42. Provencher, S. W. *Comput. Phys. Commun.* **1982**, *27*, 229.
43. Weese, J. *Comput. Phys. Commun.* **1992**, *69*, 99.
44. Istratov, A. A.; Vyvenko, O. F. *Rev. Sci. Instrum.* **1999**, *70*, 1233.
45. Hill, L. W. *Prog. Org. Coat.* **1997**, *31*, 235.
46. Lewis, L. N.; Stein, J.; Gao, Y.; Colborn, R. E.; Hutchins, G. *Platinum Met. Rev.* **1997**, *41*, 66.
47. Spiess, H. W. *Macromol. Symp.* **2001**, *174*, 111.
48. Slichter, C. P. *Principles of Magnetic Resonance*, 3rd ed.; Springer: New York, 1996.
49. Clauss, J.; Schmidt-Rohr, K.; Spiess, H. W. *Acta Polym.* **1993**, *44*, 1.
50. Lewis, L. N.; Sy, K. G.; Bryant, G. L.; Donahue, P. E. *Organometallics* **1991**, *10*, 3750.

Chapter 11

A Milestone in Biomineralization: From a Structural Assessment to a Genetic Concept of Mineral Formation. Or How the Enzyme Silicatein Forms a Solid Silica Rod

Xiaohong Wang, Ute Schloßmacher, Heinz C. Schröder, and Werner E. G. Müller*

ERC Advanced Grant Research Group at the Institute for Physiological Chemistry, University Medical Center of the Johannes Gutenberg University Mainz, Duesbergweg 6, D-55128 Mainz, Germany
*****Fax: +49 6131-39-25243; Tel.: +49 6131-39-25910; E-mail: wmueller@uni-mainz.de**

Like all structural biomaterials in Metazoa also the spicules from sponges are hierarchically organized and biofabricated. With the exception of the spicules the structural complexity of the metazoan bioskeletons can be traced back from the millimeter-scale only to the micrometer- or submicrometer-scale, while the biological and/or genetic basis controlling the synthesis of these skeletons and their building blocks remained unknown. In contrast, from the spicules of the siliceous sponges the key molecules and the molecular-biological processes, involved in their formation, have been elucidated in the last few years. Here we summarize the different levels of molecular, biological and structural hierarchies that are controlling the synthesis of the picturesquely and intricately architectured spicules. The basic enzymatic/proteinaceous machinery that facilitates the polycondensation of silicate to the bio-silica scaffold that compose the spicules are the silicateins and their interacting/mature proteins. Two isoforms of silicatein, silicatein-α and silicatein-β, have been described that catalyzes the polymerization of ortho-silicate to polymeric bio-silica enzymatically. Silicatein-α together with silicatein-β forms pentameric units that continue to grow in a linear pattern.

The silicatein-interacting protein, silintaphin-1, stabilizes the initially formed silicatein fractals [pentameric strands]; silintaphin-2 provides Ca^{2+} ions to the galectins that are required for the growth of the spicules. The primary product of the enzymatic reaction forming bio-silica is a polymeric network that is translucent. This bio-silica polymer undergoes hardening via a controlled process of syneresis. During this reaction the bio-silica acquires its characteristic morphology, form and shape. Taking together, this review attempts to overcome the frontiers in the understanding of the different levels of hierarchies, genetic, biological and structural and, by that, contributes to a rational fabrication of new bioinspired, functional material which is guided by a genetic blueprint.

Introduction

The sponges [phylum Porifera] represent the phylogenetic oldest metazoan taxon and evolved approximately 800 million years ago; during that period they had been very successful and never got extinct (*1*). The basal sponge-related hypothetical metazoan ancestor, the Urmetazoa (*2*), developed a genetic repertoire very related to those of the higher metazoan crown taxa that enabled it to survive adverse climatic conditions, even the Proterozoic snowball periods (630 to 770 Ma). Besides of the characteristic metazoan metabolic pathways (*3*) it had had been the evolutionary novelty, the first animal hard skeleton, that had been acquired by the sponges which allowed them to resist adverse environmental conditions. Already in the Porifera the two different groups of minerals, the silicon-based and the calcium-based inorganic scaffold, have been used to form their inorganic skeletal elements, the spicules; first amorphous silica in the two sponge classes the Hexactinellida and the Demospongiae, and second calcite in the calcareous sponges, the Calcarea (*4*).

The inorganic/organic composition of the siliceous sponge spicules consist of almost pure, amorphous, quartz glass SiO_2 (*5*). For a purely chemical preparation of fused quartz glass (silica) high temperatures (> 1200°C) and adverse, non-physiological conditions are required. In contrast, the siliceous sponges synthesize their bio-silica based spicules at ambient, physiological conditions. It is amazing that nature, the siliceous sponges, can produce those structures at body temperature – and even more – they form spicules with an intricate morphology which is species-specific. The sizes of those spicules range from several micrometer to 3 m, as represented by the giant basal spicules from the deep-sea glass sponge

Monorhaphis chuni (*6*). The siliceous spicule can resist heavy water movements in depths of greater than 1,000 m in the ocean without breakage. In turn, the elucidation of the composition and the formation of those rigid biological silica (bio-silica) materials had attracted material scientists, e.g. Mayer (*7*), Aizenberg et al. (*8*), Sarikaya et al. (*9*), Morse (*10*), and Fratzl et al. (*11*), and our group (*12–14*). The spicules combine unusual mechanical properties, such as strength, stiffness, and toughness. Especially the formation of the monaxonal spicules of the demosponge *Suberites domuncula*, the diactinal styles (monaxons with one end pointed and another side blunt) and the diactinal tylostyles (one end pointed and another side with a swollen knob), as well as the polyaxonal spherasters (spicules with many rays originating from a globular center) of *Geodia cydonium* has been in the focus of our group (reviewed in: (*15*, *16*)).

It was a great challenge for two research groups, for the one of Morse (see: (*10*)) which identified the protein molecule that facilitates spicule formation and our group (reviewed in: (*15*, *16*)) which discovered that this protein is a genuine enzyme. In the significant studies by the group of Morse (*10*), the native silicatein was obtained from the spicule axial filaments (Fig. 1) by treatment of spicules with hydrofluoric acid under conditions that were later shown to affect the association kinetics of the silicatein molecules to each other as well as the enzymatic function of this enzyme (see: (*15*)). A more gentle extraction procedure, omitting hydrofluoric acid and applying a buffer system based on Tris-HCl and glycerol, turned out to be more suitable to protect the catalytic function of silicatein. Likewise the method, described by us, to prepare the recombinant silicatein in *Escherichia coli* proved to be superior to the preparation described before by the Morse group (*10*). Based on these improvements, both the procedures for the preparation of the enzymes together with their application for the synthesis of novel silica-based materials, for silicatein-α (*17*) and also for silicatein-β (*18*), have been granted as patents.

These groundbreaking findings allowed an understanding of bio-silica synthesis in the sponges and a rational utilization and application of the physiologically formed bio-silica for a routine, commercial application. In contrast to the physiologically formed bio-silica, the chemical synthesis of silica, the polycondensation reactions require physiologically adverse pH conditions and high temperatures to overcome the activation energy, allowing the chemical reaction to occur. This is in contrast to the sol-gel formation processes occurring in living organisms in which the activation energy can be substantially reduced with the help of enzymes that allow the reactions to proceed on solid/fluid boundaries (*16*). Importantly, the concentrations of silicate in the aqueous milieu where the sponges live [10 and 180 μM (*19*)] are far lower than the critical concentration required for the onset of the polycondensation reaction [1 mM]. To enrich the silica concentration in an organism biological pumps are used to accumulate silicic acid against a concentration gradient under consumption of ATP (*20*, *21*). Both diatoms and sponges are provided with membrane-inserted special silica transporters that actively pump silicic acid into the organism. In addition, animals, more specific the sponges can initiate polycondensation reactions at lover silica concentration, since the Michaelis–Menten affinity constant (K_m value) of the silicatein enzyme is around the ambient silica concentration (*16*).
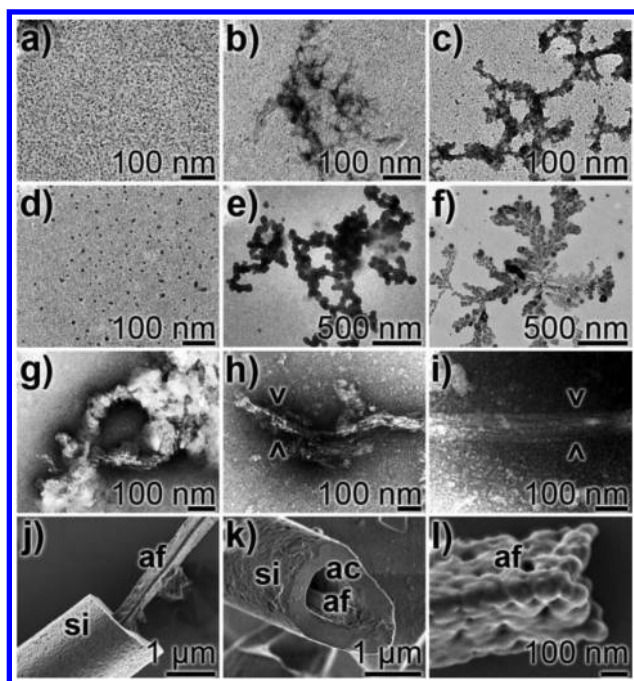
*Figure 1. Axial filament and its formation in vitro and in vivo; S. domuncula. (**a** to **f**) Formation of filamentous aggregates from recombinant silicatein monomers; TEM. (**a** to **c**) Self-assembly of recombinant silicatein-α. The samples were allowed to form aggregates for a period of 120 min (A: 0 min; B: 30 min; C: 120 min). Dendritic growth patterns were produced. (**d** to **f**) Aggregate formation of recombinant silicatein-α in the presence of recombinant silintaphin-1, added in a stoichiometric molar ratio 4:1 (silicatein-α:silintaphin-1) for a period of 0 min, 60 min and 120 min. In the intermediate stage distinct fractal-like filaments are observed. (**g** to **i**) Morphology of axial filament samples, prepared from spicules growing in primmorphs, after dissolution with HF; TEM. The structure of those filaments is not rod-shaped but fluffy. (h and i) At higher magnifications the laterally arranged filaments can be seen in a parallel arrangement (><). (**j** to **l**) Appearance of the rod- shaped axial filaments in mature spicules, located inside of the axial canal of the spicules; SEM. (j and k) Fractures through silica (si) spicules with an axial filament (af) sticking out the axial canal (ac). (l) Axial filament (af) after extensive dissolution with HF. The rope-like organization is seen.*

Results and Discussion

Genetic and Biochemical Hierarchies: Enzymatic Machinery for Soft Matter Formation

The ultimate goal in the understanding of any morphogenetic event is, at first, to elucidate the different molecules in a given regulatory network and then

to identify the underlying genes involved (Fig. 2). Using these elementary blocks a regulatory genetic architecture that is based on a few or even a single master gene can be formulated. Only recently it was possible to describe a hard skeleton formation on molecular level (reviewed in: (*15*)). This initial investigation was successfully performed with sponge spicules. By way of comparison the physiological or pathological processes involved in bone formation can only be outlined in the first approximation (*22*). The identification of silicatein, the enzyme that initiates the catalytic bio-condensation reaction (*23–25*), was a great success in understanding the biological silica formation. Silicatein is the dominant protein that builds the axial filaments, that is harbored by the central axial canal of any spicule (Fig. 1). In *in vitro* experiments, using hatching gemmules from the demosponge *Ephydatia muelleri*, it could be shown that the growth of the spicules is rapid; the 200 to 350 μm long spicules of this sponge grow with a rate of 1 to 10 μm/h. The morphogenetic process of spicule formation can be hierarchically divided into processes proceeding on the genetic/biochemical, the cellular and finally the structural level.

The Elements of the Enzymatic Machinery

The major proteins forming the enzymatic machinery of polymeric silica production are the silicateins and the silintaphins.

(A) The silicateins, being members of cathepsin L and papain family of proteases, had been discovered in the demosponge *Tethya aurantium* by the group of Morse (*23*, *24*). Soon later they were also identified in *S. domuncula* (*25*), after screening the genes of the cathepsin family (*26*). Three isoforms had been described in *T. aurantium*, silicatein-α to -γ that are slightly different in their molecular size; among them the α- and β-forms had been cloned and sequenced (*23*); Fig. 3a. Sequence similarity and phylogenetic analyses revealed that the silicateins are related to the cathepsin L family of proteases, enzymes that are involved in the hydrolytic degradation of extracellular matrix proteins. Both the *T. aurantium* and the *S. domuncula* silicateins comprise a signal peptide with a length of about 15 aa [amino acids], that is removed through the secretory pathway during translocation into the endoplasmic reticulum. The released enzyme undergoes enzymatic cleavage to the active silicatein through removal of the propeptide (*27*). In the mature, processed form the silicateins of *T. aurantium* have a molecular mass of 29, 28, and 27 kDa, respectively. For *S. domuncula* the size of the mature silicatein-α is 23 kDa (*28*). Silicatein-α is the dominant isoform, existing in the axial filament, in a 2:1 (for *T. aurantium*) (*23*) or in a 4:1 molar ratio with silicatein-β (for *S. domuncula*) (*29*). The recombinant silicateins are highly insoluble proteins (*30*), a property that can be attributed to the existence of a hydrophobic "transmembrane-like" helix at the N-terminus of the mature enzymes (*25*). The silicateins are distinguished from the cathepsins by the amino acid(s) in their active sites. The catalytic triad of the cathepsins consists of the three amino acids Cys, His and Asn (*31*), while the first aa of the sponge silicatein triad is a Ser residue; Fig. 3a. Interestingly, close to the His of the catalytic triad, a Ser cluster exists in all silicateins that comprise about 7 moieties. Since this stretch is found in the active center of the silicateins,

it is suggestive to assume that this region is involved in the binding of the enzyme to polymeric silica. In an initial approach it had been proposed that the silicatein-mediated polycondensation reaction with the ortho-silicic acid or silicon alkoxide (TEOS [tetra-ethyl-ortho-silicate]) substrates can be explain by the hydrolytic activity of silicatein toward its synthetic substrate, TEOS, or the initial formation of disilicic acid from ortho-silicic acid as the natural substrate (*24*, *32*). However, none of them is able to describe the biocatalytic formation of the polymeric silica from its monomeric precursors(s). Recently we proposed a comprehensive, new model which includes the two necessary assumptions for silicatein reaction; (*a*) implication of the crucial Ser moiety within the catalytic triad and (*b*) using ortho-silicic acid as the genuine substrate for the enzyme reaction (*33*) (Fig. 3b). In our model it is possible to explain both the initial condensation reaction, the formation of disilicic acid, as well as the subsequent oligomerization processes. The initial catalytic step involves a nucleophilic attack (S_N2 type) of the (electronegative) oxygen atom from the hydroxy group of the active site Ser to the (electropositive) silicon atom of a silicic acid molecule. This reaction is facilitated by a hydrogen bridge formation between the Ser OH and the His imidazole within the catalytic center, a reaction that increases the nucleophilicity of the Ser hydroxy group (Fig. 3b, Step 1). Then, a proton transfer from the His imidazole nitrogen (Ser•His hydrogen bond) to one of the silicon OH ligands of the pentavalent intermediate (in the transition stage) occurs, resulting in the release of a water molecule. In the next step, the silicic acid molecule which remains covalently bound through an ester-like linkage to the enzyme Ser moiety undergoes a nucleophilic attack on the silicon atom of a second ortho-silicic acid molecule, pulling it to the substrate pocket of the enzyme (Fig. 3b, Step 2). Subsequently, the nucleophilicity of the attacking oxygen atom of the first (enzyme-bound) silicic acid molecule is assumed to be increased via formation of a hydrogen bond with the imidazole nitrogen of the His. The loss of a water molecule generates a disilicic acid molecule (Fig. 3b, Step 2), which remains bound to the enzyme. Now, a rotation of the ester bond allows the interaction of a second OH ligand of the enzyme-bound silicic acid unit with the imidazole nitrogen of the His in the catalytic center, giving rise to a further growth of the disilicic acid by a third orthosilicic acid molecule (Fig. 3b, Step 3) under a release of a further water molecule. Including previous data (*34*), this model proposes a final cyclization step (Fig. 3b, Step 3). The products released from the enzyme by hydroloytic cleavage (cyclic trisilicic acid and higher oligomers) are much more reactive than the silicic acid momoners and promote the further condensation reaction.

(B) Enzyme kinetic studies were performed with recombinant silicatein-α and the model substrate bis(p-aminophenoxy)-dimethylsilane [BAPD] which contains two silicic ester-like and two silane bonds (*35*). In the optical assay applied, the temperature optimum was found within the range of 20-25°C, revealing a temperature coefficient (Q_{10}) of 2.5-fold above 25°C [35°C/25°C] and of 2.9-fold below 25°C [15°C/25°C]. The Michaelis constant (K_m) was determined to be 22.7 μM. this finding is interesting in the light of earlier findings that revealed a K_m value for human recombinant cathepsin L [an enzyme the closely related enzyme to silicatein] of 1.1 μM; for the cathepsin L reaction the

substrate benzyloxycarbonyl-Phe-Arg-4-methylcoumarin-7-amide had been used (*36*). The turnover value (molecules of substrate converted per enzyme molecule per second) for silicatein in the silica esterase assay was 5.2 close to the value found for the human cathepsin L (*37*).
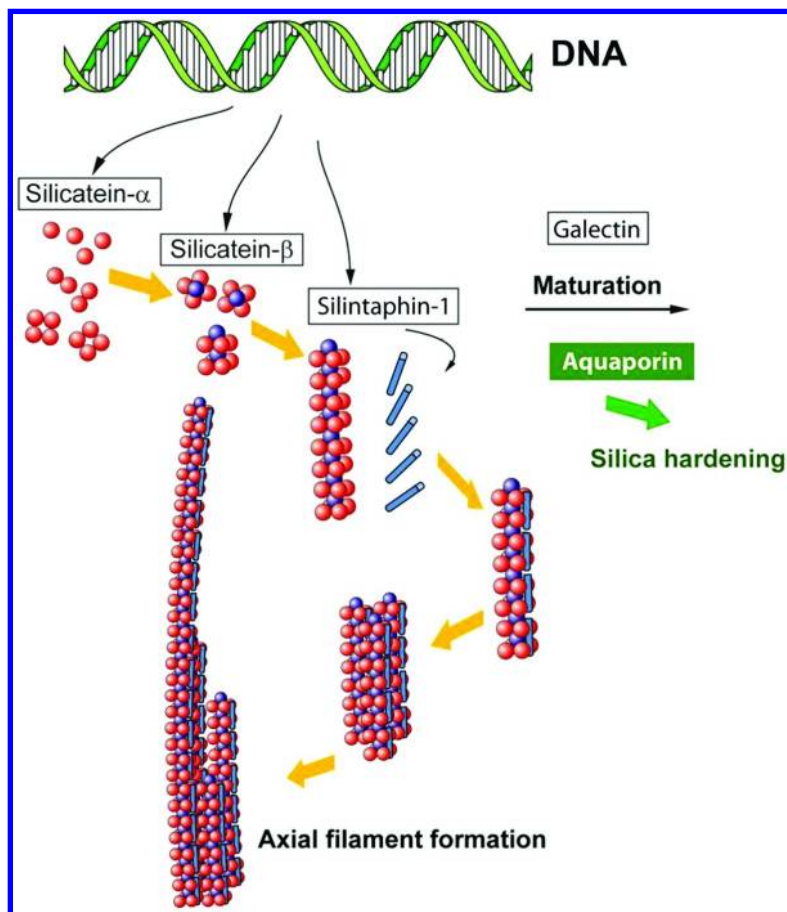
Figure 2. Proposed hierarchical genetic model controlling the synthesis of the siliceous spicules (15, 16). The spicule synthesis starts intracellularly in specialized cells, the sclerocytes, after expression of the silicateins, with their isoforms silicatein-α and silicatein-ß. In a stoichiometric manner four silicatein-α molecules form a tetramer allowing one silicatein-ß molecule to associate in the middle of the tetrad. Through axial assembly filaments are formed that are stabilized by the silicatein interactor silintaphin-1. The axial filament is harbored in the axial canal, and mediates the formation of an immature spicule rod. The formed spicules are shaped within a collagen cast and processed and aged through a process involving syneresis (expulsion of water) from the "soft" bio-silica formed by silicatein, a process facilitated by aquaporin channels inserted into the cell membranes of the adjacent cells.
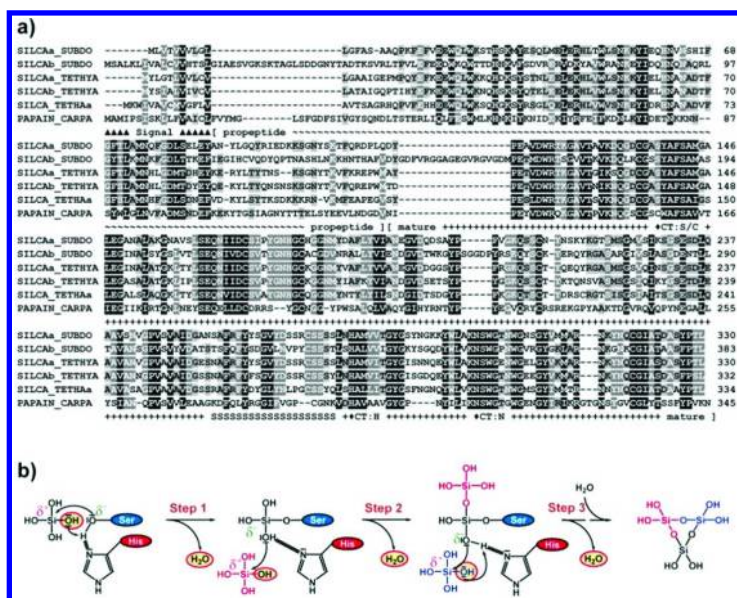
*Figure 3. Silicateines. (**a**) Alignment of selected silicateins and cathepsin L/papain. The deduced polypeptides from S. domuncula silicatein-α and silicatein-β (SILCAa SUBDO, accession number AJ272013 and SILCAb SUBDO, AJ547635.1) and T. aurantium (SILCAa TETHYA, AAD23951; SILCAb TETHYA, AF098670) have been aligned with the third T. aurantium silicatein sequence (SILCA TETHYAa, CBY80148), as well as the related proteases, papain from the papaya plant (PAPAIN CARPA, AAB02650.1). Residues conserved (similar or related to their physicochemical properties) in all sequences are shown in white on black, and those which are found in all four sequences are in white on gray. The characteristic sites in the sequences, that is, the catalytic triad (♦CT) amino acids, Ser (S) in the silicateins (and Cys (C) in cathepsin), His (H), and Asn (N), as well as the segments of the signal peptide (▴~signal~▴), the propeptide segment (~ ~ ~), and the mature enzyme (+ + +), are marked. Finally, the serine clusters (S) are underlined. (**b**) Outline of the proposed reaction mechanism of the silicatein-catalyzed polycondensation reaction using ortho-silicate as substrate and involving both the His and the Ser in the proposed catalytic reaction (21, 22). STEP 1: Nucleophilic attack of the Ser oxygen atom, negatively charged, to the silicon atom of the ortho-silicic acid substrate, positively charged, followed by transfer of a proton, coming from the Ser•His hydrogen bridge of the imidazole nitrogen of the His moiety to one OH ligand of the silicic acid molecule. After the release of a water molecule from the pentavalent intermediate, a nucleophilic attack of the oxygen atom from one of the OH ligands of the covalently bound silicic acid molecule at the silicon atom from a second orthosilicic acid molecule (in red) follows. STEP 2: Loss of a second water molecule after proton transfer from the imidazole group. The rotation of the Si–O–C bond between the disilicic acid formed and the Ser of the enzyme allows a nucleophilic attack of the oxygen atom from a second OH ligand of the first silicic acid molecule, to a third orthosilicic acid species (in blue). STEP 3: Cyclization of the resulting*

(enzyme-bound) trisilicic acid occurs that is caused by a nucleophilic attack of the (negatively charged) oxygen from an OH ligand of the terminal condensed orthosilicic acid (not shown). Finally, a reactive trisiloxane ring is formed that is released after hydrolysis of the Si–O–C bond.

(C) The activity of the silicatein-α was determined in *in vitro* assays and compared with the silica-forming activity during spicule formation *in* vivo (*30*). The *in vivo* silica-forming activity was assessed by calculating the amount of bio-silica formed during the growth of the spicules of the demosponge *Ephydatia fluviatilis*. The growth rate of those spicules with an average size of 200–350 μm and a thickness of 15 μm was determined to be 1^{-10} μm • h^{-1} (*38*). From these numbers the total weight of one spicule was calculated to be ≈ 88.3 x 10^{-9} g, which is equivalent to about 4.4 x 10^{13} molecules of bio-silica being formed during one hour in one spicule. Taking a protein content of about 5% in the spicules in account (mainly consisting of silicatein-α) (*5*), it follows that 2.2 x 10^{-10} g of protein catalyze the synthesis of 4.4 x 10^{-9} g of bio-silica per h. Since the molecular mass of mature silicatein is 25 kDa, it follows that 8.8 x 10^{-15} mol of silicatein (=5.3 x 10^9 molecules) synthesize 4.4 x 10^{-9} g [equivalent to 7.33 x 10^{-11} mol (=4.4 x 10^{13} molecules)] of bio-silica per h. In turn, and referring to native silicatein, the turnover number of silicate per silicatein on a molar basis is 8 x 10^3 molecules of converted substrate per silicatein molecule per h in spicules. With respect to recombinant silicatein-α, a value of 18.7 x 10^3 molecules per molecule of silicatein-α per h (substrate BAPD) had been determined for the esterase activity (*35*) and 5.4 x 10^3 molecules per molecule of silicatein-α per h using ortho-silicic acid as a substrate (*30*). This extent of bio-silica formation can even be increased by >5-fold, after addition of silintaphin-1, the silicatein adaptor molecule, in a 4:1 molar stoichiometric ratio (silicatein-α:silintaphin-1). Based on these calculations, it is obvious that the silica polymerization activity during spicule formation is mediated enzymatically by silicatein only.

(D) The Silintaphins, silicatein-interacting proteins. We screened for silicatein-interacting proteins applying the technique of yeast two-hybrid library screening, and could identify both silintaphin-1 (*39*), and by a solid-phase pull-down assay, we discovered silintaphin-2 (*40*). Silintaphin-1, of a size of 42 kDa comprises two distinct segments; first the pleckstrin homology domain, known to comprise strong protein:protein interacting affinities and second, towards the C-terminus, eight nearly identical repeats, each containing 10/12 aa (*39*). After raising antibodies, it could be demonstrated that silintaphin-1 is located within the axial filament silicatein, as well as in the silicatein-containing organic cylinder surrounding the growing spicules. Silintaphin-1 acts as a protein that significantly enhances the bio-silica-forming activity of silicatein; added at a molar ratio of 4:1 [silicatein-α:silintaphin-1], a 5.3- fold increase of the bio-silica-forming activity is measured (*30*).

Silintaphin-2 is the second silicatein-interactor had been identified in *S. domuncula* (*40*). This 15-kDa protein is likewise localized in the axial filament and also (mainly) in the organic cylinder of the growing spicules. Silintaphin-2 is a Ca^{2+}-binding protein which complexes four Ca^{2+} ions. It is synthesized as

a propeptide and becomes, after release to the extracellular space, processed and activated by the bone morphogenetic protein-1 (BMP-1). The activated silintaphin-2 had been shown to provide Ca^{2+} required for complex formation between the silicateins and galectins, the main components of the organic cylinder of the growing spicules (*41*).

Enzymatically Formed "Soft" Silica and Enzymatically Controlled Sol-Gel Bio-Silica Synthesis

Silicatein acts both an enzymatically active molecule, catalyzing the synthesis of an inorganic polymer (bio-silica) from inorganic monomeric precursors (ortho-silicate), and a structure-guiding scaffold protein (*29*, *42*). The enzymatic function can be characterized as an enzymatic polycondensation reaction. The characteristic feature of the enzymatically controlled sol-gel process is that the reaction proceeds at ambient temperature, physiological pH and also at silicate concentrations below 1 mM that are existing in the seawater. There 10 to 180 μM silicate are dissolved. The chemically-driven polycondensation of silica (*43*) proceeds results in the formation of 2-3 nm large colloidal particles. In the pH range of 2-7, the silica species are weakly ionized and rapidly form fibrillar aggregates allowing water molecules to fill-in the network (gel formation); Fig. 4. At pH>7 the existing charged silica particles inhibit fibril formation, but promote an Ostwald ripening process and in turn an increase in the particle size to 10-100 nm occurs. In parallel, the particle number decreases (sol formation); Fig. 4. Subsequently, the polycondensated particles undergo an aging process at higher temperature and drying before entering the phase of stabilization/sintering and glass formation (*44*).

Also the biochemically/silicatein-driven polycondensation reaction of silica follows the thermodynamic laws; however, silicatein lowers the activation energy of the exergonic polycondensation reaction. In addidion, the silicatein-mediated bio-silica formation proceeds at near neutral pH (*25*, *30*, *33*, *35*). In this environment the polycondensation involves a nucleophilic substitution reaction (S_N2) of the oxygen atom of Si-OH, resulting in the formation of a Si-O-Si siloxane linkage under the release of water. In contrast to the purely chemical polycondensation reaction, the silicatein-mediated silica formation at neutral pH leads to the formation of approximately 2.8 nm silica colloidal particles that continue to grow to 50-200 nm spheres (*45*).

Our spectroscopic analysis using the NanoSIMS technology revealed that during the enzymatically-driven reaction silicatein remains embedded within the bio-silica product (*46*). This finding implies that during the later stages of the polycondensation reaction the released water molecules remain inside the growing silica particles. The bio-silica product formed by silicatein and TEOS was analyzed by solid-state ^{29}Si NMR (nuclear magnetic resonance spectroscopy) analysis. The products formed showed a disordered, incompletely polymerized silica network (*24*). The initially formed bio-silica product represents a gelatinous amorphous silica network (Fig. 5; Fig. 6).
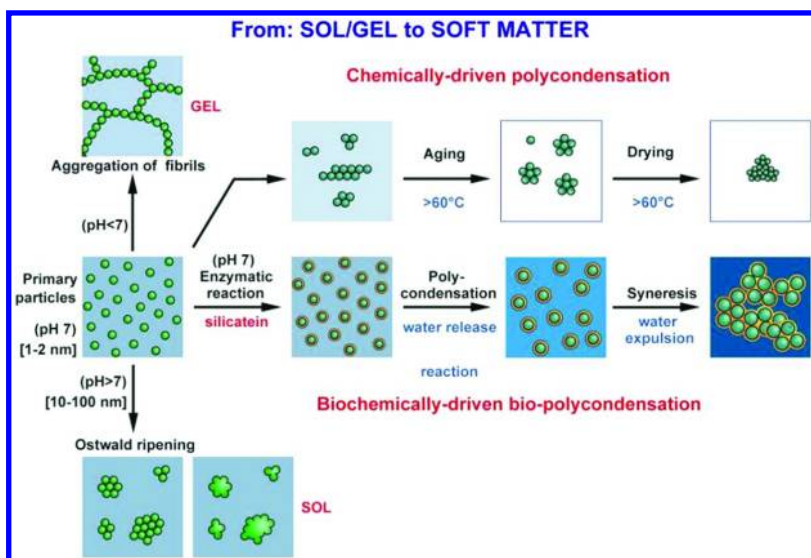
Figure 4. From sol/gel to soft matter: Chemically versus biochemically-driven polycondensation of silica (15, 16). Under acidic reaction conditions (pH<7), the silica units form fibrillar aggregates embedded in aqueous environment (gel formation). At a more alkaline milieu (pH>7), the number of particles decreases under formation of larger silica particles (10-100 nm) (Ostwald ripening process; sol formation). The chemically-driven polycondensation passes over an aging and drying process (at temperatures of >60°C) and reaches the phase of stabilization prior to the formation of glass. The silicatein/biochemically-driven polycondensation proceeds under physiological conditions, at pH 7, and undergoes water expulsion before reaching the stage of hard bio-silica material.

The ability of silicatein to associate to higher complexes had been shown by Murr and Morse, using native silicatein (*42*), and by us (*29*). Murr and Morse (*42*), by using native silicatein from the axial filament of *T. aurantium*, proposed self-assembly of silicatein molecules via fractal intermediates to stabile silicatein filaments. The authors suggest that the axial filament self-assembles from silicatein molecules [mono-/oligomers] through the formation of fractally patterned aggregates. In turn, the self-assembly of filaments from those oligomeric units proceeds progressively from an isotropic state *via* chaotic and fractal states to the ordered state, the filaments. In our studies, either by using native silicatein from *S. domuncula* axial filaments (*29*) or recombinant protein (*30*), it was visualized by TEM and SEM as well as by polyacrylamide gel electrophoresis that a stepwise assembly of the two isoforms of silicateins occurs in a stoichiometric manner. The data indicate that monomeric silicatein-α molecules form dimers and then tetramers, comprising a central opening into which one silicatein-β molecule is inserted (Fig. 2). During this protein aggregate formation, the Ser clusters of the four silicatein-α molecules are exposed to the center of the tetrad, while the active sites of the silicatein-α molecule are oriented co-axially (active

centers on the outer surface of the assembly), whereas the Ser clusters are oriented towards the center of the tetrameric silicatein complex. Furthermore the data are compatible with the assumption that the Ser clusters are likely to allow binding of the bio-silica chains formed. Within the center of a silicatein-α tetramer, one silicatein-β molecule is proposed to be inserted. The pentamers formed are aligned to filaments via fractal intermediates that are stabilized by silintaphin-1 molecules and build the backbone for the axial filaments. Using recombinant silicatein-α, the formation of filamentous aggregate via fractal-like assembly patterns can be visualized by TEM. The fractals become more prominent when the recombinant silintaphin-1 was added to recombinant silicatein-α in a stoichiometric molar ratio 1:4 during aggregate formation. In a recent study, we showed that those filaments, prepared from recombinant silicatein-α and silintaphin-1, have high enzymatic activity and strong ability to act as an *in vitro* assembled axial filament around which the ortho-silicate molecules are deposited as soft matter (*30*); Fig. 1.

Biological Hierarchy: The Soft Matter

Biochemical and molecular markers (*47*) have become available that allow a follow-up of some of the steps in the differentiation of stem cells to spicule-forming sclerocytes. With the primmorph system, it was shown that the following differentiated cell types, involved in skeletal formation, are derived from the totipotent stem cells: sclerocytes, archaeocytes, lophocytes, and chromocytes. The chromocytes (*41*) store carotenoids that are produced by bacterial symbionts in the sponge. These cells synthesize and release bone morphogenetic protein-1, a proteinase that is involved in the processing of a series of extracellular structural proteins, like in *S. domuncula*, silintaphin-2 [41]. In the latter study experimental evidence has been presented showing that the Ca^{2+}-binding protein silintaphin-2, which is formed in sclerocytes, delivers Ca^{2+} to the site of galectin filament/cylinder formation around the growing spicules (*48*). The galectin sheets provide the platform for binding of silicatein molecules, which in turn form an organic cylinder into which ortho-silicate is channeled from the sclerocytes. Collagen might be involved in the setup of the organization framework for the organic cylinder. The galectin molecules are synthesized in archaeocytes, whereas the silicateins come from the sclerocytes (*25*, *49*); Fig. 5.

Phase Separation: From Polymeric Bio-Silica to Mesoscopic Structures

The bio-silica product formed *in vitro* during polycondensation of ortho-silica in the presence of silicatein is not visible by eye-inspection. The clear solution, containing polycondensated bio-silica becomes turbid after phase separation. This process, the segregation of the liquid from the polymer, is paralleled with syneresis and occurs during the aging of silica (*50*) and has been postulated also to happen for biosilica. Recently, we succeeded to demonstrate the process of phase separation during bio-silica formation experimentally, by application of a two-phase system in which the formation of bio-silica was allowed to proceed in the upper phase, while phase-separation-inducing PEG [poly(ethylene glycol)] was added into the lower phase (*51*); Fig. 6. The silicatein reaction was performed

with 3 mM ortho-silicate (prehydrolyzed TEOS) and low concentrations of silicatein (20 µg/ml). The extent of bio-silica, formed in the presence of silicatein, was not altered during the PEG-mediated phase separation process. However, during and especially after termination of the polycondensation reaction of ortho-silicate to bio-silica, the initially glassy and translucent bio-silica polymers that are homogeneously dissolved within the reaction solution flocculate and become opaque and mechanically harden (*51*); Fig. 6. Simultaneously the viscosity of the bio-silica solution increases from 1.1 mPa/s (absence of PEG in the lower phase) to 15.3 mPas/1 (presence of PEG). PEG is a synthetic polymer. Therefore, we screened sponges for components that trigger (like PEG) the solidification process of biosilica. Knowing from previous studies that the process of hardening of bio-silica *in vivo* proceeds during maturation of the spicules, we screened for spicule-binding proteins displaying such a phase-separation property (*50*, *51*). The protein identified (Mr 22–24 kDa) was found to cause a rapid phase separation. This protein belongs to the protein family of nidogen-like proteins (mucins) that act as structural and functional phase/tissue separating molecules (*52*). The sponge nidogen/spicule-binding protein can be grouped to proteins that have the property to noncovalently polymerize (*53*). In turn, we attribute the observed phase separation of bio-silica to the type of polymerization-induced phase-separation process (*54*). In contrast, the phase-separation process of PEG bases on the property of PEG to destabilize the initial silica oligomer/water system by decreasing the hydrophilicity of the silica oligomers and by increasing the repulsive forces during silica polymerization (*55*).

Precision Bio-Silica Molding and Shaping: From Mesoscopic Structures to Precision Optical Glasses (Spicules)

The unique characteristics of the shaping of the siliceous sponge spicules is that these skeletal elements obtain their final morphology during a process of "precision glass molding" (*15*, *16*); Fig. 5. This process seems to be restricted to the siliceous sponges; the skeletons of all other metazoans are differently formed. As an example, the growth of mammalian bones occurs via deposition of hydroxyapatite crystals along an organic template either at the periosteum (outer surface) or at the endosteum (inner surface) (*56*). In contrast, spicule formation proceeds as a "replicative process" during which a fluid-elastic solid bio-silica polymer is pressed into an organic casting mold. During this molding step bio-silica undergoes a transition from soft matter to solid matter. The precision of the bio-silica glass structures is that high that e.g. the knobs of the tylostyles which likely act, in the animals, as lenses with a diameter of 10 µm do not vary by more than 10% in size. At present, such miniaturized optical structures showing excellent surface smoothness and high volume accuracy cannot be fabricated industrially. It is amazing that this biological bio-silica molding takes place at ambient temperatures, while industrially applied processes require temperatures above the glass transition temperature of 350°C (*57*).

The process of siliceous spicule formation can be dissected into the following steps: Initially the lucent soft-gel polymer is synthesized by silicatein, followed by the transition to a mesoscopic opaque gel, by water expulsion and phase separation.

Then bio-silica is pressed into a pre-formed collagen/galectin-based mold in which the final hardening process of the bio-silica takes place (Fig. 6).
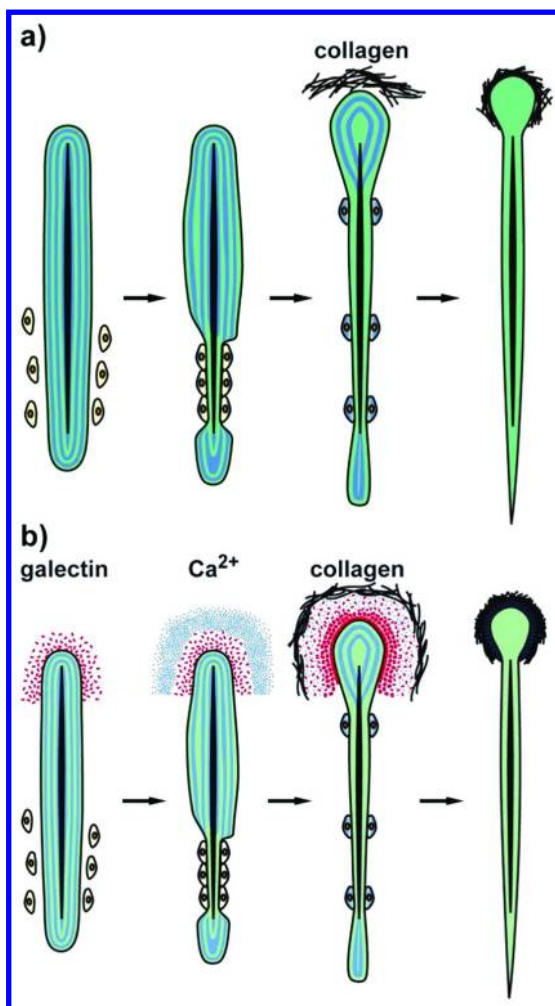
Figure 5. Precision bio-silica molding, a process during which the sponges form the intricately architectured siliceous spicules in vivo (15, 16). During this physiological molding and stamping process the microfluidic bio-silica is squeezed into an organic cast where the silica-polymer acquires the final shape and form of the spicules. (a) During the cell (c)-driven syneresis and aging of bio-silica within a growing spicule, the bio-silica scaffold is condensed and extruded (a-1 to a-4) into a collagen (col) cast. (b) Focusing on the cast formation, the process of precision bio-silica molding starts (b-1) with the synthesis of a soft bio-silica material by silicatein. After linking the galectin molecules together, by means of Ca²⁺ bridges, a mold is formed that becomes stabilized by collagen fibrils. Finally, soft bio-silica is pressed into this mold, a process followed by hardening of the spicule to a solid monolith.
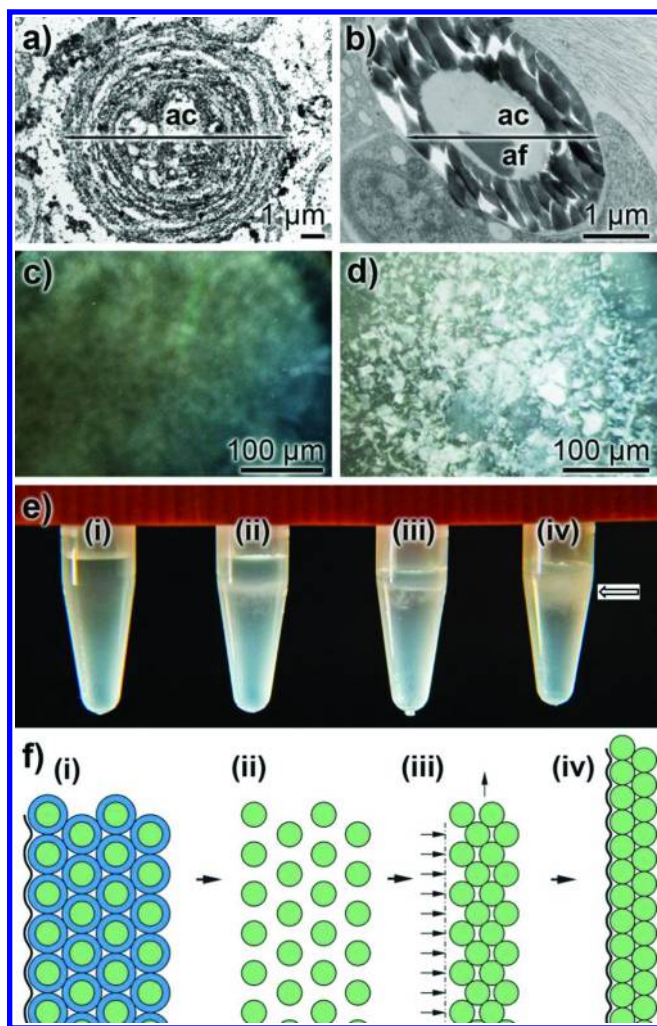
*Figure 6. Maturation steps of biosilica in vivo and in vitro (15, 16). (**a**) Extracellular maturation of spicules. TEM: immunogold labeling with anti-silicatein antibodies to highlight the silicatein molecules. During growth, organic cylinders are telescopically arranged around the axial canal (ac) which harbors the axial filament. (**b**) Section through a mature spicule, showing the axial canal (ac) in the center with its axial filament (af). The shrinkage of the diameter between the immature spicule, shown in (a), and the mature spicule, shown in (b), is striking. (**c** and (**d**) Forced bio-polycondensation/gelation reaction in the presence of 20 mg mL^{-1} recombinant silicatein-α, applying the two-phase assay system: (c) the upper layer, containing silicatein and 3 mM orthosilicate, was allowed to polycondensate for 1 h. (d) The same assay conditions, with silicatein and orthosilicate in the upper layer, but additionally with 10% w/v PEG in the lower layer. Large mesoscopic gelatinous flocs of biosilica are formed. (**e**) Mesoscopic gelatinous floc formation. In the two-phase*

assay system the upper layer was supplemented with 20 mg mL⁻¹ of recombinant silicatein and 3 mM orthosilicate. The lower layer contained PEG. Time kinetics: the reaction was run for i) 0, ii) 30, iii) 60, and iv) 180 min. The bulky bio-silica gels formed in reaction iv) are marked with an arrow. (f) Shrinkage of the biosilica network during aging and syneresis; scheme. i) The water molecules (in dark blue) are surrounding the initial biosilica nanoparticles, formed during the bio- polycondensation reaction; ii) elimination of water between the nanoparticles during syneresis; iii) continuing of the condensation process of the biosilica nanoparticles; iv) further shrinkage and denser packaging of the nanoparticles, resulting in an organized, smooth surface.

Conclusion

Bio-Silica: A Milestone in Biomineralization – Or a Paradigm Shift in Bioinorganic Chemistry

With the discovery of the silicatein protein (*10*) and the elucidation of its enzymatic function (*25*, *30*, *35*), a molecule was discovered that caused in the very last years major changes in our understanding of bio-inorganic biopolymers. The existence of such an enzyme caused a paradigm shift in the sense outlined by Kuhn (*58*). Silicatein is not merely an organic template, allowing silica to deposit as a polymer (e.g., reference (*10*)), but it is a bio-catalyst, an enzyme, that lowers the activation energy by allowing a chemical reaction to occur at lower substrate concentrations (*15*, *16*, *25*, *30*, *35*). This conceptual shift, that silicatein can be an organic template for bio-silica deposition and, in addition, acts as an enzyme accelerating this reaction, creates substantial changes in paradigms and research concepts, both in the laboratory and in the industrial practices (*59*). Surely, both organic and inorganic chemistry and certainly also biochemistry (with the focus on molecular biology) follow the rule of thermodynamics and their reactions are testable by application of a causal–analytical methodology. Wöhler (*60*) described the synthesis of an organic molecule (urea) from an inorganic precursor (ammonium cyanate), a reaction which involves both an exothermic ($\Delta H = 117$ kJ/mol) and an endothermic reaction ($\Delta H=+15.5$ kJ/mol). With the discovery of the enzymes (*61*), the elucidation of the biochemical reactions involved in the urea cycle became possible (*62*). Bio-silica is an inorganic polymer, formed by organisms, for example, diatoms or siliceous sponges, from ortho-silicate units under linking together two silanol groups to one siloxane bond. At physiological conditions (temperature and pH), this reaction does not run to an appreciable extent below an ortho-silicate concentration of <1 mm (*63*). Due to the properties of the enzyme silicatein, this polycondensation reaction proceeds even at around 100 µM (*35*), and allows the bio-polycondensation process to occur. After the formation of cyclic silicic acid oligomers (*33*), a progressive bio-silica synthesis can occur (*43*, *63*, *64*). Silicatein is the starter enzyme allowing the siloxane linkages to form, due to an interaction with the amino acids within the catalytic site of the enzyme, which facilitates the S_N2 reaction. Consequently, it is this starter reaction(s) that allows bio-polycondensation of ortho-silicate to bio-silica

to proceed at low temperature and physiological pH conditions, in contrast to purely chemically based polycondensation reactions (*65*).

In turn, this discovery of the enzymatically driven bio-silica synthesis opens a new avenue to fabricate patterned silica structures onto organic templates and by that this paradigm shift allows a major reorientation of methodology (traditional sol-to-gel polycondensation) allowing this old question to be approached in a new light (sol-to-gel biopolycondensation).

This paradigm shift of bio-polycondensation is pushed on by emerging needs in the field of biotechnology, for example for example, the development of light waveguides onto organic matrices, the taping/marking of visitors entering a security district, or the assembly of three dimensional, transistors which save operation place. Consequently, we predict that bio-polycondensation will become a key technology and will increase the economic competitiveness in order to meet the public and biomedical demands.

Acknowledgments

References

1. Wang, X. H.; Hu, S.; Gan, L.; Wiens, M.; Müller, W. E. G. *Terra Nova* **2010**, *22*, 1.
2. Müller, W. E. G.; Wiens, M.; Adell, T.; Gamulin, V.; Schröder, H. C.; Müller, I. M. *Int. Rev. Cytol.* **2004**, *235*, 53.
3. Müller W. E. G. In *Progress in Molecular and Subcellular Biology*; Müller, W. E. G., Ed.; Springer-Verlag: Berlin, Heidelberg, 1998; Vol. 19, p 89.
4. Müller, W. E. G. In *Encyclopedia of Molecular Cell Biology and Molecular Medicine*; Meyers, R. A., Ed.; Wiley-VCH Press: Weinheim, 2005; Vol.13, p 269.
5. Müller, W. E. G.; Jochum, K.; Stoll, B.; Wang, X. H. *Chem. Mater.* **2008**, *20*, 4703.
6. Wang, X. H.; Schröder, H. C.; Müller, W. E. G. *Int. Rev. Cell. Mol. Biol.* **2009**, *273*, 69.
7. Mayer, G. *Science* **2005**, *310*, 1144.
8. Aizenberg, J.; Weaver, J. C.; Thanawala, M. S.; Sundar, V. C.; Morse, D. E.; Fratzl, P. *Science* **2005**, *309*, 275.

9. Sarikaya, M.; Fong, H.; Sunderland, N.; Flinn, B. D.; Mayer, G.; Mescher, A.; Gainoa, E. *J .Mater. Res.* **2001**, *16*, 1420.

10. Morse, D. E. *Trends Biotechnol.* **1999**, *17*, 230.

11. Fratzl, P.; Weinkamer, R. *Prog. Mater. Sci.* **2007**, *52*, 1263.

12. Schröder, H. C.; Wang, X. H.; Tremel, W.; Ushijima, H.; Müller, W. E. G. *Nat. Prod. Rep.* **2008**, *25*, 455.

13. Wang, X. H.; Wiens, M.; Schröder, H. C.; Hu, S.; Mugnaioli, E.; Kolb, U.; Tremel, W.; Pisignano, D.; Müller, W. E. G. *Adv. Biomater./Adv. Eng. Mater.* **2010**, *12*, B422.

14. Wang, X. H.; Wiens, M.; Schloßmacher, U.; Jochum, K. P.; Schröder, H. C.; Müller, W. E. G. *Adv. Biomater.* **2012**, *14*, B4.

15. Wang, X. H.; Schröder, H. C.; Wang, K.; Kaandorp, J. A.; Müller, W. E. G. *Soft Matter* **2012**, *8*, 9501.

16. Müller, W. E. G.; Schröder, H. C.; Burghard, Z.; Pisignano, D.; Wang, X. H. *Chem. Eur J.* **2013**, *19*, 5790.

17. Müller W. E. G.; Krasko A.; Lorenz B.; Schröder, H. C. Silicateinvermittelte Synthese von amorphen Silikaten und Siloxanen und ihre Verwendung. EP1320624 B1, 2000.

18. Müller, W. E. G.; Schwertner, H.; Schröder, H. C.; Wang, X. H. Polypeptid eines Silicatein-ß aus Suberites domuncula, dafür kodierende Nukleinsäure, deren Verwendungen, diese Nukleinsäure umfassender Vektor und dieses Polypeptid exprimierende Wirtszelle. GPDE 10352433, 2003.

19. Maldonado, M.; Carmona, M. C.; Velásquez, Z.; Puig, M. A.; Cruzado, A.; López, A.; Young, C. M. *Limnol. Oceanogr.* **2005**, *50*, 799.

20. Hildebrand, M.; Dahlin, K.; Volcani, B. E. *Mol. Gen. Genet.* **1998**, *260*, 480.

21. Schröder, H. C.; Perović-Ottstadt, S.; Rothenberger, M.; Wiens, M.; Schwertner, H.; Batel, R.; Korzhev, M.; Müller, I. M.; Müller, W. E. G. *Biochem. J.* **2004**, *381*, 665.

22. Wang, X. H.; Schröder, H. C.; Wiens, M.; Ushijima, H.; Müller, W. E. G. *Curr. Opin. Biotechnol.* **2012**, *21*, 1.

23. Shimizu, K.; Cha, J.; Stucky, G. D.; Morse, D. E. *Proc. Natl. Acad. Sci. U.S.A.* **1998**, *95*, 6234.

24. Cha, J. N.; Shimizu, K.; Zhou, Y.; Christianssen, S. C.; Chmelka, B. F.; Stucky, G. D.; Morse, D. E. *Proc. Natl. Acad. Sci. U.S.A.* **1999**, *96*, 361.

25. Krasko, A.; Batel, R.; Schröder, H. C.; Müller, I. M.; Müller, W. E. G. *Eur. J. Biochem.* **2000**, *267*, 4878.

26. Krasko, A.; Gamulin, V.; Seack, J.; Steffen, R.; Schröder, H. C.; Müller, W. E. G. *Molec. Mar. Biol. Biotechnol.* **1997**, *6*, 296.

27. Müller, W. E. G.; Krasko, A.; Le Pennec, G.; Steffen, R.; Ammar, M. S. A.; Wiens, M.; Müller, I. M.; Schröder, H. C. In *Silicon Biomineralization: Biology - Biochemistry - Molecular Biology - Biotechnology*; Progress in Molecular and Subcellular Biology; Müller, W. E. G., Ed.; Springer Press: Berlin, 2003; Vol 33, p 195.

28. Müller, W. E. G.; Rothenberger, M.; Boreiko, A.; Tremel, W.; Reiber, A.; Schröder, H. C. *Cell Tissue Res.* **2005**, *321*, 285.

29. Müller, W. E. G.; Boreiko, A.; Schloßmacher, U.; Wang, X. H.; Tahir, M. N.; Tremel, W.; Brandt, D.; Kaandorp, J. A.; Schröder, H. C. *Biomaterials* **2007**, *28*, 4501.

30. Schloßmacher, U.; Wiens, M.; Schröder, H. C.; Wang, X. H.; Jochum, K. P.; Müller, W. E. G. *FEBS J.* **2011**, *278*, 1145.

31. Rogers, J. C.; Dean, D.; Heck, G. R. *Proc. Natl. Acad. Sci. U.S.A.* **1985**, *82*, 6512.

32. Fairhead, M.; Johnson, K. A.; Kowatz, T.; Mcmahon, S. A.; Carter, L. G.; Oke, M.; Liu, H.; Naismith, J. H.; Van Der Walle, C. F. *Chem. Commun.* **2008**, *21*, 1765.

33. Schröder, H. C.; Wiens, M.; Schloßmacher, U.; Brandt, D.; Müller, W. E. G. *Silicon* **2012**, *4*, 33.

34. Flory, P. J.; Semlyen, J. A. *J. Am. Chem. Soc.* **1966**, *88*, 3209.

35. Müller, W. E. G.; Schloßmacher, U.; Wang, X. H.; Boreiko, A.; Brandt, D.; Wolf, S. E.; Tremel, W.; Schröder, H. C. *FEBS J.* **2008**, *275*, 362.

36. Nomura, T.; Fujishima, A.; Fujisawa, Y. *Biochem. Biophys. Res. Commun.* **1996**, *228*, 792.

37. Mason, R. W. *Biochem. J.* **1986**, *240*, 285.

38. Imsiecke, G.; Steffen, R.; Custodio, M.; Borojevic, R.; Müller, W. E. G. *In Vitro Cell. Dev. Biol.* **1995**, *31*, 528.

39. Wiens, M.; Bausen, M.; Natalio, F.; Link, T.; Schlossmacher, U.; Müller, W. E. G. *Biomaterials* **2009**, *30*, 1648.

40. Wiens, M.; Schröder, H. C.; Wang, X. H.; Link, T.; Steindorf, D.; Müller, W. E. G. *Biochemistry* **2011**, *50*, 1981.

41. Müller, W. E. G.; Binder, M.; von Lintig, J.; Guo, Y. W.; Wang, X. H.; Kaandorp, J. A.; Wiens, M.; Schröder, H. C. *Biochim. Biophys. Acta, Gen. Subj.* **2011**, *1810*, 1178.

42. Murr, M. M.; Morse, D. E. *Proc. Natl. Acad. Sci. U.S.A.* **2005**, *102*, 11657.

43. Coradin, T.; Lopez, P. J. *ChemBioChem* **2003**, *4*, 251.

44. Lin, S.; Ionescu, C.; Pike, K. J.; Smith, M. E.; Jones, J. R. *J. Mater. Chem.* **2009**, *19*, 1276.

45. Woesz, A.; Weaver, J. C.; Kazanci, M.; Dauphin, Y.; Aizenberg, J.; Morse, D. E.; Fratzl, P. *J. Mater. Res.* **2006**, *21*, 2068.

46. Müller, W. E. G.; Wang, X. H.; Sinha, B.; Wiens, M.; Schröder, H. C.; Jochum, K. P. *ChemBioChem* **2010**, *11*, 1077.

47. Müller, W. E. G. *Sem. Cell Dev. Biol.* **2006**, *17*, 481.

48. Schröder, H. C.; Boreiko, A.; Korzhev, M.; Tahir, M. N.; Tremel, W.; Eckert, C.; Ushijima, H.; Müller, I. M.; Müller, W. E. G. *J. Biol. Chem.* **2006**, *281*, 12001.

49. Krasko, A.; Schröder, H. C.; Batel, R.; Grebenjuk, V. A.; Steffen, R.; Müller, I. M.; Müller, W. E. G. *DNA Cell Biol.* **2002**, *21*, 67.

50. Brinker C. J., Scherer G. W. *Sol - Gel Science: The Physics and Chemistry of Sol - Gel Processing*; Academic Press: Boston, 1990.

51. Wang, X. H.; Schloßmacher, U.; Schröder, H. C.; Müller, W. E. G. *Soft Matter* **2013**, *9*, 654.

52. Lovicu, F. J.; Chamberlain, C. G.; McAvoy, J. W. *Invest. Ophthalmol. Visual Sci.* **1995**, *36*, 1459.

53. Kang, S. H.; Kramer, J. M. *Mol. Biol. Cell* **2000**, *11*, 3911.
54. Renamayor, C. S.; Pacios, I. E. *Soft Matter* **2010**, *6*, 2013.
55. Le Bideau, J.; Miah, M. Y.; Vioux, A.; Fajula, F.; Galarneau, A. *J. Mater. Chem.* **2010**, *20*, 964.
56. Currey J. D. *Bones: Structure and Mechanics*; Princeton University Press: Princeton, 2006.
57. Firestone, G. C.; Yi, A. Y. *Appl. Opt.* **2005**, *44*, 6115.
58. Kuhn T. S. *The Structure of Scientific Revolutions*; University of Chicago Press: Chicago, 1962; p 172.
59. Potthast, T. *EMBO Rep.* **2009**, *10*, S42.
60. Wöhler, F. *Ann. Phys. Chem.* **1828**, *12*, 253.
61. Pasteur, L. *Mem. Soc. Sci. Agric. Arts.* **1857**, *5*, 13.
62. Krebs, H.; Henseleit, K.; Hoppe-Seyler's, Z. *Physiol. Chem.* **1932**, *210*, 33.
63. Belton, D. J.; Deschaume, O.; Perry, C. C. *FEBS J.* **2012**, *279*, 1710.
64. Wang, X. H.; Schloßmacher, U.; Wiens, M.; Batel, R.; Schröder, H. C.; Müller, W. E. G. *FEBS J.* **2012**, *279*, 1721.
65. Dabbs, D.; Aksay, I. *Annu. Rev. Phys. Chem.* **2000**, *51*, 601.

Quinone Tethered Silylethers: Protein Binding and Film Forming Abilities

Bigyan R. Jali and Jubaraj B. Baruah*

Department of Chemistry, Indian Institute of Technology Guwahati, North Guwahati 781 039, India
***E-mail: juba@iitg.ernet.in**

The compounds 2-(3-(trimethoxysilyl)propylthio)naphthalene-1,4-dione (**1**), 2-(3-(trimethoxysilyl)propylthio)-3-methyl-naphthalene-1,4-dione (**2**), and 2-(3-(trimethoxysilyl)propyl-thio)cyclohexa-2,5-diene-1,4-dione (**3**) were prepared by reacting 3-mercaptopropyl-trimethoxysilane with the corresponding quinone under ambient conditions. The protein binding abilities as well as film formation abilities of these three siloxyethers have been determined. The SEM studies have revealed that film formation by these compounds accompany formation of micron sized particles.

Introduction

The thiol group bearing trialkoxysilanes find great utility in preparation of hybrid-materials (*1–6*), surface-modifications (*7–14*), catalysis (*15, 16*) and in drug delivery (*17, 18*). A thiol group attached as a component of a trialkoxysilane can be easily functionalized to prepare capped metallic nano-particles (*19–22*). Such studies have helped in designing sensors. We have observed that the quinones easily lead to the formation of C-S bond without addition of a reagent. Such C-S bond forming reactions not only maintain atom economy but also lead to desired products under ambient condition (*23, 24*). Hybrid materials derived from alkoxysilane interact with proteins (*25, 26*), modifies cell membranes (*27*), causes corrosion inhibition (*28*), used in analytical chemistry for metal detections (*29, 30*) and are also used to make magnetic materials (*31*). With such diverse applications, we prepared three compounds 2-(3-(trimethoxysilyl)propylthio)naphthalene-1,4-dione (**1**), 2-(3-(trimethoxy silyl)propylthio)-3-methylnaphthalene-1,4-dione (**2**),

and 2-(3-(trimethoxysilyl) propylthio)cyclohexa-2,5-diene-1,4-dione (**3**) as shown in the chart 1 to understand their self-assembling properties and also to find out their protein binding abilities.
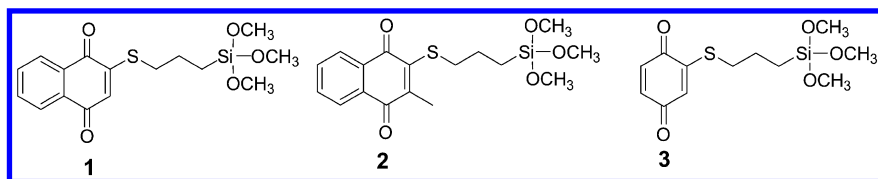
Chart 1. Some quinones bearing trimethoxysilane group

Discussion

The compounds **1-3** were prepared by reacting respective quinone with 3-mercaptopropyl-trimethoxysilane adopting procedure which was earlier followed for synthesis of similar mono-substituted C-S bonded quinones (*23*, *24*). The formation of the C-S bonded compounds in each case was confirmed by comparing the powder XRD, IR and other spectroscopic properties of the products with starting compounds. The powder XRD patterns of the starting quinones and that of the products are shown in the fig. 1a-1c. The PXRD revealed that the compounds **1-3** are less crystalline and they show broad peaks, probably due to self-assembly formation. Such self assembly may be guided by weak Si...O interactions of the silicon atoms with the carbonyl oxygen atoms. The compounds **1-3** have characteristic carbonyl frequencies at 1657 cm^{-1}, 1660 cm^{-1} and 1654 cm^{-1} respectively. The solid state UV-visible spectra of these compounds differ, the compounds **1** and **3** show one absorption each with maximum absorptions at 266 nm and 299 nm respectively; whereas the compound **2** has absorption maxima at 347 and 432 nm respectively. However, in solution (DMSO) the compound **1-3** have absorptions at 332 nm, 330 nm, 297 nm. The differences in the solution and in the solid state UV-visible spectra of these compounds suggest their ability to form self-assemblies. Although, the compounds have poor solubilities in common organic solvents as well as in water, their solubilities in dimethylsulphoxide (DMSO) were good enough to understand the film formation abilities of them and also to understand their other biological interactions. As evident from the broad powder-XRD patterns the compounds have low crystalline behavior. While preparing films of these compounds we observed simultaneous formations of micron size particles. The micron size particles were formed from cleavage of the films; as there were clear demarcations of the places from where such micron particles were formed. Representative SEM photographs showing the orifices and the micron size particles lying within and on top of the orifices as well as on the surface of films formed from compounds **1** and **3** are shown in fig. 2. From the morphological studies it is clear that the compounds **1** and **3** have similar properties to form films as well as crystalline particles whereas the compound **3** has lower tendency to form particles but forms a smooth surface of

film on glass plate. The composites of silylethers were earlier used to mimic cell membranes (*27*), thus formation of film from compound **2** may be considered as an important observation to make hydrid-materials for biological study.
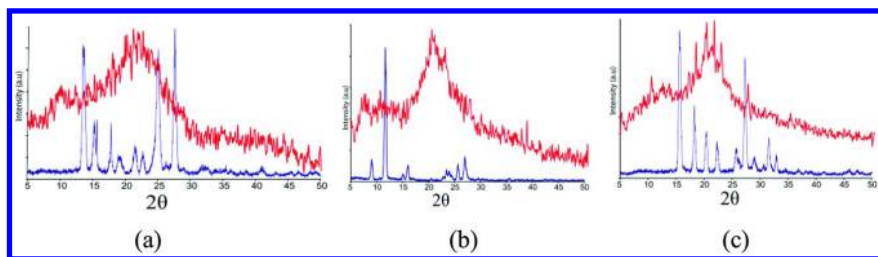
*Figure 1. Powder-XRD of (a) compound **1** (top) and 1,4-naphthoquinone (bottom); (b) compound **2** (top) and 2-methyl-1,4-naphthoquinone (bottom); (c) compound **3** (top) and 1,4-benzoquinone (bottom) (scan rate of 1° min⁻¹).*
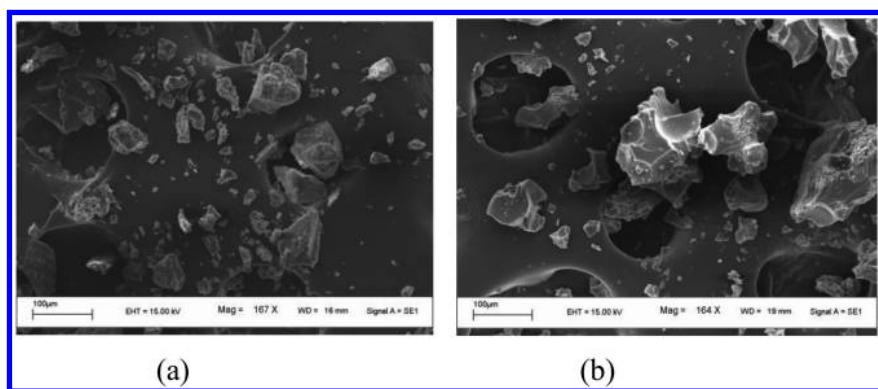
*Figure 2. The SEM figure of the film prepared from compound (a) **1** and (b) **3** showing the formation of orifices from which the micron sized particles have formed.*

These compounds interact with Bovine Serum Albumin (BSA), which could be monitored from the changes in the fluorescence emission of the BSA upon interactions. The BSA has emission from its tryptophan residues at 335 nm, and the intensity and position of this emission are guided by the local environment (*32*) . Thus, when the compounds **1-3** were allowed to interact with BSA there was decrease in emission at 335 nm in each case. The interaction of compound **1** with BSA not only quenched the fluorescence at 335 nm but on increase in the concentration of **1** resulted in generation of new emission peak at a higher wavelength, namely at 418 nm. Such change in emission passed through an isoemissive point at 375 nm (Fig 3a). Same was true in the case of the compound **2**, however, the emission at higher wavelength in the case of **2** was less prominent (Fig. 3b). In the case of compound **3** there was insignificant

changes at higher wave length and it caused quenching of fluorescence at 375 nm of BSA, despite the compound **3** had an overlapping emission with BSA. The new emission occured at higher wavelengths in the cases of **1** and **2** arose from the excess unbound compounds. This was confirmed by the comparision with the fluorescence emissions of the parent quinone compounds **1-2** at these wavelengths. Moreover these emissions were found to be environment sensitive. The environment sensitivity of fluorescence emission by quinone compounds have been well established in literature (*33*). As the emission peaks of the parent compounds **1** and **2** were away from the emission peak of BSA the binding constants of **1** and **2** were determined by using Benesi-Hildebrand equation (*34*) by the fluorescence method. These were found to be $2.787 \pm 0.026 \times 10^4$ mol^{-1}, $1.447 \pm 0.037 \times 10^3$ mol^{-1} respectively. Since the compound **3** had overlapping emission with BSA peaks, the binding constant was not been determined. The compounds **1** and **2** have similar structures, whereas, the compound **1** has a higher binding constant than compound **2**. This may be attributed to the presence of no methyl sustituent on the ring in the case of **1**, the absence ofthe methyl group enhanced the closer approach of the compound to the tryptophan residue present in the interior of the tertiary structure of the protein.
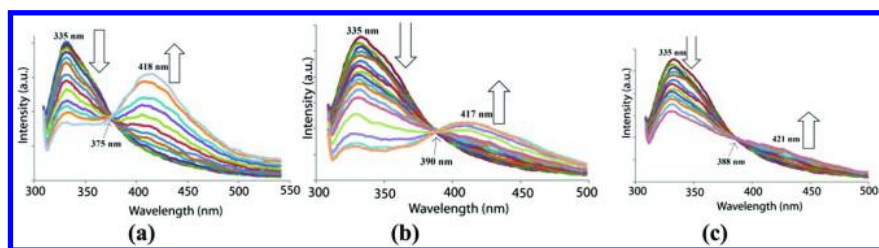
Figure 3. The changes in the fluorescence emission spectra of BSA (BSA 3μL in 3 mL buffer) addition of (a) compound 1, (b) 2, and (c) 3 with increasing concentrations in the range from 0 to 52 μM at pH 7.4 in 20 mM Tris buffer 160 mM NaCl, 50 μM ZnSO₄, pH 7.4.

The compounds **1** did not show the reversible couples of the parent 1,4-naphthoquinone, but it showed a reduction peak at E½ = - 1.13 V; whereas the compound **2** showed two one-electron reversible couples at E½ = -1.042 V (ΔEp = 69 mV and i_p/i_c = 1.4) and E½ = -1.704V (ΔEp = 115 mV and i_p/i_c = 1.16). Generally the 1,4-naphthoquinones or 1,4-benzoquinones show two one-electron reversible peaks for radical anion formation followed by formation of dianion. On the other hand, the compound **3** showed only one quasi-reversible redox couple at E½ = -1.02 (ΔEp = 538 mV and i_p/i_c = 1.41). These results showed that the functionlisation and self-assembling of the quinonic compounds **1-3** cause large devations in electrochemical properties which makes them potential candidate to make modified surfaces with varied electrochemical properties.

Conclusions

The electroactive quinone tethered trimethoxysilane compounds are capable of forming films as well as micron-sized particles. Electrochemical properties of these compounds are highly substrate dependent. Abilities of these compounds to bind to a protein have made them promising precursors to make electroactive surfaces for biological studies.

Experimental

The 1,4-naphthoquinone, 2-methyl- 1,4naphthoquinone, benzoquinone and 3-mercaptopropyl-trimethoxysilane were obtained from Sigma, USA. BSA was purchased from Fluka Germany and was used as supplied. The size and surface morphologies of the sample were investigated by Scanning Electron Microscopy (SEM) on a LEO 1430vp instrument operated at 10-15 kV. The sample was deposited onto the conductive carbon tapes, which were placed over the top of SEM Custubs. The sample was then coated with gold by sputtering for a time period of 150 s thereby making it conductive to reduce the charging effect under SEM conditions. The solid state UV-visible spectra were recorded on a Perkin-Elmer-Lambda 750 UV-visible spectrometer at room temperature. The cyclic-voltammograms were recorded on a CHI660A electrochemical work-station with a three electrodes system by dissolving adequate amounts of compound (10^{-5} M) in dry DMF with tetra butyl ammonium perchlorate as the supporting electrolyte under nitrogen atmosphere. A platinum electrode and glassy carbon electrode were used as auxiliary and working electrodes, respectively, with an Ag/AgCl electrode as the reference electrode. Fluorescence measurements were performed on fluoromax-4 spectrofluorometer using 10 mm path length quartz cuvettes with the slit width of 5 nm at 298 K. The powder X-ray diffraction were performed on a Bruker D2 diffractometer in Bragg -Brentano θ-θ geometry with Cu K α radiation ($\lambda = 1.5418$ Å) on a glass surface of an air-dried sample using a secondary curved graphite monochromator. Diffraction patterns were collected over a 2θ range of 5-50 ° at a scan rate of 1° min^{-1}.

For fluorescence titration, BSA (14 μM in 3 mL buffer solution of 20 mM Tris buffer 160 mM NaCl, 50 µM $ZnSO_4$, pH 7.40 was taken in a quartz tube and fluorescence was measure by exciting at 295 nm. Definite quantities of either of the compound **1-3** were taken out by a micro-pipette from stock solution in dimethylsulphoxide (DMSO) to add to BSA solution.

Synthesis of Compound 1

To a well stirred solution of 1,4-naphthoquinone (0.31 g, 2 mmol) in methanol (20 mL) a solution of 3-mercaptopropyl-trimethoxysilane (0.337 mL, 2 mmol) was added drop wise. The reaction mixture was stirred at room temperature for 8 hs. A brown colour precipitate of **1** was formed .The resulting mixture was filtered and dried in open air. Yield: 85% IR (KBr, cm^{-1}): 3730 (s), 3694 (m), 3622 (m), 3594 (m), 3411 (bw), 1657 (s), 1587 (m), 1551 (w), 1446 (w), 1335 (w), 1296 (m), 1254

(m), 1027 (m), 860 (m), 777 (w), 662 (s). Fluorescence emission: λ_{em} (DMSO, λ_{ex} 330 nm): 406 nm. Decomposition temp. 326 °C.

Synthesis of Compound 2

To a well stirred solution of 2-methyl-1,4-naphthoquinone (0.34 g, 2 mmol) in methanol (20 mL) a solution of 3-mercaptopropyl-trimethoxysilane (0.337 mL, 2 mol) was added drop wise. The reaction mixture was stirred at room temperature for 2 hs. A golden yellow precipitate (**2**) was formed. The mixture was filtered and the residue was dried. Yield: 92% IR (KBr, cm^{-1}): 3440 (bs), 1660 (s), 1591 (s), 1442 (m), 1383 (w), 1325 (m), 1283 (m), 1264 (m), 1118 (bm), 891 (w), 776 (m), 690 (m), 668 (m), 647 (w), 561 (w), 436 (w). Fluorescence emission: λ_{em} (DMSO, λ_{ex} 330 nm): 406 nm. Decomposition temp. 311 °C.

Synthesis of Compound 3

To a well stirred solution of 1,4-benzoquinone (0.21 g, 2 mmol) in methanol (20 mL) a solution of 3-mercaptopropyl-trimethoxysilane (0.337 mL, 2 mmol) was added drop wise. The reaction mixture was stirred at room temperature for 6 hs. A red precipitate (**3**) was obtained, which was filtered and dried in open air. Yield: 80%. IR (KBr, cm^{-1}): 3786 (w), 3725 (m), 3699 (m), 3265 (bs), 3029 (w), 1654 (s), 1515 (s), 1470 (s), 1350 (m), 1242 (m), 1209 (s), 1096 (m), 1026 (w), 889 (w), 829 (m), 760 (s), 670 (m), 608 (w), 520(w). Fluorescence emission: λ_{em} (DMSO, λ_{ex} 300nm): 338 nm. Decomposition temp. 374 °C.

References

1. Zhao, Y.; Shen, Y.; Bai, L. *J. Colloid Interface Sci.* **2012**, *379*, 94–100.
2. Ide, Y.; Kagawa, N.; Itakura, M.; Imae, I.; Sadakane, M.; Sano, T. *ACS Appl. Mater. Interfaces* **2012**, *4*, 2186–2191.
3. Barrera, C.; Herrara, A.; Zayas, Y.; Rinaldi, C. J.; Barrera, C.; Herrera, A. *J. Magn. Magn. Mater.* **2009**, *321*, 1397–1399.
4. Jesionwski, T. *Compos. Interfaces* **2009**, *16*, 115–129.
5. Yang, F.; Nelson, G. L. *J. Appl. Polym. Sci.* **2004**, *91*, 3844–3850.
6. Jo, S.; Park, K. *Biomaterials* **2000**, *21*, 605–616.
7. Yuan, B.; Chen, Q.; Ding, W. Q.; Liu, P. S.; Wu, S. S.; Lin, S.C.; Shen, J.; Gai, Y. *ACS Appl. Mater. Interfaces* **2012**, *4*, 4031–4039.
8. Baikousi, M.; Dimos, K.; Bourlinos, A. B.; Zboril, R.; Papadas, I.; Deligiannakis, Y.; Karakassides, M. A. *Appl. Surf. Sci.* **2012**, *258*, 3703–3709.
9. Seto, H.; Ogata, Y.; Murakami, T.; Hoshino, Y.; Miura, Y. *ACS Appl. Mater. Interfaces* **2012**, *4*, 411–417.
10. Farrell, M.; Beaudoin, S. *Colloids Surf., B* **2010**, *81*, 468–475.
11. Remes, Z.; Kromka, A.; Vanecek, M.; Grinevich, A.; Hartmannova, H.; Kmoch, S. *Diamond Relat. Mater.* **2007**, *16*, 671–674.
12. Chu, L.; Danials, M. W.; Francis, L. F. *Chem. Mater.* **1997**, *9*, 2577–2582.

13. Yee, J. K.; Parry, D. B.; Caldwell, K. D.; Harris, J. M. *Langmuir* **1991**, *7*, 307–313.
14. Liz-Marzan, L. M.; Giersig, M.; Mulvaney, P. *Langmuir* **1996**, *12*, 4329–4335.
15. Adam, F.; Batagarawa, M. S.; Hello, K. M.; Al-Juaid, S. S. *Chem. Pap.* **2012**, *66*, 1048–1058.
16. Zhen, B.; Jiao, Q.; Zhang, Y.; Wu, Q.; Li, H. *Appl. Catal., A* **2012**, *445*, 239–245.
17. Bariana, M.; Aw, M. S; Kurkuri, M.; Losic, D. *Int. J. Pharm.* **2013**, *443*, 230–241.
18. Zhang, Q.; Huang, R. F.; Guo, L. H. *Chin. Sci. Bull.* **2009**, *54*, 2620–2626.
19. Yoshinaga, K. *Bull. Chem. Soc. Japan* **2002**, *75*, 2349–2358.
20. Gulyas, J.; Rosenberger, S.; Foldes, E.; Pukanszky, B. *Polym. Compos.* **2000**, *21*, 387–395.
21. Xu, J.; Perry, C. C. *J. Non-Cryst. Solids* **2007**, *353*, 1212–1215.
22. Piper-Feldkamp, A. R.; Wegner, M.; Brzezinski, P.; Reed, S. M. *J. Phys. Chem. B* **2013**, *117*, 2113–2122.
23. Singh, W. M.; Baruah, J. B. *Synth. Commun.* **2009**, *39*, 1433–1442.
24. Singh, W. M.; Karmakar, A.; Barooah, N.; Baruah, J. B. *Beil. J. Org. Chem.* **2007**, *3*, 10.
25. Vargas, A.; Shnitko, I.; Teleki, A.; Weyeneth, S.; Prasinis, S. E.; Baiker, A. *Appl. Surface Sci.* **2011**, *257*, 2861–2869.
26. Hong, S. C.; Lee, J. H.; Lee, J.; Kim, H. Y.; Park, J. Y. *Int. J. Nanomed.* **2011**, *6*, 3219–3231.
27. Gong, M.; Dang, Y.; Wang, Y. B.; Yang, S.; Winnik, F. M.; Gong, Y. K. *Soft Matter* **2013**, *9*, 4501–4508.
28. Chen, J. J.; Struk, K. N.; Brennan, A. B. *Langmuir* **2011**, *27*, 13754–13761.
29. Croazza, M. Z.; Somera, B. F.; Segatelli, M. G.; Tarley, C. R. T. *J. Hazard. Mater.* **2012**, *243*, 326–333.
30. Li, X.; Ren, T.; Wang, N.; Ji, X. *Anal. Sci.* **2013**, *29*, 473–477.
31. Chen, M. A.; Lu, X. B.; Guo, Z. H.; Huang, R. *Corros. Sci.* **2007**, *53*, 2793–2802.
32. Chen, Y.; Barkley, M. *Biochemistry* **1998**, *37*, 9976–9982.
33. Itoh, T. *J. Chem. Phys.* **1987**, *87*, 4361–4367.
34. Benesi, H. A.; Hildebrand, J. H. *J. Am. Chem. Soc.* **1949**, *71*, 2703–2707.

Chapter 13

A Lesson in Limerick Enzymology

Stephen J. Clarson[*]

Department of Chemical and Materials Engineering and the Polymer Research Centre, University of Cincinnati, Cincinnati, Ohio 45221, USA
[*]**E-mail: Stephen.Clarson@UC.Edu**

Herein is presented a lesson in limerick enzymology that was given by Dr. H. N. Cheng to an aspiring poet. It should be noted that the said young and aspiring poet went to the same grammar school in Yorkshire as the late British Poet Laureate Ted Hughes (*1, 2*).

Introduction

We all know that my good friend and colleague Dr. H. N. Cheng is a renowned poet, in addition to being a fabulous scientist (*3*). I humbly submitted two limericks to H. N. for his consideration. H. N. then used his considerable knowledge of poetry to reinterpret them. I do still rather like the originals – so they are given here along with the H. N. suitably "polished" limericks.

An Enzyme Limerick

There was a new enzyme named Mitch,
Isolated from the moss in a ditch.
It transformed substrates so many,
Giving new products a plenty,
And as easy to use as a switch.

Another Enzyme Limerick

The enzyme was running amok;
Barns was watching the clock.
The reaction slowed down,
Our substrate did frown,
With pocket it did not dock.

A Lesson in Limerick Enzymology from H. N.

H. N.: As we know, in a strict sense a limerick requires the anapaestic meter (sometimes amphibrachic), with lines 1, 2, and 5 having three feet of three syllables each, and lines 3, 4 two feet of three syllables. I have slightly modified your poem to conform with the rules.

We have here a new enzyme named Rich,
Isolated from moss in a ditch.
Great ventures it conducts,
Producing "green" products,
And as easy to use as a switch.

H. N.: I think this one is a variation on the Hickory Dickory Dock rhyme. I made more changes here. Again, I tried to adhere to the rules of length and meter.

The enzyme was soon running amok;
With a frown H. N. stood by the clock.
The reaction slowed down
But the substrates turned brown.
What a comic picture for a talk!

Notes

Credit for the photograph of Ted Hughes: A portrait of Ted hughes by Rob Lycett. Date: March 19th, 1993. Location: Calder high School, Mytholmroyd, West Yorkshire. Original uploaded by Breakingthings (Transfered by Maurilbert) (Original uploaded on en.wikipedia) [CC-BY-SA-2.5-2.0-1.0 (http://creativecommons.org/licenses/by-sa/2.5-2.0-1.0)], via Wikimedia Commons.

Versions of the limericks appearing in this chapter were first printed in Cheng, H. N., Gross, R. A., Smith, P. B., Eds. *Green Polymer Chemistry: Biocatalysis and Materials II*; ACS Symposium Series 1144; American Chemical Society: Washington, DC, 2013.

References

1. Hughes, E. J. *The Hawk in the Rain*; Faber & Faber: London, 1957.
2. Hughes, E. J. *The Essential Shakespeare*; The Ecco Press: Hopewell, NJ, 1991.
3. Cheng, H. N. In *Polymer Biocatalysis and Biomaterials*; Cheng, H. N.; Gross, R. A., Eds.; ACS Symposium Series 900; The American Chemical Society: Washington, DC, 2005; p 437.

Subject Index